Mitochondrial dysfunction during ischaemia reperfusion injury in models of organ transplantation

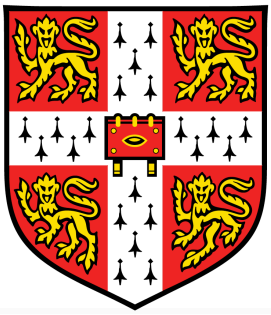

Anja Veronika Gruszczyk

MRC Mitochondrial Biology Unit

University of Cambridge

Dissertation submitted for the degree of

Doctor of Philosophy

Darwin College

April 2020

Declaration

This dissertation was written in partial fulfillment of the requirements for the degree of Doctor of Philosophy. With the exception of any collaborations that are mentioned throughout the text, this dissertation describes my own work carried out under the supervision of Prof. Michael P. Murphy and Dr. Kourosh Saeb-Parsy from April 2016 until April 2020. Any information that is derived from other sources is referenced accordingly.

Anja Veronika Gruszczyk

April 2020

Declaration

Mitochondrial dysfunction during ischaemia reperfusion injury in models of organ transplantation

Anja Gruszczyk

Abstract

Organ transplantation is the only treatment for patients with severe and irreversible organ damage. Although the efficacy of transplantation has progressed immensely in recent years, one of the most damaging factors occurring during this surgical procedure, ischaemia reperfusion injury (IRI), is still a major contributor causing poor outcome. Ischaemia arises due to the lack of blood supply, leaving the tissue without oxygen and substrates, which are crucial for energy generation. Upon reperfusion with oxygenated blood, molecular processes within mitochondria lead to the generation of reactive oxygen species (ROS), which damage the organelles and lead to cell death and ultimately tissue fibrosis. During organ transplantation, the organs are cut off the blood supply when retrieved from a donor and stored at cold temperatures while transported to the recipient. During this time the organs become ischaemic and are then exposed to reperfusion injury within the recipient. Effective therapeutics to ameliorate this injury are not available, because of our lack of understanding of some of the basic underlying molecular processes during ischaemia, as well as the damaging pathways activated by factors released upon mitochondrial damage, such as succinate or mtDNA.

In order to understand these processes better and be able to develop novel therapies, I utilised a range of models for IRI in heart, liver and kidney organ transplantation. These ranged from basic cell models to advanced *in vivo* procedures that closely replicated conventional transplantation. Finally, I compared these situations with data collected from human organs and blood during transplantation and related procedures in patients. I characterised the highly conserved decrease in the ATP/ADP ratios and the depletion of the adenosine nucleotide pools in various ischaemic tissues in a number of species over time under different temperatures. This work indicated the important mitochondrial and metabolic changes that occur in organs during storage and reperfusion in the recipient. I then used this knowledge to develop an

improved mouse cardiomyocyte model for the assessment of IRI in vitro. For this, I utilised primary adult murine cardiomyocytes to demonstrate succinate accumulation during ischaemia as the metabolic factor that leads to mitochondrial ROS production during IRI. This led on to an exploration of potential drugs targeted to inhibit complex II as a possible therapy. Furthermore, I investigated the release and efflux of accumulated succinate and the mitochondrial damage associated molecular patterns (mtDAMPs) mtDNA upon reperfusion in this cell model. This was compared with the role of circulating mtDNA in mice undergoing transplantation and also in patients during liver transplant surgery. Hence, I could determine a time course of mtDNA release from mitochondria into the cytosol, as well as from cells into the circulation. Furthermore, I could show that the release of mtDNA was enhanced by opening of the mitochondrial permeability transition pore (MPTP), and that this could be inhibited using the MPTP inhibitor cyclosporin A.

Overall, this work has generated new insights into the contribution of mitochondrial dysfunction to IRI during organ transplantation and has contributed to the development of potential therapies to ameliorate this damage

Acknowledgements

First, I want to thank Mike for giving me the opportunity to do what I love most in such an incredible environment. Thanks to you I grew a lot, scientifically and personally. And thanks for being such a strong support, especially throughout the writing phase - I don't think the result would have been the same otherwise.
And thank you to Kourosh for providing a lab culture that is based on caring for each other - I have never experienced anything like this before and it feels great to know that I will always be part of the KSP family.

I am grateful for all the guidance and support I received while writing up, specifically from Hiran, Abigail and Nikola. I really value your constructive criticism.

Thanks to all my amazing co-workers, who never failed to see when things were hard and supported me whenever possible. Especially Fay, who has become a big part of my PhD life, Nils, and obviously Hiran, who probably is one of the kindest people I have ever met.
And of course, I would have never made it without the KSP lab, above all Krish, Nikola and Tim. Can't wait for our next retreat!

I want to say special thanks to all our collaborators who were the ones truly making this work possible. I am especially grateful to Dr. Ina Jochmans for providing me with invaluable liver transplant samples. And to all the surgeons who surprised me with their enthusiasm towards our research and their interest in even the slightest discovery - this definitely was a huge motivation!
And I am grateful for the donors and their families, without whom this project would not have been possible.

Finally, a big thank you to all my awesome friends in Cambridge, Köln and all over the world, who supported me throughout every difficult phase. Especially to Marisa and the dinner crew– I cannot (and don't want to) imagine a life without you anymore!
Und danke natürlich an meine Familie, ohne Euch geht eh gar nix – KOCHAM CIĘ!

Abbreviations

All abbreviations, unless listed, are as described in the "Instructions to Authors" of the Biochemical Journal (http://www.biochemj.org).

ΔP	proton motive force
ΔpH	pH gradient
ΔΨ	membrane potential
2'3'-cGAMP	cyclic guanosine monophosphate–adenosine monophosphate
3NPA	3-nitropropionic acid
Acetyl-coA	Acetyl-Coenzyme A
ADP	adenosine-5'diphosphate
AIM	absent in melanoma 2
AK	adenylate kinase
ALT	alanine aminotransferase
AST	aspartate aminotransferase
AMP	adenosine-5'monophosphate
AMPK	5'AMP-activated protein kinase
AMS	acetoxymethyl succinate
AN	anoxia
ANT	adenosine nucleotide translocase
ATP	adenosine-5'triphosphate
BCA	bicinchoninic acid
BSA	bovine serum albumin
cGAS	cyclic GMP-AMP synthase
CI	cold ischaemia
CI-V	respiratory chain complexes 1-5
CM	cardiomyocytes
CoQ	Coenzyme Q
CpG	5'C-phosphate-G 3'
CsA	cyclosporin A
Cyt c	cytochrome c
Cyto	cytosol
D-loop	displacement loop
d	days
ddPCR	droplet digital PCR
DIC	dicarboxylate carrier

DMEM	Dulbecco's Modified Eagle's Medium
DMM	dimethyl malonate
DMSO	dimethyl sulfoxide
DNA	deoxyribonucleic acid
dNTP	deoxyribonucleotide triphosphate
dsDNA	double stranded DNA
DSM	disodium malonate
eGFR	epidermal growth factor receptor
ELISA	enzyme-linked immunosorbent assay
EQ	equilibration
ER	endoplasmic reticulum
ESC	embryonic stem cells
ETC	electron transport chain
EVNP	ex vivo normothermic perfusion
FAD	flavin adenine dinucleotide
FADH2	flavin adenine dinucleotide (reduced)
FAM	6-carboxyfluorescein
FBS	foetal bovine serum
FeS	iron-sulfur cluster
FMN	flavin adenine mononucleotide
FWD	forward (primer)
gGT	gamma-glutamyltransferase
Gpx	glutathione peroxidase
GR	glutathione reductase
Grx	glutaredoxin
GS	glycogen synthase
GSH	glutathione (reduced)
GSSG	glutathione disulfide
H+	proton
H_2S	hydrogen persulfide
HEK	human embryonic kidney
HEPES	4-(2-hydroxyethyl)-1-piperazineethanesulfonic acid
HEX	hexachloro-fluorescein
HIF-1α	hypoxia-inducible factor-1α
HILIC	hydrophilic interaction liquid chromatography
HLA	human leukocyte antigen
IFN (β)	interferon (β)
IL (6)	interleukin (6)
IMM	inner mitochondrial membrane
IMS	inter membrane space
IPC	ischaemic preconditioning
IRI	ischaemia reperfusion injury
IS	ischaemia
IVC	inferior vena cava

KIM-1	kidney injury molecule-1
LAD	left anterior descending artery
LC-MS/MS	liquid chromatography tandem mass spectrometry
LDH	lactate dehydrogenase
Log	logarithm
M199	medium 199
MCT (1)	monocarboxylate transporter (1)
MEM	minimal essential medium
MitoPQ	MitoParaquat
MnSOD	manganese superoxide dismutase
MPTP	mitochondrial permeability transition pore
Mt	mitochondrial
mtDAMP	mitochondrial damage associated molecular pattern
mtDNA	mitochondrial DNA
NAD	nicotinamide adenine dinucleotide
NADH	nicotinamide adenine dinucleotide (reduced)
ND (1&5)	NADH: Ubiquinone Oxidoreductase Core Subunit (1&5)
nDNA	nuclear DNA
NGAL	neutrophil gelatinase-associated lipocalin
NLRP (3)	nucleotide-binding oligomerisation domain, leucine rich Repeat and Pyrin domain containing
O_2-	superoxide
OMM	outer mitochondrial membrane
OXPHOS	oxidative phosphorylation
PAGE	polyacrylamide gel electrophoresis
PAMP	pathogen associated molecular pattern
PBS	phosphate buffered saline
PCA	perchloric acid
PCR	polymerase chain reaction
Pi	phosphate
PK	pyruvate kinase
Prx	peroxiredoxin
PVDF	polyvinylidene difluoride
Q	ubiquinone
QH_2	ubiquinol
qPCR	quantitative PCR
R	reperfusion
RET	reverse electron transport
REV	reverse (primer)
ROS	reactive oxygen species
Rpm	revolutions per minute
RT-PCR	real-time PCR
SDH	succinate dehydrogenase
SDS	sodium dodecyl sulfate

SN	supernatant
ssDNA	single stranded DNA
STING	stimulator of interferon genes
T141990	Tyrode's Buffer + 10 uM MCT1 inhibitor AR-C141990
TBE	Tris/Borate/EDTA buffer
TCA	tricarboxylic acid cycle
TE	Tris-EDTA buffer
TLR (9)	toll-like receptor (9)
TOM	translocase of the outer membrane
TPP	triphenyl phosphodium
Trx	thioredoxin
TTFA	thenoyltrifluoroacetone
UV	ultraviolet light
VDAC	voltage-dependent anion channel
WI	warm ischaemia
wk	weeks

Table of content

Chapter 1

Introduction

1.1 General Introduction

In recent years, an increasing number of organs have been donated for transplantation, but not all of them can be used due to excessive damage to these organs during the transplantation process. This leads to a significant mismatch between the number of people worldwide who rely on a transplant and the number of available donor organs of sufficient quality to produce successful outcomes following the stresses occurring during donation, preservation and anastomosis upon transplantation (Matesanz et al., 2012). It is therefore important to reduce damage to these donated organs at all stages of transplantation to increase the pool of available organs and to improve the outcome for graft recipients. Furthermore, most of the research to date on improving transplant outcome has focused on surgical procedures and also on the immunological aspects of transplantation which has enabled successful and widespread organ transplantation. However, less research has been carried out on the metabolic aspects of transplantation. While, during the development of organ transplantation, there was a focus on developing preservation solutions and on how to sustain organs during cold preservation, these developments have not been reassessed or built on in recent years. Over this time there have been many developments in our understanding of the metabolic underpinnings of factors that can affect organ function and injury during transplantation. This is especially relevant with regard to the effects of ischaemia and ischaemia-reperfusion injury during transplantation surgery on the function and health of organs.

Ischaemia-reperfusion (IR) injury is inevitable during transplantation and is a major contributor to early graft dysfunction and failure (Cavaillé-Coll et al., 2013; Perico et al., 2004; Summers et al., 2010; Zhai et al., 2013). During organ storage the blood supply, which usually provides energy-yielding molecules and oxygen, is blocked. Without this blood supply, the lack of oxygen means that metabolic pathways within the cell switch to anaerobic metabolism to enable energy production by glycolysis. The organelles inside cells that require oxygen for their metabolism and are therefore most sensitive to its absence are mitochondria. Mitochondria make energy available in the form of an adenosine triphosphate (ATP) to ADP ratio which is sustained by utilising the mitochondrial protonmotive force, which comprises a pH gradient and a membrane potential across the mitochondrial inner membrane. This proton motive force is developed by transferring electrons through respiratory complexes within the mitochondrial inner membrane and simultaneously pumping protons across the membrane (Mitchell, 1961). The electrons are finally accepted by oxygen at complex IV of the respiratory chain, producing water (Watt et al., 2010). If this oxygen is missing, the electron transport

cannot be completed and the aerobic energy production is stopped. Furthermore, reoxygenation causes the production of mitochondrial reactive oxygen species (ROS), which has been recognised to play a central role in the pathology of ischaemia reperfusion injury in various pathologies, such as heart attack and stroke (Baines et al., 2005; Brealey et al., 2002; Brooks et al., 2009; Chen et al., 2015; Kuznetsov et al., 2004; Zhang et al., 2007).

During ischaemia, cells and organs are forced to maintain their ATP/ADP ratio anaerobically and utilise internal energy stores, leading to a drop in energy availability as ischaemic time increases. Ultimately, this leads to cell death unless oxygen is restored. One way to prolong the ischaemic time that organs can survive is via methods to store organs at low temperatures and to use preservation solutions (Monbaliu et al., 2009). However, even under these conditions, prolonged preservation time can cause long-term damage to grafts that means they do not function appropriately in the recipient and this can also be followed by chronic organ rejection. During transplantation of the heart, which is very sensitive to ischaemia, an increase in mortality one year after transplantation occurs when the organ was stored for more than 3 h (Stehlik et al., 2010). However, little is known about how increased cold storage time may lead to a poor outcome for the patient.

In this thesis I explore the ways in which mitochondrial function can contribute to the damage that occurs to organs during the transplantation process. In the introduction I first provide some background on transplantation and then I discuss relevant aspects of mitochondrial metabolism, function and dysfunction before describing how understanding these processes may contribute to improvements in outcome for transplantation patients.

1.1.1 Necessity for improvement

Although an increasing number of people donate organs, and the techniques for transplantation have improved considerably in recent years, there is still a major need for improvement in organ quality and viability. Much research has understandably focused on understanding the immunological aspects of transplantation and how this contributes to the long-term rejection that lead to graft dysfunction. As shown in FIGURE 1, a gradual increase in the number of donors in the UK was reported between 2017/18 and 2018/19 (Great Britain and Department of Health & Social Care, 2018; NHS Blood and Transplant, 2015). These donors can contribute various numbers of organs, dependent on patient death and health conditions. Strikingly, although more patients are willing to become organ donors, fewer organs were actually transplanted (Figure 1.1). These data retrieved from the annual blood and transplant

report from the NHS does not specify why these organs could not be utilised for transplantation, but often this is due to underlying pathological conditions in the donor, complications during the transplantation surgery or elevated ischaemic damage to the organ, all of which may lead to delayed graft function followed by chronic graft failure and/or rejection. These data show that the quality of organ donation has to be improved in order to allow the transplantation of more organs with successful engraftment.

The molecular basis of the cellular damage that occurs during the transplantation process is still poorly understood and needs much more detailed analysis. Throughout the surgical procedure, organ damage can occur due to the lack of oxygen, but paradoxically the damage can be further exacerbated after the organ has been transplanted into a recipient and reconnected to the blood supply. This reperfusion and reoxygenation activates molecular processes that can lead to cellular damage and even activate long-term immunological responses as explained in more detailed further on in this chapter. In summary, although the success of organ transplantation has improved over the last few years, the quality of the donated organs can be poor, making them unsuitable for transplantation. In order to improve organ survival, the underlying cellular processes that cause organ damage and delayed graft function need to be better understood so that therapies targeted at preventing them can be developed.

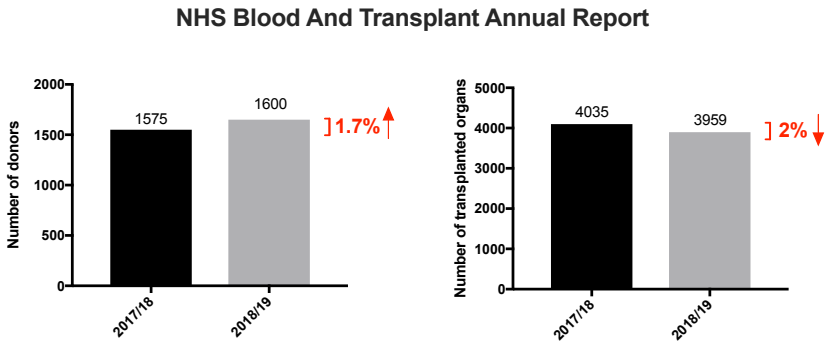

Figure 1.1: Organ demand in the UK 2017-2019. The NHS Blood and Transplant annual report provides information about the amount of patients waiting for an organ donation, the number of retrieved organs and the number of successful transplantations in the UK. In the year 2017/2018, 1575 patients donated organs, one year later this number increased to 1.7% to 1600. In contrast to this, the number of transplanted organs decreased by 2% from 4035 in 2017/2018 to 3959 total number of all transplanted organs in the UK in 2018/2019.

1.1.2 General introduction to transplantation

Organ transplantation is the only available cure for patients with end-stage organ failure after all other medical therapies have failed (Morris, 2004). In a surgical procedure, vital organs are retrieved from a donor and transplanted as so-called grafts into a recipient. During this process, the organs are retrieved in a given order: first, lungs and heart are obtained, before liver, spleen and pancreas can be removed and finally the kidneys and other organs are collected (Figure 1.2). Donation can occur from a living or deceased donor. In our research, we focus on donation after death, which can substantially impact the quality of the organs and therefore transplantation outcome.

There are two main categories of deceased donors which are differentiated as shown in Figure 1.2. Donors after brain death (DBD) are patients that show no brainstem activity and are therefore pronounced brain dead (Barker and Markmann, 2013). The criteria for brain death have been established in 1968 in Harvard (Beecher, 2007) and allow DBD donation, which is the major source of donor organs in most Western countries (NHS Blood and Transplant, 2015b). Although these patients show no brain activity, they are still kept on life support that maintains a beating heart and therefore constant perfusion and supply of oxygenated blood to the organs throughout the body. Despite this, brainstem death does inflict huge stress on the body and causes changes in haemodynamic, endocrine and metabolic processes which may impact the quality of the donated organs and therefore affect the short- and long-term outcomes for recipients (Hodgson et al., 2017).

So-called DCDs, donors after cardiac death, are patients that have undergone cardiac arrest and are therefore pronounced dead. In addition, irreversibility of death has to be proven by a five-minute waiting period after cardiac arrest, in case of spontaneous re-activation of the heart (2009). Due to this interrupted blood supply, the donor is subjected to an inevitable period of ischaemia while organs in the body are deprived of oxygenated blood. This primary ischaemia to DCD organs results in poorer graft quality and transplantation outcome compared to DBD. Despite this, because of the chronic shortage of organs from DBD donors, DCD donation has become more prevalent recently, and ischaemic organs have been increasingly utilised successfully in transplantation (Hodgson et al., 2017).

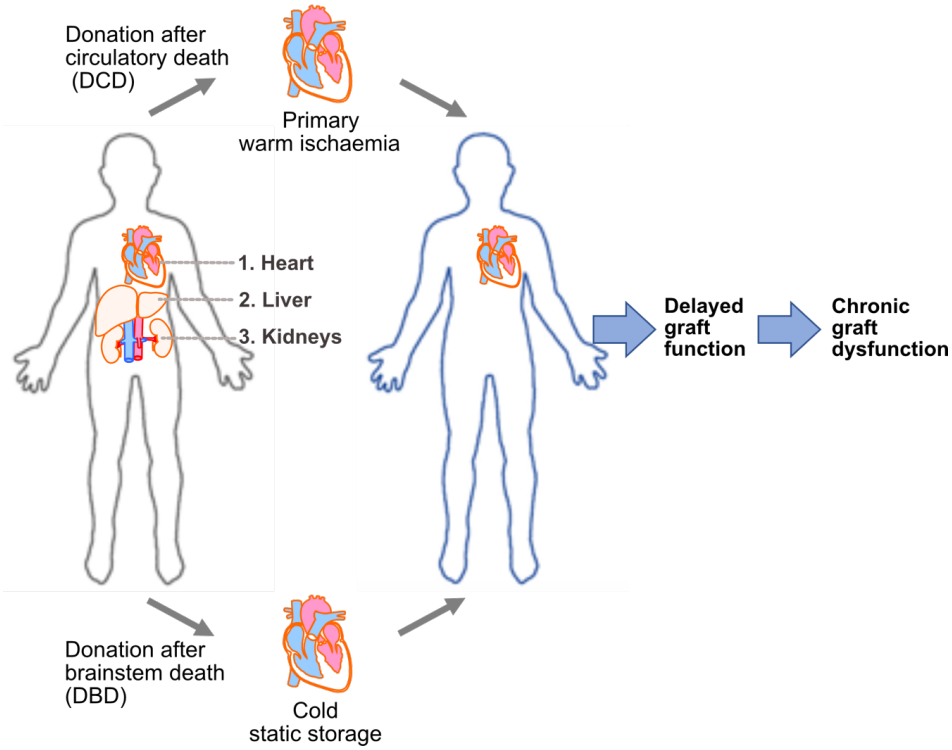

Figure 1.2: Schematic overview over the two main forms of organ donation after death Two main forms of organ donation after donor death are differentiated: donation after brain stem death (DBD) and donation after cardiac death (DCD). In both cases the donor is declared dead and organs can be retrieved in a fixed order, whereby heart and lungs are retrieved first, then liver, pancreas and spleen, before finally kidneys and other organs are taken. During DCD donation, the donor died of cardiac arrest resulting in interrupted perfusion of the organs and therefore primary warm ischaemia. During DBD donation, the donor brain shows no function anymore, but the heart remains beating, keeping the organs within the patient perfused. This way, primary warm ischaemia is ameliorated and retrieved organs are cooled down rapidly and stored on ice undergoing cold ischaemia until they are transplanted. The amount of warm ischaemia that occurred before transplantation affects surgery outcome. Elevated ischaemic times lead to delayed graft function and finally chronic graft dysfunction and rejection.

To summarise, organ transplantation is the major therapy to ensure survival for patients with organ failure after all other medical interventions have failed. Although best results are obtained with donation after brain death, not enough DBD organs are retrieved to meet demand, making DCD donation more prevalent, despite the additional primary ischaemia. In addition, there is also the inevitable damage that occurs to organs during DBD, as well as DCD donation, due to ischaemia during transport of the donated organ from donor to the recipient. Together these create the need for good preservation methods to maintain high graft quality and make organs that are currently discarded usable for transplantation.

1.1.3 Organ preservation

Organs that are retrieved for transplantation are subject to damage due to the cellular processes occurring upon death within the body or primary ischaemia when the blood supply is interrupted. Furthermore, retrieved organs have to be transported to and transplanted into the recipient, which induces additional ischaemic periods. In order to minimise the ischaemic damage and the subsequent IR injury, organ preservation procedures are used. The beneficial effects of cold preservation on graft-outcome were first explored in the 1960s, when researchers discovered that organ cooling could ameliorate ischaemia reperfusion injury. For example, Calne et al. showed that kidneys that were rapidly cooled could survive 12 hours storage on ice (Monbaliu et al., 2009; Pegg et al., 2006). This led to the adoption of organ preservation by cold static storage for transplantation. During cold static storage, the organ is flushed with cold preservation solution and kept cold in a bag filled with this solution on ice. More recently, a number of alternative techniques have been developed in which the organs are stored and transported while being perfused *ex vivo* under hypo- or normothermic conditions. During *ex vivo* perfusion, the organ is attached to a pump and continuously perfused with an oxygenated perfusion solution in a closed circuit. Although cold storage is less expensive and therefore widely used, *ex vivo* perfusion techniques are being increasing used to improve graft quality and are described in more detail below. A final important point is that the usage of preservation and perfusion solutions opens up the possibility to supplement them with therapeutic compounds during ischaemia as well as upon reperfusion, which will be discussed in more detail later on in this chapter.

1.1.3.1 Cold static storage

Cold static storage preservation is the most commonly performed method for retrieved organs in the UK and worldwide (Opelz and Dohhler, 2007). The organ is flushed immediately upon collection from the donor with ice-cold preservation solution and maintained in the solution on ice at approximately 4°C. On ice, most organs are viable for several hours, and can be safely transported to other hospitals where they can be transplanted into recipients. The preservation solution is usually starch-rich, acellular and able to flush out residual blood from the vessels. Three solutions are commonly used for organ preservation in the UK: University of Wisconsin solution (UW, from Viaspan), histidine tryptophan-ketoglutarate (HTK, from Custodiol) and a proprietary solution from Celsior. All of these have similar beneficial effects on graft function during storage and early after transplantation (O'Callaghan et al., 2012). All

of these solutions are similar in design. For example, they aim to counteract osmotic fluid shifts that occur during prolonged ischaemia and hypothermia, which will result in cell swelling and loss of structural integrity. Furthermore, they have a strong pH buffering capacity to counteract the increased lactate accumulation. Finally, the electrolyte composition, especially the content of potassium and sodium, is crucial to control and maintain the ion balance between cells and the extracellular matrix (Bond et al., 2009). A comparison of the three solutions described above is presented in table 1.1. The preferred preservation material used in the Department of Surgery at the University of Cambridge is the University of Wisconsin solution from Viaspan.

Table 1.1: Composition of cold static storage solutions used to store donated organs upon retrieval, before transplantation. UW= University of Wisconsin, HTK= histidine tryptophan-ketoglutarate, Osm= osmotic pressure.

Solution name	[Na+] mmol/ L	[K+] mmol/ L	[Mg2+] mmol/ L	[Ca2+] mmol/ L	pH	Buffer	Osm (mOsm/l)	Colloid	Imper-meants	Anti-oxidants
UW	30	125	5	N.A.	7.4	Phos-phate	325	HES	Lacto-bionate / Raffi-nose	Allopurinol , glutathion e
HTK	15	10	4	0.015	7.0 2- 7.2	Histi-dine	310	N.A.	Manni-tol	Histidine/ tryptophan / mannitol
Celsior®	100	15	13	0.25	7.3	Histi-dine	320	N.A.	Lacto-bionate / Manni-tol	Histidine/ mannitol/ glutathion e

1.1.3.2 Ex vivo organ perfusion

Besides static cold preservation, continuous *ex vivo* perfusion is another way to preserve organs and has the major advantage that the continuous perfusion with oxygenated preservation fluid helps to prevent excessive IR injury. Perfusion pumps can be utilised to shorten the ischaemic period as the organ is perfused with solutions that supply oxygen, metabolites and energy substrates. Apart from monitoring ischaemic times, there is no reliable

way to determine organ quality before reperfusion thus *ex vivo* perfusion also offers the possibility to investigate damage parameters and to determine whether the organ has the potential to recover from the ischaemia it sustained during retrieval. *Ex vivo* perfusion may also help ameliorate some aspects of IR injury which can lead to the release of damage and cell death markers during reperfusion within the recipient activating immune responses. Because the organ is first perfused *ex vivo*, these markers are washed out. In addition, their analysis provides information about the level of IR injury and the potential for successful engraftment. Furthermore, marginal organs can be reconditioned and recover when perfused *ex vivo* because of the re-established supply with nutrients and oxygen. Finally, this technique offers the possibility to deliver therapeutic molecules using the energy- and oxygen-rich perfusion solution.

Ex vivo perfusion systems have been developed specifically for lungs, heart, liver and kidneys and are categorised into either hypothermic or normothermic perfusion. During hypothermic perfusion, the organ is kept cool (e.g. 4°C) after retrieval and throughout perfusion (Watson and Dark, 2012). During *ex vivo* normothermic perfusion (EVNP), the organ is warmed up by using a perfusion solution at 37°C which is pumped through the tissue. Both perfusion techniques have shown beneficial effects on transplant outcome (Hessheimer et al., 2015; Hosgood et al., 2015). Here, I focus on EVNP because it is widely used in the Department of Surgery, Cambridge.

A schematic overview of organ retrieval and EVNP is depicted in Figure 1.3. The organs are retrieved during which they are subjected to an initial period of warm ischaemia within the donor as the blood supply is disrupted and before the organ is retrieved from the body. The graft is then rapidly cooled with cold preservation solution and stored on ice, where it undergoes cold ischaemia. Following this, it is either transported to the recipient, or further preserved via *ex vivo* perfusion. On EVNP the efficiency of perfusion and recovery of organ function, such as urine output from perfused kidneys, can be assessed and the graft is the implanted into the recipient. Flushing the organ with preservation solution, or with leucocyte depleted blood, also enables the organ to be treated with anti-inflammatory or anti-oxidant compounds to reduce IR injury and improve graft function.

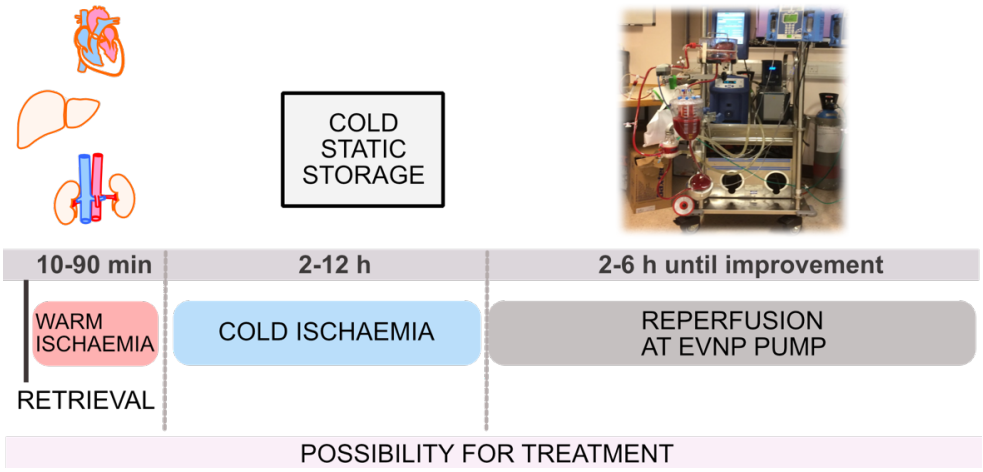

Figure 1.3: Schematic model of ex vivo normothermic perfusion systems. In order to improve organ quality after retrieval, the grafts can be perfused on ex vivo normothermic perfusion (EVNP) machines. During donation, organs are subjected to a short period of warm ischaemia followed by a longer period of cold ischaemia while the organ is stored on ice. Ex vivo perfusion enable the possibility to improve graft function and also offer a platform for surgeons to assess quality of the graft. Organs can be perfused with leucocyte-depleted blood for up to 6 h on such a pump and therefore ischaemic times can be ameliorated, and this also offers the possibility to induce therapeutic treatment in form of drugs.

Altogether, approaches to organ preservation are crucial to minimise damage and increase graft function upon transplantation. Cold static storage is efficient and low in cost, but *ex vivo* perfusion systems such as EVNP offer a number of potential advantages, including the possibility to assess the amount of damage that occurred to the organ, and to "recondition" marginal organs before implanting them into the recipient.

1.1.4 Organ-specific introduction into transplantation

Although the basic biochemical processes that lead to tissue damage remain broadly the same for different organs, the different cell types and structures of organs lead to different susceptibility to damage during ischaemia and upon reperfusion in the recipient. Some organs tolerate ischaemia better than others and can be stored on ice for longer (table 1.2).

Table 1.2: Maximal cold storage time (without any warm ischaemia) different human organs can tolerate. Adapted from O'Callaghan et al., 2012**.**

Organ	Number of hours (maximum)
Heart	6
Lung	8
Liver	12-16
Pancreas	16-18
Kidney	24-28

Consequently, organs are retrieved from the donor in a specified order, which is not only due to their accessibility within the body but is also based on how well they tolerate ischaemia. Below, I outline some of the organ-specific aspects of transplantation, because the differences between organs is important in understanding how to ameliorate excessive damage and IR injury during organ transplantation.

1.1.4.1 Heart transplantation

The heart is generally the first organ that is retrieved after donor death. It is also sometimes retrieved in combination with the lungs. The surgeon will cross-clamp the ascending aorta to stop blood supply in the body and avoid spillage during surgery. Immediately after cross-clamping, the heart (with or without lungs) is retrieved, perfused with cold storage solution and stored on ice or attached to a perfusion pump and perfused with leukocyte-depleted blood. The organs are then transported immediately to the recipient. The heart does not tolerate more than a few minutes of warm ischaemia at 37˚C, but at 4°C on ice it is viable for a few hours and is usually transplanted within 4 hours of retrieval. This is one of the reasons why DCD hearts are still used relatively infrequently for transplantation because it is unclear how much warm ischaemic damage the heart has sustained. Despite this, DCD donors are now being used for heart transplants in the UK and preliminary outcome data support successful recovery of the recipients (Large et al., 2017).

1.1.4.2 Liver transplantation

The liver can tolerate ischaemia much better than the heart. This may be in part because hepatocytes are highly regenerative and can survive significant stress, such as several hours of ischaemia (Zhai et al., 2013). Furthermore, the liver often contains large energy stores which facilitates recovery after reperfusion. During organ retrieval, after the heart and lungs have been removed, the liver and its surrounding organs are taken next. It is not clear which of the remaining organs best tolerates ischaemia.

1.1.4.3 Kidney transplantation

Even though the liver has greater glycogen stores than the kidney, few other organs can tolerate ischaemia as well as kidneys. This, and its position deep within the body, are why this organ is retrieved late in the process, just before skin or retina. Therefore, kidneys nearly always undergo a significant period of primary warm ischaemia during transplantation, before they are flushed with cold- storage solution and stored on ice for up to 12 hours before transplantation (O'Callaghan et al., 2012; van der Vliet et al., 2011). Kidneys are complex organs with diverse types of cells, some of which are chronically hypoxic *in vivo*, and are therefore thought to be more tolerant to ischaemia. As kidneys filter toxic and damaging factors from the blood, they come in contact with damaging factors released into the circulation after surgery, including proteins, DNA molecules and metabolites that can signal to the innate inflammatory system. These and other forms of stress during organ transplantation can lead to acute kidney injury (AKI), which is seen often in patients with graft dysfunction (Jochmans et al., 2017).

1.1.5 Ischaemia reperfusion injury in organ transplantation

The outcome of transplantation depends on several factors including damage to the donated organ as well as graft rejection within the recipient. Immunological rejection of the organ has historically been the biggest challenge and consequently research still focuses on understanding the role of the adaptive immune response and HLA (human leucocyte antigen) mismatching of donor and recipient. Organ transplantation in fact only became widely available due to the development of immunosuppressants, notably the T-cell proliferation

inhibitor cyclosporin A (Morris, 2004; Umland et al., 1999). The first successful clinical transplant was performed in 1954 on identical twins, avoiding HLA mismatching and the following immune responses (Merrill, 1956). Nowadays, donor and recipient are matched as closely as possible and that, in combination with long-term immunosuppression, has made successful engraftment possible (Morris, 2004). Nevertheless, graft failure does still occur, leading to secondary organ damage and sepsis in patients. Delayed graft function within the recipient often occurs when the organ does not perfuse well upon implantation. There can be several causes for this, for example previously unnoticed pathologies or tumours within the graft, or underlying health conditions in the recipient. However, the most common reason for poor graft performance seems to be associated with elevated ischaemic damage and ischaemia reperfusion injury (Zhao et al., 2018).

1.1.5.1 Organ damage and long-term rejection and graft dysfunction

The lack of oxygen supply that occurs due to ischaemia during transplantation surgery decreases energy supply and prevents the graft from performing vital metabolic processes leading to graft dysfunction after transplantation (Wang et al., 2019b). Another cause for long term graft dysfunction is the damage that occurs upon reperfusion of the transplanted organ. The sudden re- oxygenation when the organ is reconnected to the recipient`s blood supply leads to the production of reactive oxygen species that damage cell membranes, proteins and DNA that can lead to cell damage and death (Chouchani et al., 2016). The factors released from dead and dying cells can also enter the circulation and lead to an immunological response in the recipient. The recipient`s immune system can then attack the damaged graft and cause long term rejection. The underlying cellular processes that cause IR injury during transplantation are discussed in detail below.

1.2 Ischaemia reperfusion injury at the cellular level

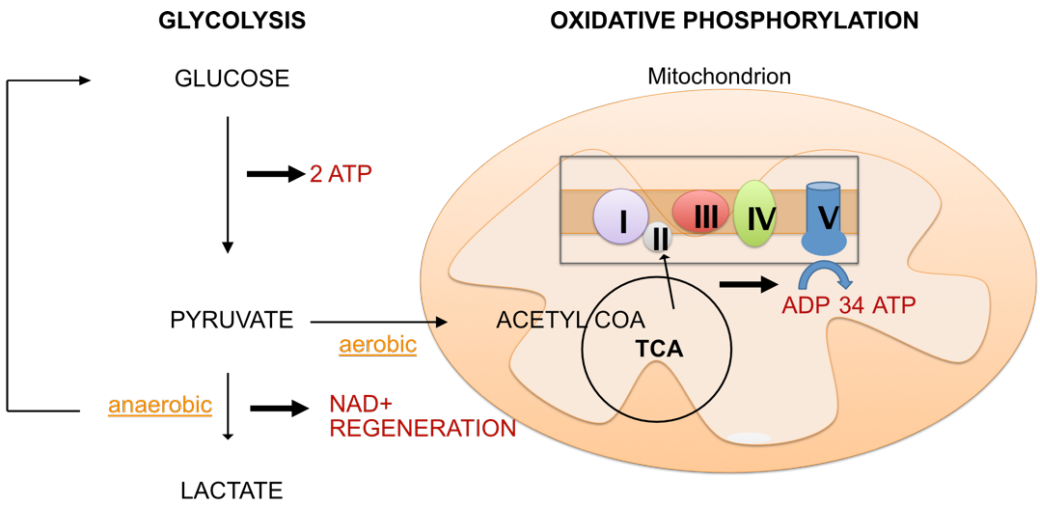

Figure 1.4: Aerobic and anaerobic metabolism. During aerobic conditions, cells generate some energy via aerobic glycolysis, but most of it utilising mitochondrial respiration. During glycolysis, glucose is broken down to pyruvate, generating ATP. Under aerobic conditions, pyruvate is further broken down to acetyl-coA, which feeds into the mitochondrial tricarboxylic acid cycle (TCA). The TCA generates reducing agents, which enable ATP production via oxidative phosphorylation in mitochondria. Under anaerobic conditions, pyruvate cannot be broken down into acetyl-coA, but is metabolised to lactate, thereby regenerating the reducing agent NAD+, which maintains glycolysis as long as glucose stores are available.

As depicted in Figure 1.4, during ischaemia, aerobic metabolic processes are shut down and switched to anaerobic metabolism. Under aerobic conditions, energy in form of the ATP/ADP ratio is produced either via glycolysis in the cytosol of a cell, or via oxidative phosphorylation in mitochondria. The nutrients that are broken down to provide energy substrates are delivered by the blood stream and include amino acids, carbohydrates and fatty acids. All of these can be broken down and enter the mitochondrial tricarboxylic acid cycle (TCA) to be utilised for ATP production (Chandel, 2015). While carbohydrates are broken down to glucose which is broken down further in the cytosol generating ATP before entering the TCA as pyruvate under aerobic conditions, amino acids and fatty acids can only fuel this mitochondrial energy production via the TCA cycle and β-oxidation. Different cell types can specialise on one or the other nutrient, for example red blood cells, which do not contain mitochondria, rely solely on glycolysis, while cardiomyocytes mainly utilise fatty acids (Grynberg and Demaison, 1996).

Because of the lack of oxygen and external nutrients during ischaemia, the only way to generate energy is by utilising stored energy in the form of glycogen, which can be degraded to glucose and used for anaerobic glycolysis. Anaerobic glycolysis takes place in the cytosol and leads to lactate formation to generate ATP and recycle NADH back to NAD (Stettner and Segre, 2013) (Figure 1.4). This can generate enough ATP to maintain vital processes in the cell until glycogen stores run low. Therefore, the amount of stored glycogen may, in part, determine how long cells can survive the lack of oxygen.

During ischaemia, energy-dependent processes within the cell have to be maintained to enable survival (Figure 1.5). Among these, the ATP-consuming Na^+/K^+ and Ca^{2+} ion pumps at the plasma membrane are necessary to assure cell volume stability and to avoid cell swelling. Inhibition of these pumps by a lowered ATP/ADP ratio upon prolonged ischaemia, will lead to water influx into the cells leading to swelling, rupture of the plasma membrane and finally bursting of the cells, which is a major cause of cell death during prolonged ischaemia (Karmazyn, 1999; Murphy and Steenbergen, 2008).

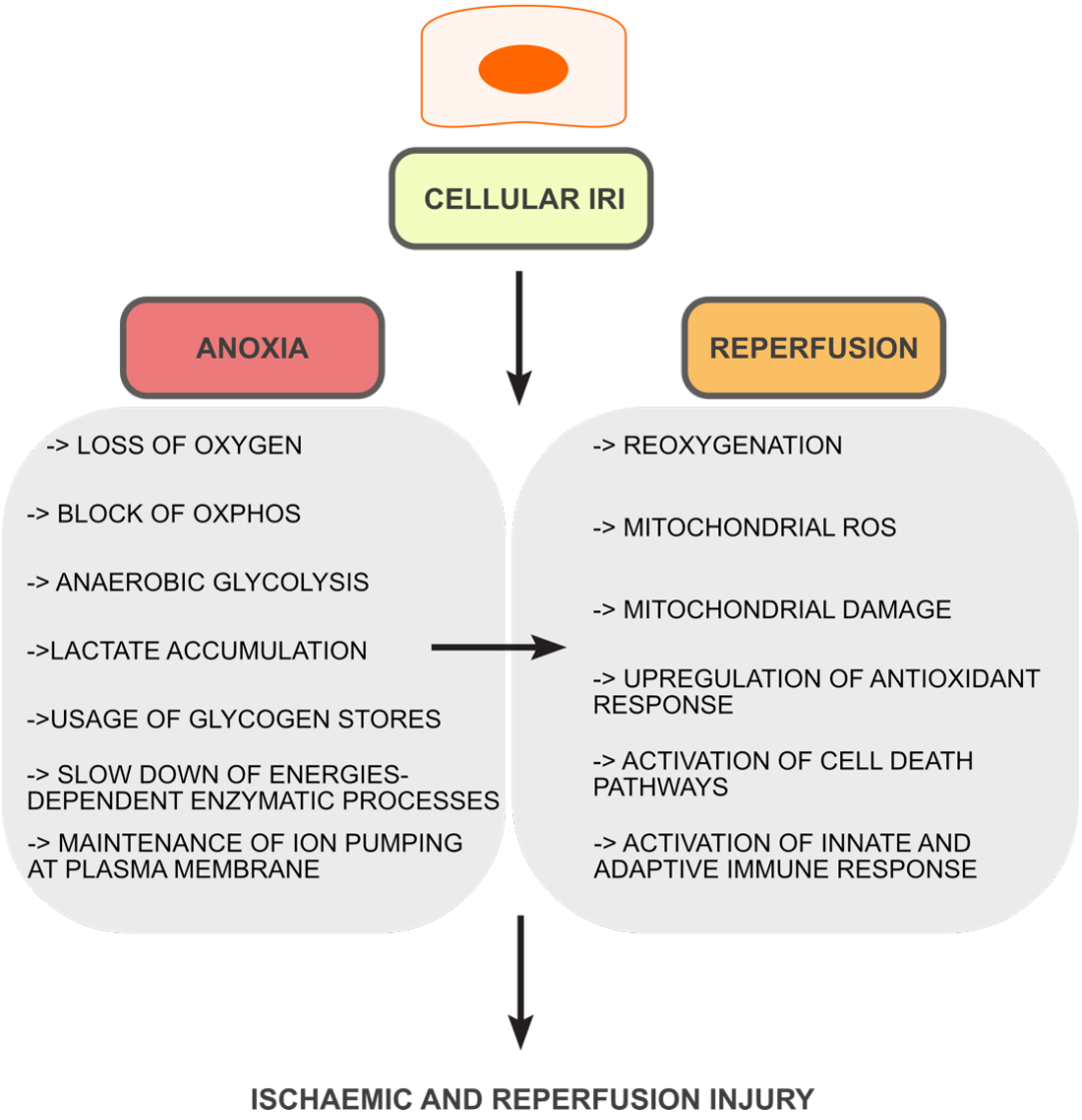

Figure 1.5: Schematic overview of hallmarks of cellular ischaemia and reperfusion leading to ischaemia reperfusion injury. Distinct cellular processes occur during ischaemia and upon reperfusion which are characteristic for the lack of oxygen or the reoxygenation leading to ischaemia reperfusion injury (IRI). During anoxia, loss of oxygen causes a block in mitochondrial respiration. The cell therefore has to generate ATP via anaerobic glycolysis causing accumulation of lactate and usage of its glycogen stores. Reduced energy availability leads to the slowdown of non-essential enzymatic processes and maintenance of crucial processes like ATP-dependent ion pumping at the plasma membrane. Upon reoxygenation, restored oxygen leads to a burst in mitochondrial reactive oxygen species (ROS) and therefore oxidative damage to the organelles. Mitochondria in turn upregulate their antioxidant response to rescue cell survival. Elevated oxidative damage will overwhelm the antioxidant response and activate cell death as well as immune response pathways. These are hallmarks of ischaemia reperfusion injury in cells.

Eventually ischaemia will lead to cell death if oxygenation is not restored, but ironically upon restoration of oxygenation at reperfusion further damage occurs (Figure 1.12). During reperfusion, as oxygen re-enters the cell, respiration starts again and mitochondrial ATP production resumes. However, the sudden re-oxygenation leads to an excessive generation of ROS causing oxidative damage to mitochondria that can lead on to damage to the whole cell. The generation of ROS by mitochondria during IR is discussed in detail in a later section, after a more general introduction of mitochondria. Importantly, the damage to mitochondria by IR injury leads to the activation of a number of processes that contribute to activation of the immune response and this is described in the following section.

1.2.1 Differences between the cellular response to hypoxia and anoxia

The processes described above occur in the complete absence of oxygen and a sudden re-appearance of this gas. It is difficult to investigate precisely when anoxia, reperfusion or hypoxia occur *in vivo*. In organ transplantation, the organs are retrieved, left over blood is flushed out and they are stored for several hours before they are transplanted and suddenly reperfused with oxygenated blood. Because of this, we can assume that in this scenario true anoxia and sudden reperfusion is occurring. In other physiological conditions, during a heart attack for example, where a blocked blood vessel will stop blood supply to some heart tissue, it is more difficult to determine how much true anoxia occurs in comparison to hypoxia. In this case, the blocked vessel will lead to an immediate stop in blood supply, however there may still be some residual perfusion through collateral vessels. This will result in a hypoxic period. Similarly, it is possible that the ischaemic cells are provided with some oxygen from surrounding cells and are therefore exposed to severe hypoxia rather than true anoxia during a heart attack. Upon removal of the blockage, the success of re-oxygenation depends on the survival of the vessel. The blood vessel, especially smaller branches of the vessel, might have been so severely damaged, or are still blocked by residual debris, that they cannot transport any blood to the tissue anymore. The vessels have to slowly recover, which can take days and may result in a not homogenous perfusion of the tissue, leaving some affected cells hypoxic rather than anoxic for an increased period of time.

The amount of true anoxia versus hypoxia in *in vivo* scenarios, other than transplantation, is most likely highly variable dependent on the specific case and injury. Therefore, it is important to understand each of these scenarios in detail to be able to draw conclusions which can then be transferred onto the patient`s situation.
On a cellular level, hypoxia is very different to anoxia. During hypoxia limited oxygen amounts are still available and therefore the electron transfer slows down, there is a highly reduced CoQ pool, decreased membrane potential and therefore less ATP production. The highly reduced CoQ pool might lead to a small amount of succinate accumulation. The respiratory chain will not stop fully and therefore some membrane potential will be impaired but still functional, maintaining essential mitochondrial processes like metabolism and protein import. Additionally, because some membrane potential is contained, the ATP synthase does not have to run backwards and decrease the adenosine nucleotide pool even further. AMPK will sense the decreased ATP/AMP ratios, as well as Hif1a will be stabilised due to the decreased availability of oxygen and therefore start transcriptional activation of antioxidants and other proteins (Li et al., 2015).

Due to this, reperfusion will have a less damaging effect in hypoxic compared to anoxic conditions. The decreased succinate accumulation will cause minor revers electron transport (RET) at complex I and therefore some ROS but not such a big burst in ROS as after true anoxia. These ROS molecules can sometimes be scavenged by antioxidants that have been produced due to the Hif1a hypoxic response. Massive oxidative damage can therefore often be prevented and mitochondrial function rescued.

As described before, it is difficult to distinguish which scenario is happening *in vivo* in patients, but it is most likely a combination of events. Organ transplantation offers a unique situation with clear starting and end points of anoxia and reperfusion and therefore enables detailed analysis of IR injury without influence of the cellular hypoxic response.

1.2.2 Cellular immune response after IRI

The immune response in patients after transplantation results in part from the fact that the donated organ contains foreign antigens. Donors and recipients are HLA class matched before transplantation and thus rejection due to an immediate inflammatory rejection response due to

the adaptive immune response is relatively rare (Corry et al., 1973). Nevertheless, there is still an increased immune response detectable after transplantation that is due to the cellular damage that occurs to the transplanted organ releasing cytosolic and organelle contents to trigger an innate immune response (Land et al., 1994). These potential immune responses to tissue damage during transplantation are considered below.

1.2.2.1 Adaptive immune response

The adaptive immune response is mediated by different forms of B and T cells and macrophages. These cells circulate through the body and recognise patterns in the circulation that are foreign to the body, such as those due to bacterial infection that could result in sepsis (Li et al., 2019; Zhang et al., 2010a). During an adaptive immune response, B cells recognise the molecular patterns on the surface of bacteria as foreign and release factors that will activate T cells which will move towards the origin of the foreign molecules and attack them. Macrophages are immune cells that engulf and degrade foreign cells and molecules (Ermin and Sewell, 2011). The adaptive immune response is a complex cascade of myriad cell types signalling to each other by the production of molecules such as interleukins. Interleukins (IL) are proteins that are produced after transcriptional activation of inflammatory pathways in T cells in response to different transcriptional activators that allows a specific immune response to infection or damage (Weinberg et al., 2015; Wood et al., 2012). It is this response that contributes to organ rejection in transplantation and which is counteracted by immunosuppressants. However, here I am most concerned with the activation of the innate immune response by tissue damage during transplantation and this is discussed below.

1.2.2.2 Innate immune response

While the adaptive immune response covers a complex reaction of different cell types in a cascade, started and kept alive through stimuli and interleukins, the sterile innate immune response (not activated by pathogens and pathogen associated molecular patterns, PAMPs) occurs within cells that are not necessarily immune cells, but which go on to regulate transcription of response genes to different stress situations. This is generally mediated by receptors within the cell that are activated by damage associated stimuli called damage associated molecular patterns (DAMPs). An overview over important innate immune response pathways is depicted in Figure 1.6.

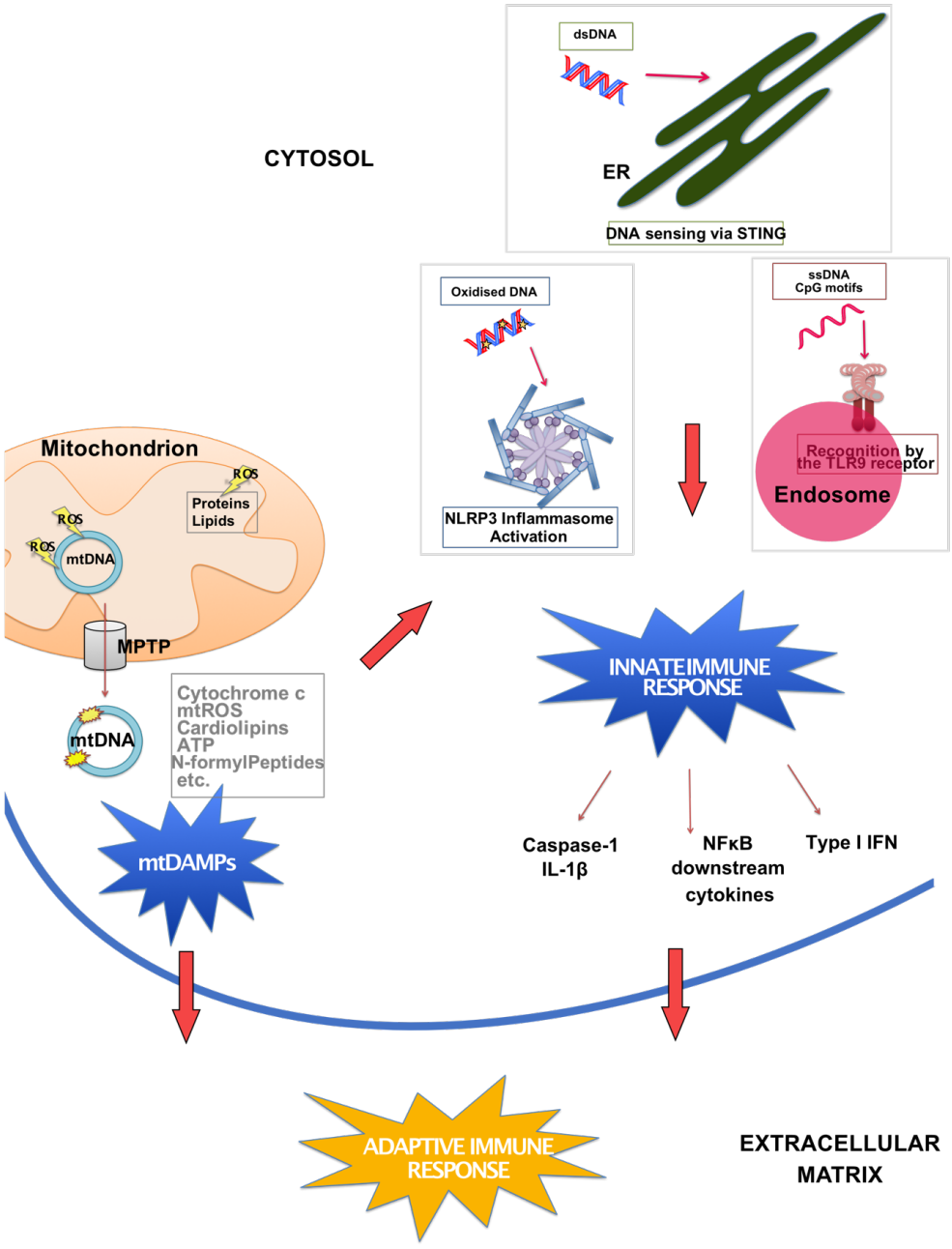

Figure 1.6:The role of damage associated molecular patterns in activating the adaptive immune response. Figure legend on the following page.

Figure 1.6: The role of damage associated molecular patterns in activating the adaptive immune response. Upon mitochondrial damage, reactive oxygen species (ROS) will oxidise and therefore damage mitochondrial content like mtDNA, proteins and lipids and cause the formation and opening of a permeability transition pore (MPTP) in the inner membrane, followed by outer membrane permeabilization and the release of mitochondrial content into the cytosol. These function as mitochondrial damage associated molecular patterns (mtDAMPs), which include N-formyl peptides and cardiolipin as well as mtDNA. mtDAMPs can be released from cells and activate the adaptive immune response directly, and they have been shown circulating in patients with pathologies causing mitochondrial dysfunction. But increasing evidence implicates a role for mtDAMPs, especially mtDNA, in activating the innate immune response as well. mtDNA for example is thought to be able to activate three distinct intracellular pathways: cytosolic dsDNA is recognised by the protein cGAS, which activates the ER-linked protein STING. ssDNA on the other hand activates toll-like receptor 9 (TLR9) on the ER or endosomes, and oxidised mtDNA has been shown to facilitate the assembly of the NLRP3 inflammasome. All of these activate various innate immune responses, which will stimulate activation of the adaptive immune system upon release from injured cells.

1.2.2.2.1 Damage associated molecular patterns

DAMPS are molecules like DNA, proteins or metabolites that are not usually available in the cytosol of a healthy, undamaged cell. Upon cellular stress, these molecules are released into or generated within the cytosol and then trigger an innate immune response. The naming of DAMPs is derived from the molecules that are most commonly responsible for the adaptive immune response, pathogen associated molecular patterns (PAMPs). These are molecules, like DNA and proteins, from bacteria or other pathogens that can infiltrate an organism. Cells from the adaptive immune response recognise patterns on the DNA, like decreased methylation profiles, or protein modifications, that are not common in the host organism, and start reacting against these patterns to avoid inflammation and sepsis. DAMPs function in a similar way as molecular patterns that are not abundant in the cytosol in healthy cells, they are recognised after release or production as a sign of damage (Seong and Matzinger, 2004). In this way, cells can sense and respond to damage by upregulating repair mechanisms and by initiating an inflammatory transcriptional response to signal to surrounding cells that damage has occurred. The release of DAMPs into the circulation will also activate cells from the adaptive immune response, so that after a primary innate immune response due to cell damage, the adaptive immune response is activated downstream of injury (Hanson et al., 2016; Tang et al., 2012). This occurs frequently in surgery in general due to tissue damage, as well as in organ transplantation. Some of these pathways are described in more detail below.

1.2.2.2.2 Inflammasomes

Inflammasomes are protein complexes that form upon activation with inflammatory stimuli. Four different forms of complexes have been described in the nucleotide- binding oligomerisation domain-like receptor (NLR) family: NLRP1, NLRP3, NLRP6 and NLRC4. All of these contain a nucleotide- binding oligomerisation domain to bind ribonucleotide-phosphates for self-oligomerisation and a leucine-rich domain for ligand recognition (Groß et al., 2016; He et al., 2016). Another inflammasome complex, which belongs to the PYHIN (pyrin and HIN domain-containing) family is called AIM2. All of these complexes contain the NLR core proteins and assemble with Apoptosis-associated speck like protein containing a caspase recruitment domain (ASC). Upon stimulation with an inflammatory stimulus, oxidative or cellular stress, ASC recruits caspase 1. NLR, ASC and caspase 1 form the complete inflammasome complex (Arnoult et al., 2011).

One of the most abundant and highly activated inflammasomes is the NLRP3 inflammasome, which is known to be activated by mitochondrial DAMPs such as ROS and also by mtDNA fragments. It has been proposed that the assembly of the NLRP3 complex occurs at the surface of mitochondria and is dependent on the abundance of mitochondrial membranes and specifically on the translocation of cardiolipin to the outer membrane. Double stranded cytosolic DNA has been shown to be recognised and bound by the AIM2 inflammasome, which also assembles with ASC and caspase 1. The different stimuli for the different inflammasomes and the cellular specificities or abundance of the various inflammasomes is largely unknown. After stimulation and assembly, the inflammasomes activate caspase 1, which cleaves the pro-interleukins 18 and 1b to their mature forms interleukin type 18 (IL-18) and 1β (IL-1β). These interleukins function as general activators of macrophages and therefore increase the immune response to the damaged tissue (Collins et al., 2004; Shimada et al., 2012).

1.2.2.2.3 Toll-like receptors

Another prevalent innate immune pathway, is through toll- like receptor (TLR) activation. Toll- like receptors are a family of immunoreceptors, usually expressed on endosomes. These receptors typically consist of dimers that are anchored in the membrane and reach their coiled-coiled domains towards potential substrates. TLRs trigger the translation of different

interleukin proteins upon activation. Different TLRs recognise different stimuli and promote the expression of specific interleukins and therefore enable a specific and fine-tuned immune response dependent on the underlying stimuli (Boros and Bromberg, 2006; Eltzschig and Eckle, 2011). The receptor TLR9, for example, specifically recognises unmethylated CpG motifs, which rarely occur on nuclear DNA, but which are often found on bacterial or mitochondrial DNA. Upon recognition of these CpG motifs, they activate MyD88 which in turn leads to activation of NfκB contributing to the transcription of the inflammatory cytokine interleukin type 6 (IL-6) (Akira and Hemmi, 2003; Alegre et al., 2008).

1.2.2.2.4 The cGAS/STING response

Recently, another cytosolic pathway activating the innate immune response has been described. The cytosolic protein cGAS recognises free double-stranded DNA within the cytosol. It binds the DNA and produces the intermediate signalling nucleotide cyclic guanosine monophosphate (cGAMP). cGAMP binds to the endoplasmic reticulum protein STING, which in turn activates NfκB, as well as interferon type 1 production (Li et al., 2015; Xia et al., 2016). Interferons are proteins that are released upon infection, often viral infections, from host cells and signal to, and activate immune cells. In this, interferons function in a similar way to interleukins, as signalling molecules for immune cells, which they activate and guide towards the origin of injury.

A number of different innate immune response pathways have been described in various cell types, but which non-immunological cells can activate the innate immune response and produce interleukins or interferons to stimulate the adaptive immune response is still being investigated. Furthermore, although these immunity pathways have been discovered in various pathological scenarios, it is not yet known which of these are most relevant for ischaemia reperfusion injury in the context of transplantation.

In general, a large number of changes occur throughout the cell during ischaemia and especially upon reperfusion. The impact of these processes is particularly significant on those organelles that use oxygen for oxidative phosphorylation, the mitochondria. Mitochondria are at the centre of the metabolic and energetic changes that occur during ischaemia and reperfusion. Therefore, my research focuses on investigating how ischaemia reperfusion injury

impacts mitochondria during organ transplantation. Thus, in the next sections, I discuss those aspects of mitochondrial that are important for IR injury in cells.

1.3 Mitochondria

1.3.1 General

Mammalian cells have between 1000 and 10 000 mitochondria, dependent on the cell type. Only a few cells, such as red blood cells, do not contain these organelles. Mitochondria are composed of an outer membrane (OMM), an inner membrane (IMM), the inner mitochondrial space (IMS) between the two membranes and the matrix in the centre of the organelle (Figure 1.7) (Frey and Mannella, 2000). The IMM forms tongue-like structures that reach into the centre of the mitochondria, called cristae. These are highly important to transfer electrons, pump protons and thus build up a proton motive force and generate ATP.

The origin of mitochondria as described in the endosymbiont theory suggests that ~1.5 billion years ago a proteobacterium was incorporated by an archaeon (Gray, 2012; Lane and Martin, 2010; Schwartz, 1982). They developed a co-dependent metabolism with the proteobacterial endosymbiont providing aerobic respiration, energy production, electron transfer and other crucial metabolic processes, the proteobacterium gained essential amino acids, proteins and metabolites from its host. Because of this endosymbiosis, mammalian mitochondria contain mitochondrial DNA (mtDNA) and inner membrane components such as cardiolipin, that differ from the rest of the cell and are more similar to molecules found in bacterial. Some of these crucial mitochondrial functions are discussed here.

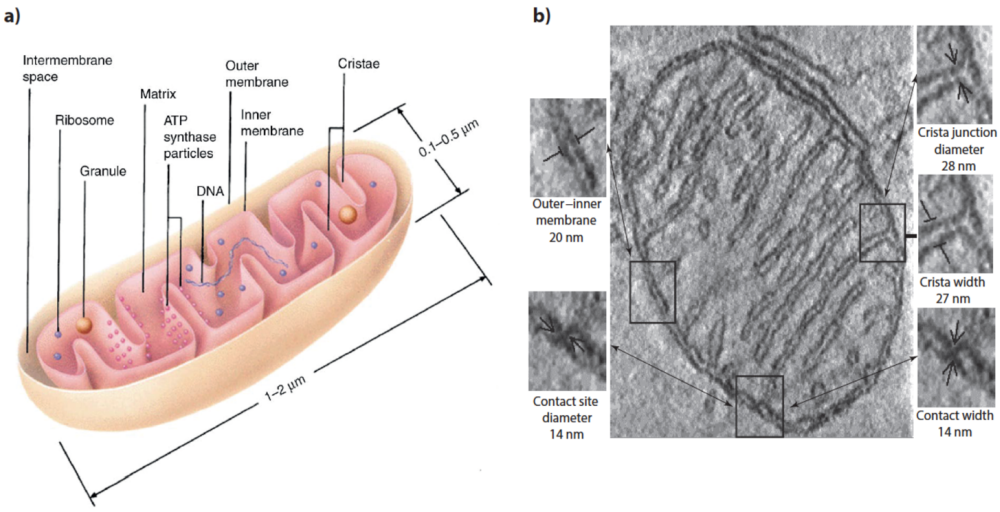

Figure 1.7:Mitochondrial structure. *a) Schematic representation of mitochondria, their membranes and matrix content. b) Electron micrograph of mitochondria, indicating sub organellar compartments and cristae structure. Figure adapted from Frey and Mannella, 2000.*

1.3.2 Mitochondrial DNA

Each mitochondrion contains 2 to 10 copies of circular DNA (Wiesner et al., 1992). In humans this genome contains 16 569 DNA base pairs, which encode for 13 proteins, 2 ribosomal subunits and 12 tRNAs (Figure 1.8). It has two origins of replication, one for the light strand and one for a heavy strand. There are nearly no non-coding regions on the mitochondrial genome, except for a 100 base pair region close to the origin of replication for the light strand, the D-loop, which is a regulatory region for mitochondrial DNA (mtDNA) expression. The 13 proteins encoded by mtDNA are all components of the respiratory chain or ATP synthase complexes that sit in the inner mitochondrial membrane. The translation machinery for these proteins is thus also retained within mitochondria to produce these proteins. Most mitochondrial proteins (~1,500) are nuclear encoded, translated in the cytosol and transported into mitochondria (D'Souza and Minczuk, 2018). Many, but not all contain an N-terminal mitochondrial targeting sequence (MTS) that is recognised by cytosolic transport proteins and locates them to mitochondria where they are imported via the OMM and brought to their destination within the organelle.

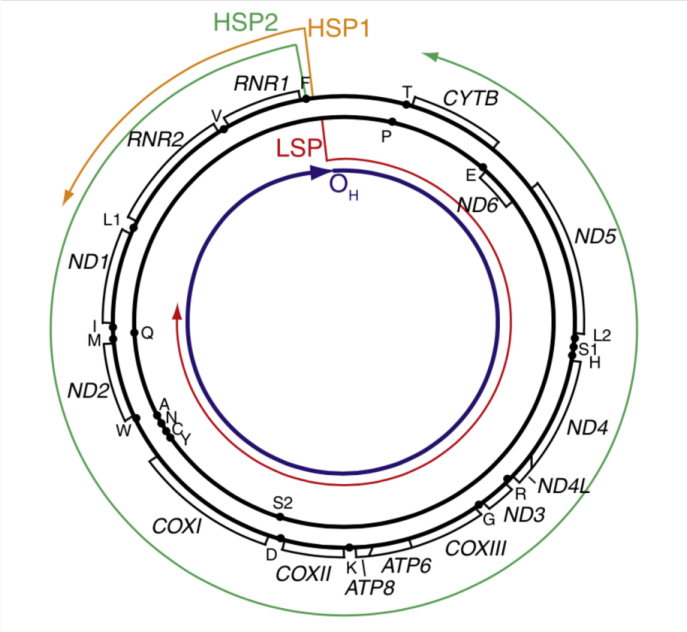

Figure* 1.*8*: *The structure and organisation of mitochondrial DNA. *Mitochondria contain their own DNA, which is located in the mitochondrial matrix in close proximity to the inner mitochondrial membrane, where it is exposed to reactive oxygen species generated by the respiratory chain. Mammalian mtDNA encodes for 13 polypeptides, 22tRNAs and 2rRNAs. The rest of the respiratory apparatus is encoded by nuclear DNA, with proteins being imported into the mitochondria. Adapted from Campbell et al., 2012.*

1.3.3 Oxidative Phosphorylation

A crucial role of mitochondria is oxidative phosphorylation (OXPHOS) (Figure 1.9). Four protein complexes in the IMM are responsible for electron transport from acetyl-CoA, a breakdown product of carbohydrates and fatty acids via the electron carriers NADH and $FADH_2$ to oxygen with three of them being used to pump protons across the mitochondrial inner membrane to generate a proton motive force (ΔP) (Sazanov, 2015). The ΔP is composed of a pH gradient (ΔpH), because the mitochondrial matrix is more basic than the IMS and cytosol, and a membrane potential (ΔΨ) across the IMM (more negative in the matrix) (Mitchell, 1961). This ΔP is then used to drive ATP synthesis by the ATPsynthase by transporting protons through the IMM.

1.3.3.1 Electron transport chain

Electrons are received from the electron donor NADH at complex I, leading to an oxidation of NADH to NAD+. The electrons move through complex I via an FMN cofactor and 7 iron-sulfur clusters until they are finally transferred to ubiquinone that is thus reduced to ubiquinol. Ubiquinol then transfers electrons onto complex III, the ubiquinol-cytochrome c reductase, while reducing cytochrome c. Finally, the electrons are transported from cytochrome c onto complex IV. There they are transferred onto the final electron acceptor oxygen resulting in the production of water. Complex I is not the only enzyme that can retrieve electrons from electron donors, complex II, also known as succinate dehydrogenase, can receive electrons from succinate, which is oxidised to fumarate passing electrons on to FAD which is reduced to $FADH_2$ and are then transferred onto ubiquinone producing ubiquinol, which is then oxidised at complex III.

At complexes I, III and IV, protons are pumped out of the matrix into the inter membrane space. This generates the ΔP, is necessary to make ATP, but also for many other mitochondrial processes such as protein import and metabolite transport (Mitchell, 1961; Sazanov, 2015).

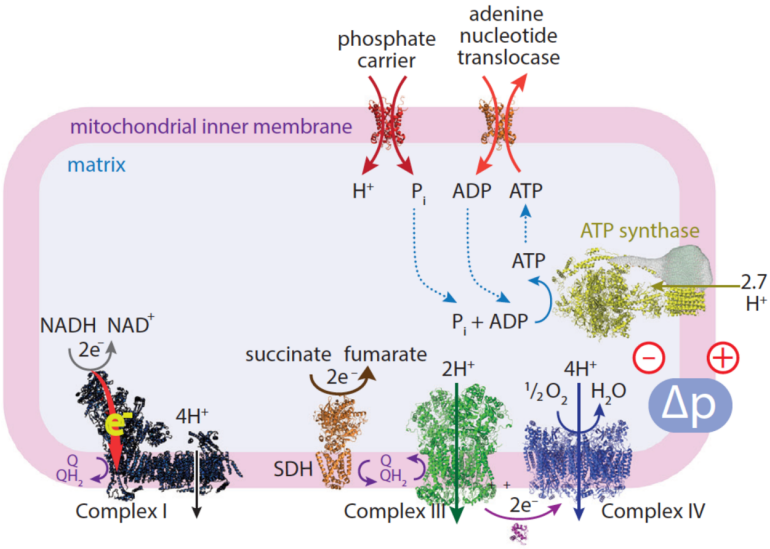

Figure 1.9:: An outline of mitochondrial oxidative phosphorylation showing the respiratory chain, ATP synthesis and the export of ATP from the mitochondrion. Electrons are fed into the respiratory chain from NADH into complex I or from the $FADH_2$ on complex II. The electrons are transferred to oxygen via complex III, Cytochrome c and complex IV. Electron transfer enables proton pumping at complexes I, III and IV, generating the Δp across the inner mitochondrial membrane. The Δp is utilised by the mitochondrial ATP synthase to synthesise ATP from ADP and organic phosphate (Pi). Pi is imported into mitochondria via the phosphate carrier, ATP is exported into the cytosol by the adenine nucleotide translocase in exchange for ADP. Figure adapted from Chouchani et al., 2016..

1.3.3.2 ATP production

The mitochondrial proton motive force is utilised predominantly by another complex in the IMM, the ATP synthase (Figure 1.9). This complex uses the ΔP to generate ATP from ADP and phosphate (Pi). It consists of a core stalk, situated in the IMM that is in close apposition to a stator arm. A c-ring is attached to this asymmetric stalk and rotates causing a conformational change that favours phosphorylation of ADP to form ATP. The ATP synthase exists in dimers in the cristae of the IMM which are responsible for the cristae membrane shaping. Protons that have been actively pumped out of the mitochondrial matrix by complexes I, II and IV re-enter the matrix through the ATP synthase driven by the ΔP to make ATP. The enzyme complex utilises the H+ molecules passing through its membrane arm to move the rotor ring of the ATP synthase at the matrix side. This conformational change is used to combine phosphate groups onto ADP producing ATP. ATP is then exported to the cytosol for energy requiring processes. The Pi for phosphorylation is imported into the matrix via the phosphate carrier and ATP is exported from the matrix in exchange for ADP by the adenine nucleotide translocase (ANT) (Watt et al., 2010).

1.3.3.3 The tricarboxylate acid cycle and fatty acid oxidation

Mitochondria generate ATP via oxidative phosphorylation using electrons derived from the electron donors NADH and $FADH_2$ within the mitochondria matrix. These electron carriers are generated in large part by the citric acid cycle, also called the tricarboxylate or Krebs cycle. Glucose and fatty acids are broken down under aerobic conditions to acetyl-CoA in the mitochondrial matrix. This metabolite then enters the TCA, an 8-enzyme series of reactions that results in amino acid precursors, co-factors (CoA-SH), electron carriers (NADH, $FADH_2$ and QH_2) and energy equivalents (GTP or ATP) as well as CO_2 and H_2O by-products (Akram, 2014). The full cycle is depicted in Figure 1.10A. Fatty acids are rich in energy; hence their oxidation produces more than double the amount of energy compared with carbohydrates (Houten and Wanders, 2010; Röhrig and Schulze, 2016). They are broken down to acetyl-coA by β-oxidation which also generates NADH and FADH2 which are passed on the electron transport chain (Figure 1.10B).

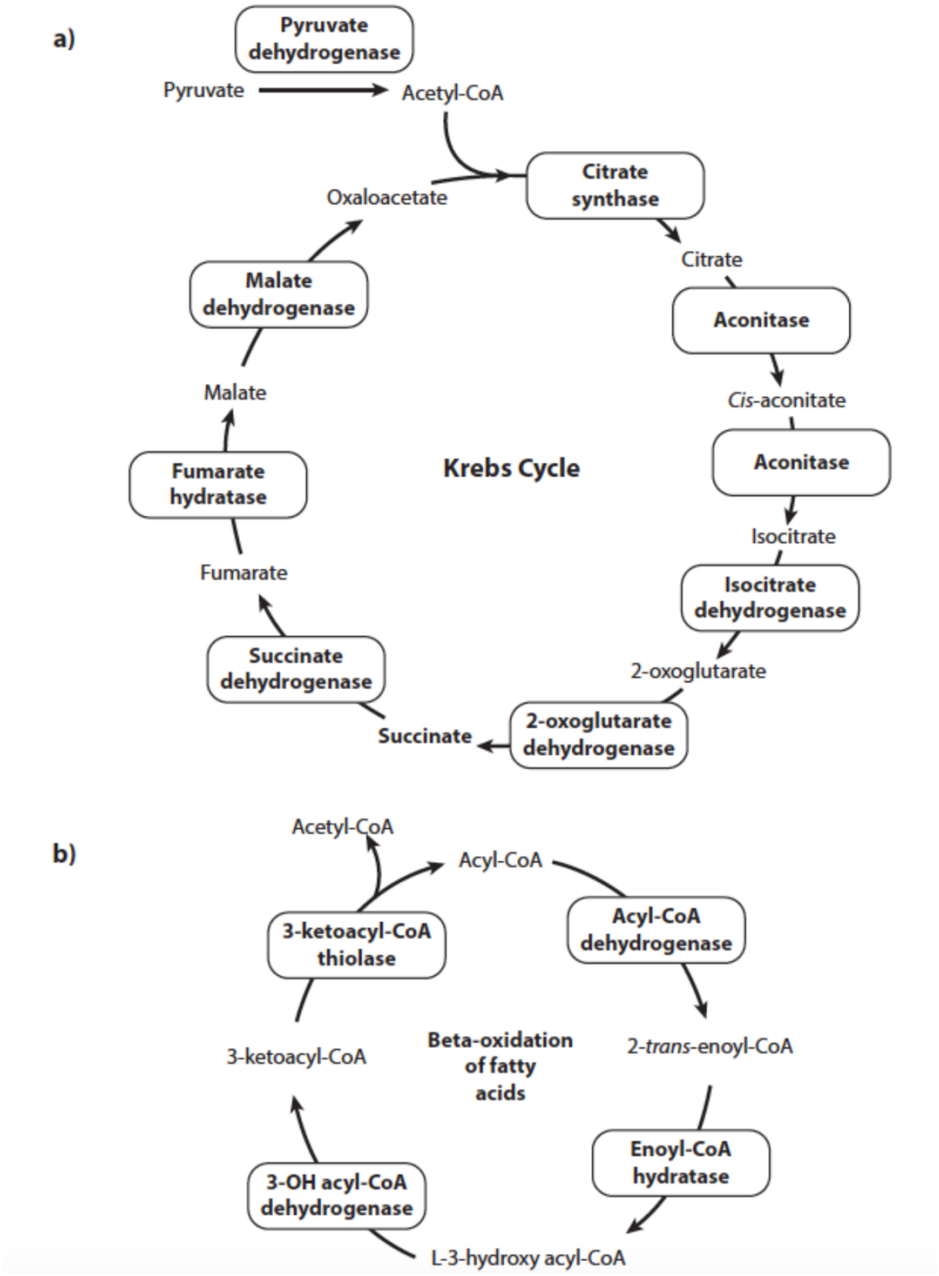

Figure 1.10: The tricarboxylic acid cycle and b-oxidation of fatty acids. a) Schematic of the tricarboxylic acid (TCA) cycle. The TCA cycle takes acetyl-CoA from sources such as glycolysis and ß-oxidation through a series of redox reactions with electrons transferred to cofactors NAD+ and FAD. b) ß-oxidation of fatty acids: Fatty acids are coupled to CoA and transported into mitochondria. They are subsequently oxidised, with the release of acetyl-CoA and an acyl-CoA. Adapted from Dr. Hiran Prag.

1.3.4 Mitochondrial calcium metabolism and the permeability transition pore

Calcium concentrations in the cytosol are carefully controlled and changes are used in a range of signalling processes. For signalling purposes, calcium levels can rise in the cytosol, however if calcium levels rise too high this can lead to extensive cell damage. Therefore, it is essential that excessive calcium is removed from the cytosol (Nicholls and Crompton, 1980). The organelle that is mainly responsible in regulating cytosolic calcium is the endoplasmic reticulum (ER) that sequesters calcium and can then release calcium in close proximity to mitochondria. The ER and mitochondria are in close contact at mitochondrial associated membranes (MAMs) (Pinton et al., 2008). At these locations, the ER releases calcium and mitochondria take it up via a transporter protein in their inner membrane the calcium uniporter. Through this, the levels of calcium within the mitochondria respond to those in the cytosol and can activate mitochondrial dehydrogenases. In addition, this uptake process also allows the mitochondria to contribute to buffering excessive calcium in the cell, by sequestering excess calcium that is then slowly re-released into the cytosol. The uptake of calcium by mitochondria is driven by $\Delta\Psi$ and fascilitated trhough the mitochondrial calcium uniporter (Pan et al., 2013).

However, uptake of too much calcium by mitochondria can lead to cell damage by induction of a non-specific pore in the IMM, called the mitochondrial permeability transition pore (MPTP) (Bernardi and von Stockum, 2012; Lemasters et al., 2009). Mitochondrial oxidative stress and extrusion of protons, rectifying intracellular pH, cause increased calcium influx and therefore opening of the MPTP followed by mitochondrial swelling until the mitochondrial membranes rupture and released mitochondrial content contributes to cell death (Andrienko et al., 2017; Bernardi et al., 2015).

The MPTP is a non-selective channel within the IMM, enabling molecules of <1500 kDa to pass freely through the normally impermeable membrane. Although the structure of the MPTP is not definitively known, the *cis-trans* prolyl isomerase, cyclophilin D is clearly a critical component of the pore. CypD is important to IR injury, which has been shown because $CypD^{-/-}$ mice are resistant to IRI (Baines et al., 2005; Nakagawa et al., 2005). The MPTP was recently proposed to involve the F_OF_1-ATP synthase, with F_OF_1-ATP synthase dimers forming to create a calcium-dependent channel. The elevated Ca^{2+} is thought to displace the functionally important Mg^{2+} bound at the catalytic site, triggering MPTP formation (Alavian et al., 2014; Bernardi, 2018; Bernardi and Di Lisa, 2015; Bernardi and von Stockum, 2012).

The oligomycin sensitivity conferring protein (OSCP) subunit of the F_OF_1-ATP synthase has also shown implications in MPTP formation and has been thought to interact with CypD; though, some evidence suggests OSCP may act independently of CypD in MPTP activation (Baines et al., 2005; Beck et al., 2016; Bernardi and Di Lisa, 2015).

Opening of the MPTP leads to membrane potential collapse, cessation of respiration and mitochondrial swelling, leading to OMM permeabilisation and release of Cyt *c* (Eefting, 2004). This in turn will activate apoptotic and necrotic cell death signalling cascades as well as further ROS production. This ROS causes additional damage directly through lipid peroxidation, DNA oxidation and matrix metalloproteinase activation (Andrienko et al., 2017; Nelson and Melendez, 2004).

This above described oxidative damage leads to the activation of cytosolic stress response pathways as a result of the released mitochondrial contents into the cell via the pore, activating additional cell death and innate immune pathways. Finally, there is compelling evidence that this induction of the MPTP and the resulting signalling cascades are major contributors to cell death and damage following IR injury primarily due to the elevated mitochondrial ROS and calcium (Briston et al., 2017; Rottenberg and Hoek, 2017).

1.3.5 Mitochondrial reactive oxygen species

Besides facilitating essential metabolic processes and the production of energy, mitochondria are also a major source of reactive oxygen species within the cell (Arnoult et al., 2011; Murphy, 2009; Tormos et al., 2011). Reactive oxygen species (ROS) are oxygen containing molecules that can react and damage non-specifically a range of biomolecules. ROS such as superoxide can be generated by the reaction of single electrons coming from the respiratory chain and reacting with oxygen. There are mitochondrial and cytosolic enzymes such as superoxide dismutase which converts superoxide (O_2-) to hydrogen peroxide (H_2O_2) (Murphy, 2009). Mitochondria generate ROS mainly under conditions, when either there is a high NADH/NAD+ ratio in the matrix or when ATP synthesis at the ATP synthase is low, resulting in a high ΔP and reduced CoQ pool.

Complex I is one of the main sources of mitochondrial superoxide, producing it during forward electron transfer under certain conditions, but particularly by reverse electron transfer (RET) (Chouchani et al., 2014a, 2016; Murphy, 2009; Pryde and Hirst, 2011). ROS is produced during forward electron transfer when O_2 reacts with fully reduced FMN on Complex I. The proportion of FMN that is fully reduced is determined by the NADH/NAD+ ratio. A high

NADH/NAD+ ratio occurs when the respiratory chain is blocked by damage or ischaemia. ROS production by RET occurs under conditions of a highly reduced CoQ pool combined with a high ΔP which drives electrons back into Complex I, reducing NAD+ to NADH at the FMN site, as described in more detail later, this can occur upon reperfusion after ischaemia (Chouchani et al., 2014a).

ROS can also be generated at complex III (Murphy, 2009; Quinlan et al., 2013) when the lifetime of the semiquinone radical at the Qo site is increased, leading to it donating an electron to O_2 to form superoxide. Under normal physiological conditions, this ROS production at complex III seems to make up just a small amount of the mitochondrial ROS production. However, the presence of the complex III inhibitor antimycin greatly enhances this ROS production by stabilising a semiquinone radical at the Qo site (Nicholls and Ferguson, 2013; Quinlan et al., 2013).

The excessive production of ROS by mitochondria would always lead to oxidative damage if it were not for the range of mitochondrial antioxidant defence mechanisms (Figure 1.11). These include the enzymatic metabolism of superoxide via superoxide dismutases (Murphy, 2009). This process can convert superoxide to H_2O_2 to stop it causing damage to iron sulphur centres. However, H_2O_2 itself can also cause oxidative damage, for example in the presence of ferrous iron it can generate the damaging hydroxyl radical and it can also directly oxidise thiols on proteins. There are a group of thiol systems in the mitochondrial matrix (Figure 1.11) that are responsible for preventing oxidative damage by removing ROS such as hydrogen peroxide (Murphy, 2009). Peroxiredoxins (Prx) are thiol peroxidases that act to maintain the redox balance of the cell by scavenging H_2O_2 (Murphy, 2016). Mammals possess 6 Prx isoforms, two of them are located in mitochondria. A redox-sensitive cysteine in the Prx active site can be oxidised by H_2O_2, generating a disulphide leading the Prx to form homodimers, which temporarily inactivates the protein. This can be reversed by thioredoxin (Trx), which reduces the disulphide bond to a dithiol (Collins et al., 2012). The thioredoxin is then reduced by thioredoxin reductase. Glutathione (GSH) is a small peptide that has protective roles in antioxidant defence, especially via maintenance of thiol status (Marí et al., 2009; Murphy, 2016). In the mitochondrial matrix, GSH is oxidised to glutathione disulphide (GSSG) through the action of glutathione peroxidase (Gpx1) which reduces H_2O_2 to H_2O. GSSG is reduced back to GSH by glutathione reductase (GR), using NADPH as an electron donor. GR maintains the mitochondrial matrix GSH pool highly reduced (95-99%) with some oxidised GSSG (Nicholls and Ferguson, 2013).

Although ROS is generated under physiological conditions in cells, the levels are usually low. Increased ROS can occur under certain conditions like IR injury, cell death or aging. These elevated ROS levels affect cell fate because they cause damage to the cells and tissue, but they also function as signalling molecules communicating mitochondrial dysfunction and damage to neighbouring cells.

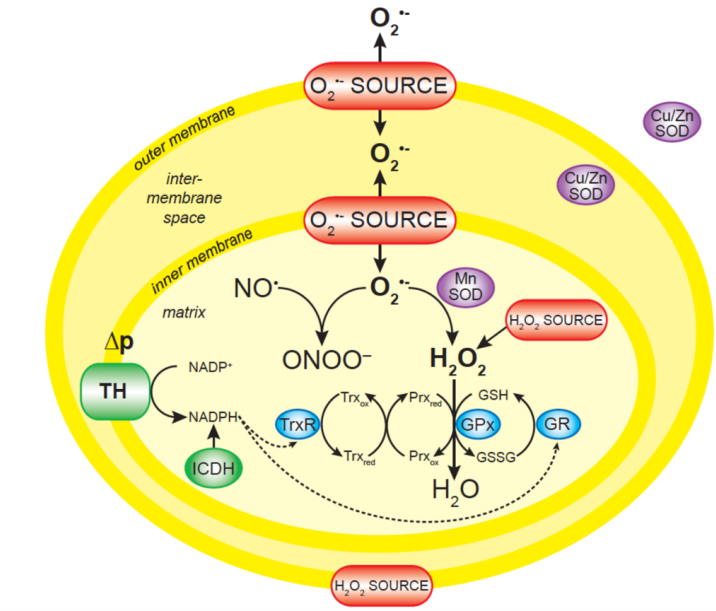

Figure 1.11: Overview over mtROS and the antioxidant response. Superoxide (O_2-) is produced in the matrix and metabolised to hydrogen peroxide (H_2O_2) by manganese superoxide dismutase (MnSOD). H_2O_2 is metabolised to H_2O by the peroxidases peroxiredoxin (Prx) and glutathione peroxidase (Gpx). Oxidised Prx can be regenerated by thioredoxin (Trx). Reduced Trx levels are controlled by thioredoxin reductase (TrxR), which in turn is regulated by the NADPH/NADP+ pool. Gpx uses glutathione (GSH) to reduce oxidised peroxidases, such as Prx. The oxidised Gpx is recycled by glutathione reductase (GR). Furthermore, membrane permeable H_2O_2 can leave the mitochondria directly. TH: transhydrogenase. Figure adapted from Murphy, 2009.

1.3.5.1 Mitochondrial oxidative damage

Elevated production of ROS in mitochondria can overwhelm the antioxidant defences and cause severe cellular damage contributing to many pathologies (Di Meo et al., 2016) (Figure 1.12). ROS produced within mitochondria, can damage mitochondria themselves. The mitochondrial membrane is very accessible to ROS and the unsaturated fatty acids in the membranes are susceptible to lipid peroxidation, leading to increased generation of F2-isoprostanes. Damage to membrane lipids also increases membrane permeability which may

uncouple OXPHOS and decrease ATP production (Murphy, 2016). Furthermore, oxidative damage can cause mutations and deletions, which can be removed by mitochondrial DNA repair mechanisms when occurring in limited amounts. However, when the accumulation of damaged mtDNA exceeds a threshold this will cause disruption to the electron transport chain (ETC). Finally, ROS damage can also lead to the oxidation of proteins, altering protein structure and leave them incapable of performing their enzymatic reactions.

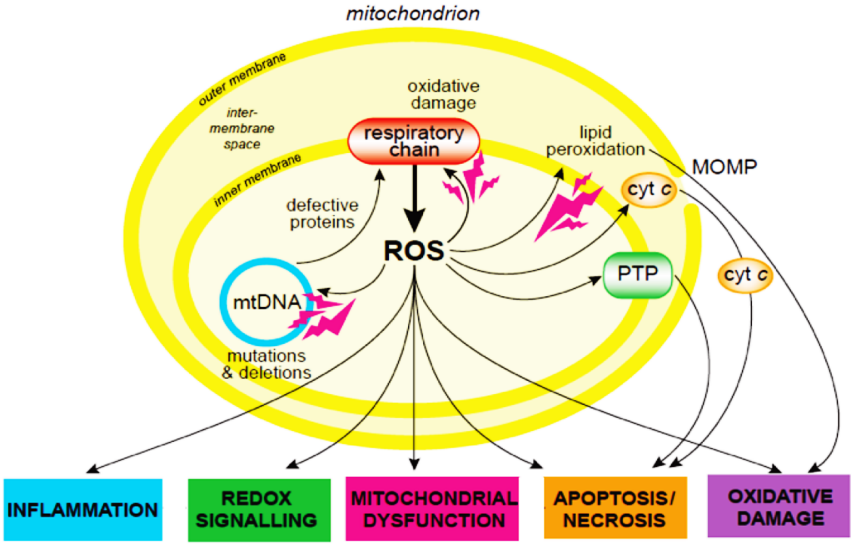

Figure 1.12: mtROS damage and signalling. Reperfusion after ischaemia causes a burst of mitochondrial ROS at complex I of the respiratory chain, including superoxide and hydrogen peroxide. This burst of mtROS starts a range of pathological processes within the cell. It causes mitochondrial dysfunction directly by damaging the mitochondrial respiratory chain causing oxidative damage to lipids (lipid peroxidation), proteins and mtDNA (causing mutations and deletions). Furthermore, mtROS can act as a cellular signalling mechanism, contributing to the formation and opening of the permeability transition pore (PTP) and the induction of apoptotic or necrotic cell death pathways, e.g. through the release of cytochrome c (cyt c) and opening of a mitochondrial outer membrane pore (MOMP). ROS plays a central role in redox signalling contributing both directly and indirectly to inflammation by activating innate inflammatory pathways as a response to cellular injury. Figure adapted from Murphy, 2009.

ROS can also have a beneficial role by acting as redox signals within the cell, enabling communication between the mitochondria and the cytosol and nucleus. A direct way of ROS signalling is via H_2O_2, which can rapidly diffuse through membranes (Murphy, 2009) and therefore efficiently signal about changes in mitochondrial status to activate responses of the cell by altering enzyme activity via reversible oxidation of cysteine thiols or by acting on redox

sensitive proteins (Finkel, 2012; Holmström and Finkel, 2014). For example, the cytosolic transcription factor HIF-1a is stabilised by mitochondrial ROS and leads to transcriptional adaptation (Mills et al., 2016).

Thus, ROS can be a damaging agent within cells on the one hand, but also function as direct or indirect signalling molecules on the other hand, enabling cells to adapt to the stress. Understanding the role of mitochondrial ROS in pathology may help elucidate how diseases occur and in the development of therapies.

1.3.6 Involvement of mitochondria in the activation of cell death

Mitochondria are central to different forms of cell death. One of the most important and crucial ones being programmed cell death via apoptosis (Wang and Youle, 2009). Upon cellular damage and following apoptotic signalling, the anti-apoptotic Bcl-2 family of proteins become inactivated, promoting alteration of the pro-apoptotic proteins, Bax and Bak on the outer mitochondrial membrane, where they oligomerise and permeabilise the OMM (Nagata, 2018). Due to this, inner mitochondrial proteins such as cytochrome c, are released into the cytosol activating the apoptotic cascade. Cytochrome C interacts with APAF1, a protein of the apoptosome complex, which enables assembly of the apoptosome with caspase 9 and cytochrome c. The Apoptosome is a complex which cleaves the inactive form of caspase 3 producing its active form which starts a cascade of caspase activation. These caspases start degrading cytosolic content leading to cell death (Taimor, 2000; Wlodkowic et al., 2011).
Necrosis on the other hand is a process of cellular death after acute and severe damage and trauma, unlike the programmed and regulated cell death during apoptosis (Fink and Cookson, 2005).Acute loss of cellular homeostasis leads to disruptions in ion handling, with mitochondrial calcium particularly affected (Kwong and Molkentin, 2015). Mitochondrial calcium overload is associated with mitochondrial swelling and leads to the opening of the mitochondrial permeability transition pore (MPTP), as described in section 1.3.4. This rapidly dissipates the Δp, required for ATP synthesis, with organelle rupture and following cellular death.

In general, cell death leads to the rupture or degradation of the plasma mebrane and therefore the release of intracellular content, like the abundant protein lactate dehydrogenase as well as inflammation activation signals like cytokines (Fink and Cookson, 2005). Mitochondria are at

the centre of sensing cell damage and can activate programmed or none-programmed cell death pathways, dependent on severity of the damage.

1.3.7 The role of mitochondria in inflammation

Mitochondrial damage can lead to the release of damaging molecules into the cytosol, where these activate response pathways that will determine cell fate. Some of these have been shown to activate the innate immune response pathways within cells and lead to the production of inflammatory signalling molecules like cytokines. Within the cell, mitochondria are key players in starting the cytosolic response pathways, including inflammasomes and TLRs as described before (Figure 1.7). A well-studied example, is the NLRP3 inflammasome, a cytosolic protein complex that assembles upon stimulation with factors like cytochrome c, ROS, oxidised mtDNA, which are all released from damaged mitochondria. The molecules that are released from mitochondria and start inflammatory reactions are called mitochondrial damage associated molecular patterns (mtDAMPs). If these molecules are released into the circulation upon cell death or through cellular release, they can even activate inflammatory cells and cause an immune reaction in the whole body (Mills et al., 2017; West et al., 2011, 2015; Zhang et al., 2010a).

1.3.7.1 mtDAMPs

Mitochondrial DAMPs are particular interesting in activating the innate immune responses. Mitochondria were originally independent organisms which explains why some of the translational modifications on proteins and also modifications on DNA, like methylation, vary inside mitochondria from the cytoplasm. As a result, they are easily distinguishable from the normal cytoplasmic content when they leave mitochondria and enter the cytosol, or blood (Wenceslau et al., 2014). There, they are recognised as DAMPs and signal cell damage to the surrounding cells and the adaptive immune system. Protein modifications that are known to function as DAMP are for example N-formyl peptides. Additionally, ATP and ROS can take over these roles as well (Zhang et al., 2010a). But the probably best understood and most relevant DAMP is mtDNA as is described below.

1.3.7.1.1 mtDNA as DAMP

mtDNA has a distinct structure and similar to bacterial DNA, the total amount of methylated DNA bases is small in comparison to nuclear DNA. The release of mtDNA has been shown to be released from mitochondria into the cytosol where it activates the innate immune response via cGAS. Other immune pathways could also be activated by released mtDNA, in particular the NLRP3 inflammasome, the TLR9 receptor or sensing via the cGAS/STING pathway, all of which have been described earlier. While the NLRP3 inflammasome formation is facilitated by oxidised mtDNA, TLR9 is activated after binding of distinct unmethylated, single-stranded CpG motifs. cGAS senses double-stranded DNA molecules within the cytosol. The diversity of DNA that can activate distinct innate immune pathways is intriguing and further research is necessary to fully understand if different cellular stressors can activate specific immune responses (Kausar et al., 2020; Shimada et al., 2012; Wenceslau et al., 2014; West et al., 2015).

To summarise, several pathways have been described that activate the innate immune response and many of them involve free mitochondrial DNA. The variety of immunological pathways involving mtDNA is striking and evokes even more interest in understanding the role of mtDNA as signalling molecule after mitochondrial injury or dysfunction. Nevertheless, we are just starting to understand how mitochondria are involved in cellular and whole-body immune responses. In this thesis, I will try to investigate some of these pathways further and will evaluate the role of mitochondrial DNA later on.

1.4 Ischaemia reperfusion injury in mitochondria

Next, I am going to focus on how mitochondria contribute to IR injury in more detail than previously.

1.4.1 Mitochondrial metabolism during ischaemia

During ischaemia, the NADH/NAD+ ratio increases and the ubiquinone pool is fully reduced, both of which will lead to the reduction of fumarate to succinate at complex II. Therefore, an accumulation of succinate is detectable during ischaemia and it increases with time of

ischaemia (Chouchani et al., 2014a). The accumulation of succinate during ischaemia is a mechanism that is conserved among different species and in different models for ischaemia (Bundgaard et al., 2019; Kohlhauer et al., 2019; Martin et al., 2019). This reversal of complex II is limited by the availability of fumarate. So far it is not clear where all the fumarate is coming from, that is used to make succinate. Precursors may be transported into mitochondria via the malonate/aspartate shuttle or be a by-product of the TCA within mitochondria.

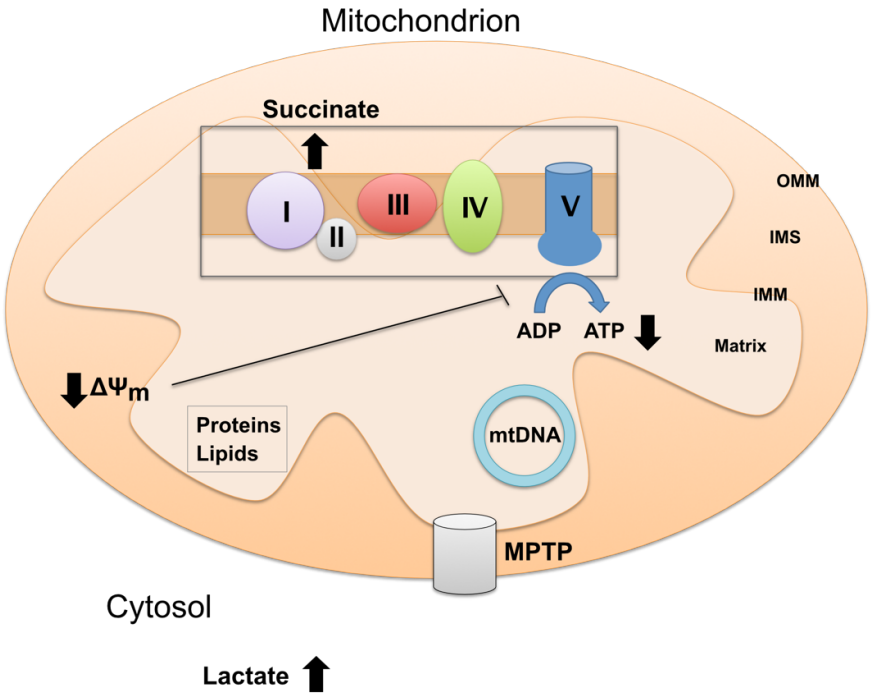

Figure 1.13: Overview of mitochondrial processes during ischaemia. The lack of oxygen affects mitochondrial processes because it blocks the respiratory chain and leads to a loss of mitochondrial membrane potential. Accumulation of NADH during ischaemia causes a reduced CoQ pool at complex I. This drives reversal of SDH and therefore accumulation of succinate. The blockage of oxidative phosphorylation inhibits ATP production causing loss of adenosine nucleotides. Anaerobic glycolysis in the cytosol is utilised to generate ATP and the NAD+ pool leading to acidification because of lactate accumulation. IMM= inner mitochondrial membrane, OMM= outer mitochondrial membrane, IMS= inter membrane space, MPTP= mitochondrial permeability transition pore.

Additionally to succinate accumulation during ischaemia, the reduction in the availability of ATP. If oxygen is missing, the production of ATP will slow down. Usually, ATP is used in such a way that ATP -> ADP + Pi leading to production of ADP from ATP. The enzyme

adenylate kinase can use ADP to produce ATP in the following reaction: 2 ADP <-> ATP + AMP. If the equilibrium of the reaction shifts because ATP is used up the enzyme will use up ADP to generate ATP. This will lead to a reduction of the ATP and ADP pools and an increase in AMP, which then is further degraded to hypoxanthine and xanthine (Chouchani et al., 2014a; Takeda et al., 2004). This means that after prolonged ischaemia the adenine, and other, nucleotide pools are severely depleted which can make it difficult for metabolism to restart when ischaemia is over.

During ischaemia the mitochondrial ATP synthase can start running backward hydrolysing ATP and pumping protons out of the mitochondrial matrix while it is splitting ATP into ADP and Pi. This will stabilise the proton motive force for a while. There are other features characteristically for ischaemia. For example, anaerobic conditions will force cells to perform anaerobic glycolysis producing lactate, as described in detail before. This leads to an accumulation of lactate and with that a reduction in the cytosolic pH. In summary, accumulation of succinate, lactate, loss of adenine nucleotides and changes in the cellular pH are hallmarks of ischaemia that can give some information about the severity of ischaemia (Figure 1.13).

1.4.2 Mitochondrial metabolism upon reperfusion

The reintroduction of oxygen upon reperfusion enables the accumulated succinate to be oxidised by complex II and for complexes III and IV to generate a proton motive force across the IMM again. This oxidation of succinate will also reduce the ubiquinone pool. This together with the high protonmotive force will drive reverse electron transport (RET) and facilitates a burst of ROS production at complex I that underlies the ROS production upon IR injury (Chouchani et al., 2016).

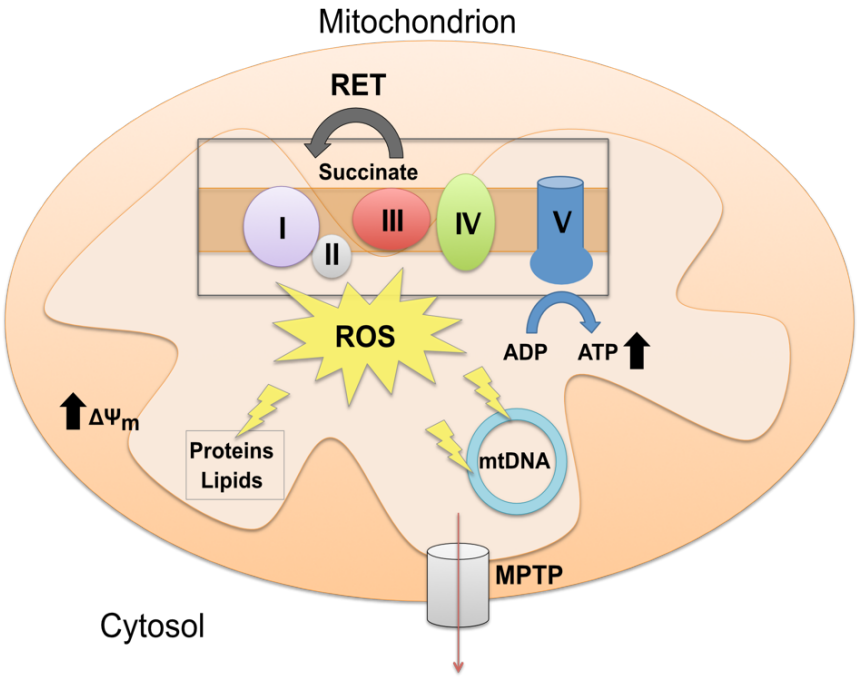

Figure 1.14: Overview of mitochondrial processes during reperfusion. Upon reperfusion, a highly reduced CoQ pool and reduced membrane potential enforced by the accumulated succinate drive reverse electron transport (RET) at complex I. Reverse electron transport allows electrons to flow backwards through complex I onto the flavin mononucleotide. Here, they reduce O_2 to superoxide causing a burst in reactive oxygen species (ROS). Stabilisation of the electron transport chain permits reactivation of the ATP Synthase and ATP production, if adenosine nucleotides are abundant. The burst of ROS damages mitochondrial molecules, above all membrane lipids, proteins and mtDNA. Reduced ATP availability, destabilised membrane potential causing calcium influx and increased oxidative damage will lead to the opening of the mitochondrial permeability transition pore (MPTP) and allow the release of mitochondrial content into the cytosol.

The massive burst in superoxide exceeds the capacity of antioxidant mechanisms in mitochondria and plays a major pathological role during the return of blood flow after a period of ischaemia, such as during a heart attack, stroke or surgery (de Vries et al., 2013). To summarise, mitochondrial processes during ischaemia lead to the accumulation of succinate, will cause ROS production by RET at complex I upon reperfusion. This leads to ischaemia reperfusion injury causing cellular damage and finally cell death (Figure 1.14).

1.4.3 Mitochondrial response to ischaemia reperfusion injury

The mitochondrial ROS generation upon reperfusion results in opening of the PTP starting a cytosolic response cascade leading to the production of signalling molecules of the immune response and activation of cell death pathways (Green, 2004; Vringer and Tait, 2019).

1.4.3.1 Opening of the mitochondrial permeability transition pore upon IR injury

Oxidative damage will lead to the opening the MPTP (Andrienko et al., 2017; Halestrap, 2004; Rottenberg and Hoek, 2017). This marks the final response of mitochondria to severe stress and leads to the release of mitochondrial matrix proteins, metabolites and DNA into the cytosol, where they are involved in different cytosolic cell death and immune responses.

1.4.3.2 Immune response upon IR injury

Although MPTP opening upon reperfusion has been investigated *in vitro* and *in vivo* in different experimental models (Halestrap, 2004; Luongo et al., 2015; Rottenberg and Hoek, 2017), less is known about the release of potential mitochondrial DAMPs into the cytosol and circulation during IR injury. A few studies showed an increase in IL6 in the circulation upon cardiac as well as renal IR injury using *in vivo* models. This suggests that mtDNA, which can activate TLR9, is involved in inflammation upon IR injury (Akira and Hemmi, 2003; O'Neill et al., 2009). Although NLRP3 inflammasome activation as well as cGAS/STING pathway activation have been reported in other pathologies and upon mitochondrial damage, their involvement in the immune response upon IR injury remains to be elucidated (García and Chávez, 2007; García et al., 2005; Liu et al., 2016a; Maekawa et al., 2019).

To summarise, opening of the MPTP upon IR injury causes the release of mtDAMPs into the cytosol as well as into the circulation causing activation of the innate immune response (Figure 1.15). Not much is known about the time course of mtDAMP release and specific inflammatory pathways involved in inflammation upon IR injury. But mtDNA might be an interesting candidate to investigate further, due to its role in several immune pathways and the fact, that IL6 levels are elevated upon ischaemia reperfusion injury.

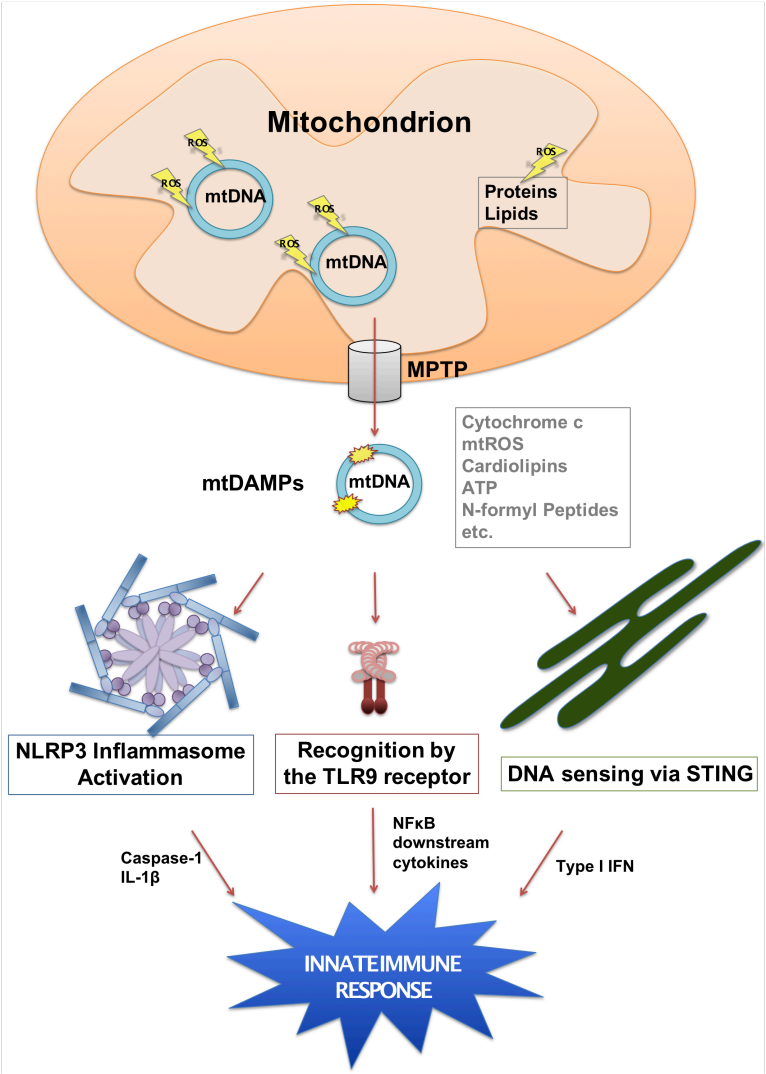

Figure 1.15: Schematic model of mtDAMP release upon ischaemia reperfusion injury and the role of mtDNA in activating the innate immune response. Schematic hypothesis of the role of mtDNA as mtDAMP in activating the innate immune response. Upon ischaemia reperfusion injury, reverse electron transport causes a burst in ROS, which damages mitochondrial content like lipids, proteins and mtDNA. It is possible that the mitochondrial permeability transition pore opens and releases mitochondrial damage associated molecular patterns into the cytosol. One of them is mtDNA, which in the cytosol could potentially be involved in activating immune pathways. As described earlier, three pathways are known to be activated by DNA molecules: the NLRP3 inflammasome that leads to caspase-1 activation and IL1β production; the toll like receptor 9, located primarily at endosomes, activating the NfκB response; or the ER- linked cGAS/STING pathway leading to interferon type 1 production.

1.4.3.3 Cell death upon mitochondrial damage

Energy-dependent as well as -independent cell death pathways are both elevated upon mitochondrial damage in different pathologies (Galluzzi et al., 2012; Green, 2004). Apoptosis is an energy-dependent programmed cell death pathway known to be closely linked to mitochondrial function. Necrosis on the other hand is highly immunostimulatory and occurs in the absence of ATP as well, causing plasma membrane rupture and release of cytosolic content into the extracellular matrix or circulation. While apoptosis has been shown to be the dominant cell death pathway occurring upon IR injury in hypoxic cell models (Eefting, 2004), tissues are thought to be primarily necrotic upon severe IR injury (Gottlieb, 2011). Due to the lack of cell models resembling *in vivo* conditions for IR injury, our understanding of the activation of the different cell death pathways under these conditions is still poor.

In summary, mitochondria are at the centre of IR injury, not just because of metabolic changes that occur within mitochondria during anoxia, but also because of a burst in ROS generation due to RET at complex I and subsequent oxidative damage. Furthermore, following mitochondrial damage, these organelles are involved in activating the cellular response to IR injury, in form of innate immune cascades as well as cell death.

1.5 Therapeutic approaches on mitochondria to ameliorate ischaemia reperfusion injury

Understanding cellular processes that occur during ischaemia and upon reperfusion opens new ways and possibilities to prevent this damage. IR injury can be divided into three different phases: the ischaemic period, the reperfusion phase and the injury response. This allows several different possibilities to intervene in ischaemia reperfusion injury and decrease damage. One possibility is to use mitochondria-targeted therapies to ameliorate pathologies (Horton et al., 2008; Murphy, 2009; Smith and Murphy, 2010) (Figure 1.16). Therapeutic compounds such as antioxidants can be targeted to mitochondria by attaching them to a lipophilic, cation. The charge will draw the compound via the plasma membrane potential into cells where it will further follow the membrane potential and enter mitochondria. A widely used group to do this is the lipophilic triphenyl phosphonium (TPP) cation. This can pass through membranes due to its charge and the large mitochondrial membrane potential. Several

compounds linked to TPP have been developed in the last years, such as MitoSNO or MitoQ, which will be described in more detail later on (Murphy, 2016).

1.5.1 Interventions during ischaemia

One of the crucial metabolic changes during ischaemia is the accumulation of succinate which arises in part due to reversal of complex II. This accumulation can potentially be prevented using inhibitors of complex II during ischaemia and thereby decrease the injury upon reperfusion. Different forms of malonate a competitive inhibitor of complex II have been used to ameliorate IR (Chouchani et al., 2016; Martin et al., 2019; Valls-Lacalle et al., 2018). Malonate is structurally similar to succinate and acts as a competitive inhibitor, so their effects can be reversed after the malonate has been used to decrease oxidative damage.

1.5.2 Interventions during reperfusion

Upon reperfusion, the initiating damaging factor is the ROS burst through RET at complex I. Inhibiting ROS production directly could thus decrease damage upon reperfusion. Analysis of the active/deactive transition of complex I revealed that a cysteine, Cys39, was exposed in the deactive state that complex I adopts during ischaemia. A TPP compound, MitoSNO, has been developed to target this cysteine and block it, and thereby lock complex I in the deactive state when added at reperfusion and thereby disable RET and excessive ROS production. Studies have shown that mice treated with MitoSNO during cardiac ischaemia and reperfusion show reduced ROS and injury levels upon reperfusion (Chouchani et al., 2016; Prime et al., 2009). Additionally, it is possible to target the ROS produced and prevent oxidative damage. The mitochondria-targeted antioxidant MitoQ can decrease oxidative damage inside mitochondria. Similar to MitoSNO, it contains a TPP group, which ensures mitochondrial localisation of the antioxidant. The beneficial effects of MitoQ have been shown in various studies of diseases that are all linked through the prevention of oxidative damage via MitoQ (Dare et al., 2015; Murphy, 2016).

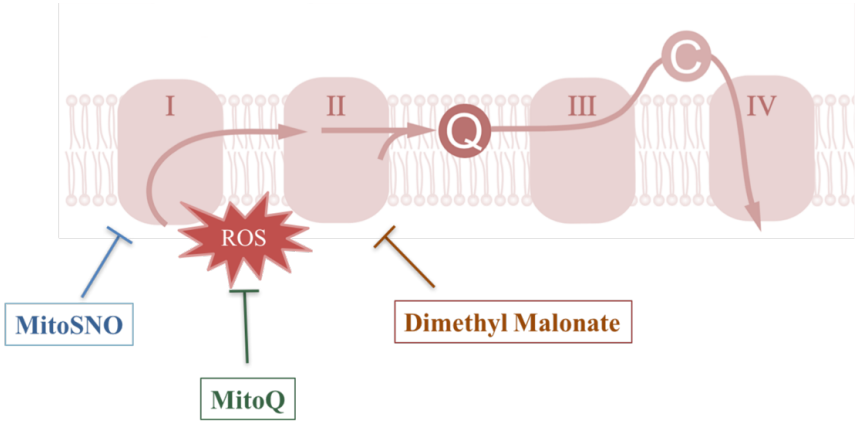

Figure 1.16: Therapeutic approaches to ameliorate IRI in mitochondria. Schematic overview over therapeutic approaches to ameliorate ischaemia reperfusion injury. The main goal is to reduce the production of ROS upon reperfusion after ischaemia, which occurs at complex I due to reverse electron transport. The mitochondria-targeted compound MitoSNO blocks structural changes of complex I during anoxia, which facilitate RET and therefore ROS production. Dimethyl malonate on the other hand inhibits complex II and therefore succinate accumulation, which maintains a reduced CoQ pool upon reperfusion that ultimately drives RET. Finally, the mitochondria-targeted antioxidant MitoQ can ameliorate ROS directly and avoid oxidative damage upon reperfusion.

1.5.3 Inhibition of the immune activation

Finally, another approach to prevent IRI in mitochondria to rescue cells and therefore tissues from necrosis, is prevention of mitochondrial death or dysfunction after primary reperfusion damage has already occurred. One final step after mitochondria dysfunction is opening of the MPTP. Therefore, inhibiting the opening of this pore could prevent cell death. Cyclosporin A is an inhibitor of the pore opening and some studies have shown that cyclosporin A can ameliorate IRI in transplantation, however the exact mechanisms of this process are still not completely understood (Hausenloy et al., 2012; Nighoghossian et al., 2016). It may be possible to block TLR9 using a CpG antagonists (primers) and additionally inhibit cGAS using inhibitors like the compound Ru.521 (InvivoGen) to prevent the immune reaction. This, in combination with apoptosis inhibition, could prevent cell death and the release of cytokines to the circulation.

In general, all of these therapeutic approaches have difficulties e.g. the importance of correct timing and dosing to be effective without inhibiting essential cellular pathways. Therefore, it is first crucial to understand the pathological processes occurring during ischaemia and reperfusion. Additionally, it is important to note that the best therapeutic approach in the future may be a combination of treatments. In order to understand their

function perfectly, they will have to be analysed *in vitro* and *in vivo* to understand the cellular response but also mimic a clinical scenario.

1.6 Summary

To summarise, our current understanding of IR injury, is that mitochondrial processes are at the centre of this pathology. IR which plays an important role in diseases such as heart attack and stroke (Eltzschig and Collard, 2004; Gürtl et al., 2009). Our hypothesis is that this type of cell damage also contributes to poor outcome in organ transplantation. However, a detailed understanding of the role of mitochondria and IR injury in models of transplantation is lacking, which if developed may lead to new therapies to improve the outcome for transplantation patients.

1.7 Aims

The overall aim of this study is to investigate the role of mitochondria in IR injury in clinical and experimental models of organ transplantation. This will also be extended to simpler *ex vivo* and *in vitro* models in order to analyse in detail the cellular processes occurring during ischaemia and upon reperfusion, including the role of mtDNA as mtDAMP in activating the innate immune response.

1.7.1 Understanding energy demand during ischaemia in tissue

The first aim of this study is to investigate which changes in the ATP/ADP ratios and adenosine nucleotide pools occur during ischaemia in different organisms and organs. The focus is on the time course and effects of temperature during ischaemia, because in clinical scenarios of organ transplantation various periods of cold as well as warm ischaemia occur. Additionally, the differences between different organs and their energy demand during ischaemia are investigated in various mammalian species and compared to non-mammalian species.

1.7.2 Establishment of a cellular model to investigate succinate accumulation and efflux during ischaemia and reperfusion

In order to be able to isolate and analyse cellular processes and their impact during IR injury in more detail, it is necessary to utilise a simpler model. Therefore, I established a cellular IRI model that mimics the physiological conditions that occur during transplantation. Primary adult cardiomyocytes are used in combination with an anoxic chamber to reduce oxygen levels rapidly to below 1 particle per million of oxygen. This cell model replicates *in vivo* IRI and allows a detailed analysis of underlying cellular pathways.

I utilise this model to investigate accumulation of succinate during anoxia and its efflux upon reperfusion further. Finally, I explore the possibility of interfering at different sites and timepoints during ischaemia and reperfusion using mitochondria-targeted compounds to ameliorate injury.

1.7.3 Investigation of mtDNA release upon IRI *in vitro*

The anoxic cell model is then utilised to investigate if mtDNA is released from mitochondria to the cytosol upon reperfusion injury and further on into the extracellular matrix from damaged cells. Hence, I am especially interested in examining whether released mtDNA upon ischaemia reperfusion injury is involved in the activation of cytosolic innate immune responses within these primary cells.

1.7.4 Investigation of mtDNA release as mtDAMP *ex vivo* and *in vivo*

Finally, the role of mtDNA as a DAMP is explored in models of organ transplantation. I investigate if elevated levels of mtDNA can be found in the circulation of perfused organs and patients that have undergone ischaemia reperfusion injury. Additionally, I analyse further if circulating mtDNA levels in patients correlate with other, known organ damage markers and provide insight into the severity of IR injury and mitochondrial damage during organ transplantation.

Chapter 2

Material and Methods

2.1 Chemicals and stocks

All reagents were obtained from Merck (formerly Sigma-Aldrich), UK unless otherwise specified.

Stock solutions were stored at 4°C, unless otherwise stated, and enzyme glycerol stocks were stored at -80°C.

Experiments were performed and samples and solutions kept at room temperature during experiments, unless stated otherwise.

Solvents used for the preparation of samples for LC-MS were of high-pressure liquid chromatography (HPLC) grade (Thermo Fisher Scientific).

pH of solutions was corrected at the temperature of use (as indicated), using a calibrated pH meter (3310; Jenway, UK).

Water used in all experiments, unless specified, was Milli-Q filtered to a resistivity of 18.2 MΩ at room temperature (R/=nnT) (Merck, UK).

2.1.1 Compounds and inhibitor stocks

Rotenone (experimental concentration: 1 μM), TTFA (experimental concentration: 1 mM), 3-nitropropionic acid (3-NPA; experimental concentration: 500 μM) and disodium malonate (experimental concentration: 10 μM) and dimethyl malonate (experimental concentration: 10 mM) were dissolved in absolute ethanol.

MCT1 inhibitor AR-C141990 (Tocris, UK) (experimental concentration: 10 μM) and Digitonin (experimental concentration: 30 μg/mL) in water.

Cyclosporin A (experimental concentration: 200 nM) and Ru.521 A (experimental concentration: 2 μg/mL) in DMSO.

The compounds MitoPQ (experimental concentration: 0.01 nmol), MitoQ (experimental concentrations: 50 and 100 μM), MitoSulf (experimental concentration: 1 μM) and MitoNap (experimental concentration: 1μM) were synthesised in the lab of Professor Richard Hartley (WestCHEMSchool of Chemistry, University of Glasgow, UK) and dissolved in absolute ethanol or DMSO at stock concentrations of 100 mM Compounds were diluted from stock solutions in water and adjusted to pH 7 with KOH to experimental concentration.

2.2 Animal work

2.2.1 Mouse work

2.2.1.1 Mouse strain and animal husbandry

C57BL/6 mice were purchased from Charles River Laboratories (Margate, UK). C57BL6/NZB conplastic mice were a gift from José Antonio Enríquez and were maintained by Dr. Stephen Burr, Chinnery Lab, Mitochondrial Biology Unit (Latorre-Pellicer et al., 2016). All animal experiments were approved by the UK Home Office under the Animals (Scientific Procedures) Act 1986 and followed the University of Cambridge Animal Welfare Policy.

Mouse hearts and kidneys were retrieved from male C57BL/6 mice (Charles River Laboratories, UK) at 6-8 weeks of age. Animals were kept on 12 h light/dark cycles in specific pathogen-free animal facilities with *ad libitum* access to food and water. For cardiomyocyte isolation, mice were culled by cervical dislocation.

2.2.1.2 Energy metabolism during organ storage in murine heart

Adenosine nucleotide changes during organ storage were measured in whole murine hearts exposed to variable periods of warm or cold ischaemia and compared to baseline normoxic hearts. The animal work was performed by Dr. Jack Martin, sample retrieval, handling and freezing by me.

The donor animals were anaesthetised with isoflurane (Abbott Laboratories, US) and oxygen at 2 l/min. The animals' rectal temperature was measured continuously using a rectal thermometer and maintained at 37°C ± 1°C using a relayed variable heat mat (Kent Scientific). Animals were culled via exsanguination by division of the IVC and aorta and the heart was retrieved.

For analysis of cold ischaemia (CI), hearts were placed directly in 10 mL University of Wisconsin (UW) solution (Viaspan, Cold Storage Solution, Bridge to Life Ltd, USA: hydroxyethyl starch 50 g/l, lactobionic acid 105 mM, KH_2PO_4 25 mM, MgSO 5 mM, raffinose 30 mM, adenosine 5 mM, allopurinol 1 mM, glutathione 3 mM, KOH 100 mM, pH 7.4 at 1-2°C) upon retrieval of the heart. To analyse warm ischaemia, the excised heart was left in the abdomen of the animal and maintained at 37°C on a heat mat.

2.2.1.2.1 Clamp freezing

To measure ATP and ADP concentrations in the heart under baseline normoxic conditions, as close as possible to those *in vivo*, the still-beating hearts of anesthetised mice were rapidly frozen within 10 seconds using Wollenberg clamps (manufactured by Josh Firman, LMB Workshop, UK) at liquid nitrogen (LN_2) temperature (Figure 2.1).

In order to freeze samples, the clamps were cooled for 2 mins in LN_2 just before sample retrieval. A tissue sample was then placed with forceps (room temperature warm) on the clamp blade and rapidly clamped. The clamps were then cooled again in LN_2 for ~10 secs, freezing the tissue.

Then, the clamps were opened (in close proximity to the dry ice, careful not to drop the tissue) and the tissue was rapidly transferred into pre-cooled (on dry ice) Eppendorf tubes using pre-cooled forceps. Samples were stored at –80°C until further analysis.

Figure 2.1: Wollenberger clamps. Representative Image of Wollenberger clamps, cooled down in LN_2.

2.2.1.3 Energy metabolism during organ storage in murine kidney

Changes in adenosine nucleotides during warm or cold ischaemia in murine kidneys were analysed in a similar experimental procedure as in hearts. The animal procedures were performed by Dr. Timothy Beach.

Briefly, mice (~ 25 g) were anaesthetised with inhaled isoflurane (Abbott Laboratories, US) and oxygen at 2 l/min. Temperature was measured continuously using a rectal thermometer and maintained at 37°C ± 1°C using a heat mat (Kent Scientific). Animals were then culled via exsanguination by division of the IVC and aorta and one kidney rapidly clamp frozen as base line control, the other kidney subjected to either warm or cold ischaemia before clamp freezing, as described before. Cold ischaemia was induced by placing the kidney into 10 mL UW solution (Viaspan) on ice, while warm ischaemia was induced by maintaining the kidney in the abdomen of the animal at 37°C. Clamp frozen samples were transferred to pre-cooled tubes and stored at –80°C until further analysis.

2.2.1.4 mtDNA release upon IR injury in murine kidneys

In order to investigate mtDNA release from murine kidneys upon ischaemia and reperfusion injury, a model of bilateral renal vascular occlusion (Chiao et al., 1997) was optimised and performed by Dr. Timothy Beach.

Briefly, a laparotomy was performed on anaesthetised and temperature-controlled mice, and vascular clamps (8 mm, interFocus Fine Science Tools, Cambridge, UK) were placed over the renal hilum on one kidney to induce unilateral renal ischaemia. The other unclamped kidney served as control. At the end of 25 min of warm ischaemia, the clamps were removed and reperfusion of the kidneys confirmed by return of blush colour. Kidneys underwent 25 min of ischaemia followed by 24 h of reperfusion. At the end of the study protocol, the animals were euthanised (Schedule 1 method of cervical dislocation under terminal anaesthesia) and a blood sample was collected using a heparinized syringe. These samples were compared to samples from animals subjected to sham surgery without any induction of ischaemia.

2.2.1.5 Murine heterotopic heart transplantation

The murine heterotopic heart transplant model was originally described by Corry et al., 1973, and performed here by Dr. Jack Martin. Donor animals were anaesthetised with isoflurane (Abbott Laboratories, US) and oxygen at 2 l/min. The animals' rectal temperature was measured continuously using a rectal thermometer and maintained at 37°C ± 1°C using a relayed variable heat mat (Kent Scientific, UK). 100 IU heparin (Leo Pharma A/S, Ballerup,

Denmark) was administered in 100 µL 0.9% w/v sodium chloride via central vein injection using a 1 mL syringe attached to a 31-gauge needle. Animals were exsanguinated by division of the IVC and aorta. The IVC (caudal caval vein), left SVC (cranial caval vein) and right SVC (cranial caval vein) were ligated, the fat and connective tissue dissected between the aorta and pulmonary artery and the ascending aorta divided, followed by division of the descending one. The left and right pulmonary arteries were divided as well and the donor heart was flushed with 500 µl Soltran (Baxter Healthcare) via a fine bore (0.28 x 0.165 mm) polyethene tube (Portex tubing, Smith Medical International Ltd, UK). The pulmonary veins were then ligated, the heart excised and stored in UW (Viaspan) until implantation. Hearts were either immediately retrieved with no additional warm ischaemia or left for 6 or 12 minutes prior to performing the standard retrieval operation.

The donor heart was transplanted heterotopically into the abdomen of the recipient animal using a modified microsurgical technique previously described (Liu et al., 2016). The recipient mouse was anaesthetised with isoflurane (Abbott Laboratories, US) and oxygen at 2 l/min and the animal's rectal temperature was measured continuously using a rectal thermometer and maintained at 37°C ± 1°C using a relayed variable heat mat (Kent Scientific, UK). The tissue overlying the abdominal aorta and IVC was divided by dissection, the posterior lumbar vessels were identified and ligated using 7-0 silk ties. Vascular clamps were applied and the IVC was emptied with a 31-gauge needle.

The donor heart was then retrieved from cold storage and placed into the right side of the recipient's abdomen where sutures were placed between the donor and recipient vessels using 10-0 nylon Bearä surgical suture on a round bodied 4 mm (3/8) needle (Bear Medic Corp., Tokyo, Japan). Then the clamps were removed and contraction of the heart monitored. Following reperfusion, the recipient's skin was closed and animals were recovered in an incubator at 28°C overnight on soft, dry bedding with food and water. 24 h after surgery, the animals were culled via exsanguination, abdominal blood samples retrieved and tissue clamp frozen.

2.2.1.6 In vivo LAD infarct model

The left artery descending occlusion (LAD) model was as previously described (Chouchani et al., 2014b; Methner et al., 2014), to reflect ischaemia reperfusion injury as seen in patients after heart attack. The LAD surgeries were performed by Dr. Victoria Pell or Dr. John Mulvey (Department of Medicine, University of Cambridge, UK). Briefly, 8 to 10-week-old, male

C57BL/6 mice (~25 g; Charles River Laboratories, UK) were anaesthetised by administration of sodium pentobarbital (70 mg/kg intraperitoneally), intubated, ventilated and kept at 37°C using a rectal thermometer-controlled heat mat (TCAT-2LV, Physitemp, USA). Ventilation frequency was maintained at 110 breaths/min. The heart was exposed, a suture was placed around the prominent branch of the left anterior descending (LAD) and passed through a small plastic tube used to initiate ischaemia by pressing the tube against the heart occluding this LAD. Mice were subjected to 30 min of ischaemia and 120 min of reperfusion via removal of the suture, before ischaemic as well as control tissue was cut out and rapidly clamp frozen, within ~10 seconds. The control tissue was retrieved first, and consisted of ventricular tissue from the part of the heart that was still perfused throughout the experiment. Samples were stored at -80°C until experimental analysis.

2.2.2 Pig work

2.2.2.1 Porcine strain and animal husbandry

Large white male (Landrace) pigs (50 ± 5 kg) were supplied by Huntington Life Sciences, Huntington, UK and were acclimatised for a minimum of 7 days prior to experiments, with *ad libitum* access to food and water. All animal experiments were approved by the UK Home Office under the Animals (Scientific Procedures) Act 1986.

2.2.2.2 Energy metabolism during organ storage in porcine heart

Pig heart tissue was retrieved with the help of Dr. Kourosh Saeb-Parsy and Dr. Mazin Hamed from the Department of Surgery, University of Cambridge, UK. Pigs were sedated and received narcotic analgesia (ketamine 10 mg/kg, midazolam 0.1 mg/kg, medetomidine 0.02 mg/kg). General anaesthesia was induced using intravenous propofol (10 mg/mL) and remifentanil (6 µg/mL) through a peripheral vein. Animals were intubated and ventilated with intermittent positive pressure ventilation. Heart rate, blood pressure and O_2 saturation was monitored throughout the procedure. At the time of exsanguination, the thoracic cavity was accessed through the diaphragm and the apex of the heart (~ 20 - 30 g) was amputated with a scalpel. From this, a full thickness tissue sample (~ 100 mg) was immediately excised and clamp frozen using Wollenberger clamps as described above, taking ~30 seconds from

exsanguination to freezing. The rest of the apex was cut into cubes of ~3x3 cm, ~100 mg. These samples were either transferred to UW (Viaspan) storage solution at ~ 2˚C (cold ischaemia) or stored in Eppendorf tubes at 37°C on a heat block (Thermo Fisher Scientific, UK, warm ischaemia). At various time points, the tissues were then frozen utilising Wollenberger clamps as described before and stored at -80°C until analysis.

2.2.3 Human tissue

Heart biopsies were taken from deceased human organ donors aged 36-69 (Chapter 3). Ethical approval for the studies was obtained from NRES Committee East of England-Cambridge South (REC Reference 15/EE/0152). Informed consent was obtained from donor families for use of tissue for this study.

2.2.3.1 Energy metabolism during organ storage in human heart

Hearts declined for transplantation from deceased human organ donors, undergoing donation after brainstem death (DBD), were offered for research purposes after obtaining consent from the donor families. Consent was obtained by Dr. Jack Martin and the following sample retrieval performed by Dr. Kourosh Saeb-Parsy from the Department of Surgery, University of Cambridge, UK. Upon exsanguination of the donor as part of the organ retrieval process, a sample (~3 g) of myocardium from the still-beating heart was removed from the organ and clamp frozen within 10 seconds. After this control sample was frozen, another piece of myocardial tissue was retrieved and cut into cubes of ~3x3 cm, ~100 mg each. These samples were either transferred to UW (Viaspan) storage solution at ~ 2˚C or stored in Eppendorf tubes at 37°C on a heat block (Thermo Fisher Scientific, UK) to induce cold and warm ischaemia, respectively. At various time points, the tissues were then frozen utilising Wollenberger clamps and stored at -80°C until analysis.

2.2.3.2 Ex vivo perfusion of discarded organs

Donated human organs that were declined for transplantation but offered for research were retrieved after obtaining consent from the donor families. Human kidneys were accepted and handled by Dr. Mazin Hamed, human livers by Prof. Christopher Watson, Department of

Surgery, University of Cambridge, UK. Human organs were subjected to varying periods of warm and cold ischaemia, before they were perfused for up to 6 h at an *ex vivo* normothermic perfusion machine (EVNP) in the Department of Surgery as previously described (Harper et al., 2008). The perfusion machine was developed by Prof. Michael Nicholson and Dr. Sarah Hosgood at the Department of Surgery. This model has been optimised and reported as a method for understanding IR injury in porcine kidneys (Harper et al., 2008; Hosgood et al., 2012) and for screening potential therapeutics (Hosgood and Nicholson, 2010; Hosgood et al., 2011).

The circuit includes a paediatric centrifugal pump, pressure transducer, heat exchanger (Grants Instruments, Cambridge, UK) and temperature probe (Acorn, Oakton Instruments, Vernon Hills, IL, USA). Disposable perfusion sets (Medtronic, Watford, UK) are used for each experiment and consist of a biohead pump, venous reservoir, polyvinyl chloride (PVC) tubing and membrane oxygenator (Minimax Plus, Medtronic).

The disposable perfusion set is connected to a custom-made glass chamber (University of Leicester, UK) where the organ lies during the perfusion period. Prior to placing the organ in this chamber, the arteries and veins were cannulated with soft silastic catheters (Pennine, UK), which were tied in place with 4-0 vicryl suture (Ethicon, Johnson & Johnson, Livingstone, UK). The catheters were connected to the perfusion set and the circuit was primed with leucocyte depleted blood. The total circulating volume was 1 litre. The circulating perfusate was oxygenated with 95 % O_2/ 5 % CO_2 at 0.5 L/min at a temperature of 37°C. The perfusion pressure was set to a mean arterial pressure of 85 mmHg.

Tissue as well as blood (and urine) samples retrieved at different time points throughout the perfusion.

2.2.4 Trachemys scripta

2.2.4.1 Turtle strain and animal husbandry

Male and female red-eared slider turtles (*Trachemys scripta elegans*) were purchased from eNASCO (Fort Atkinson, WI, USA) and kept in the animal facility at the Department of Bioscience, Aarhus University, for several months before being used for experiments. Turtles were kept at 25°C in aquaria with free access to basking platforms on a 12:12 light/dark cycle and fed three times a week with dry pellets and raw krill. All experiments were conducted by

Dr. Amanda Burghaard at the University of Aarhus, Denmark in accordance to animal welfare standards of the UK Home Office and the laws for animal care and experimentation in Denmark.

2.2.4.2 Energy metabolism during anoxia in turtle heart

To investigate conserved pathways during ischaemia, we investigated changes in adenosine nucleotide pools during anoxia in red-eared slider turtles.

Anoxic turtles were kept submerged in water continuously bubbled with N_2, while normoxic turtles were allowed free access to air. Anoxic turtles were removed from the tanks with their heads pressed into their shields to limit their access to breathing. Turtles were euthanized with an overdose of 1 mg/kg pentobarbital injected in the supravertebral sinus. They were then kept at room temperature until the corneal reflex was gone after ~5 min and beheaded. Hearts were quickly dissected out and a ventricular sample (~50 mg) was immediately frozen in LN_2 and stored at −80 °C. All data was collected on heart ventricles which is referred to as turtle hearts.

2.2.5 Drosophila melanogaster

Additionally, we investigated ATP and ADP ratios during anoxia in the fruit fly *Drosophila melanogaster*, a species known to survive prolonged hypoxia.

Fruit flies were maintained and experiments conducted at 25ºC on a 12 h light:12 h dark cycle at 60% humidity using standard sugar/yeast/agar (SYA) media (Bass et al., 2007). Flies were tipped onto fresh food every 2 - 3 days. Flies were reared at standard larval density and enclosing adults were collected over a 12 h period. Flies were mated for 48 h before sorting into male and female populations.

To investigate adenosine nucleotide degradation in flies, they were either maintained at 25°C in a fly incubator under normoxia or subjected to anoxia at 25°C in an anoxic chamber. For reperfusion experiments, flies were removed from the anoxic chamber and incubated in a fly incubator before lysis. Changes in nucleotides after 1, 3 or 5 h of anoxia or after 60 min anoxia followed by 5 min, 2 or 24 h of reperfusion were determined. These experiments were performed in collaboration with Dr. Federica De Lazzari (University of Padova, Italy).

2.3 Mammalian cell culture

2.3.1.1 Cell culture media, buffers, reagents and cell lines

- Complete medium: Dulbecco's Modified Eagle's Medium (DMEM, Gibco): high glucose (4.5 g/l), GlutaMAX™ (2mM), sodium pyruvate (110 mg/mL); supplemented with 10 % (v/v) feta bovine serum (FBS) (E.U.-approved, South American origin, Gibco), 100 U/mL penicillin and 100 µg/mL streptomycin (Gibco);
- Cell freezing medium: 90% (v/v) FBS, 10% (v/v) dimethyl sulfoxide (DMSO) (Fisher BioReagents);
- Phosphate-buffered saline (PBS): Dulbecco's phosphate-buffered saline (Gibco) without calcium, magnesium or phenol red; 137 mM NaCl, 2.7 mM KCl, 8 mM Na_2HPO_4, and 2 mM KH_2PO_4
- Trypsin: Trypsin-EDTA (0.25%), phenol red (Gibco);
- Cell lines: Human Embryonic Kidney (HEK 293) cell line (HEK-BLUE, InvivoGen); murine macrophages (Raw264.7)

2.3.1.2 Growth and maintenance of mammalian cell lines in culture

Adherent cell lines (HEK-BLUE and Raw264.7 cells) were routinely cultured in T-75 treated, vented flasks (Nuncon Delta; Thermo Fisher Scientific, UK) in complete medium. Cells were incubated in a humidified incubator (37°C, 5% CO_2,) and maintained at sub-confluence (< 75% confluency). Therefore, cells were split regularly by removal of medium prior to two washes with 5 mL pre-warmed PBS. PBS was completely removed before the addition of 2 mL pre-warmed Trypsin distributed across the cellular surface of the flask. Cells were left to dissociate at 37°C for 3 min before the addition of 8 mL pre-warmed complete growth medium and resuspension by gentle pipetting. The required volume of suspension was subsequently transferred to a new T-75 flask containing 10 mL fresh, pre-warmed complete growth medium at a 1/10 dilution. Medium was replaced every 2 to 3 days.

2.3.1.3 Freezing, storing and re-thawing cell lines

Cells in T-75 flasks were trypsinised, resuspended and counted by a Trypan Blue Exclusion assay. Cell suspension (10 µL) was mixed with the same volume of Trypan Blue stain 0.4% (Invitrogen) and the mix was loaded on a Countess cell counting chamber slide (10 µL per chamber). Live cells can exclude the stain, while dead cells are stained blue. A Countess II FL haemocytometer (Invitrogen) counts and quantifies living and dead cells per mL. After quantification, the cells were pelleted by centrifugation at 500 x g for 5 minutes. The supernatant was aspirated and cells were gently resuspended in cell freezing medium at a density of 1 000 000 cells/mL. 1 mL cell suspension was transferred into each cryovial and placed in a Nalgene Mr. Frosty freezing container, which contains isopropyl alcohol to facilitate a slow (~1°C/min) cooling rate. The container was stored at -80°C for a minimum of 24 h, after which cryovials were transferred to LN_2 for long-term storage. To re-thaw and culture cells, frozen cell stocks were thawed rapidly in a 37°C water bath before transferring the cell suspension to a fresh T-75 flask containing 10 mL complete medium (pre-warmed at 37°C) and the medium was replaced with 10 mL fresh medium after 24 h.

2.3.2 ESC derived cardiomyocytes

Embryonic stem cell derived cardiomyocytes were compared to primary adult cardiomyocytes regarding their tolerance to anoxia reoxygenation. This work was performed in collaboration with Dr. Johannes Bargehr from the Department of Medicine, University of Cambridge, UK. Cardiomyocytes were differentiated and cultured in the Department of Medicine, before being transferred to the Mitochondrial Biology Unit, where experiments were performed.

Briefly, hESCs (RUES2, female line, Rockefeller University, National Institutes of Health (NIH) registry number 0013) were maintained in irradiated complete medium containing bFGF (4 ng/mL, Peprotech). Cells were seeded as single cells (1×10^5 cm^{-2}) on Matrigel (BD Biosciences)-coated plates with conditioned medium including Chiron 99021 (1 µM, Cayman Chemical) and ROCK inhibitor (Y-27632) (Bargehr et al., 2019). The following day (day 0), the medium was aspirated and cells were fed with RPMI medium (glucose (2 g), pH indicator (phenol red, 5 mg), salts (6 g sodium chloride, 2 g sodium bicarbonate, 1.512 g disodium phosphate, 400 mg potassium chloride, 100 mg magnesium sulfate, and 100 mg calcium nitrate) supplemented with B27 (Invitrogen) containing Activin-A (100 ng/mL)) for 18 h. On

day 1, medium was aspirated and cells were fed with RPMI medium plus B27 containing BMP4 (5 ng/mL) and Chiron 99021 (1 μM) for 48 h. On day 3, medium was aspirated and replaced with RPMI medium plus B27 containing Xav 939 (1 μM, Torcis). On day 5, the medium was replaced with RPMI medium plus B27. On day 7, the medium was replaced with RPMI containing B27 with insulin (Invitrogen) and was consequently replaced every other day. Anoxia and reoxygenation was induced as described for adult primary cardiomyocytes below.

2.3.3 Primary adult cardiomyocytes

2.3.3.1 Cardiomyocyte isolation

In order to investigate ischaemia reperfusion injury in detail on a cellular level, I developed an *in vitro* model utilising primary adult murine cardiomyocytes that were isolated using a collagenase-based preparation. In short, cannulated mouse hearts were perfused via the aorta with collagenase to digest the heart and release the cardiac cells (Graham et al., 2013; Li et al., 2014).

C75BL/6 mouse hearts were retrieved after the animals were culled via cervical dislocation. The organ was accessed via the thoracic cavity through the diaphragm and the tissue was dissected after division of the ascending and descending aorta. The heart, which kept beating for ~5 seconds, was immediately placed in a mixture of ice and perfusion buffer (table 2.1) to rapidly cool the organ. Next, fat and lung tissue were trimmed off, and the aorta was cannulated through the aortic branch on a Langendorff apparatus and tied safely with 4-0 nylon Bearä surgical sutures (Figure 2.2). The heart was then retrogradely perfused at 37°C at roughly 1 drop every 3 sec (3mL/min) first for 5 min with perfusion buffer. This buffer was then supplemented with 200 g/mL (final concentration) Liberase (Collagenase I and II mixture from Roche, diluted in 50 mL perfusion buffer and 3 μL 1 M CaCl) and the organ perfused at 37°C for approximately 20 min, until almost completely dissolved, which was monitored by checking that the heart lost its firm structure and became soft and pale.

Next, ventricles were removed, the heart was covered with Stop buffer (Perfusion buffer supplemented with 1 mg/mL BSA) and carefully pipetted up and down before being transferred into a 15 mL Falcon tube. The cells were topped up to 5 mL with Stop buffer and allowed to settle via gravity separation. Fibroblasts settled first, the cardiomyocyte-containing supernatant was transferred to a fresh tube after ~10 min and topped up with Stop buffer to 5

mL total volume. Ca^{2+} tolerance of the cells was increased by adding 10, 25 and 50 µL of 100 µM Ca^{2+} every 15 min to 5 mL of cells in Stop buffer. The cells were washed 3 times with Stop buffer containing a final Ca^{2+} concentration of 1 mM. The cell suspension was divided onto 60x15 mm or 40x12 mm glass dishes, which have been treated with laminin. The smaller dishes were plated with approximately 50 000 cells, the bigger ones with 100 000 cells.

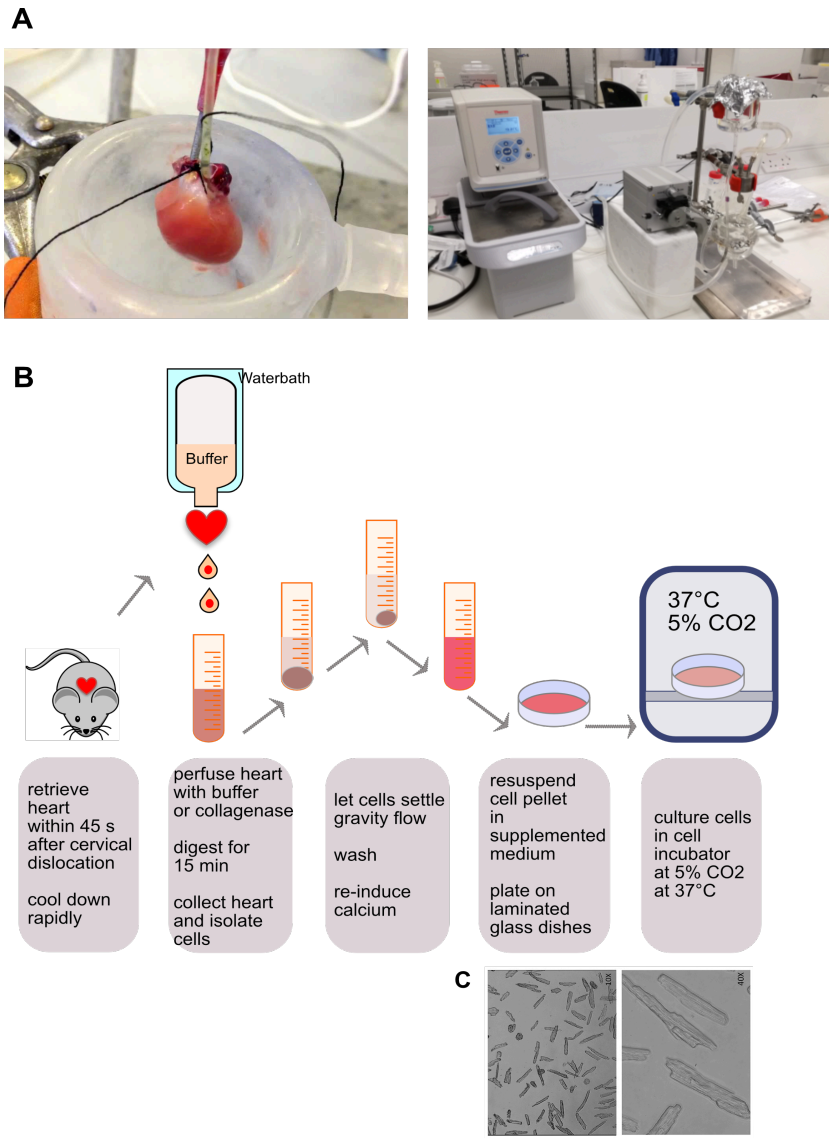

Figure 2.2: Isolation of adult murine cardiomyocytes. (A) Representative picture of a cannulated mouse heart at a Langendorff perfusion pump, next to a picture of the perfusion apparatus, including water bath, pump and buffer reservoirs. (B) Workflow schematic of cardiomyocyte isolation including digest and various washing steps before the cells are resuspended in culture medium, plated and maintained in at 37°C, 5% CO2. (C) Representative pictures of isolated cardiomyocytes after plating at 4 x and 10 x magnification.

2.3.3.2 Cardiomyocyte culture

Cardiomyocytes were cultured on glass dishes and maintained at subconfluence at 37°C in a humidified 5% CO_2 incubator. The 60x15 mm or 40x12 mm glass dishes were rinsed with 70% ethanol, before they were washed 3 times with 1 mL PBS and laminated with 1 mL laminin (150 µL of laminin stock in 10 mL of sterile water) (Laminin stock from Engelbreth-Holm-Swarm murine sarcoma basement membrane, Sigma-Aldrich, UK). The plates were incubated for 2 h at 37°C and the laminin solution was aspirated before cardiomyocytes were transferred onto the plates.

The cells were cultured in M199 medium supplemented with 100 U/mL penicillin, 100 U/mL streptomycin, 161 mg/500mL L-carnitine, 282.5 mg/mL creatine and 312 mg/mL taurine.

For long term culture (up to 2 days), 1 µL/mL 25 mM Blebbistatin was added to block cardiomyocyte contraction. Spontaneous, non-controlled beating of the cells would lead to excessive ATP consumption and calcium influx, which is a huge cellular stressor.

To count, 10 µL cells were mixed carefully with 10 µL Trypan blue (under usage of a cut pipette tip) and subjected onto a Neubauer chamber. Cells on the outside of the grid were counted, divided by 8 and 0.04, then multiplied by 2000 to give the number of cells per mL.

2.3.3.3 Anoxia and reperfusion in isolated cardiomyocytes

Ischaemia is the lack of oxygen which occurs in various human diseases. Some organisms, like certain microbiota, survive or even preferably live under anoxia. In order to study these, anaerobic chambers and gloveboxes are utilised. These gloveboxes are air sealed and maintain a different atmospheric environment within, compared to the normal air outside. Nitrogen gas is used to replace oxygen and air inside the chamber, leading to total oxygen concentrations of 0.1-10 ppm (part per million) inside the glovebox.

The mechanism by which oxygen is removed, while nitrogen floods the chamber, utilises copper metal catalysts (Figure 2.3). In order to maintain the low concentration of oxygen, gloveboxes contain airlocks or transfer chambers to enable transfer of samples or materials into the chamber. These transfer chambers purge excess oxygen before the door into the actual chamber can be opened and the items transferred into it. Additionally, temperature controls, in form of a water bath or ice bath, are attached to the glovebox to allow manipulation of the internal temperature to maintain the desired experimental conditions.

The amount of oxygen contained within items that are going to be placed in the chamber, determines how long it has to be purged before being transferred into the chamber. Some materials, like plastic, contain oxygen and need to be purged for 15 min to 4 h, dependent on the size and amount of plastic. We therefore decided to use glass petri dishes to culture cells. Glass contains less oxygen and can be purged within 5 min, so that the cells do not have to be maintained in the transfer chamber for excessive amount of time.

Necessary equipment and solutions were degassed overnight prior to the start of the experiment. The experiments in this chamber in the Hirst Lab, Mitochondrial Biology Unit, Cambridge, UK, were done at 10-0.4 parts oxygen per million.

Cardiomyocytes were washed once with normoxic Tyrode's buffer (37°C) before 2 mL of fresh buffer were added to each dish. Experiments were performed in either hypoxic buffer, or in Tyrode's buffer. The MCT1 inhibitor AR-C141990 from Tocris was used at a concentration of 10 μM in Tyrode's buffer.

(Cells from a 'control start' dish were lysed immediately, 'control end' dishes were kept at 37°C, 5% CO_2 until the end of the experiment.) The other dishes were degassed for 10 min followed by transfer into the anoxic chamber onto a heat block at 37°C. Anoxia was induced for different time points before the cells were lysed (in a buffer suitable for the assay performed afterwards), transferred to Eppendorf tubes, moved out of the chamber and immediately snap frozen on dry ice. Cells that underwent reperfusion received buffer replacement with fresh Tyrode's buffer (for up to 15 min reperfusion) or M199 medium (for longer reperfusion) and were transferred out of the chamber. The dishes were then incubated for different reperfusion time points at 37°C, 5% CO_2 and lysed afterwards.

To induce hypoxia, cells were cultured on laminated 6-well plates (CoStar), washed and put into experimental buffers as described above, before being incubated for different time points at hypoxia inside the CLARIOStar Plus plate reader from BMG Labtech. There, the plates were kept at 0.1% O_2, 5% CO_2 at 37°C, then retrieved and cells lysed immediately.

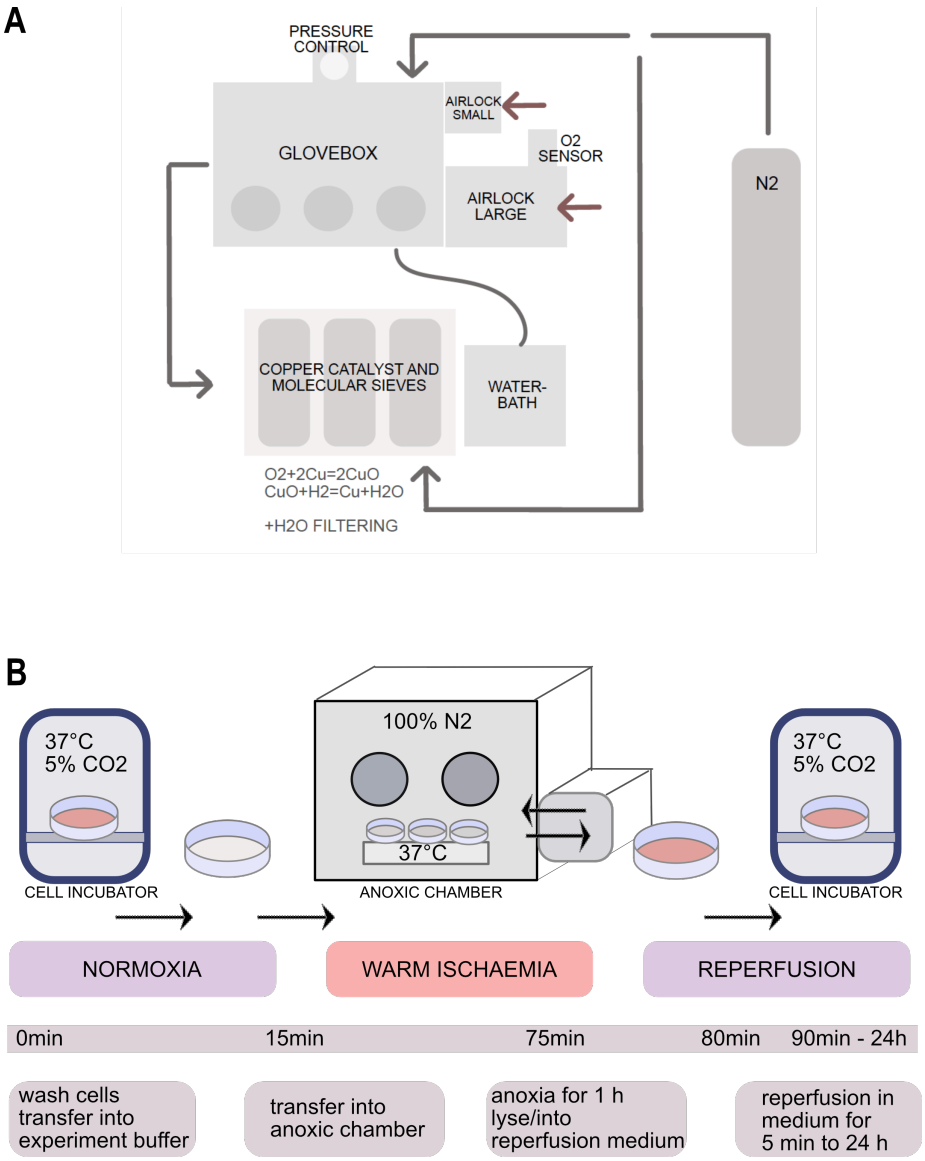

Figure 2.3: Schematic picture of an anoxic chamber and cardiomyocyte treatment to induce IRI. (A) An anoxic glovebox is sealed from the surrounding air and filled with nitrogen. An oxygen sensor monitors residual oxygen concentrations within the chamber. Airlocks provide the possibility to move samples and materials into the chamber upon degassing. Temperature within the box is maintained with a water bath and the oxygen concentrations maintained low via copper catalysation. (B) Workflow and time schedule of inducing anoxia and reoxygenation to cardiomyocytes.

Hypoxic buffer is a lactate-based buffer that overloads the cells with lactate at a lower pH of 6.4 which mimics conditions of hypoxia or anoxia, characterised by anaerobic glycolysis, leading to the production of excess lactate and therefore cellular acidification. Tyrode's buffer, on the other hand, is a simple glucose-based buffer at physiological ph. Our research has

shown that (cardiac) cells are capable of excreting excess metabolites from their cytosol. In order to control the lactate efflux, we investigated another buffer system which consists of Tyrode's buffer supplemented with an inhibitor of the lactate transporter in the plasma membrane MCT1 (Roth et al., 2014; Wendt et al., 2009).

Table 2.1: Solutions and reagents used to isolate cardiomyocytes and induce normoxic or anoxic conditions.

Solution	Reagents
Perfusion Buffer	133 mM NaCl, 4.7 mM Kill, 0.6 mM KH_2PO_4, 0.6 mM NaH_2PO_4, 1 mM Hepes, 1.2 mM $MgSO_4$, 12 mM $NaHCO_3$, 10 mM $KHCO_3$, 30 mM Taurine, 10 mM Butanedione monoxime, 5.5 mM Glucose, pH 7.4 (with KOH)
Normoxic Tyrode's Buffer	137 mM NaCl, 5.4 mM KCl, 0.4 mM $MgCl_2x6H_2O$, 10 mM Hepes, 10 mM Glucose, 1 mM $CaCl_2$, pH 7.4 (with KOH)
Hypoxic Buffer	1 mM KH_2PO_4, 10 mM $NaHCO_3$, 2.5 mM $MgCl_2x6H_2O$, 25 mM Hepes, 74 mM NaCl, 14.7 mM KCl, 10 mM Lactate, 1.2 mM $CaCl_2$, pH 6.2 (with HCl)

2.3.3.4 Cytosol extraction

To investigate mtDNA release from mitochondria upon IRI, cytosolic fractions were extracted using digitonin treatment (West et al., 2015).

For digitonin extraction, cells (100,000 cells/plate) were subjected to anoxia and reoxygenation as described above. The culture medium was removed after reperfusion, cells

were washed once with PBS, scraped with a plastic cell scraper and transferred to 1.5 mL Eppendorf tubes. The cells were pelleted via centrifugation for 1 min at 300 x g at room temperature and gently resuspended in 50 µL PBS. Half of the cells was transferred to a fresh Eppendorf tube and used for whole cell extraction. The other 25 µL were carefully mixed with 300 µl KCl buffer substituted with 30 µg/mL digitonin (prepared freshly, dissolved in MiliQ water). The samples were then incubated at room temperature for 10 min to allow digitonin to penetrate the plasma membrane and release the cytosolic content. Next, they were spun for 3 min at 1000 x g, resulting in cell membranes and organelles being pelleted and cytosolic content suspended in the supernatant. This supernatant (~300 µL) was pipetted into a fresh tube, the pellet was used for Western Blot analysis to confirm presence of membrane and mitochondrial proteins. The supernatant was further spun for 10 min at 10, 000 x g to remove residual debris (which was then discarded) and the supernatant then transferred to a fresh tube. These cytosolic fractions were stored at -80°C before being used for further analysis, e.g. DNA extraction.

2.4 Cell Death and Viability Assays

2.4.1 Lactate dehydrogenase release

LDH is a stable enzyme that is very abundant in cellular cytoplasm and is released into the surrounding environment after the cell loses membrane integrity during cell death. The more cell damage occurs, the more enzyme can be detected in cell supernatant or blood and plasma samples.

Cells were plated at 100,000 cells/plate and subjected to different experimental conditions of anoxia and/or reperfusion. 1000 µL supernatant were collected from the samples and then spun for 10 min at 1000 x g at 4°C and stored in a fresh Eppendorff tube at -80°C. For analysis of cell death, lactate dehydrogenase levels were measured using the Roche (Sigma-Aldrich) cytotoxicity kit, utilising the reaction of LDH with its substrate lactate via reduction of NAD+. 100 µL supernatant were transferred to a CoStar 96-well plate. Each plate also contained a positive control of cell lysate from 100,000 cells in 1% Triton-X100 and appropriate blanks.

The substrate solution was freshly prepared with 11.25 mL of dye solution A, which was mixed with 250 µL of catalyst solution B. 100 µL of this substrate solution were added to each

sample. The plate was incubated at room temperature for 15 or 30 min before absorbance at 450 and 620 nm was measured on a microplate reader (CLARIOStar *PLUS*, BMG Labtech).

2.4.2 Caspase-Glo 3/7 assay

The cell death pathway apoptosis is characterised by the activation of caspase 9, an enzyme that will cleave pro-caspases 3 and 7 to their mature form, which starts a cascade of cellular content breakdown leading to cell death. In order to measure the amount of apoptotic cell death, here, the Caspase-Glo 3/7 assay (Promega, USA) was utilised to assess caspase 3 and 7 activity as an indicator for apoptosis.

The assay utilises caspase cleavage of a luminogenic substrate resulting in generation of a luminescent signal which is proportional to the amount of caspase activity present. The kit has been used following manufacturer's instructions. A reaction mixture is provided in the kit containing cell lysis buffer and caspase substrate which exhibits luciferase activity upon cleavage. Cells were plated at 100,000 cells/well on 6-well plates (CoStar) 24 h before treatment (anoxia, anoxia and reoxygenation, UV irradiation). The cells were then washed once with 1 mL PBS, before 500 µL Caspase-Glo 3/7 reagent was added to the wells and the plate incubated for 60 min at room temperature, protected from light. Finally, luminescence was measured using a CLARIOStar Plus plate reader (BMG Labtech).

2.5 Metabolite Analysis

2.5.1 Measuring cell and tissue ATP/ADP ratios by bioluminescence

2.5.1.1 Background

The luciferase/luciferin bioluminescence reaction can be utilised in a sensitive assay to measure adenosine triphosphate (ATP) and adenosine diphosphate (ADP) in extracts from cells and tissues (Strehler, 1974). ATP concentrations can be determined against ATP standards by measuring light production in a luminometer. Furthermore, ADP in cells and tissues can be measured by first degrading the endogenous ATP with ATP sulfurylase and then enzymatically converting endogenous ADP to ATP using a pyruvate kinase/phosphoenolpyruvate mix (Figure 2.4). Nucleotides were extracted from cells or snap-frozen tissue samples using perchloric acid to rapidly denature any endogenous proteins that

may alter the relative levels of ATP and ADP. The acidified, deproteinised extract is then neutralised with potassium hydroxide (in the presence of the pH buffer MOPS), forming a $KClO_4$ precipitate. Enzymatic reactions are then performed on the neutralised supernatant.

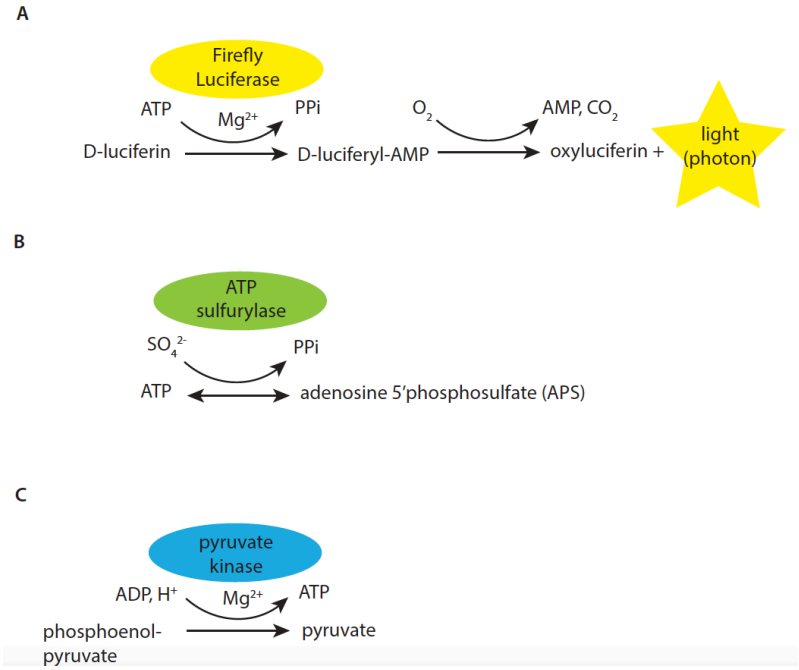

Figure 2.4: Reactions involved in measurement of ATP and ADP by luciferase/luciferin bioluminescence. (A) Photons are produced in proportion to ATP, D-luciferin and luciferase concentrations; (B) ATP sulfurylase catalyses the adenylation of sulfate using ATP, producing APS and PPi; (C) Pyruvate kinase catalyses the phosphorylation of ADP, forming ATP and pyruvate. Adapted from Dr. Elizabeth Hinchy.

2.5.1.2 Stock Solutions

- ADP and ATP stock solutions: 20 mM stocks (sodium salts) in HCl-acidified H_2O (pH 1-2), snap frozen in 100 µL aliquots, stored at -80°C;
- Perchloric acid ($HClO_4$) extractant (PCA): 3% (v/v) $HClO_4$, 2 mM Na_2EDTA, 0.5% (v/v) Triton X-100, stored at 4°C;
- Potassium hydroxide solution (KOH): 2 M KOH, 2 mM Na_2EDTA, 50 mM MOPS, stored at 4°C;
- Tris-acetate (TA) buffer: 100 mM Tris, 2 mM Na_2EDTA, 50 mM $MgCl_2$ (pH 7.75 with glacial acetic acid), stored at 4°C;
- D-Luciferin sodium salt: 2 mM in TA buffer, snap frozen in 200 µL aliquots in opaque Eppendorf tubes and stored at -80°C;

- Luciferase from *Photinus pyralis* (firefly): 1 mg lyophilised preparation (~150 µg luciferase protein) in 1.86 mL TA buffer (25% (v/v) glycerol) (~ 80 µg protein/mL), snap frozen in 100 µL aliquots in opaque Eppendorf tubes and stored at -80°C;
- Phosphoenolpyruvate cyclohexylammonium salt (PEP): 114 mM in TA buffer, snap frozen in 150 µL aliquots and stored at -80°C;
- Tris-HCl buffer: 100 mM Tris-HCl, 10 mM $MgCl_2$ (pH 8.0) stored at 4°C;
- Guanosine 5′-monophosphate disodium salt hydrate (GMP): 100 mM in Tris-HCl buffer, stored at 4°C;
- Sodium molybdate (Na_2MoO_4): 1 M in MQ H_2O, stored at 4°C;
- Bovine serum albumin (BSA) fatty acid free (Sigma): 100 mg/mL in TA buffer snap frozen and stored at -80°C;

2.5.1.3 Working solutions (prepared just before use)

- 2X ATP sulfurylase assay buffer (250 µL per reaction): 20 mM Na_2MoO_4, 5 mM GMP, 0.2 U ATP sulfurylase (New England Biolabs), Tris-HCl buffer to 250 µL, stored on ice until use;
- Pyruvate kinase / PEP mix (10 µL per reaction): 100 mM PEP, 6 U pyruvate kinase suspension (type II, from rabbit muscle: P1506), stored on ice until use;
- Luciferase/Luciferin mix (100 µL per reaction): 7.5 mM DTT (from 1 M stock made in MQ H_2O), 0.4 mg/mL BSA, 1.92 µg luciferase/mL, 120 µM luciferin, TA buffer (25% (v/v) glycerol) to 100 µL, stored at RT (protected from light).

2.5.1.4 Preparation of ATP and ADP standard curves

ATP and ADP (20 mM stocks) were thawed quickly at 37°C and then serially diluted in ice-cold PCA to make standard curves, typically ranging between 0 (100 % v/v PCA) and 10 µM in 1 mL aliquots.

2.5.1.5 Nucleotide extraction from cells and tissues

Cells were plated at a density of 50,000 cells/3 cm plate (HEK, ESC cardiomyocytes, RAW264.7) or 50,000 cells/40 mm glass dish (adult cardiomyocytes) and subjected to anoxia

and reoxygenation. Samples were then washed rapidly with ice-cold Tyrode's buffer on ice and immediately lysed in ice-cold PCA (500 µL per plate). Lysed cells were scraped from the plate surface with a plastic cell scraper and lysate was transferred to 1.5 mL Eppendorf tubes stored at -80°C until further analysis.

Tissue samples were clamp frozen, as described before, and stored at -80°C. For adenosine nucleotide analysis, ice-cold PCA (500 µL) was added to 5 mg weighed tissue in hard tissue homogeniser tubes (CK28 – 2 mL, Bertin Instruments) on dry ice and the solution was homogenised using a Precellys machine (Precellys 24 Tissue homogeniser, Bertin Instruments) in two circles of 15 seconds at 6000 x g until the sample was fully dissolved. Tubes were then centrifuged (14,000 x g for 10 min at 4°C) and diluted to 1 mg frozen homogenate extract /mL PCA in 500 µL aliquots. Dissolved samples were analysed on the same day.

2.5.1.6 Neutralisation of PCA extracts and standards

400 µL of ATP and ADP standards and ice-cold PCA extracted samples had their pH adjusted to 6.5-7.5 by addition of ice-cold KOH solution (containing MOPS as a pH buffering agent) of about 110 µL for cell samples and 135 µL for standards and tissue extracts. Each tube was vortexed immediately after KOH addition for 5 s until formation of a white precipitate ($KClO_4$). Samples were placed back on ice to allow the precipitate to settle. The pH of the neutralised supernatant was tested by pipetting 2 µL of each sample onto pH indicator strips (Sigma, pH 4.5-10.0). If a sample remained too acidic, a further 2-10 µL of KOH was added, the sample vortexed and the pH re-checked. This step was repeated until the optimum pH was achieved. After neutralization was confirmed, the white $KClO_4$ precipitate in all samples was pelleted by centrifugation (3,000 x g for 1 min at 4°C) and supernatants were stored on ice. The volume of added KOH was noted to enable later calculation of accurate nucleotide concentrations.

2.5.1.7 ATP/ADP measurements

Light emission from the luciferase/luciferin reaction in the presence of ATP (from standards and extracts) was recorded using a luminometer (Berthold Technologies AutoLumat LB 953 Multi-Tube luminometer; software: Eg&g Berthold Tubemaster Version 1.0 (1997-99)) fitted

with an autoinjector to deliver the luciferase/luciferin solution to individual tubes. Samples were loaded in luminometer tubes (Sarstedt Röhren tubes (5 mL, 75 X 12 mm, PS)). TA buffer (400 µL) was added to all luminometer tubes (and maintained at RT) before sample additions, as follows:

- ATP measurement in ATP standards: neutralised ATP standard supernatant (100 µL) was added to TA buffer (400 µL) in luminometer tubes (in duplicate or triplicate);
- ATP measurement in samples: neutralised sample supernatant (100 µL) was added to TA buffer (400 µL) in luminometer tubes;
- ADP - ATP measurement in ADP standards: neutralised ADP standard supernatant (100 µL) was added to TA buffer (400 µL) in luminometer tubes (in duplicate). PK/PEP cocktail (10 µL) to be added later to convert the ADP to ATP;
- ADP - ATP measurements in samples: neutralised sample supernatant (250 µL) was added to 2X ATP sulfurylase assay buffer (250 µL), vortexed briefly and incubated at 30°C for 20 min with gentle shaking. Samples were centrifuged (17,000 x g for 1 min at RT), boiled at 100°C for 5 min and cooled on ice. ATP sulfurylase-treated sample (the ATP should now be degraded) (200 µL) was added to TA buffer (400 µL) in luminometer tubes (in duplicate). PK/PEP cocktail (10 µL) to be added later to one of the duplicate tubes to convert the ADP to ATP. The other duplicate tube (without addition of PK/PEP cocktail) served as an ATP 'blank' value.

The autoinjector was washed (6 x 100 µL injections) with 0.5 M HCl, then washed with 0.5 M NaOH and finally washed three times with MQ H_2O. The washings (collected in luminometer tubes) were discarded. Just before running the samples, the autoinjector was primed (6 x 100 µL injections) with freshly made Luciferase/Luciferin mix. The mix was collected in a clean luminometer tube and recycled back into the working stock Falcon tube for use in the assay.

Sample running:

Prepared luminometer tubes containing samples and standards were placed in the luminometer. PK/PEP cocktail (10 µL) was added to all tubes requiring an ADP to ATP conversion. The tubes were mixed gently and placed back in the luminometer in the correct order. All tubes were incubated in the luminometer for 30 min at 30°C to allow the ADP to ATP conversion to proceed. The assay was commenced with the following settings: read time: 30 s, background read time: 5 s, cycle time: 40 s, post-injection delay: 5 s, total time: 80 s, temp.: 30°C, injection vol.: 100 µL.

Emitted light, recorded as Relative Light Units (RLU) was analysed using Microsoft Excel and GraphPad Prism 5.0. Volume-corrected ATP standard curve values (nmol ATP/tube) were plotted against corresponding RLU values (expressed as mean and range/SEM of duplicates/triplicates). A linear regression was performed to assess the linearity of the standard. Then the RLU values of the samples (for ATP and ATP 'blank' measurements) were plotted against the standard curve and unknown values (in nmol/mg or 10,000 cells) were calculated from a linear regression analysis. Finally, the ratio of ATP/ADP in the samples was calculated as follows: Sample ATP values/ (Sample ADP values–Sample ATP 'blank' values).

2.5.2 Succinate

2.5.2.1 Ischaemic treatment of cardiomyocytes for metabolomic analysis

Cardiomyocytes were plated at 100,000 cells/well on 60 mm glass dishes or at 50,000 cells/40 mm diameter dish and incubated overnight in M199 medium. Media was aspirated and the cells washed once with pre-warmed PBS. The solution was then replaced with 2 or 1 mL Tyrode's buffer and tested compound in 1 µL DMSO or vehicle control (DMSO) was added. Cells were incubated for varied time points of ischaemia prior to extraction. With plates in the anoxic chamber, 1000 µL supernatant was removed for extraction and cells washed once with PBS. 1 mL MS extraction buffer (30% acetonitrile, 50% methanol, 20% water) was added to the plates. After 5 min of incubation, the cells were placed on dry ice outside the chamber. Cells on a control plate or in reperfusion experiments were washed and same volumes of MS extraction buffer was added in the same way.

2.5.2.2 Extraction of cells for LC/MS-MS

To extract metabolites from cell samples and quantify them using LC/MS-MS, I used an acetonitrile and methanol-based approach to deproteinise the samples and obtain isolated metabolites, which were run on a LC/MS-MS and quantified against standard curves.

Succinate was extracted from cell samples that were treated as described above. After MS extraction buffer had been added to the plates, they were incubated on dry ice for 15 min. 20 µL internal standard (retrieved from Dr. Hiran Prag, MRC Mitochondrial Biology Unit, Cambridge) was added onto the plates, the cells scraped from the plate surface with a plastic cell scraper and lysate was transferred to 1.5 mL Eppendorf tubes. The tubes were then placed

on a Thermoshaker for 15 min, 4°C at 1400 rpm. The cell suspensions were next incubated at -20°C for 1 h, prior to centrifugation at 17, 000 x g, 10 min, 4°C. The resulting supernatant was centrifuged again at the same conditions and transferred to mass spectrometry eligible glass vials (1.5 mL screw cap, clear glass vials, Shimadzu). The vials were labelled and stored at -80°C (for up to 1 month) before analysed by LC-MS/MS.

For the extraction of incubated cell supernatant, 1000 µL supernatant was centrifuged at 17, 000 x g, 10 min, 4°C before 50 µL the supernatant transferred to 1.5 mL Eppendorf tubes containing 750 µL MS extraction buffer and 20 µL internal standard. The supernatants were then processed as described above (15 min incubation at 4°C, 1 h incubation at -20°C, centrifugation).

2.5.2.3 LC/MS-MS of succinate

LC-MS/MS analysis of succinate was performed using an LCMS-8060 mass spectrometer (Shimadzu, UK) with a Nexera X2 UHPLC system (Shimadzu, UK). Samples were stored in a refrigerated autosampler (4°C) upon injection of 5 µL into a 15 µL flow through needle. Separation was achieved using a SeQuantr ZICr-HILIC column (30°C column temperature; MerckMillipore, UK). A flow rate of 200 µL/min was used. The mass spectrometer was operated by Dr. Hiran Prag (MRC Mitochondrial Biology Unit, University of Cambridge) who acquired spectra using Labsolutions software (Shimadzu, UK) and calculated succinate concentrations from standard curves in MS extraction buffer.

2.5.3 Lactate measurements

Lactate was measured in cell supernatants or in cell pellets concentrations using the colorimetric Abcam Lactate Assay Kit (ab65331). Cells were plated at 100,000 cells/plate and subjected to different experimental conditions of anoxia and/or reperfusion. 1000 µL supernatant were collected from the samples and then spun for 10 min at 1000 x g at 4°C before further analysis. For analysis of the intracellular lactate content, the cardiomyocytes were washed and lysed in 200 µL Assay buffer/100,000 cells by scraping them down and repeating three freeze/thaw cycles and vigorous vortexing in between these cycles. The samples were spun down for 2 min at 14,000 x g at 4°C and the supernatant kept for deproteinization. Therefore, 25 µL 5 M perchloric acid were added to each tube, followed by 47 µL of 3 M potassium hydroxide to neutralise the samples. After spinning for 5 min at 14,000

x g at 4°C, the supernatant was used to determine lactate concentrations using the Abcam Lactate Assay Kit according to the manufacturer's instructions.
Therefore, according to the manual instructions, a standard curve was prepared via serial dilution of the kit's standard concentrate in Assay buffer to concentrations between 0 and 10 nM. 50 µL of each standard, blank or sample were pipetted into a CoStar 96-well plate in triplicates. Then, a reaction master mix was prepared containing 46 µL Assay buffer, 2 µL Substrate mix and 2 µL Enzyme mix per reaction. 50 µL of this master mix were added to each well and the reaction was incubated for 30 min at 400 rpm at room temperature. The output was measured on a microplate reader (CLARIOStar *PLUS*, BMG Labtech) at OD 450 nm.

2.6 DNA Analysis

2.6.1 DNA extraction

DNA was extracted from whole cells (100,000 per sample) or tissue (5 mg) using the QIAmp DNA Blood and Tissue Mini Kit (#69504, QIAGEN, UK) according to the manufacturer's instructions. For DNA extraction from cell supernatant, cytosolic fractions, serum or urine samples, the QIAmp DNA Blood Mini Kit (#51104, QIAGEN, UK) was used. In this case, liquid samples were spun for 5 min at 1000 x g and the supernatant again for 10 min at 13,000 x g before DNA extraction.
For extraction from cell supernatant, cytosolic fractions, serum or urine samples, 20 µL proteinase K mixture from the kit were added to 200 µL sample and incubated for 10 min at 56°C on a heat block (Thermo Fisher) before continuing with DNA extraction via ethanol precipitation as described below.
In order to extract DNA from whole cell or tissue samples, 20 µL proteinase K mixture was added to each sample and 180 µL of the kit's lysis buffer ATL and incubated at 56°C until fully lysed or up to 2 h.
Afterwards, 200 µL 100% ethanol were added and vortexed. The sample was then transferred onto QIAmp Mini spin columns and spun down for 1 min at 14,000 x g. The flow through was discarded and 700 µl washing buffer AW1 added to the column. After spinning this again and

discarding the flow through, 700 µL washing buffer AW2 were added. The columns were then spun twice to remove all residual ethanol.
DNA was eluted in buffer EA as follows: 30 µL was added to the column for cells, supernatant, cytosol, serum or urine samples and 100 µl for cells or tissues. The elution buffer was incubated on the column for 2 min before the column was spun for 1 min at 14,000 x g and the flow through was collected in a fresh Eppendorff tube.
DNA concentrations were measured using Nanodrop 2000 (Thermo Scientific, UK) and diluted in TE buffer (Tris-EDTA:10 mM Tris-Cl, 1 mM EDTA, pH 8; form the QIAGEN kits) to 1 ng/µL or 3 ng/µL dependent on the desired experiment. Extracted DNA was stored at -20°C until further analysis.

2.6.2 Measuring Damage to mtDNA

2.6.2.1 8-OHdG quantification

Reperfusion upon ischaemia leads to excessive ROS production. DNA is one of the main targets of oxidative attacks, and it is widely thought that continuous oxidative damage to DNA is a significant contributor to development of cancers and elevated immune responses. Among numerous types of oxidative DNA damage, the formation of 8-hydroxydeoxyguanosine (8-OHdG), an oxidised modification at guanine bases in DNA, is a ubiquitous marker of oxidative stress. During the repair of damaged DNA *in vivo* by exonucleases, the resulting 8-OHdG is excreted without further metabolism into urine. In order to measure oxidative damage to DNA upon IRI in isolated cardiomyocytes, I utilised the OxiSelect Oxidative DNA Damage ELISA Kit (Cell Biolabs, Inc., USA), which is a competitive enzyme immunoassay in which the quantity of 8-OHdG is determined by comparing its absorbance with that of a known 8-OHdG standard curve.

The assay was performed following the manufacturer's instructions. First, standards were prepared freshly by serial dilutions to generate standard curves in a range from 0 to 20 ng/mL. Next, 50 µL standards, samples, controls or blanks were added to the 8-OHdG conjugate coated plate in triplicates and incubated for 10 min at room temperature, 400 rpm. Then, 50 µL anti-8-OHdG antibody were added to each well and incubate at room temperature for 1 h at 400 rpm.

After that, the plate was washed three times with 300 µl washing buffer, before 100 µL secondary antibody were added and incubated for 1 h at room temperature at 400 rpm. After washing three times, 100 µL of substrate solution were added and incubated for 30 min at room temperature, 400 rpm. Finally, 100 µL stop solution is added and the absorbance at 450 nm measured within one hour using a microplate reader (SpectraMax. Plus 384 Microplate Reader, Molecular Devices, UK). 8-OHdG concentrations were quantified against a standard curve calculated from the linear regression of the absorbance of the standards at known concentrations.

2.6.2.2 QPCR assay to measure oxidative damage on mtDNA

Damage to mtDNA can be assessed using a quantitative PCR method. Some types of oxidative damage to DNA, such as strand breaks, and some oxidised bases, can block the progression of the polymerase during PCR. For a given target sequence, any damage of this kind results in a reduction in amplification. By controlling the number of cycles in the PCR to ensure that the reaction remains within a linear amplification phase, the amount of product at the end of the reaction is proportional to the starting template amount. This allows for comparison of DNA damage between different samples. A long target (~10 kb) is used to assess mtDNA damage, and a short (≥200 bp) target is used to control for fluctuations in mtDNA copy number.

DNA, which has been extracted and diluted to 3 ng/µL as previously described, was amplified using the TaKaRa LA Taq PCR kit (New England Biolabs), which lacks proof reading activity. Primers were ordered from Sigma Aldrich. Sequences are described table 2.3.

Each sample was amplified in duplicates, along with a control containing 50% DNA (dilution of one of the control samples) and a non-template control (using H_2O in place of DNA template).

Each PCR reaction was a total of 40 µL, consisting of 15 ng (5 µL) DNA template and 35 µL PCR mastermix containing 1U TaKaRa LA Taq. The mastermix was made up as described in table 2.2.

Table 2.2: Composition of a mastermix reaction for the oxidative damage qPCR assay. All reagents were obtained from the TaKaRa LA Taq kit (Takara, Japan). The water utilised was nuclease-free water (Invitrogen, UK).

Reagent	Stock	1 reaction [µL]	Final concentration
Buffer	10 X	5	1.25 X
BSA	10 mg/mL	0.5	125 ng/µL
dNTPs	10 mM	1	0.25 mM
FWD primer	10 µM	2	0.5 µM
REV primer	10 µM	2	0.5 µM
Mg^{2+}	25 mM	2	1.25 mM
Taq polymerase	25 U	0.2	0.125 U
H_2O	-	22.3	-
Total	-	35	-

Table 2.4: DNA sequences of primer pairs used for the qPCR assay in mouse, pig and human samples. Primers were previously designed by former lab members Dr. Angela Logan and Dr. Anna Dare.

Primer	DNA Sequence
Mouse_FWD	5'-GCC AGC CTG ACC CAT AGC CAT AAT-3'
Mouse_REV SHORT	5'- GCC GGC TGC GTA TTC TAC GTT A -3'
Mouse_REV LONG	5'-GAG AGA TTT TAT GGG TGT AAT GCG G-3'
Pig_FWD SHORT	5'- CAA CCG CAT CGG AGA CAT TGG -3'
Pig_FWD LONG	5'- TCA GGA CAC CCA AAT GGT GCA A -3'
Pig_REV	5'- TGC TGA GGG CAA TCA GGG ATG -3'
Human_FWD SHORT	5'-CCC CAC AAA CCC CAT TAC TAA ACC CA-3'
Human_FWD LONG	5'- TCT AAG CCT CCT TAT TCG AGC CGA-3'
Human_REV	5'-TTT CAT CAT GCG GAG ATG TTG GAT GG-3'

Parameters for the short mitochondrial target are:

- X cycles of (x = 16 for mouse, 16 for pig and 18 for human samples):
  - 30 seconds at 94°C
  - 45 seconds at 64°C
  - 45 seconds at 72°C
- followed by 10 min at 72°C.

Parameters for the long mitochondrial target are:

- one minute at 94°C,
- Y cycles of (y = 18 for mouse, 18 for pig and 20 for human samples):
  - 15 seconds at 94°C
  - 12 min at 64°C
- followed by 10 min at 72°C.

Where X and Y are the number of cycles where the PCR is linear i.e. amplification of the 50% control yields ~50% product as the 100% sample (40-60% is considered linear). This has been determined using control samples before the start of the experiments.

As described below, PCR products were quantified using the PicoGreen assay (Invitrogen, UK) and run on a 0.8% agarose gel to check that products are of the expected size.
Each sample was corrected to the non-template control. Amplification of the long target was then normalised to amplification of the short target, and amplification relative to an untreated control was calculated for each sample.

2.6.2.3 Gel electrophoresis

To confirm the products amplified by PCR were of the correct size, electrophoresis was performed. Therefore, 10 µL of the amplified DNA samples were mixed with 2 µL loading dye (6x stock: 0.25% (w/v) bromophenol blue, 0.25% (w/v) xylene cyanol FF, 30% (w/v) glycerol in H_2O; New England Biolabs, UK) were loaded on to a 1% (w/v) agarose gel in 100 mL TBE buffer (100 mM Tris base, 100 mM Boric acid, 2 mM Na_2EDTA) supplemented with

5 µL GelRed™ (Invitrogen, UK). Two separate ladders were run with the gel. A 1 Kb and a 100 bp ladder (both from New England Biolabs, UK), for this, 1 µl ladder was mixed with 1 µL loading dye and 8 µL nuclease-free water (Invitrogen, UK). The samples were separated by running the gel in TBE buffer for approximately 60 min at 100 V. The gel was visualised on a UV transilluminator and photographed with ImageLab software.

2.6.2.4 PicoGreen Assay for DNA quantification

PCR products were quantified by PicoGreen assay (Invitrogen, UK). For this, a standard curve was prepared freshly each time via serial dilution of lambda DNA at a known concentration in TE buffer (Tris-EDTA:10 mM Tris-Cl, 1 mM EDTA, pH 8; provided in the assay kit). 10 µL standard, sample or blank were pipetted in triplicates into a 96-well plate (CoStar) and 90 µL TE buffer was added to each well. 200X PicoGreen dye was diluted 1:200 in TE buffer and 100 µL dye dilution was added to each well. The plate was incubated at room temperature at 400 rpm protected from light for 4 min before fluorescence was measured at excitation/emission 488/515 nm using a microplate reader (SpectraMax. Plus 384 Microplate Reader, Molecular Devices, UK). The final concentration of standards was between 0-500 ng/mL and a linear regression standard curve was calculated using Excel. Sample DNA concentrations were quantified against this standard curve.

2.6.3 Droplet digital PCR

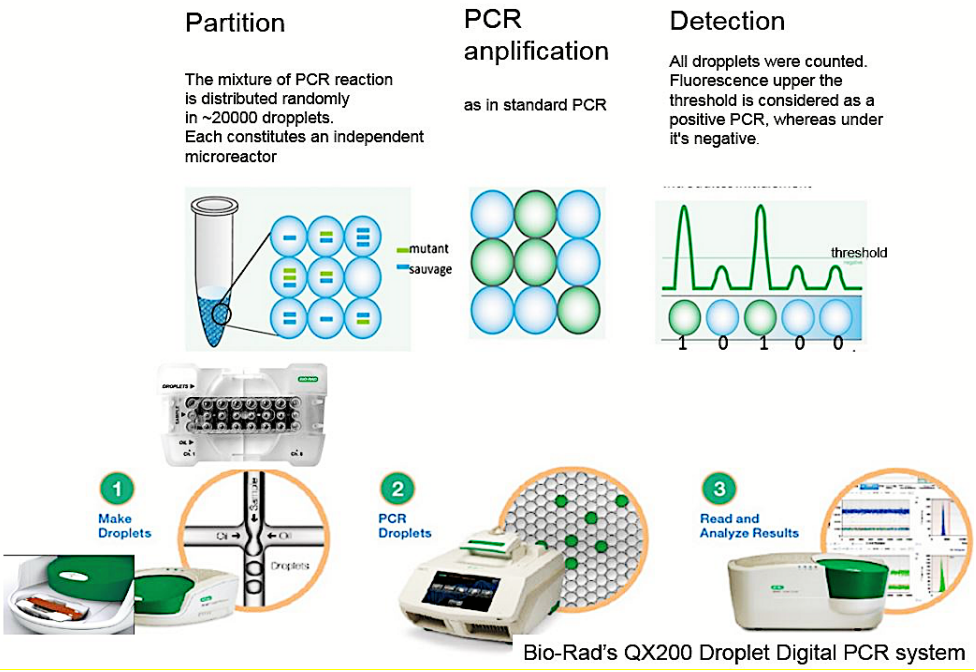

Figure 2.5: Schematic overview of droplet digital PCR. First, sample and mastermix are distributed into oil droplets, the PCR is then amplified and probe fluorescence measured. This is quantified against the number of droplets using Quantilife software. Adapted from BIORAD.com.

Droplet digital PCR (ddPCR) is a highly sensitive approach to reliably measure small amounts of DNA. In this method, the PCR reaction is performed first and the amplicons are separated into thousands of droplets by spraying the mastermix into oil, forming an emulsion with oil droplets and PCR mix. Each oil droplet contains its own real-time PCR reaction and the droplets are quantified as positive or negative for the reaction. This enables immediate quantification when the amount of used DNA is known.

Small amounts of free circulating DNA were measured using droplet digital polymerase chain reaction (ddPCR). Serum samples were spun for 10 min at 1600 x g. The supernatant was then spun for 10 min at 16,000 x g before DNA was isolated using the DNeasy Blood kit (QIAGEN) without cell lysis with buffer GQ. DNA was quantified with 'Nanodrop' and diluted to 1 ng/µL for this assay. Primers and probes were ordered from Sigma (tables 2.4 & 2.5; murine nuclear beta-actin FAM and mitochondrial ND5 HEX, or human ND1 FAM and RNaseP HEX). Each PCR reaction was a total of 22 µL, consisting of 1 ng DNA template (1 µL), 21 µL PCR

mastermix including primers, probes and 1U Taq (table 2.6). In each PCR reaction, a mitochondrial and a nuclear gene were amplified to enable direct comparison within each sample of mitochondrial to nuclear DNA. The BIORAD ddPCR Automated Droplet Generator was used to generate ddPCR droplets according to the manufacturer's instructions and the plate sealed at 174°C before the PCR has been run within 2 h of droplet generation.
The parameters for the PCR are as described below:

- 40 cycles of:
  - 30 seconds at 94°C
  - 45 seconds at 64°C
  - 45 seconds at 72°C
- followed by 10 min at 72°C.

After completion of the program, the droplets were read within 2 days. The plate was placed into the BIORAD Droplet Reader and the fluorescence of the real-time PCR probes was measured. The results were analysed using the BIORAD Quantilife software.

Table 2.5: ddPCR primer sequences. FWD= forward primer, REV= reverse primer**.**

Primer	Sequence 5'- 3'
FWD murine HEX_ND5	CTGCTCTTTCCCAGACGAGG
REV murine HEX_ND5	AAGGCCACTTATCACCAGC
FWD murine FAM_ßactin	ACCTAATTAAACACATCAACTTCCC
REV murine FAM_ßactin	GACTCAGTGCCAGGTTGTAA
FWD human HEX_RNaseP	AGATTTGGACCTGCGAGCG
REV human HEX_RNaseP	GAGCGGCTGTCTCCACAAGT
FWD human FAM_ND1	CGAGCAGTAGCCCAAACAAT
REV human FAM_ND1	CGGTTGGTCTCTGCTAGTGT

Table 2.6: ddPCR probe sequences.

Probe	Sequence 5'- 3'
murine HEX_ND5	ACACCACCACATCAATCAAATTCTCCTTCA
murine FAM_ßactin	ATTGCCTTTCTGACTAGGTG
human HEX_RNaseP	CCAGAGGCGGCCCTAACAGGGC
human FAM_ND1	CCTGCCATCATGACCCTTGGCCA

Table 2.7: Composition of ddPCR mastermix. Probes and primers were ordered from Sigma, UK. The ddPCR Supermix for probes (no dUTP), containing buffer, dNTPs and Taq enzyme, was obtained from BIORAD (#1863024, BIORAD, UK).

	Stock	1 reaction (µl)	final conc.
Buffer	10 X	5	x1
HEX Probe	10 mg/mL	0.5	100 ng/µL
FAM Probe	10 mM	1	200 µM
F primer HEX	10 µM	2	20 pmol
R primer HEX	10 µM	2	20 pmol
F primer FAM	10 µM	2	20 pmol
R primer FAM	10 µM	2	20 pmol
H_20	-	22.3	-
total		21	

2.6.4 Pyrosequencing

In order to analyse in detail the mitochondrial genotype of mouse samples for BL6/NZB versus BL6/J in preparation for future experiments including this conplastic mouse line, pyrosequencing was performed. In this method, a short DNA fragment is amplified via PCR using biotinylated primers. This biotinylation is used to bind the DNA fragments to streptavidin covered beads and to sequence it using labelled DNA bases that are attached to the template fragment. This sequencing method is quick and cheap due to the fact that a single short template of DNA is sequenced, and it is more sensitive and accurate than common PCR to genotype mouse strains.

DNA was extracted from tissue or blood as described before and a 150 base pair fragment of mitochondrial gene ND1 was amplified using the QIAGEN Pyromark PCR kit (#978705).

Primers (table 2.7) have been designed and ordered by Dr. Stephen Burr (Chinnery Lab). 5 µL DNA at 3 ng/µl were mixed with 22.5 µL PCR master mix (table 2.8) and run at following conditions:

- 45 cycles of:
  - 30 seconds at 95°C
  - 30 seconds at 54°C
  - 30 seconds at 72°C
- followed by 10 min at 72°C.

Table 2.8: Primer sequences for pyrosequencing of an ND1 template. Primers were obtained from Dr. Stephen Burr and ordered from Sigma-Aldrich, UK. FWD= forward primer, REV= reverse primer.

Primer	Sequence 5'- 3'
FWD ND1	CAG CCG CTA TTA AAG GTT CG
REV ND1	AGA GTG CGT CAT ATG TTG TTC

Figure 2.6: Composition of PCR mastermix for pyrosequencing of an ND1 template. Primers were obtained from Dr. Stephen Burr. Other components were included in the QIAGEN Pyromark PCR kit (#978705).

	Stock	1 reaction (µl)	final conc.
Master Mix	2 X	12.5	x1.1
Coralead concentrate	-	2.5	-
F primer biotinylated	10 µM	0.5	222 pmol
R primer	10 µM	0.5	222 pmol
H_20	-	6.5	-
total		22.5	

The PCR product was run on a 1.5% agarose gel to confirm that the PCR worked.

Next a 11 base long fragment covering a single nucleotide polymorphism of the BL6/NZB mitochondrial background in the ND1 gene was sequenced in a QIAGEN Pyromark Q48 sequencer.

The machine was set up, washed and primed first according to the manufacturer's instructions. Then, 10 µl PCR product and negative control (excluding DNA, to confirm specificity of detection) were mixed with 3 µl streptavidin beads (included in the Pyromark Kit) in wells of a PyroMark Q48 Disc (#974901). The disc was placed into the sequencing machine and the program set up by Dr. Stephen Burr used to sequence the DNA fragment. During this procedure, first, a NaCl degradation buffer washed off the antisense strand from the PCR product that is bound to the streptavidin beads via its biotinylated forward primer. In the next step, single bases were added, releasing light upon binding to the DNA strand. The luminescence was measured in the PyroMark Q48 and then analysed using the PyroMark Q48 autoprep software. If the DNA fragment contained a T, it was of a BL6/J background, a C was of an NZB background. An example is depicted in Figure 2.6.

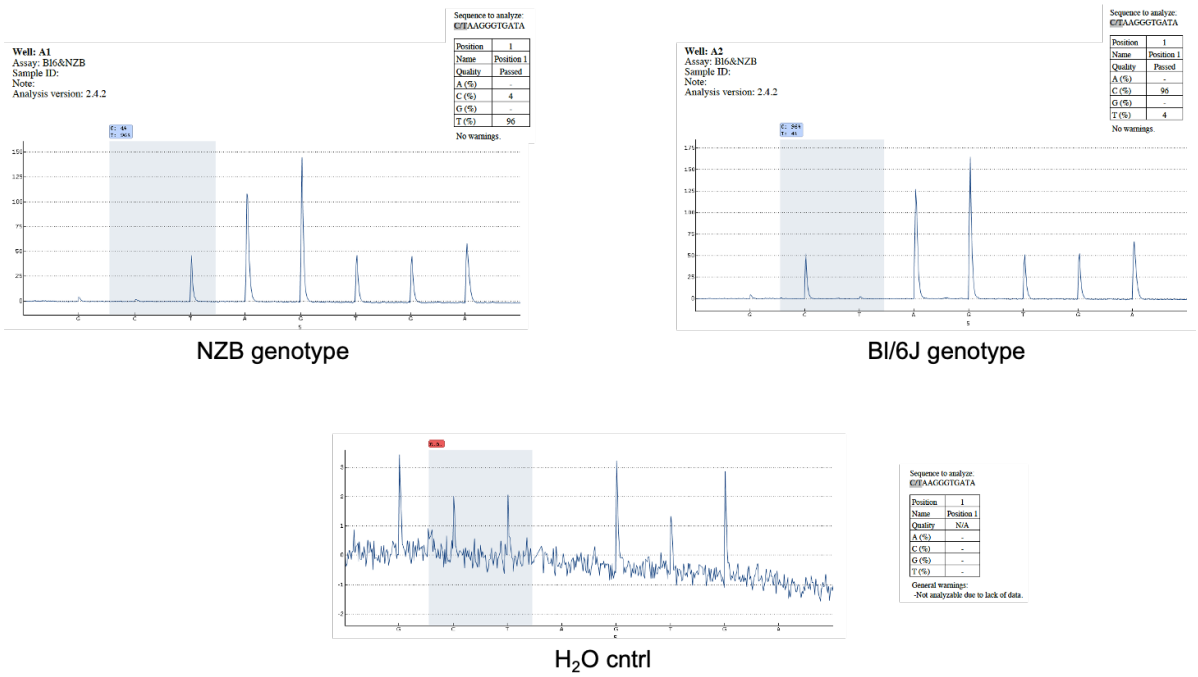

Figure 2.7: Representative data of C57BL/6 and NZB ND1 pyro sequences. The data represent sequences obtained after pyrosequencing, showing the SNP between NZB and BL/6J genome shown as different peaks in the grey box. Water control samples show no sequence.

2.7 Protein Analysis

2.7.1 Protein concentration assays

2.7.1.1 Protein extraction

Proteins were extracted from cells in order to analyse expression and localisation of target proteins. To evaluate that the digitonin cytosol extraction was effective, proteins were extracted from the remaining membrane pellets, quantified and analysed via Western blotting to ensure that mitochondrial fractions were intact in the pellet rather than released into the cytosolic fraction.

Cells, plated at 100,000 cells/plate, were lysed with radioimmunoprecipitation assay (RIPA) buffer. This lysis buffer contains of 10 mM Tris-Cl (pH 8.0), 1 mM ethylenediamine tetra-acetic acid (EDTA), 1% Triton X-100, 0.1% sodium deoxycholate, 0.1% sodium dodecyl sulfate (SDS), 140 mM NaCl and 1 tablet Complete protease inhibitor cocktail (Sigma-Aldrich).

Cells were washed once with ice cold phosphate buffered saline (PBS). Then 100 µL RIPA buffer/100,000 cells were added, the cells scraped with plastic cell scrapers while the plate was kept on ice, and the cell suspension was then transferred into 1.5 mL Eppendorff tubes. The samples were next incubated for 30 min on ice before spinning for 30 min at 14,000 x g at 4°C. The supernatant was transferred into fresh Eppendorff tubes and protein concentrations were determined as described below.

2.7.1.2 Bicinchoninic acid assay

Protein concentrations from previously described extracted protein samples were measured using the bicinchoninic acid (BCA) assay utilising the Pierce BCA Protein Assay Kit (ThermoScientific, UK). This is a colorimetric assay in which peptide bonds of the proteins react with BCA, which contains bicinchoninic acid, sodium carbonate, sodium bicarbonate, sodium tartrate and copper(II)sulfate pentahydrate.

The protein peptide bonds reduce Cu^{2+} ions from the copper(II)sulfate to Cu^{+}, proportionally to the protein concentration. The Cu^{+} ion forms a purple-coloured complex with bicinchoninic acid, which strongly absorbs light at a wavelength of 562 nm.

Standards were prepared with 2 mg/mL BSA in RIPA buffer serially diluted to concentrations between 0-2 mg/mL. 10 µL standard, blank or samples were pipetted in triplicates onto a 96-

well plate (Corning, CoStar). 200 µL BCA assay reagent (Reagent A (1% (w/v) BCA, 2% (w/v) Na_2CO_3, 0.16% (w/v) $Na_2C_4H_4O_6$, 0.4% (w/v) NaOH and 0.95% (w/v) $NaHCO_3$, pH 11.25) was mixed with
reagent B (4% (w/v) $CuSO_4.5H_2O$) in a 50:1 ratio) was added and incubated, protected from light, for 30 min at 37°C before the colour change intensity was measured in a microplate reader (SpectraMax. Plus 384 Microplate Reader, Molecular Devices, UK) at 562 nm. A standard curve was calculated via linear regression and protein concentrations quantified against this.

2.7.1.3 ELISA: IFNβ, cGAMP, KIM, NGAL

Some protein levels have been measured using enzyme-linked immunosorbent assays (ELISA). This assay uses immunohistochemical properties of antibodies to visualise proteins in a concentration-dependent manner. For that, antibodies specific for the protein of interest are linked to a 96-well plate. Samples, standards or blanks are incubated on this plate overnight and during this, the proteins of interest bind to the antibodies on the plate. After washing off excessive samples, a horseradish peroxidase (HRP) linked secondary antibody is added. This binds the protein-bound primary antibody. Excessive secondary antibody is washed off and after addition of peroxidase substrate the amount of bound enzyme can be measured on a microplate reader as intensity of absorbance.
Specifically, the ELISA kits IFNβ (Mouse IFNβ Quantikine ELISA, R&D systems, UK), 2'3'-cGAMP (Mouse 2'3'-cGAMP ELISA Kit, Cayman chemical, USA), KIM-1 (Human TIM-1 (HAVCR1) ELISA Kit, Thermo Scientific, UK) and NGAL (Human NGAL ELISA Kit, Cohesion Bioscience, UK) have been used according to manufacturer's instructions.
The kits provide a plate with pre-attached primary antibodies, standards, controls, washing buffer, secondary antibody, HRP substrate and stop solution.
First, standards were prepared freshly in serial dilutions to generate standard curves in the sensitivity range recommended by the manufacturer (0-50 pg/mL β-IFN,0- 500 ng/mL 2'3'-cGAMP, 0-2000 pg/mL KIM-1, 0-80 ng/mL NGAL). Next, 50 µL standard, sample, control or blanks were added to the plate in triplicates and incubated overnight at 4°C, 400 rpm. After that, the plate was washed three times with 300 µL washing buffer, before the secondary antibody was added and incubated for 2 h at room temperature at 400 rpm. After washing three

times again, the HRP substrate solution was added and incubated protected from light for 45 min at room temperature, 400 rpm. Finally, a stop solution was added and the absorbance measured within one hour in a microplate reader (SpectraMax. Plus 384 Microplate Reader, Molecular Devices, UK) at 450 nm. Protein concentrations were quantified against a standard curve calculated from the linear regression of the absorbance of the standards at known concentrations.

2.7.2 Immunohistochemistry

2.7.2.1 Western Blot analysis

Proteins can be separated by their size on gels, because they move along electric current due to their negative charge. The bigger the protein, the less easily it moves through the pores in the gel. After separation of the proteins on a gel, they can be transferred onto a membrane and probed with antibodies. Antibodies are proteins that bind to a specific protein peptide sequence. In this assay, HRP-linked secondary antibody binds to the primary antibody can later be visualised after addition of its substrate (Burnette, 1981).

Protein concentrations were first determined via BCA assay as described above. 30 µg protein was then aliquoted, 8 µL 6 x Laemmli buffer (125 mM Tris (pH 6.8), 6% (w/v) sodium dodecyl sulphate (SDS), 40% (v/v) glycerol, 25 mg/mL bromophenol blue and 5% (v/v) β-Mercaptoethanol) was added and the volume topped up to 50 µL, before the samples were denatured by heating (95°C, 5 min) and left to cool at room temperature. Samples were briefly centrifuged before loading onto pre-cast MiniProtean 4-20% tris-glycine gels (8.6 x 6.7 x 0.1 cm; BioRad, UK). 5 µL molecular weight marker were also loaded (Precision Plus Protein Dual Color Standards; BioRad, UK). Proteins were electrophoresed using SDS-running buffer (25 mM Tris (pH 8.3), 192 mM glycine, 0.1% (w/v) SDS) at 110 V for ~1 h in a BioRadMiniProtean Tetra Vertical Electrophoresis cell (BioRad, UK) until the dye front had reached the bottom of the gel.

Proteins were transferred to a PVDF membrane (0.45 µm pore size, Immobilon-P PVDF Membrane; Merck Millipore, UK) for semi-dry transfer. The membranes were transferred using Trans-Blot Turbo™ Transfer packs (BIO-RAD: 1704157) at 2.5 A and 25 V (max) for 7 min in transfer buffer (25 mM Tris, 192 mM glycine, 20% (v/v) methanol, pH 8.4 (unadjusted) at 4°C).

The membrane was blocked in 100% Odyssey PBS blocking buffer (gentle shaking, 1 h, RT; LI-COR Biosciences, UK) before rinsing the membrane with PBST and incubating with primary antibodies in 4% blocking buffer/PBST (gentle shaking, 1 h at RT or overnight at 4°C). The membrane was washed in PBST (3 x 5 min) before incubating in the dark with secondary antibodies in 4% blocking buffer/PBST (gentle shaking, 1 h). After the secondary incubation, the membrane was washed firstly in PBST (gentle shaking, 2 x 5 min) before being washed in PBS alone (gentle shaking, 2 x 5 min) and developed using enhanced chemiluminescence (Amersham ECL Prime; GE Healthcare, UK) according to manufacturer's instructions.

2.7.2.2 Immunofluorescence

In order investigate mtDNA release into the cytosol after anoxia and reoxygenation, I performed immunofluorescence microscopy experiments. This method utilises the binding of antibodies to target proteins in cells immobilised on glass coverslips. Binding of a fluorescent secondary antibody allows visualisation and analysis of cellular localisation.

2.7.2.2.1 Coverslip and cell preparation

First, coverslips (25 mm diameter, Thermo Scientific, UK) were laminated with 5 mg/mL laminin (Laminin from Engelbreth-Holm-Swarm murine sarcoma basement membrane, Sigma-Aldrich, UK) diluted in water. Briefly, coverslips were incubated in 4 cm glass dishes covered with 1 mL of laminin solution for 1 h at 37°C, as described before for cardiomyocyte plates. Next, cardiomyocytes were plated onto these plates at 1,000,000 cells/plate and cultured at 37°C at 5% CO_2 overnight, before anoxia and reoxygenation experiments were performed as described before.

2.7.2.2.2 Fixation with paraformaldehyde

After treatment, cardiomyocytes on coverslips in glass dishes were washed twice with 1 mL PBS, before they were fixed with paraformaldehyde. 500 µL of ice cold 4% paraformaldehyde in PBS (pH 7.4) was added to the washed coverslips and incubated for 30 min at room temperature. Next, the paraformaldehyde solution was removed and the cells washed twice with 1 mL PBS.

2.7.2.2.3 Permeabilization

After fixation and washing, the cell membranes were permeabilised by adding 500 µL of 0.1% Triton X-100 in PBS onto the coverslips and 15 min incubation at room temperature. The Triton-X-100 was then removed and the cells washed again twice with 1 mL PBS.

2.7.2.2.4 Blocking

Before antibody treatment, the cells were blocked to reduce unspecific binding. Therefore, 500 µL of 2% BSA in PBS were added to the coverslips and incubated at room temperature for 60 min.

2.7.2.2.5 Immunostaining

After removal of the blocking solution, 500 µL primary antibodies, diluted in 0.1% BSA in PBS, were added to the coverslips and incubated for 3 h at room temperature or overnight at 4°C. The primary antibody solution was then removed and the cells were washed twice with 500 µL PBS.

Antibodies:

Primary:

1:500 anti-ds DNA, mouse from Abcam (ab27156)

1:500 anti-TOM20, rabbit from Cell Signalling Technology Inc. (mAb #42406)

Secondary:

1:1000 anti-mouse Goat/IgG Alexa Fluor 594 from ThermoFisher Scientific (AB_2762825)

1:1000 anti-mouse Donkey/IgG Alexa Fluor 488 from ThermoFisher Scientific (AB_2762833)

Next, the coverslips were incubated in 500 µL secondary antibodies, diluted in 0.1% BSA in PBS, for 1 h at room temperature, protected from light. Finally, the antibodies were removed

and the cells incubated with Hoechst dye (1:10,000 in PBS) for 15 min at room temperature, protected from light. The solution was then removed and the cells washed three times with 500 µL PBS.

2.7.2.2.6 Mounting

Finally, coverslips were mounted onto microscope slides (Thermo Scientific, UK). To do this, a drop of mounting medium (Thermo Scientific, UK) was added onto labelled microscope slides and coverslips carefully placed onto this, with the cells facing downwards into the mounting medium. The microscope slides were protected from light and let dry over night or for 4 h, before visualisation by fluorescence microscopy using the Zeiss LSM 880 confocal microscope. After analysis, slides were stored at 4°C.

2.8 Immunoactivation Assays

2.8.1 Macrophage activation

In order to investigate if ischaemia reperfusion injury can activate the immune response, I performed a macrophage activation assay. RAW264.7 murine macrophages were cultured on 96-well (CoStar) at a density of 10,000 cells/well in 180 µl culture medium and incubated with 20 µL supernatant from cardiomyocytes that had been subjected to anoxia and reoxygenation. After incubation for 24 h, the supernatant from RAW264.7 cells was retrieved and nitrite formation from nitric oxide measured via the Griess assay as an indication of cell activation.
To do that, Griess reagent (2.3 mL Phosphoric acid (85%), 1 g Sulfanilamide, 0.1 g Naphtylethylenediamine and 97.7 mL MilliQ water) was prepared and protected from light. A standard curve was prepared via serial dilution of sodium nitrite ($NaNO_2$) in culture medium in a range from 0 to 1000 µM. Next, culture medium blanks, standards and supernatant samples were pipetted in triplicates at 50 µL/well on a 96-well plate (CoStar). 50µL of Griess reagent were added on top of each sample and incubated for 10 min at room temperature at 200 x g, while protect from light. Finally, absorbance was measured at 540 nm in the reader machine (SpectraMax. Plus 384 Microplate Reader, Molecular Devices, UK).

2.8.2 HEK TLR9

In order to investigate immune responses via TLR9 activation, I utilised a HEK-BLUE TLR9 cell line from InvivoGen (HEK-BLUE mTLR9, #hkb-mtlr9, InvivoGen, France), which transiently expresses plasma membrane-localised TLR9, as well as SEAP (secreted embryonic alkaline phosphatase), a phosphatase that is expressed under a promotor activated upon NFκB stimulation after TLR9 activation. Therefore, activation of TLR9 will cause expression of this phosphatase. Incubated in a detection medium, phosphatase activity can be detected as a change of medium colour and quantified by measuring changes in absorbance at 625 nm.

HEK-BLUE TLR9 cells were cultured on 96-well plates (CoStar) at a density of 10,000 cells/well in 180 µL culture medium and incubated for 24 h with 20 µL supernatant from cardiomyocytes that had been subjected to anoxia and reoxygenation. As a positive control, HEK-BLUE TLR9 cells were incubated with a synthetic oligonucleotide containing a CpG motif known to activate TLR9 (ODN2006, #tlrl-2006, InvivoGen, France) and an antagonistic oligonucleotide of the potent inhibitory sequences are (TTAGGG) (ODN2088, #tlrl-2088, InvivoGen, France). Both were diluted in nuclease-free water and used at a final concentration of 1 µM. Wells containing medium only were used as blanks.

After incubation for 24 h, 100 µL supernatant from the cells were retrieved and transferred to a fresh 96-well plate, before 100 µl HEK-Blue Detection medium (#hb-det2, InvivoGen, France) were added and the plate incubated for 30 min at 37°C. Detection medium allows the detection of SEAP as the reporter protein is secreted by the HEK-BLUE cells into their supernatant and the medium contains a specific SEAP colour substrate. The hydrolysis of the substrate by SEAP produces a purple/blue colour that can be easily detected with the naked eye or measured with a spectrophotometer.

After 30 min incubation, absorbance was measured at 625 nm in a plate reader (SpectraMax. Plus 384 Microplate Reader, Molecular Devices, UK), an example is presented in Figure 2.7.

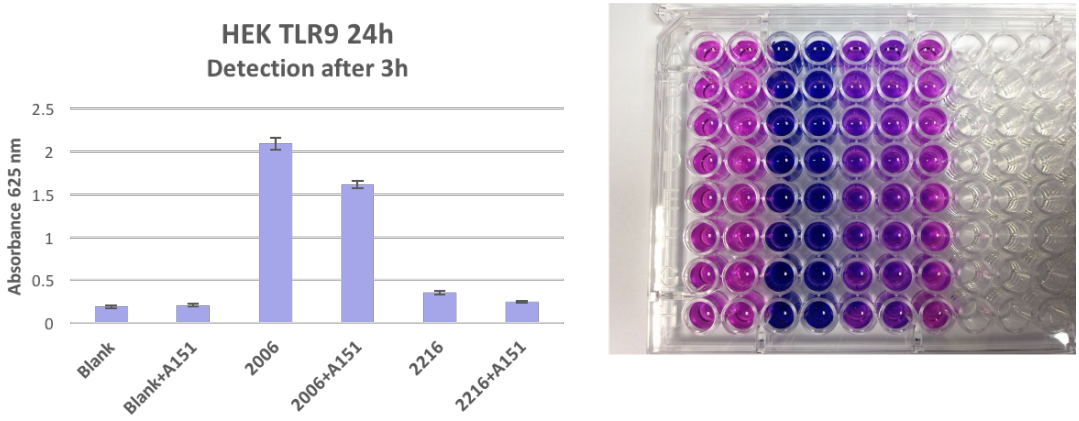

Figure 2.8: Picture of HEK-BLUE TLR9 cells after treatment with agonist and/or antagonist in detection medium. Absorbance was measured at 625 nm.

2.9 Statistics

Data presented in this thesis are represented as mean ± standard error of the mean (S.E.M.) or standard deviation (S.D.) as indicated, with 'n' values representing either the number of independent experiments or biological replicates as indicated in figure legends. Statistical analysis was performed using Prism 7.0 (GraphPad, USA). Comparisons between two datasets were assessed via two-tailed unpaired Student's t-tests, assuming equal variance. For comparison of multiple datasets, one or two-way ANOVA was used, with the appropriate correction for multiple comparisons. The p value, or associated probability, was considered significant if *$p<0.05$; **$p<0.01$; ***$p<0.001$, ****$p<0.0001$.

2.10 Collaborations

Where experiments have been conducted by or with collaborators, these are explicitly stated in the text and figure legend. *In vivo* experiments were conducted by Dr. Jack Martin (murine heart ischaemia and heterotopic heart transplantation), Dr. Timothy Beach (murine renal ischaemia and model for IRI), and Dr. Kourosh Saeb-Parsy (human heart tissue), all from the Department of Surgery, University of Cambridge, UK. Human liver transplantation and sample retrieval was performed by Dr. Ina Jochmans and colleagues at the University Hospital

in Leuven, Belgium. Partial nephrectomy surgery was undertaken by Prof. Grant Stuart and colleagues (Department of Surgery, University of Cambridge, UK). The murine LAD model was performed by Dr. Victoria Pell and Dr. John Mulvey in the lab of Dr Thomas Krieg (Department of Medicine, University of Cambridge, UK). *In vivo* work on *Trachemys scripta* red-eared slider turtles was performed by Dr. Amanda Bundgaard at the University of Aarhus, Denmark, and Drosophila melanogaster fruit flies were analysed with the help of with Dr. Federica De Lazzari (University of Padova, Italy).

Ex vivo experiments were conducted by Dr. Mazin Hamed and Dr. Kourosh Saeb-Parsy (porcine and human kidney perfusion), Mr. Stephen Large and Mr. Aravinda Page (porcine heart EVNP) at the Royal Papworth Hospital, Cambridge, UK and Prof. Chris Watson from the Department of Surgery, Cambridge, UK (human liver EVNP). Langendorff procedures on murine hearts were performed by Dr. Dunja Aksentijevic from the Queen Mary University, London, UK.

Other human organ samples were retrieved with the help of Dr. Krishnaa Mahbubani, Department of Surgery, Cambridge, UK.

Mice for cardiomyocyte isolation were provided by Ms Volha Sauchanka (Krieg Lab, Department of Medicine, University of Cambridge, UK).

ESC derived cardiomyocytes were generated in the lab of Dr. Sanjay Sinha and were cultured by Dr. Johannes Bargehr from the Department of Medicine, University of Cambridge, UK.

Access to the anoxic chamber was enabled by Prof. Judy Hirst and her Lab at the MRC Mitochondrial Biology Unit, University of Cambridge, UK.

LC-MS/MS metabolite analysis was performed by Dr. Hiran Prag (MRC Mitochondrial Biology Unit, University of Cambridge, UK).

Chapter 3

ATP/ADP ratios and adenosine nucleotide levels during ischaemia

3.1 Introduction

All life is possible due to energy storage in form of adenosine triphosphate (ATP), adenosine diphosphate (ADP) and adenosine monophosphate (AMP). For example, if the Δp is high and ADP is available, then the mitochondrial ATP synthase will use this Δp and an ADP plus Pi to produce ATP. The ATP is then rapidly transported out of mitochondria via the adenosine nucleotide transporter (ANT) in exchange for ADP. Therefore, a major way in which ATP is produced is within mitochondria where the reaction ADP + Pi <-> ATP favours the production of ATP. ATP can also be degraded when the ATP synthase in the inner mitochondrial membrane runs backwards and breaks down ATP to produce ADP and free phosphate (Pi). Another important reaction involved in ATP and ADP production is by the enzyme adenylate kinase which transfers a phosphate group from ATP onto AMP leading to the production of two ADP molecules. Depending on the availability of adenosine nucleotides in the cell this reaction can be shifted to favour the production of ADP, or ATP and AMP.

ATP is also generated in the cytosol by substrate-level phosphorylation during glycolysis as well as by oxidative phosphorylation and some tissues are glycolytically more active in the absence of oxygen, where pyruvate will be converted to lactate to enable glycolysis to continue. In contrast, for most aerobic cells glycolysis generates pyruvate, which is then transported into mitochondria to generate acetyl CoA by pyruvate dehydrogenase. This then leads onto activation of the Krebs cycle which then drive ATP synthesis by oxidative phosphorylation, thereby sustaining a high ATP/ADP ratio, which can be upregulated under conditions to respond to extra energy requirements such as exercise (Watt et al., 2010).

Depending on the metabolic state of the cell, the demand for ATP will alter potentially leading to an increase in production under aerobic conditions mainly via oxidative phosphorylation (OXPHOS), and for this, ATP production is tightly regulated to ensure that the cell can respond to increased energy demand. Much of the mitochondrially-produced ATP is transported into the cytosol, where it is used by a broad range of enzymes to enable the functioning of vital processes within the cell. This ATP is typically broken down to ADP, although for some enzymes AMP and pyrophosphate are produced. The balance between ATP and ADP pools is at the centre of energy production and is usually controlled by adapting mitochondrial and glycolytic ATP production to energy demands, in order to maintain a substantial ATP/ADP ratio. For example, in cells the ATP/ADP ratio varies from 10-20 in

isolated cells, dependent on the cell type. Furthermore, the ATP/ADP ratio can vary from 3-12 varying in different tissues. Tissues with a high energy demand such as the heart and skeletal muscle

usually maintain a high ATP/ADP ratio of around 6-12, while tissues with lower energy demand such as the kidney have lower ATP/ADP ratios of about 3-5 (table 3.1).

As shown in table 3.1, ATP and ADP values can be measured using a range of techniques, for example by chemiluminescence, by nuclear magnetic resonance (31P-NMR) spectroscopy, or by high- performance liquid chromatography (HPLC).

Table 3.1: Overview of adenosine nucleotides and ATP/ADP ratios in different tissues and species in the literature. HPLC= high- performance liquid chromatography, ATP=adenosine triphosphate, ADP= adenosine diphosphate, AMP= adenosine monophosphate.

SPECIES	TISSUE/CELL TYPE	ATP [µmol/ g]	ADP [µmol/ g]	RATIO	AMP [µmol/ g]	METHOD	IN VIVO/VITRO	REFERENCE
MURINE	HEPATOCYTES	2.4 mM	0.4 mM	6	-	LUMINESCENCE ASSAY	IN VITRO	(Kane et al., 1985)
MURINE	PANCREATIC ISLETS	-	-	8.6	-	LUMINESCENCE ASSAY	IN VITRO	(Schultz et al., 1993)
RAT	LIVER	12.4	3.19	3.9	0.58	ENZYMATICALLY	IN VITRO	(Soboll et al., 1978)
RAT	LIVER	6.73	3.09	2.27	0.59	HPLC	IN VITRO	(Zager et al., 1991)
RAT	KIDNEY	6.75	2.80	2.45	0.63	HPLC	IN VITRO	(Zager et al., 1991)
RAT	HEART	21.2	3.60	5.9	0.645	HPLC	IN VITRO	(Williams et al., 1996)
RAT	HEART	19.6	0.16	122.5	1.27 [nmol/ g]	31P-NMR	IN VITRO	(Williams et al., 1996)
RAT	LIVER	50	20	2.5	-	HPLC	IN VITRO	(Maida et al., 2016)
PORCINE	KIDNEY	-	-	0.23	-	LUMINESCENCE ASSAY KIT	IN VITRO	(Kay et al., 2011)
PORCINE	LIVER	2.25	-	-	-	ENZYMATIC ANALYSIS	IN VITRO	(Kang et al., 2018)
HUMAN	RED CELLS	3.64	-	-	-	LUMINESCENCE ASSAY KIT	IN VITRO	(Planker et al., 1983)
HUMAN	PANCREATIC ISLETS	7.1	3.27	2.17	-	ENZYMATIC ANALYSIS	IN VITRO	(Salehi, 2004)
HUMAN	MUSCLE	5.35 [µmol/ g]	5.18 [nmol/ g]	1033	-	31P-NMR	IN VIVO	(Wu et al., 2007)
HUMAN	LIVER	-	-	6.5	-	LUMINESCENCE ASSAY KIT	IN VITRO	(Bruinsma et al., 2016)
HUMAN	PANCREAS DBD	48.2 [µmol/ g]	-	-	-	LUMINESCENCE ASSAY KIT	IN VITRO	(Leemkuil et al., 2018)
HUMAN	PANCREAS DCD	8.4 [µmol/ g]	-	-	-	LUMINESCENCE ASSAY KIT	IN VITRO	(Leemkuil et al., 2018)

During conditions of increased work, when the consumption of ATP is elevated, or when glycolysis or OXPHOS cannot provide enough ATP to meet demand, then ADP will accumulate and the ATP/ADP ratio will decrease. This in turn regulates the activity of adenylate kinase which will respond by shifting the equilibrium of its reaction (2ADP <-> ATP + AMP) towards ATP production, with two ADP molecules being used to produce one ATP and one AMP molecule (Figure 3.1). In turn, the AMP pool will increase and will activate further downstream cellular processes, such as the energy sensor AMPK, thus activating a number of catabolic pathways in order to maintain the supply of ATP to the cell (Lindberg and Hansen, 1967) (Figure 3.1).

While the above reactions are operational there are a series of feedback mechanisms that act to maintain the ATP/ADP ratio. However, as AMP accumulates to a greater amount, it is broken down further in a series of degradation steps to adenosine and a further series of breakdown products. Some of these are shown in Figure 3.1: It can be seen that AMP is first broken down to adenosine by nucleotidases, and this adenosine is then deaminated by adenosine deaminase to produce inosine (Figure 3.1). Then, nucleoside phosphorylase breaks down inosine to form hypoxanthine. Finally, this purine is further degraded to xanthine, hypoxanthine and uric acid by the enzyme xanthine oxidoreductase. This degradation will occur under conditions such as ischaemia which are important to my consideration of the role of ATP/ADP in organ storage during transplantation.

While energy-dependent processes are driven by the ATP/ADP ratio, rather than the concentration of ATP per se, eventually if ADP is not available anymore, neither mitochondrial OXPHOS or glycolysis can produce any ATP and cells will not be able to maintain the ATP/ADP ratio, leading to energy dependent processes being defective and thus culminating in cell death. This mode of cell death can occur after energy depletion due to prolonged ischaemia.

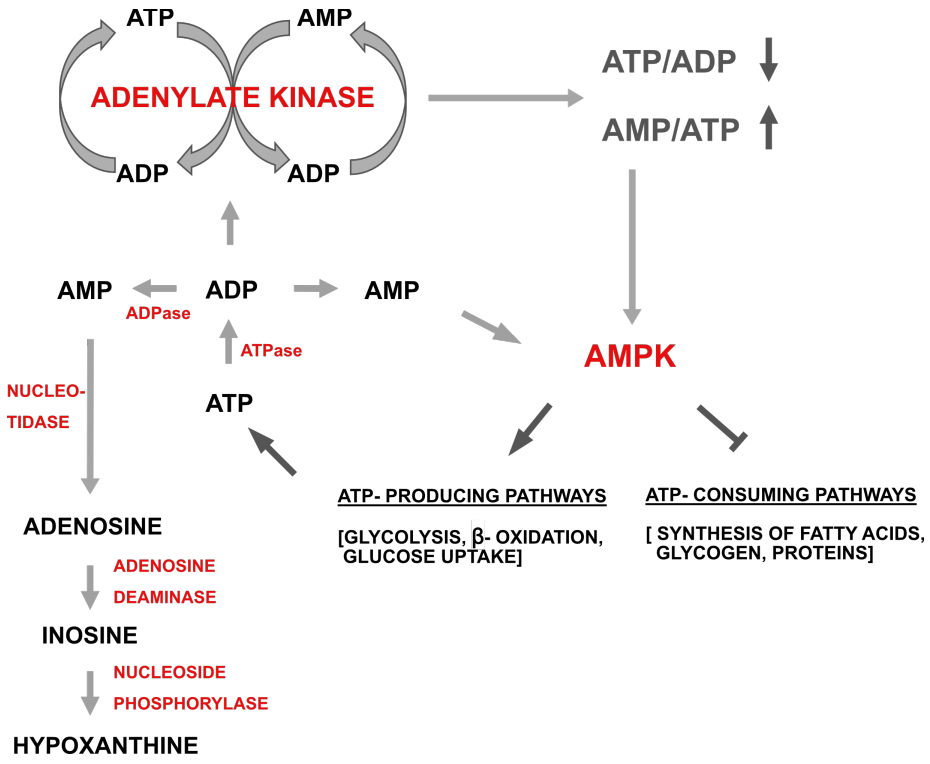

Figure 3.1: Schematic overview over ATP consumption, Adenylate kinase activity and AMPK activation. Increased ATP consumption causes elevated ADP levels. These shift the adenylate kinase reaction to produce ATP and AMP in the following way: 2 ADP -> ATP + AMP. During conditions of restricted ATP production, like ischaemia, this will lead to decreased ATP/ADP and increased AMP/ATP ratios. These in turn cause an activation of the AMP Kinase and downstream pathways which will promote ATP- producing processes and block ATP-consuming ones. ATP consumption results in increased ADP and AMP levels which in turn activate AMPK and adenylate kinase. AMP can further be degraded to adenosine, then by adenosine deaminase to inosine and finally by nucleoside phosphorylase to hypoxanthine. Enzymes are presented in red. ATP= adenosine triphosphate, ADP= adenosine diphosphate, AMP= adenosine monophosphate, AMPK= AMP Kinase.

This is in part because the lack of oxygen during ischaemia will block OXPHOS, as described in detail in the introduction. The only way to generate ATP under these circumstances of ischaemia is via anaerobic glycolysis. But during ischaemia there is no supply of glucose from the circulation and thus the cells can only use glycogen to supply glucose for glycolysis during ischaemia. Glycolysis can then continue to generate ATP within the cell until the glycogen stores are used up, or glycolysis is prevented, for example by the accumulation of NADH. However, once glycolysis stops, either because the cell has run out of glycogen, or because the flux through the pathway is blocked, then the ATP/ADP ratio and the adenosine nucleotide pools will start to decline leading to cell death. Upon reperfusion of

the tissue after ischaemia, the higher the ATP/ADP ratio and the bigger the pools of ATP and ADP, the more likely the tissue is to survive; therefore, it may be therapeutically beneficial to prevent the loss of adenosine nucleotide pools during ischaemia to assist tissue recovery upon reperfusion.

It is known that short periods of ischaemia and reperfusion before a severe heart attack or stroke improve patients' outcome but so far, the reason for this is not known. This so-called ischaemic preconditioning (IPC) has been shown to be an effective means of cardioprotection(Downey et al., 2007; Murry et al., 1986; Schott et al., 1990; Yang et al., 2010). IPC is the process of subjecting the heart to sub-lethal levels of ischaemia, then reperfusion, as a method of priming the organ against a subsequent, more pronounced ischaemic insult. Multiple cycles of ischaemia/reperfusion are administered, with 5 min ischaemia and reperfusion a common protocol for IPC, since the initial observations of its cardioprotective effects (Murry et al., 1986; Pell et al., 2018). IPC is a robust and species-independent method of cardioprotection, though the protective mechanism is not fully understood. There are many hypotheses trying to explain how this so-called ischaemic preconditioning (IPC) prevents ischaemia-reperfusion damage, e.g. increased antioxidant response due to small amounts of ROS released during reperfusion periods or increased adenosine nucleotide pools(Downey et al., 2007; Schott et al., 1990; Yang et al., 2010; Yellon and Downey, 2003). Furthermore, IPC induces a number of signalling pathways with activation of adenosine, bradykinin and opioid receptors leading to protein kinase C (PKC) activation. Phosphorylation of proteins by PKC, lead to the activation of PI3K and other survival pathways(Iliodromitis et al., 2007; Pickard et al., 2017). Thus, activation of these pathways leads to a therapeutic window, whereby reduced damage from subsequent IR events occurs. It is possible that IPC works via a combination of different processes that are activated due to the short periods of ischaemia and reperfusion but in order to fully understand this, further investigation is necessary and a detailed analysis of adenosine nucleotide pools in tissues after IPC might give insight into which molecular processes occur.

While we still lack understanding in how mammalian metabolism is affected by ischaemic periods and how IR injury can be prevented, another research approach to find therapeutic targets and investigate the underlying cellular processes, is to compare IRI in mammalian species to species that tolerate prolonged anoxia and hypoxia. Due to collaborations of the Murphy lab, here, I focus on the freshwater turtle species *Trachemys*

scripta as well as *Drosophila melanogaster*, which can survive for a prolonged period after reperfusion.

Trachemys scripta are highly anoxia-tolerant and can survive several weeks without oxygen at low temperatures (Bickler and Buck, 2007; Ultsch, 1989). Thereby, they rely on stored glycogen to produce energy via anaerobic glycolysis leading to increased lactate production (Ultsch, 2006; Warren et al., 2006). Interestingly, lactate accumulates first in cells allowing NAD+ regeneration, but is then exported to the blood plasma, where it is buffered by calcium carbonate that originates from the turtle shell. This is possible because the turtles maintain a low heart-beat allowing metabolite circulation even during prolonged anoxia (Jackson and Heisler, 1982; Warren et al., 2006). So far it is not known if other metabolic changes, like the accumulation of succinate, occur as well in this species and if turtles degrade their adenosine nucleotide pool to xanthine and hypoxanthine as described for mammals, or if they maintain a stable adenosine nucleotide pool throughout prolonged anoxia.

Drosophila melanogaster are a widely used biological tool especially due to their importance as genetic tool. This species can easily be genetically modified allowing the investigation of the role of single proteins in pathologies like IR injury. Interestingly, these flies tolerate prolonged hypoxia well. They can be maintained at 5% O_2 for hours without any immediate IR injury. 24 h later, these flies are hit by ischaemia reperfusion injury which is shown in decreased lifespan (Farahani and Haddad, 2003; Hanson et al., 2016). Although many pathways have been discovered that enhance the IR injury in flies, not much is known about why these flies tolerate prolonged hypoxia at all. Importantly, this species slows down their metabolism significantly during hypoxia and during anoxia is fully paralysed. During this time, they maintain energy levels utilising glycogen stores, which has been shown been shown by loss of intracellular glycogen via electron microscopy (Zhao and Haddad, 2011; Zhou et al., 2008). Upon reoxygenation, the flies awaken and maintain to survive without any immediate injury for 24 h. The metabolic changes and breakdown of adenosine nucleotides have not been investigated during anoxia and upon reoxygenation in this model so far and differences between this species and mammals might give rise to better understanding of crucial metabolic processes that cause IR injury.

To summarise, ongoing metabolic processes during ischaemia cause a decrease in ATP/ADP ratios and the loss of adenosine nucleotides. The ATP/ADP ratio decreases with the severity of the ischaemia and furthermore the ability to recover the ATP/ADP ratio upon reperfusion decreases. Thus, it is crucial to analyse the adenosine nucleotide pools and the ATP/ADP ratio,

rather than solely the amount of ATP that is available in order to understand energy demand and usage in tissue during ischaemia and during IR injury.

3.2 Aim

The aim of this part of my thesis is to investigate changes in ATP and ADP pools and in ATP/ADP ratios during ischaemia in different tissues from a number of different organisms during ischaemia at various temperatures. To do this, I utilised a chemiluminescence approach (see 2. Materials and methods) to measure the ATP and ADP levels in rapidly frozen samples from models of transplantation in murine and porcine hearts. Furthermore, I characterised the adenosine nucleotide pools in samples from hearts of human organ donors. To extend these findings, I also compare these results to turtle and fly samples to assess whether the decreases in ATP and ADP during prolonged ischaemia is conserved among different species. Finally, I also assessed how adenosine nucleotides change in a murine model for heart attack. These finding will help to understand whether loss of ATP and a decrease in ATP/ADP ratios is a universally conserved marker of ischaemia that can be used to analyse the severity of ischaemia.

3.3 Results

3.3.1 ATP degradation in samples during freezing and storage

The aim of this study was to determine ATP and ADP levels and calculate the ATP/ADP ratios in different tissues, to investigate their potential as a hallmark of ischaemia. The first step was to determine how tissue samples should be prepared and stored to minimise ATP and ATP degradation.

In order to determine the best way of freezing tissue samples, I first compared snap freezing (dropping tissue samples into liquid nitrogen) to clamp freezing (clamping the tissue between aluminium blocks that have been cooled in liquid nitrogen). These clamps, known as

Wollenberger clamps, should far more quickly freeze the tissue due to rapidly spreading the tissue as a thin layer over the surface of the cold metal, which has very good heat transfer. Heart tissue samples were cut into pieces of approximately 1x1 cm, because this size is small enough to freeze rapidly yet large enough to give enough tissue for several experiments. Samples that were simply snap frozen were transferred into pre- cooled vials, sealed and dropped into a Nalgene Dewar with 4 L liquid nitrogen. Although retrieving the samples and putting the vials into liquid nitrogen does not take longer than 30 seconds, we do not know how long it takes until the tissue is frozen to its core within the cryo- vial, as the heat transfer is slowed by the insulating plastic and air. In comparison, we also used pre- cooled Wollenberger clamps (see Figure 2.1). In this system, the tissue is rapidly flattened and frozen throughout within seconds on the surface of the metal. As shown in Figure 3.2 A, control samples from murine heart tissue, that were clamp frozen, have an ATP/ADP ratio of ~7 while snap-frozen heart tissue gave a ratio of ~2, this suggests that during the slower cooling via snap- freezing the sample loses ATP by hydrolysis as the tissue slowly freezes. This difference is especially visible following the nucleotide analysis (Figure 3.2 C). In comparison to the clamp frozen samples, there is a major reduction in ATP levels and a corresponding increase in those of ADP, leading to a large reduction in the measured ATP/ADP ratios in snap- frozen samples. Therefore, it is crucial to clamp freeze samples as quickly as possible because a delay in freezing already causes degradation of ATP due to residual enzymatic activities in the cooling tissue.

ATP is not likely to be stable long term in the acidic extracts used for the chemiluminescence analysis. Thus, after clamp- freezing, the tissue samples are then stored at -80°C and samples are only lysed in acid on the day the assay is run. This is done in a 5 M perchloric acid solution that denatures all the proteins. As determined in Figure 3.2 A, C; 3 months of storage of frozen tissue at -80°C causes some loss of ATP and a change in the ATP/ADP ratio. As expected, storage at higher temperatures leads to a bigger reduction in ATP levels and a more rapid decrease in the ratios (Figure 3.2 B, D) while lower temperatures can slow this degradative process down. Tissue that was rapidly retrieved and cooled down to various temperatures for 12 min before clamp- freezing maintained more adenosine nucleotides the colder the temperature was, with 4°C barely causing any loss of nucleotides.

All together, these results about the relative instability of ATP within samples leads to three important working principles: 1) all tissue samples should be analysed within three months of lysis and storage at -80°C; 2) all samples must be kept frozen at all times between first

sampling of the tissue until final analysis; 3) tissue samples have to be rapidly clamp- frozen in liquid nitrogen using Wollenberger clamps.

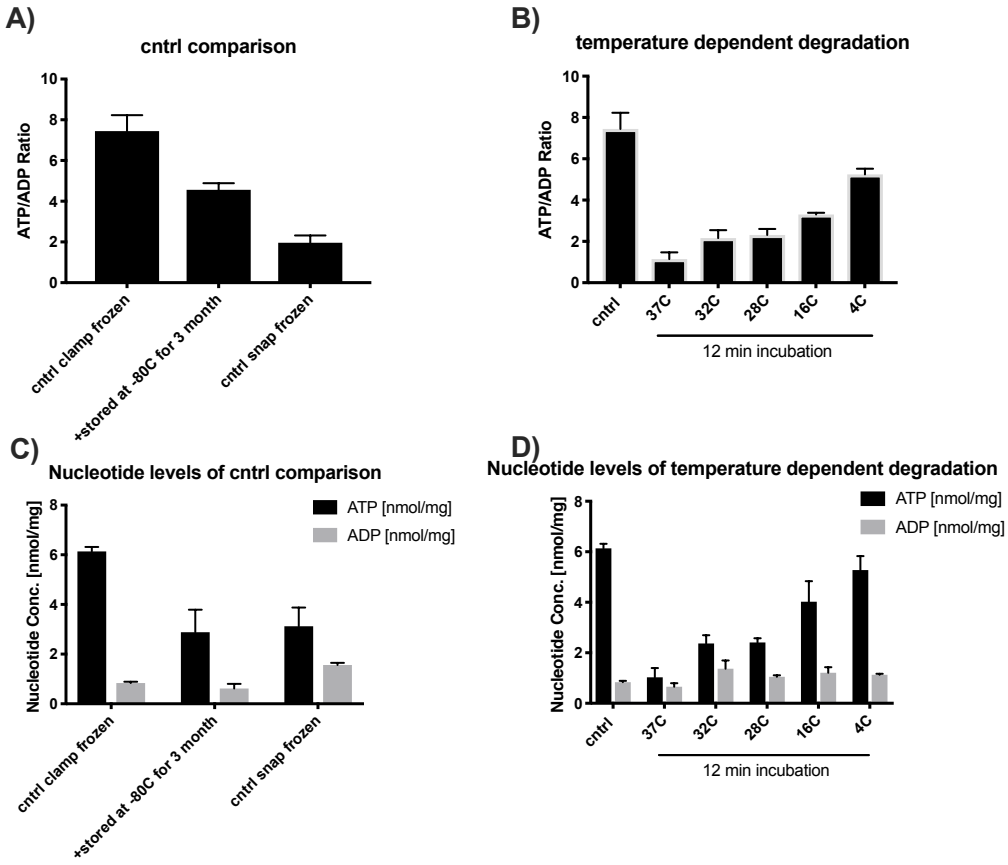

Figure 3.2: Degradation of adenosine nucleotides and decrease in the ATP/ADP ratios during tissue sample storage. Adenosine nucleotides were measured in heart tissues using a Luciferase luminescence assay. Murine heart samples were rapidly frozen using Wollenberger clamps or snap frozen in liquid nitrogen (A, C). These samples analysed 1 months after retrieval, or after storing them at -80°C for 3 months (A, C). Heart tissue was retrieved and rapidly transferred onto a heat block at various temperatures before being clamp frozen and lysed in perchloric acid before analysis (B, D). ATP and ADP were measured (C, D) and the change in adenosine nucleotides presented as ratio of ATP to ADP (A, B). Nucleotide concentrations are measured in nmol/mg. n= 2-4 biological replicates, data are mean ± S.D., no statistical analysis due to low number of samples.

3.3.2 Comparison of ATP and ADP levels in different human tissues

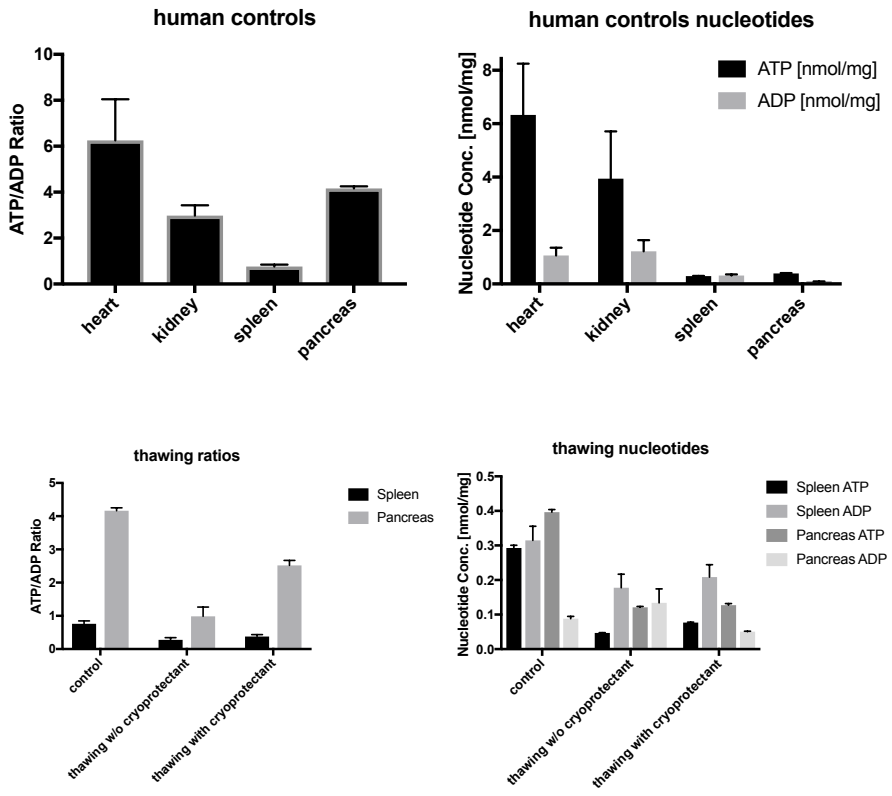

Figure 3.3: ATP/ADP ratios and adenine nucleotide samples in human spleen, pancreas, kidney and heart tissue. Tissue samples were retrieved from human organs that were rejected for transplantation but donated for research. The organs underwent an initial period of warm ischaemia before samples were clamp frozen, stored at -80°C and processed within 1 month. Adenosine nucleotides were measured using a Luciferase luminescence assay and the change in nucleotides presented as ratio of ATP to ADP (A). Nucleotide concentrations are measured in nmol/mg (B). Spleen and pancreas samples were frozen and thawed with or without the cryoprotectant glycerol and ATP/ADP ratios (C) and nucleotide concentrations (D) determined. n= 2-4 biological replicates, data is mean ±SD. no statistical analysis due to low number of samples.

The above analysis of mouse tissue provided me with ways of assessing ATP and ADP levels. As part of my research will be on the analysis of adenine nucleotides in human tissue samples, I next wanted to confirm that I could extend this work to these samples. This was important to do, as the analysis of human samples comes with particular challenges as often it is not possible to retrieve these samples under conditions as controlled as we have used for mice. Furthermore, I also wanted to investigate if different human tissues have different baseline levels of ATP and ADP, to see how these compared with mice and also to assess how freezing and thawing impacts the adenosine nucleotide pool.

As I am affiliated with the Department of Surgery, I could access discarded human organs immediately after retrieval from human donors. These organs were retrieved during transplant surgery, but could not be used for donation due to various reasons, including excessive donor age, underlying pathologies, tumours or the lack of a suitable recipient. After obtaining approval from the donor's family and ethical approval described in detail in the methods, these discarded organs were utilised for research purposes under the supervision of Dr. Krishnaa Mahbubani at the Department of Surgery, Cambridge, UK. As shown in Figure 3.3 A- B, the different human organs- heart, kidney, spleen and pancreas - show different ATP/ADP ratios and pool sizes for adenine nucleotides. It is important to note that during organ retrieval, the heart is retrieved first, the spleen and pancreas later and kidneys were retrieved last (up to 2 h until kidney retrieval). These organs retrieved later on during this process also show the lowest ATP/ADP ratios and adenosine nucleotide concentrations.

3.3.3 Adenosine nucleotide pools during ischaemia in models for organ transplantation

Organ transplantation is often the last available therapy for patients with severe organ failure. Different factors influence the outcome of the surgery, for example immunological responses and rejection are well known to affect the patient's recovery, but damage to the donated organ by other mechanisms can also have impact on the recipient's recovery as well. This damage can occur during the surgery process due to ischaemic damage itself, or during the reperfusion of the organs within the recipient. This is important as both ischaemia and reperfusion are inevitable during most forms of organ transplantation and the extent varies dependent on the type of organ that is retrieved and the procedure followed. Focussing on ischaemia, during transplant surgery there are two broad types of ischaemia that occur, first the organ is at body temperature (37°C) until retrieval, and is then cooled down on ice to ~4°C and stored cold until transplantation. We have shown recently that this temperature change affects two main metabolic processes during ischaemia: the accumulation of succinate and the maintenance of adenosine nucleotides (Martin et al., 2019).

3.3.3.1 Murine heterotopic heart transplantation

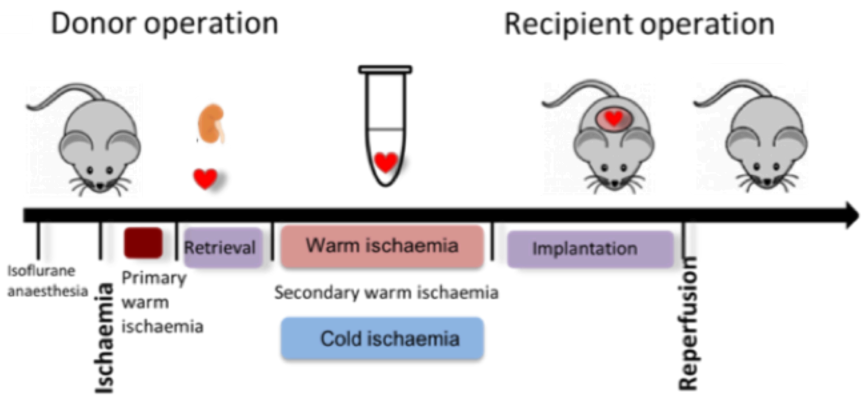

Figure 3.4: Schematic model of heterotopic transplantation. Organs, primarily hearts, are retrieved from anaesthetised BL6J wild type mice during which they undergo a period of primary warm ischaemia. Organs are then subjected to additional warm or cold ischaemia before being transplanted into the abdomen of a recipient mouse, where the heart is subsequently perfused. Therefore, the heart is connected to the inferior aorta and vena cava and can pump blood without affecting the recipient`s circulation.

For this study, Dr. Jack Martin developed a heterotopic murine heart transplant model that mimics human transplant surgery. In this model, a heart from a mouse donor is transplanted into the abdomen of a recipient and connected to the descending aorta and inferior vena cava. This model enabled us to mimic ischaemia as it occurs in human heart transplantation. All surgeries were performed by Dr. Jack Martin, before I retrieved, froze and processed samples. We utilised this model to investigate the above-mentioned different forms of ischaemia that occur during transplantation, the primary warm ischaemic period at ~37°C was followed by a cooling period and cold ischaemia at ~4°C as depicted in figure 3.4.

3.3.3.2 Effect of slow cooling during ischaemia on ATP/ADP ratios in murine heart samples

The surgical procedure during transplantation in human patients as well as in our heterotopic heart transplant model includes several temperature changes that are associated with ischaemic damage and are difficult to control precisely due to variation in surgical procedures. As shown in our paper (Martin et al., 2019), it takes more than 15 min to cool the core of a pig heart down to 4°C when storing it on ice and perfusing it with a cold solution (Figure 3.5). Because

the pig heart is about the same size as a human heart (~300 g) and the cooling procedures were identical to those during human heart transplantation, we therefore assume that during transplantation, an organ will spend several minutes under ischaemia at different temperatures between 37 and 4°C before longer storage at 4°C.

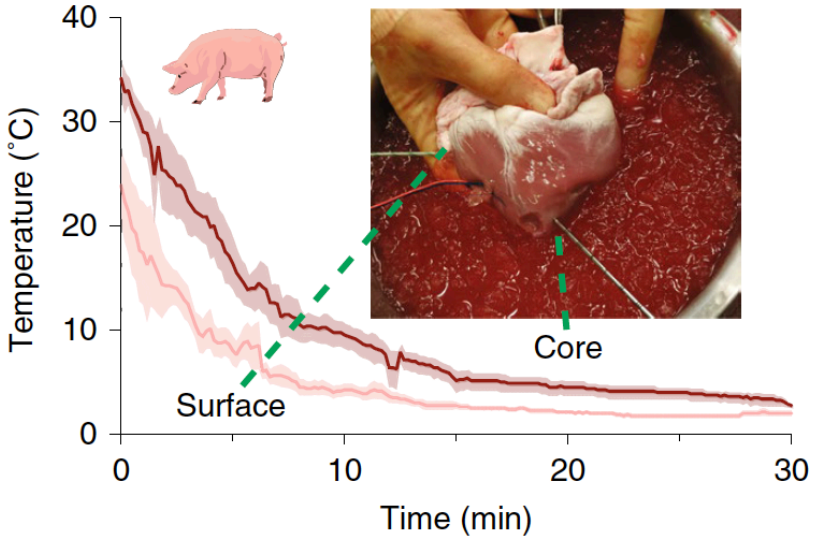

Figure 3.5: Surface and core temperature of pig heart following retrieval. Following retrieval from an anaesthetised pig, the heart was flushed with cold University of Wisconsin (UW) solution and immersed in slushed ice. The inset shows the temperature probes, which were subjected to the surface and the core of the organ. Temperature was measured over a time period of 30 min. The mean temperature (n = 4) every 10 s is shown ±S.E.M. (shaded). Surface temperature is presented in pink, core temperature in red. Modified from Martin et al., 2019.

I investigated here if ATP/ADP ratios and adenosine nucleotide levels are good markers to understand the severity of ischaemia in such conditions. To do this, I investigated the impact of different temperatures during ischaemia on adenosine nucleotides in heart tissue, at first in the mouse model.

Anaesthetised mice were culled by exsanguination, the heart was retrieved as quickly as possible (~10 sec) and placed into 2 mL Eppendorf tubes and incubated at 37, 32, 28, 16 or 4°C for 12 or 60 minutes. Then, the hearts were clamp frozen and processed as described before to analyse adenosine nucleotide levels (Figure 3.5). The ATP/ADP ratios clearly show that even after 12 min incubation at 16°C or higher, ATP is rapidly degraded in comparison to control samples, which were rapidly frozen immediately upon retrieval. After 60 min

incubation, even samples that were stored at 4°C show a reduction in ATP levels, while at higher temperatures most ATP is already degraded to ADP (Figure 3.5 B).

Altogether, these data show that adenosine nucleotides are lost more rapidly at high temperatures which underlines the importance of cooling down the organs as fast as possible, because even temperatures as low as 16°C lead to a severe reduction in ATP/ADP ratios after a short period of time.

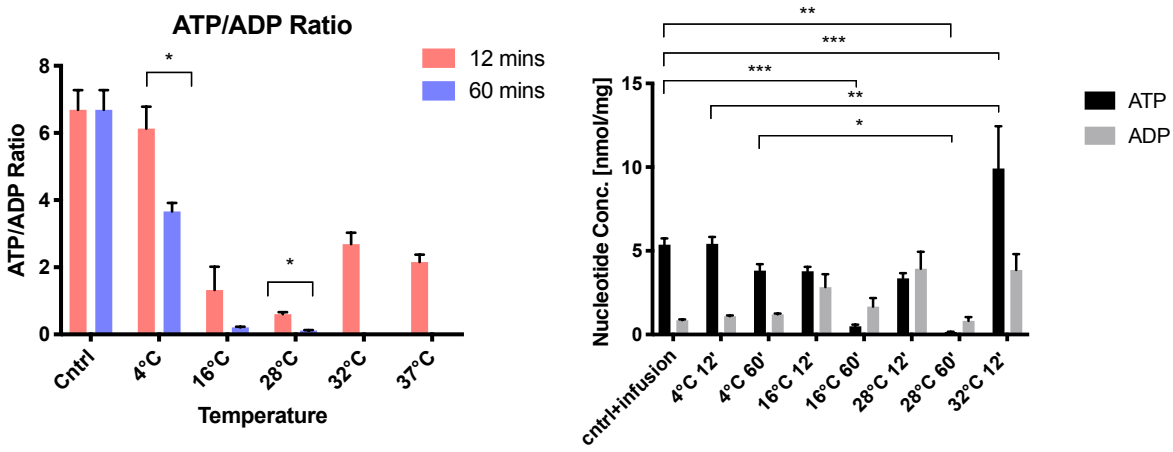

Figure 3.6: Effects of different temperatures on ATP/ADP ratios in murine heart samples. ATP/ADP ratios were determined in murine hearts with ischaemia administered at 4°C, 16°C, 28°C, 32°C and 37°C for 12 or 60 min. ATP and ADP concentrations were measured using a Luciferin-based assay and the change in adenosine nucleotides presented as ratio of ATP to ADP (A). Nucleotide concentrations are measured in nmol/mg (B). Independent normoxic controls were used for each data sets. Hearts were retrieved, rapidly transferred onto a heat block at different temperatures for 12 or 60 min of ischaemia before being rapidly clamp frozen using Wollenberger clamps. Frozen samples were stored at -80°C and processed within 1 month. Data are mean ±SEM n=7, statistical analysis was performed via two-way ANOVA. *P < 0.05, **P < 0.005, ***P < 0.001.

3.3.3.3 Effect of warm and cold ischaemia on ATP/ADP ratios in murine heart samples

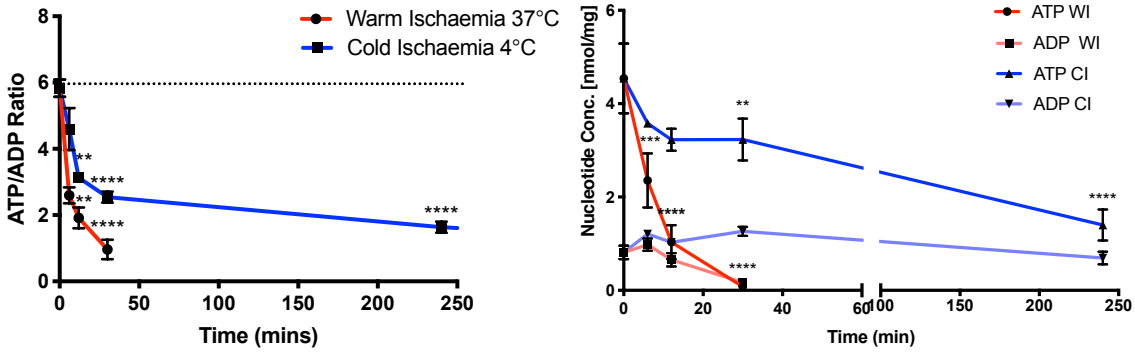

Figure 3.7: Effect of warm and cold ischaemia on ATP/ADP ratios in murine heart. ATP and ADP concentrations were determined measuring ATP-dependent Luciferase activity. **(A)** ATP/ADP ratios have been measured in mouse hearts, which have undergone warm ischaemia at 37°C (WI) or cold ischaemia at 4°C (CI) for 6, 12, 30, 240 and 480 min before being rapidly clamp frozen and analysed within 1 month. The dotted line represents the control ratio. Warm ischaemic samples are presented in red, cold ones in blue. **(B)** Data points for the adenosine nucleotide concentrations in nmol/mg of the same WI and CI samples are shown. Data are mean ±SEM n=7, statistical analysis was performed via two-way ANOVA. **P < 0.01, ***P < 0.05, ****P < 0.001.

Having shown that this method of ATP and ADP analysis worked well in tissue samples, next, I focused on the two main forms of ischaemia that occur during organ transplantation: warm (WI) at 37°C and cold ischaemia (CI) at 4°C. I directly compared the relative changes in the adenosine nucleotide pools between these two different temperatures over 8 hours in the mouse heart (Figure 3.7). At both temperatures, ATP/ADP ratios and ATP levels decrease rapidly initially, but the reduction at 37°C is much more severe and continues to decrease, while storage at 4°C maintains higher levels of these for longer. It can be seen that 4 h after retrieval of the tissue, nearly all the ATP and ADP is degraded in the samples that were incubated at 37°C, while the ATP and ADP levels declined far more slowly at 4°C. These results show that ATP/ADP ratio and ATP and ADP levels are preserved at 4°C in comparison to 37°C, confirming that as expected lower temperatures slow down metabolic processes leading to less loss of adenosine nucleotides.

3.3.3.4 A porcine model for ischaemia in heart tissue

While mouse and other small rodent models are widely used, and give vital information about mammalian biological processes, due to their small size they are often somewhat different from the human situation. This is especially so in terms of drug delivery, surgical techniques, and for processes that depend on size, such as heat exchange and metabolic rate. Bigger animal models, like pig models, are thus more relevant in the final stages of the development of medical therapies due to the similarity in size with human organs. It is therefore important to investigate the metabolic changes that occur in pigs in disease models. In collaboration with Dr. Kourosh Saeb-Parsy, Dr. Mazin Hamid and Dr. Jack Martin, we developed a model for ischaemia and reperfusion in porcine heart and analysed adenosine nucleotide concentrations in heart wedge biopsies.

In order to carry out this study, pigs were anaesthetised and underwent a renal surgical procedure as part of another study first. The diaphragm was then opened, the still beating heart accessed and first a control sample of the beating heart retrieved. This control sample was clamp frozen immediately, before other heart tissue biopsies where sampled from the heart, cut into pieces of approximately 1x1 cm^2 and stored either at 37°C for warm or at 4°C for cold ischaemia. These samples were clamp frozen at different timepoints from 6 min to 24 h.

3.3.3.5 Effect of warm and cold ischaemia on ATP/ADP ratios in porcine heart samples

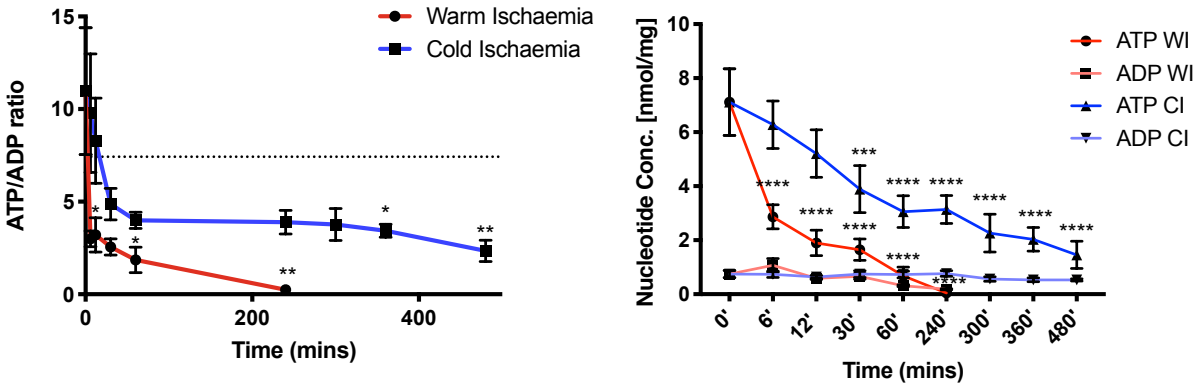

Figure 3.8: Effect of warm and cold ischaemia on ATP/ADP ratios in porcine heart samples. ATP/ADP ratios in pig hearts that have undergone warm or cold ischaemia for 6, 12, 30, 60, 240, 300, 360 or 480 min. Heart tissue samples were retrieved and rapidly transferred to ice for cold ischaemia at 4°C (CI) or on a heat block for warm ischaemia at 37°C (WI). Samples were clamp-frozen after different time points of ischaemia and stored at -80°C before being processed within 1 month. A control was retrieved from the beating pig heart just after application of terminal anaesthesia and exsanguination and immediately clamp frozen. Adenosine nucleotides were measured using a Luciferase luminescence assay and the change in nucleotides presented as ratio of ATP to ADP (A). Nucleotide concentrations are measured in nmol/mg (B). The dotted line indicates the control value. n= 5 biological replicates, data are mean ±SEM, statistical analysis was performed via two-way ANOVA. *P < 0.05, **P < 0.01, ***P < 0.001, ****P < 0.0001.

ATP/ADP ratios and adenosine nucleotide concentrations were determined as described before (figure 3.8). As already shown in murine tissue, ATP nucleotides rapidly degrade during warm ischaemia, while they are more stable in cold ischaemia. After 30 min of cold ischaemia, almost half of the ATP is degraded. On the other hand, three quarters of the ATP was broken down within the first six minutes of warm ischaemia. ADP values are maintained at much more stable levels in comparison to this and only start being depleted after 30 min warm ischaemia while they are maintained stable for over 4 h at 4°C. The ATP levels at the start are higher in comparison to murine ATP pools, at ~7 nmol/mg wet weight. Nevertheless, these results show that the adenosine nucleotide pools behave consistently during warm and cold ischaemia in different mammalian animal systems.

3.3.3.6 Effect of warm and cold ischaemia on ATP/ADP ratios in human heart samples

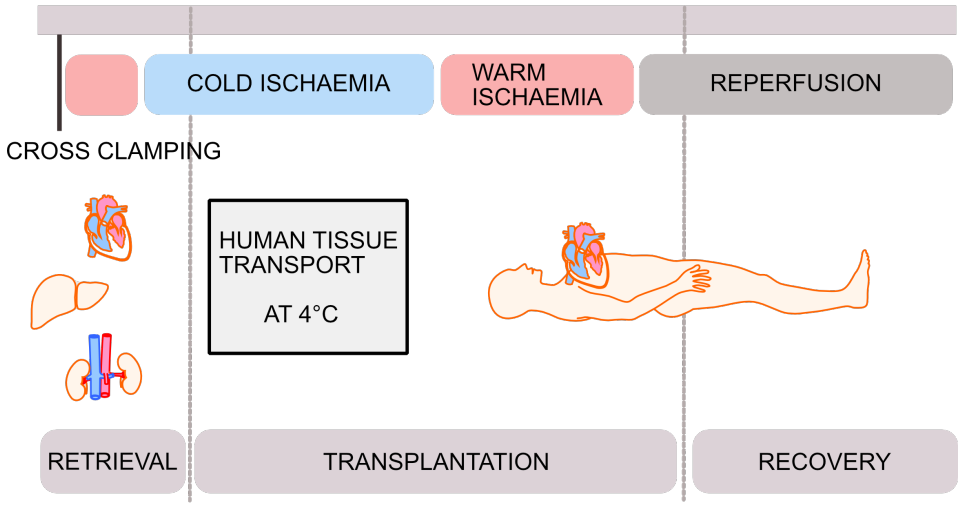

Figure 3.9: Schematic models of ischaemia reperfusion injury in human organ transplantation. Organs are retrieved in a defined order after cross clamping of the aorta in the human organ donor. During this time, organs undergo a period of primary warm ischaemia. Upon retrieval, organs are cooled down to 4°C rapidly via flushing with cold storage solution on ice. Like this, they are stored and transported until being transplanted into a recipient patient. In the patient, the organ undergoes a period of secondary warm ischaemia while being transplanted into the body, warmed up to body temperature and reperfused in the recipient. Ischaemia reperfusion injury occurs during reperfusion and recovery has to be monitored during long- term reperfusion.

Although we discovered above that the adenosine nucleotide pools and ratios behave consistently in small and large animal models, the most relevant species for our research is humans. We want to discover the underlying mechanisms for ischaemic damage in transplanted human organs in order to develop therapies and improve transplant outcome. Therefore, it is crucial to investigate metabolic changes during ischaemia in human tissue directly. We developed a similar model for inducing warm or cold ischaemia as described for the pig heart experiments and translated this into human heart samples and analysed ATP/ADP ratios and adenine nucleotide levels. Dr. Jack Martin recruited organ donors that had died of brain stem death (DBD), instead of cardiac death (DCD), in order to avoid ischaemia prior to the transplant surgery procedure as highlighted in the introduction and figure 3.9. In total we managed to retrieve samples for research from four donors, whose details are summarised in table 3.2. These donor hearts could not be used for transplantation due to reasons that suggested that heart damage was elevated, e.g. indicated by elevated levels of the damage

marker troponin or blood pressure, or in case of donor 1 due to a short cardiac arrest before death.

In order to retrieve organs from a donor, the surgical procedure is strictly time scheduled to avoid increased ischaemia to the retrieved organs. First, the surgeon will cross clamp the aorta to shut down the blood supply to the body (Figure 3.9). Immediately after this, the heart and lungs are retrieved for transplantation. After that, the liver, pancreas and spleen are retrieved, before finally the kidneys can be removed from the donor. The strictly timed procedure leaves just a small window to access samples from the beating heart before global ischaemia is induced to the donor via cross- clamping. Dr. Saeb- Parsy retrieved a wedge biopsy of approximately 5x3 cm from a ventricle of the heart which was clamp frozen immediately and functions as a control sample for the beating, non-ischaemic heart. Another wedge biopsy was retrieved seconds after the control sample, and cut into pieces of ~1 cm^3. These samples were stored either at 37°C or at 4°C for up to 24 h, similar to the procedure described for the porcine heart ischaemia experiments. Freezing of the control sample occurred within approximately 30 sec, handling of the other samples took another 30-45 sec.

Table 3.2: Characteristics of the 4 human DBD donors, whose heart samples were retrieved for succinate and ATP/ADP measurements.

Donor	Gender	Age	Smoker	BMI	Cause of Death	Lactate [mmol/L]	Cardiac Arrest	Respira-tory Arrest	Additional Information
1	Female	36	No	24.8	ICH	2.6	Yes (15 min)	Yes	Asthma
2	Male	54	No	31.4	ICH	1.4	No	No	MCA Clipped 1987, Hypertension
3	Female	67	No	25.8	ICH	1.1	No	No	Depression, Colon adenocarcinoma 58 months prior to admission, Adjuvant chemotherapy
4	Female	69	Yes	30.1	ICH	1.3	No	No	Hypercholesterolaemia, Heavy alcohol intake (9 units/day)

The samples, that were retrieved with consent of the donors' families for research, where analysed for metabolites and adenosine nucleotides as described before. The donor demographics (table 3.2) show that the four patients differed from each other in age, gender, BMI and lifestyle. This is reflected in differences in the ATP/ADP ratios in the control samples. A comparison of these samples is depicted in Figure3.10 D. The samples have been analysed in duplicate (except for donor H2) and the ATP/ADP ratios compared to each other to assess the variability of the basal ratios in different human donors. Two of the donors have lower ratios (~5) than the other two (~8) which could be linked to the amount of time it took to retrieve the samples during surgery, or it might reflect how healthy the donor heart was at the time of death of the patient. There are no donor characteristics in common between the donors with similar ratios, therefore we cannot determine the exact reason for the variability. Even so, overall the heart samples behaved similar not showing any statistically significant difference during ischaemia so that during warm ischaemia, ATP was rapidly decreased within 6 minutes and almost fully depleted after 60 min of warm ischaemia. The ratios were much more stable in cold ischaemia for up to 60 min before they slowly decreased. They reached a level comparable to 6 min warm ischaemia after 4 h of cold ischaemia. These results are similar to those obtained in the pig heart ischaemia model and confirm this rapid ATP depletion in warm but prolonged ATP stabilisation in cold ischaemia is universal and consistent between different species, including humans. In addition, it shows that porcine models are good surrogates for modelling the effects of ischaemia seen in human hearts.

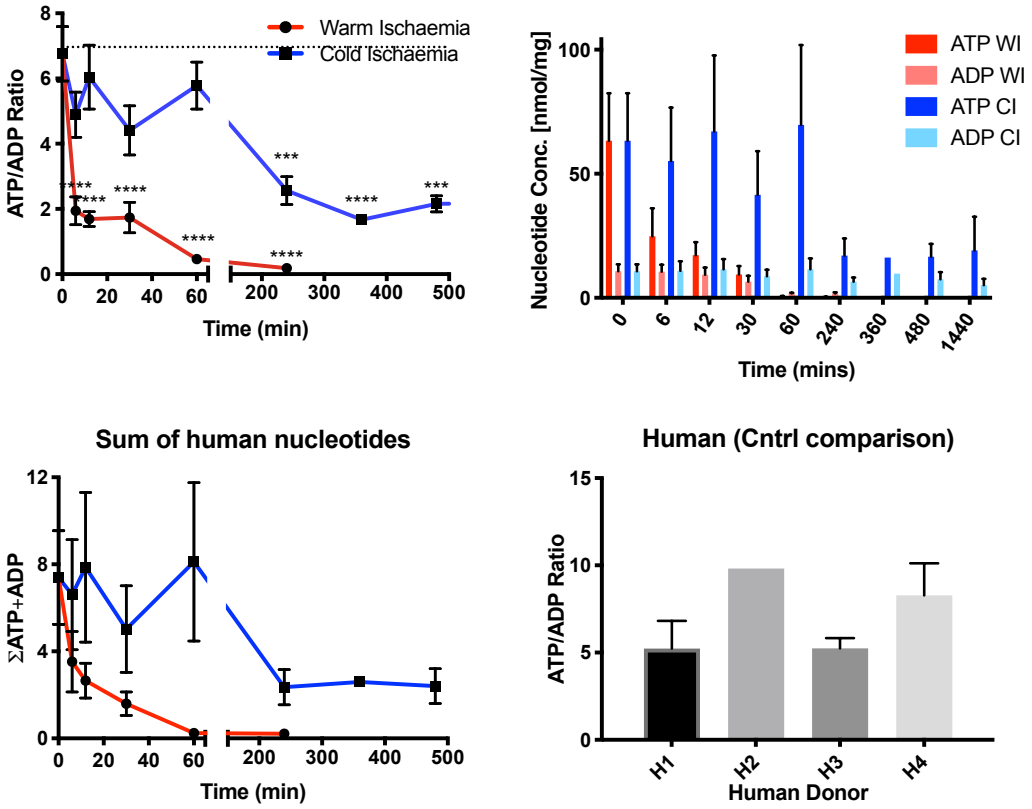

Figure 3.10: Effect of warm and cold ischaemia on ATP/ADP ratios in human heart samples. ATP and ADP concentrations were determined measuring ATP-dependent Luciferase activity. ATP/ADP ratios (A), adenosine nucleotide concentrations (B) and sum of the nucleotides (C) was determined in samples from human DBD donor hearts. A control sample was retrieved immediately upon cross- clamp from the still beating heart and rapidly clamp- frozen. Further tissue samples were retrieved and rapidly transferred onto ice for cold ischaemia (CI) at 4°C or onto a heat block at 37°C for warm ischaemia (WI). ATP/ADP ratios and nucleotide concentrations in nmol/mg were determined in the human heart sections after warm ischaemia has been initiated for 6, 12, 30, 60 and 240 min or cold ischaemia for 6, 12, 30, 60, 240, 300, 360, 480 and 1440 min. The dotted line indicates the control value. Nucleotide concentrations were used to calculate the sum of nucleotides. (D) Comparison of ATP/ADP ratios in control samples of the 4 different human donors. n= 4 biological replicates, data are mean ±SEM, statistical analysis performed via two-way ANOVA, significant data is indicated with asterices: ***P < 0.001, ****P < 0.0001.

3.3.4 A murine model for kidney ischaemia

The kidney is also susceptible to ischaemia reperfusion injury after transplantation. After heart or liver transplantation, patients often develop secondary organ damage in form of acute kidney injury (AKI) followed by long term kidney dysfunction. We are therefore also interested in how kidneys behave during ischaemia and want to analyse changes in adenosine nucleotide pools during warm and cold ischaemia. Furthermore, although the underlying

mechanisms during ischaemia are thought to be broadly similar in all tissues, the amount of ischaemic damage that occurs varies depending on the type of tissue. Some organs are more susceptible to injury upon ischaemia and reperfusion than others. The heart cannot tolerate ischaemia well, while other organs like kidneys can survive far longer ischaemic periods (as described in the general introduction). One hypothesis is that the kidney is inherently much more glycolytic than the heart and can therefore maintain their ATP/ADP ratio during ischaemia better than the heart that uses mainly the β-oxidation of fatty acids which requires oxygen and consequently cannot take place during ischaemia. Furthermore, the kidney is to some extent pre-adapted to ischaemic injury, because parts of the organ undergoes periods of hypoxia during its normal function. Here, we investigate changes in adenosine nucleotides in mice that were anaesthetised and the kidneys were removed by Dr. Timothy Beach. Here, one of the kidneys was clamp frozen immediately as a control and the other one was removed from the donor mouse and transferred onto ice for cold ischaemia or to a heat block at 37°C for warm ischaemia before I retrieved samples at different time points.

3.3.4.1 Effect of warm and cold ischaemia on ATP/ADP ratios in murine kidney samples

As described above, murine kidneys were stored for different time points, up to 8 hours, at 4°C on ice or for up to 4 hours at 37°C. Samples were then clamp frozen and their adenosine nucleotide pools measured as described above. Figure 3.11 indicates that the measured ATP/ADP ratios in heart and kidneys vary drastically. While the murine control heart shows ratios of approximately 6-7, the kidney has an average ratio of about 3. Consistent with the differences in adenine nucleotides between cold and warm ischaemia in the heart, 6 min of warm ischaemia caused a severe reduction in the ATP/ADP ratio, while the levels are maintained stable at higher ratios in cold ischaemic samples for up to 60 min and are still relatively high even after 8 h of ischaemia. Warm ischaemic samples show a severe loss of ATP already after 6 min and continue decreasing ATP levels for up to 60 min of warm ischaemia, until barely any ATP is left. The trend in heart and kidney during warm and cold ischaemia is therefore consistent, the same accounts for the amount of adenosine nucleotides in the different tissues. In kidney control samples, we could measure an average of 4 nmol/mg ATP and 1 nmol/mg ADP which is comparable to detected nucleotide levels in murine heart control samples (see Figure 3.6). This finding underlines the fact that rapid adenosine nucleotide degradation occurs at warm temperatures, but not cold ones, and that this is a

conserved mechanism during ischaemia throughout all energy demanding tissues and has to be monitored closely in order to understand the severity of ischaemia the organ has undergone.

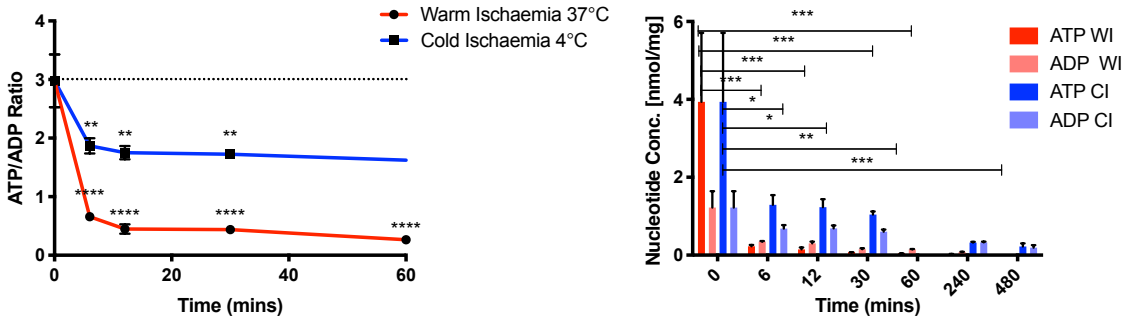

Figure 3.11: Effect of warm and cold ischaemia on ATP/ADP ratios in the murine kidneys. ATP/ADP ratios in mouse kidneys that have undergone warm or cold ischaemia for 6, 12, 30, 60, 240 or 480 min. Kidneys were retrieved and rapidly transferred to ice for cold ischaemia at 4°C (CI)or kept in the heated body for warm ischaemia at 37°C (WI). Samples were clamp- frozen after different time points of ischaemia and stored at -80°C before being processed within 1 month. Adenosine nucleotides were measured using a Luciferase luminescence assay and the change in nucleotides presented as ratio of ATP to ADP (A). Nucleotide concentrations are measured in nmol/mg (B). The dotted line indicates the control value. n= 4 biological replicates, data are mean ±SEM, statistical analysis was performed via two-way ANOVA. *P < 0.05, **P < 0.01, ***P < 0.005, ****P < 0.0001.

Altogether, I could show that during organ storage adenosine nucleotides are degraded rapidly, independent of the type of tissue or species, but dependent on the temperature. This highlights the importance of rapidly cooling down organs that are retrieved for transplantation, because already after 6 min of warm ischaemia there was almost full loss of ATP.

3.3.5 Adenosine nucleotide pools during ischaemia and upon reperfusion in models for organ transplantation

Decreases in adenosine nucleotide levels during ischaemia are highly conserved among different species and organs and are therefore good markers for the effect of ischaemia on tissue function. Upon reperfusion, tissue is subjected to IR injury and takes some time after

this to either recover or die. It is therefore important to monitor this recovery, or failure to do so, early after the reperfusion of the ischaemic tissue.

3.3.5.1 Effect of ischaemia reperfusion injury on ATP/ADP ratios in porcine heart samples

A porcine model for ischaemia and reperfusion has been developed in collaboration with Mr. Stephen Large and Mr. Aravinda Page at the Royal Papworth Hospital. Hearts were retrieved from anaesthetised pigs and stored on ice for 4 h, before being perfused with neutrophil depleted blood using an *ex vivo* normothermic perfusion pump (EVNP) (Figure 3.12 A). Wedge biopsies were snap frozen upon retrieval of the heart, after 4 h of ischaemia and 1 h after reperfusion at the EVNP. This experimental set up is close to the situation during human heart retrieval and perfusion before transplantation of the organ and therefore provides relevant information about metabolic changes during transplant surgery.

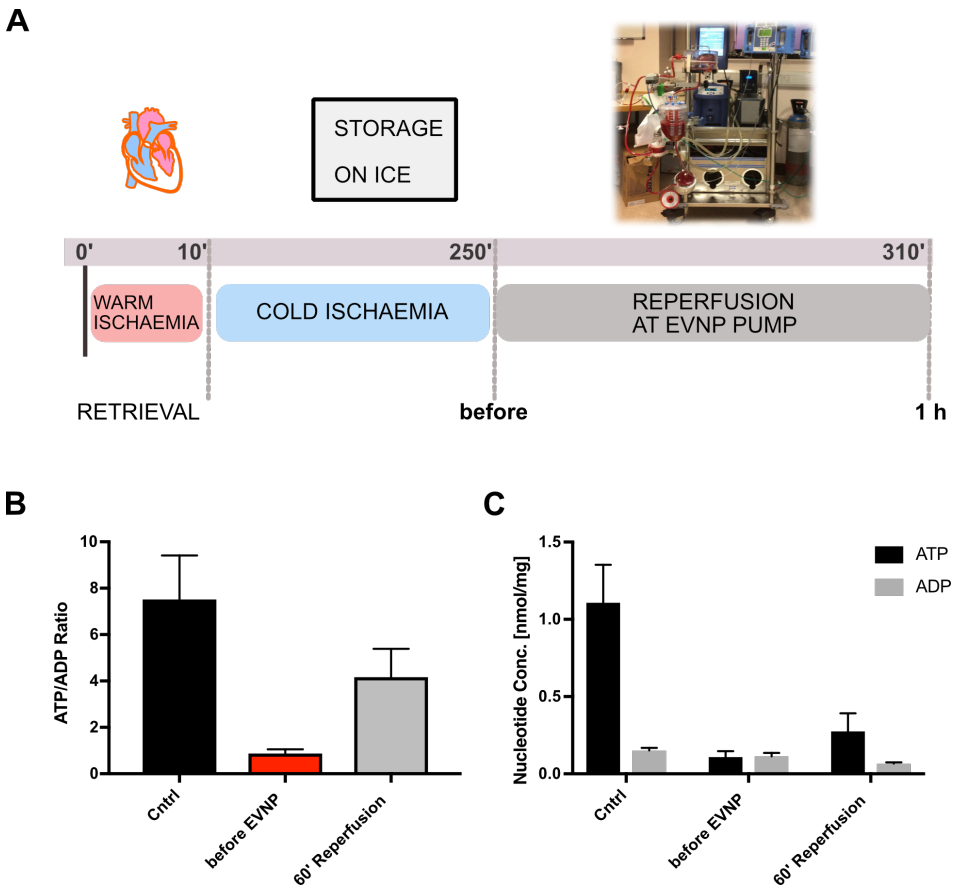

Figure 3.12: Changes in adenosine nucleotides and ATP/ADP ratios in porcine heart during ischaemia and upon reperfusion. ATP/ADP ratios in pig hearts that have undergone a model of transplantation. Hearts were retrieved in a surgical procedure and a control sample was snap-frozen after retrieval of the heart. After this initial period of warm ischaemia, the hearts were transferred onto ice for 4 h, before being reperfused on an ex vivo normothermic perfusion machine for 60 min with neutrophil depleted blood. Samples were snap frozen at the end of ischaemia, before reperfusion, and 60 min after reperfusion (A). Adenosine nucleotides were measured using a Luciferase luminescence assay and the change in nucleotides presented as ratio of ATP to ADP (B). Nucleotide concentrations are measured in nmol/mg (C). n= 4 biological replicates, data are mean ±SEM. 1-way ANOVA was performed with no significant results between before and after EVNP in (B) p= 0.5983 and (C) p= 0.7592.

These samples were snap frozen by our collaborator Dr Amanda Bundgaard, who does not have access to Wollenberger clamps, and therefore some nucleotides were degraded during the prolonged freezing process. As described before, this was because some enzymatic reactions still occur during slow freezing, as well as during the long surgical procedure and preparations for transplantation. Due to this, the ATP and ADP concentrations in the control samples are very low at ~1 nmol/mg or 0.15 nmol/mg respectively while they were much higher in the controls that were rapidly retrieved and clamp frozen (Figure 3. 8). Nevertheless, the ratios still give an indication about energy availability in the heart tissue before or after EVNP. As is shown in Figure 3.12, the ATP/ADP ratio is high in control samples before ischaemia, very similar to ratios obtained in the other pig model utilised. After severe ischaemia, the ratio drops below 1 and barely any nucleotides are detectable. One hour of reperfusion can increase ATP concentrations slightly and decrease the ADP, thereby increasing the ATP/ADP ratio to 4, but cannot fully recover the nucleotide pools and ATP/ADP ratio. Prolonged reperfusion needs be investigated in the future in this model to determine if the nucleotide pools recover.

3.3.5.2 Effect of ischaemia and reperfusion on ATP/ADP ratios in human liver samples

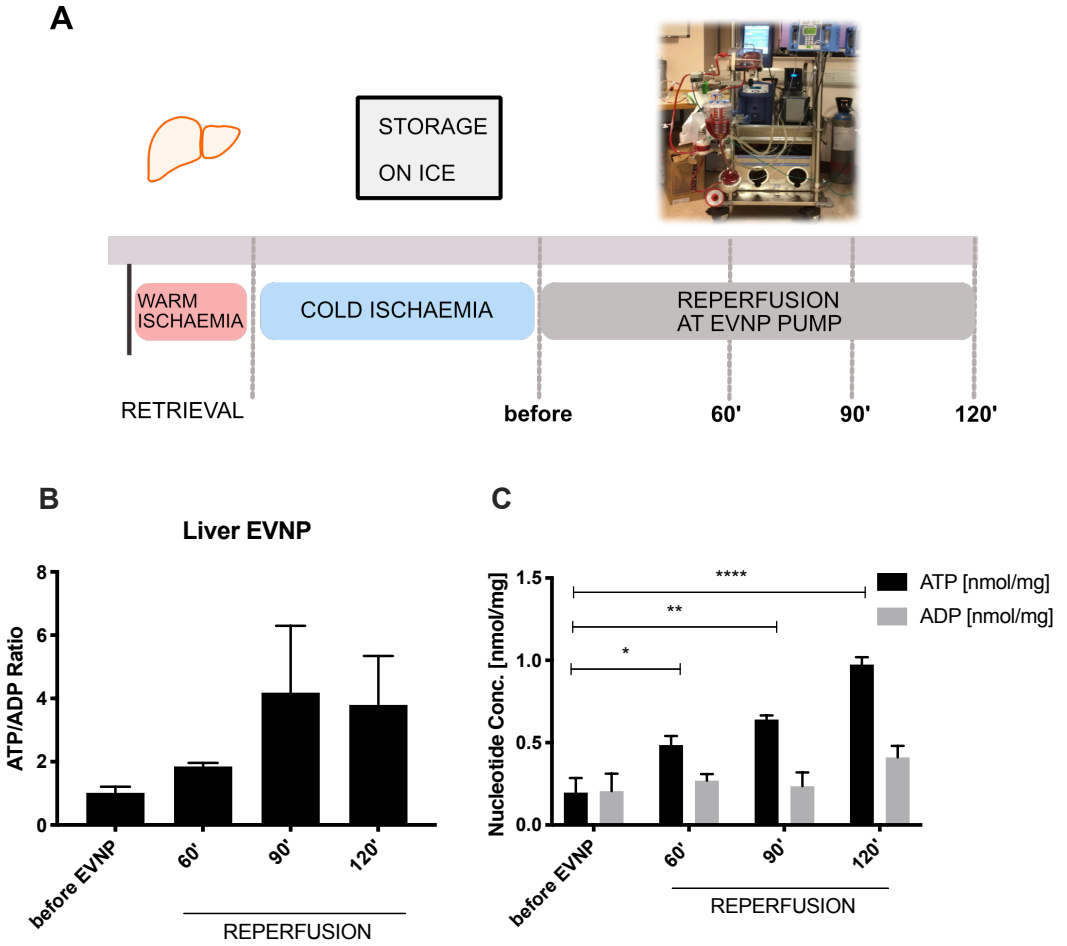

Figure 3.13: ATP/ADP ratios in human liver biopsies after ischaemia and ex vivo normothermic perfusion. ATP/ADP ratios in human livers that have undergone a model of transplantation. The organs were retrieved for organ donation, but rejected for transplantation and donated for research instead. They underwent an initial period of warm ischaemia and where then stored on ice at 4°C for several hours, before being reperfused with neutrophil depleted blood for up to 2 h. Samples were snap- frozen before initiation of reperfusion on an ex vivo normothermic perfusion machine and after 60, 90 and 120 min of reperfusion (A). Adenosine nucleotides were measured using a Luciferase luminescence assay and the change in nucleotides presented as ratio of ATP to ADP (B). Nucleotide concentrations are measured in nmol/mg (C). n= 3 biological replicates, data are mean ±SEM, statistical analysis via one-way ANOVA either not significant (B) at p= 0.3987, or significant as indicated with asterices: *P < 0.05, **P < 0.005, ****P < 0.0001.

In this study, in collaboration with Prof. Chris Watson form the Department of Surgery, human livers were retrieved for transplantation and after retrieval stored on ice at 4°C, before undergoing EVNP for 2 h (Figure 3.13 A). Wedge biopsies were retrieved every 30 min after

the first hour of perfusion and adenosine nucleotide content was determined. Unfortunately, we could not retrieve a control from the organ before transplantation and therefore before start of ischaemia. Additionally, wedge biopsies of approximately 3x3 cm were cut out of surface parts of the perfused organ, transferred into cryo-vials and snap instead of clamp frozen and might therefore have lost some ATP during freezing. In general, as depicted in Figure 3.13, there was not much loss or increase of ATP/ADP ratios during the course of perfusion suggesting that the liver is capable of maintaining its energy pool during short ischaemic periods and reperfusion. In comparison to data retrieved from the human heart, the liver showed much lower nucleotide concentrations, either due to lower baseline levels of adenosine nucleotides, or due to the long ischaemic times that the liver has already been exposed to during organ retrieval. Upon perfusion, an increase in ATP levels and ATP/ADP ratios is detectable, but both showed a tendency to stay low, perhaps indicating severe, non-recoverable IR injury to the organ. In summary, this preliminary dataset on liver reperfusion after ischaemia highlights that *ex vivo* perfusion can increase adenosine nucleotides, but that this recovery takes time.

3.3.6 Changes in adenosine nucleotides during ischaemia and reperfusion in a murine heart attack model

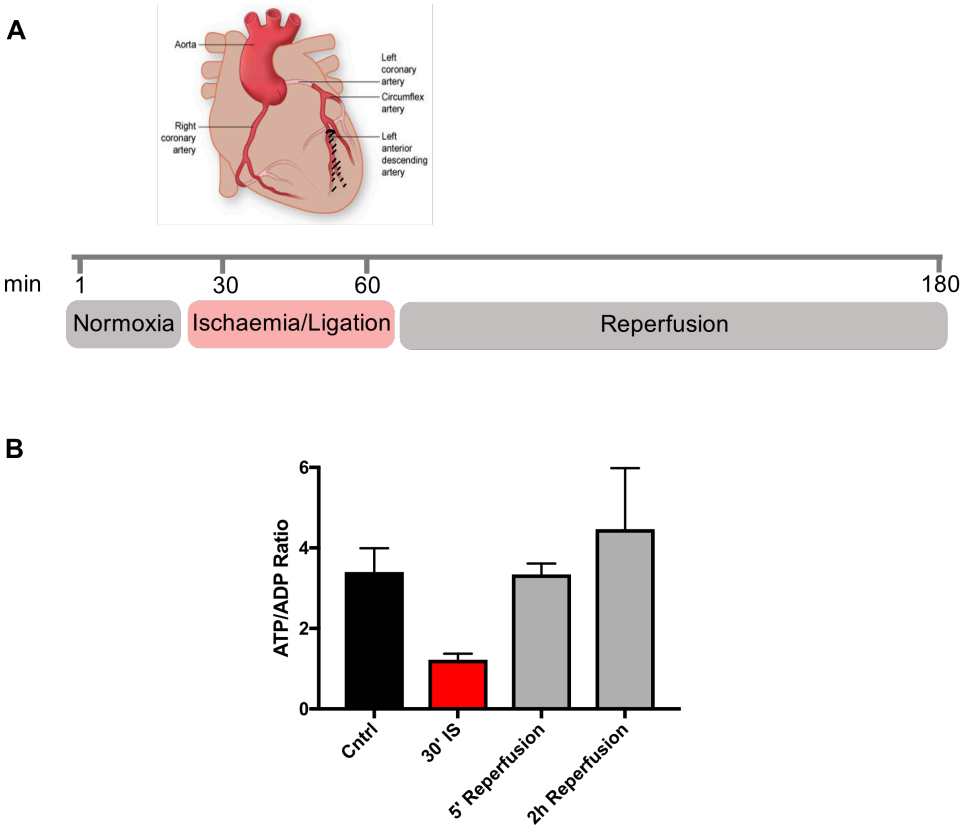

Figure 3.14: A murine model for ischaemia reperfusion injury after heart attack. (A) Schematic overview over the LAD model. The left artery descending (LAD), one of the biggest arteries in the heart is occluded with a *thread* to block blood supply to a part of the left ventricle. After a normoxic equilibration period of 30 min, ischaemia is subjected for 30 min, before the LAD blockage is removed and the tissue reperfused for up to 2 h. (B) ATP/ADP ratios were determined in murine hearts with ischaemia administered to the left ventricle via LAD occlusion for 30 min followed by 5 or 120 min of reperfusion. ATP and ADP concentrations were measured using a Luciferin-based assay and the change in adenosine nucleotides presented as ratio of ATP to ADP. Independent normoxic controls were used for each data sets. Hearts were retrieved and rapidly clamp frozen using Wollenberger clamps. Frozen samples were stored at -80°C and processed within 1 month. n= 3 biological replicates, data are mean ±SEM. Statistical analysis via one-way ANOVA, not significant at p= 0.0914.

During organ transplantation, the whole organ is exposed to ischaemia. Therefore, all cells lack a source of oxygen and struggle to maintain their energy balance. Other diseases associated with IR injury such as stroke and heart attack differ from this because a small part of the tissue is ischaemic but surrounding areas are still provided with oxygen and metabolites

from the blood supply. In order to investigate differences between partial ischaemia and global ischaemia in the heart, and also to generate insights into IR injury in heart attack, we utilised an established murine heart attack model in collaboration with Dr. Thomas Krieg from the Department of Medicine (Chouchani et al., 2014a; Methner et al., 2014). In this model, the left anterior descending artery (LAD) is ligated with a thread to induce ischaemia and can be opened up again to induce reperfusion after a period of ischaemia (FIGURE 14 A). This is similar to a blockage in a vessel during a heart attack that can be removed in patients by removing the blockage by primary percutaneous coronary intervention. During this procedure the mouse is anaesthetised and cardiac function such as heart rate, pressure, volumes pumped and ECG can be monitored. Regarding analysis of adenine nucleotides, this model is different from the heterotopic heart transplant model in one key aspect: while in transplant models the whole heart underwent ischaemia and is clamp frozen, in the LAD model, only a part of the tissue is ischaemic and is frozen and analysed. For this, the ischaemic tissue has to be cut out and separated from the normoxic/perfused part of the heart after ischaemia, or after ischaemia and reperfusion, and this section of the heart is then clamp frozen after this. However, this process is inevitably slower than clamping the whole heart and in addition it can be difficult to cleanly separate ischaemic and non-ischaemic tissue. An additional difference to the murine transplant model is that the ischaemic tissue is directly connected to healthy, functioning heart tissue and could thereby interact with neighbouring healthy cells.

As depicted in Figure 3.14 the general procedure for the LAD model includes an initial normalisation period, in which the anaesthetized mouse is prepared and the heart rate monitored at normoxia for 30 min. Then the LAD is ligated followed by 30 min of ischaemia. The body temperature of the mouse is maintained at 37°C during all of these steps via a heat mat. Reperfusion is then induced after these 30 min of ischaemia via reopening of the LAD by removing the ligating thread and the heart is then perfused for up to 3 hours before the ischaemic/reperfused tissue of the left ventricle is clamp frozen. As shown in Figure 3.14, 30 min of ischaemia leads to a significant decrease in ATP/ADP ratios, but this ratio recovers quickly upon subsequent reperfusion. This model closely mimics the ischaemia and subsequent reperfusion injury that occurs in heart attacks in patients and thus the changes we see in adenine nucleotides are likely to mimic the situation in that pathology. Hence, the loss of adenosine nucleotides and the decrease in the ATP/ADP ratio are likely to be typical of ischaemia. The situation after reperfusion in the LAD model was somewhat different from reperfusion after severe global ischaemia, in that the ATP/ADP ratios recovered more quickly upon reperfusion.

3.3.6.1 Effect of ischaemic preconditioning on ATP and ADP in murine heart samples

In the search for new therapies to ameliorate IR injury in patients. There has been a long-standing interest in better understanding the beneficial effects of preconditioning of the organ by a mild bout of IR injury prior to a subsequent, more severe damaging level of IR injury, as described before in the introduction to this chapter. This so-called ischaemic preconditioning (IPC) has been long known to be beneficial and lead to less severe damage upon reperfusion. In collaboration with Dr. Thomas Krieg and Dr. Victoria Pell, we could show that infarct size of the murine heart is reduced (Figure 3.15 A) if the heart was subjected to preconditioning prior to ischaemia in a LAD model for IPC. The mechanism by which this preconditioning is affecting tissues and cells and prevents subsequent IR injury is still unknown, but we could exclude that it is due to changes in metabolite accumulation during ischaemia after IPC, which is one of the hallmarks of ischaemia *in vivo* (Figure 3.15 B) (Pell et al., 2018).

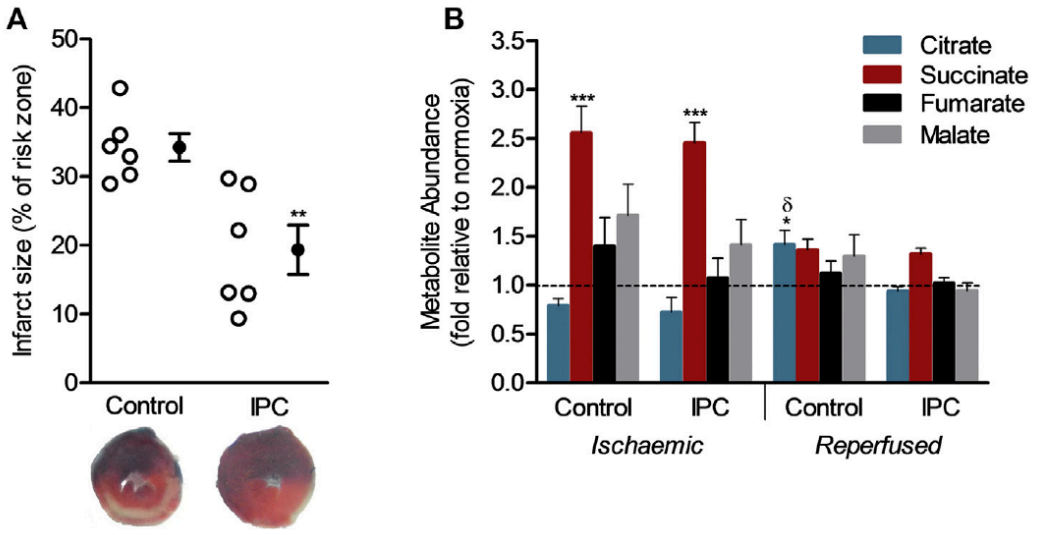

Figure 3.15: The effect of ischaemic preconditioning on metabolite abundance during IR injury in the in vivo mouse heart. This graph has been retrieved and modified from Dr Victoria Pell and published in Pell et al., 2016. The previously described LAD occlusion model was utilised to mimic heart attack in mice. Mice were either subjected to 30 min of normoxia followed by 30 min of ischaemia upon LAD occlusion or ischaemic preconditioning (IPC) due to repeated ischaemia and reperfusion periods before 30 min of ischaemia. (A) Preconditioning reduced infarct size in vivo as presented in reduced infarct size during ischaemia. Representative cross-sections from mouse hearts after myocardial infarction are shown. Infarcted tissue is white, the area at risk is red, and non-risk tissue is dark blue (n=6). **p < .01 (two- tailed Student's t-test). B) Metabolite abundance following 30 min ischemia or following 1 min reperfusion after ischaemia was measured via liquid chromatography- mass spectrometry. Data are expressed as fold change relative to time-matched normoxic shams (n=7–8). *p < .05, ***p < .001 vs normoxia, δp < 0.05 vs reperfusion + IPC (one-way ANOVA with Tukey's post-hoc analysis). Mean ± SEM. Modified from Pell et al. 2018.

These results were published by Pell et al., 2018 and additionally, we wanted to investigate whether short periods of ischaemia followed by reperfusion influence the adenosine nucleotide pools and/or ATP/ADP ratios. To do this we used this LAD ligation model including ischaemic preconditioning and then investigated tissue samples for changes in adenine nucleotides. The LAD surgeries were performed by Dr. Victoria Pell. Briefly, we induced 3 periods of 5 minutes ischaemia followed by reperfusion to precondition the organ before an additional 30 min of ischaemia and then reperfused the heart (Figure 3.16 A). To analyse the effect of preconditioning, I analysed the heart tissue after preconditioning, but prior to reperfusion, at which end the tissue was retrieved, frozen and then analysed for adenine nucleotides.

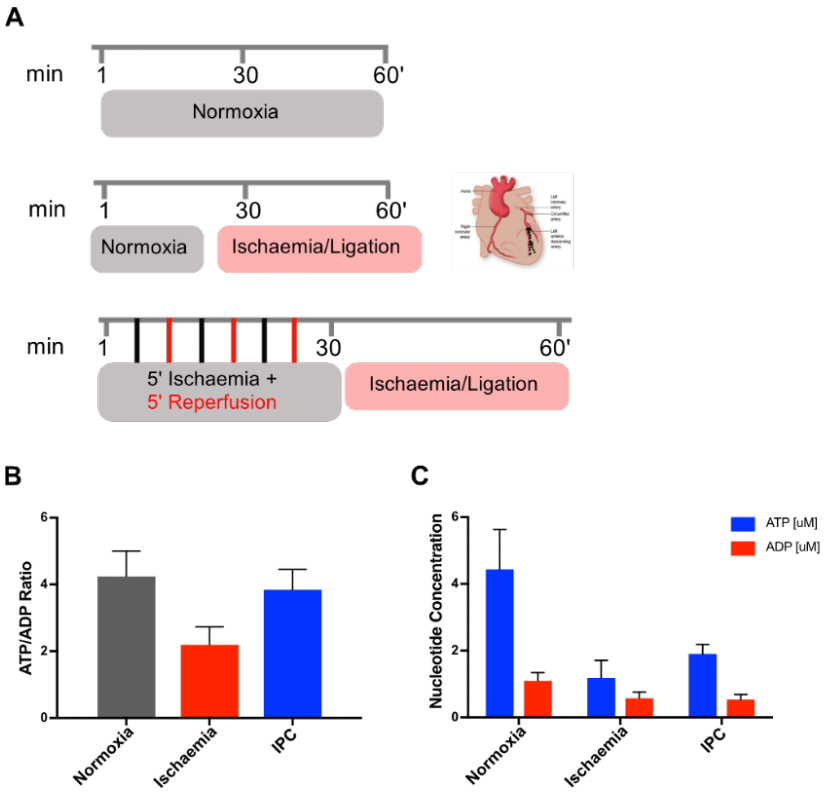

Figure 3.16: Ischaemic preconditioning in a murine model for heart attack. The previously described LAD occlusion model was utilised to mimic heart attack in mice. A schematic timeline of the model is presented in (A). Mice were either subjected to 60 min of normoxia without occlusion of the LAD, or 30 min of normoxia followed by 30 min of ischaemia upon LAD occlusion or ischaemic preconditioning (IPC) via repeated ischaemia and reperfusion periods before 30 min of ischaemia. To induce preconditioning, samples underwent 3 times 5 min of ischaemia followed by 5 min of reperfusion, before the additional 30 min of ischaemia were administered. Adenosine nucleotides were measured in heart tissues using a Luciferase luminescence assay and the change in nucleotides presented as ratio of ATP to ADP (B). Nucleotide concentrations are measured in nmol/mg (C). Samples were rapidly frozen using Wollenberger clamps and analyse within 1 months. n= 3 biological replicates, data are mean ±SEM, statistical using Student`s t- test was not significant p= 0.702.

I compared the levels of adenine nucleotides following this preconditioning protocol with the results in the hearts of mice that underwent a mock procedure but with no LAD ligation ("Normoxia") and mice that underwent 30 min of normoxia followed by 30 min of ischaemia ("Ischaemia") (Figure 3.16). The ATP/ADP ratios clearly show a reduction in the ischaemic samples compared to the control normoxic samples. The samples that have undergone preconditioning showed no significant difference in their ATP/ADP ratios. The nucleotide levels show that the reduction in ATP levels in the ischaemic samples is severe in comparison to the control samples. The preconditioned samples have severely reduced ATP levels as well (Figure 3.16 C), but slightly more ATP is left than in the ischaemic samples, while ADP concentrations do not change between ischaemia only and IPC samples. Although the differences are not significant, the data suggest that there may be an impact on the balance between ATP and ADP and it is possible that this can be sensed by sensitive cellular mechanisms that maintain the ATP/ADP ratios in favour of ATP production. However, more work is required to assess this.

While these preliminary results did not show significant differences, they may suggest a trend, that may be worth assessing in more detail in the future give an interesting insight into how ischaemic preconditioning has its beneficial effects.

3.3.6.2 Effect of selective mitochondrial ROS production on ATP and ADP in murine heart samples

While the assessment of adenosine nucleotide levels after ischaemic preconditioning was not immediately informative, we wanted to investigate if mitochondrial ROS production could affect ATP/ADP ratios, as seen before in cell models (Hinchy et al., 2018). To do this, we extended the LAD ligation model to assess the effect of the mitochondria-targeted ROS-producing agent MitoParaquat (MitoPQ), which is a Paraquat redox cycling molecule that is linked to a TPP moiety and due to its positive charge targeted to mitochondria *in vivo*, where it produces superoxide at complex I (Figure 3.17 A) (Robb et al., 2015).

The LAD surgeries were performed by Dr. John Mulvey and as published in Antonucci et al., 2019, we discovered that MitoPQ treatment decreased infarct size in LAD occluded murine hearts, as shown in Figure 3.17. The hearts were treated in vivo 10 min before induction of ischaemia either with a vehicle, control compound or 0.01 nmol MitoPQ. Ischaemia was induced for 30 min, before samples were retrieved and infarct size as dark areas investigated.

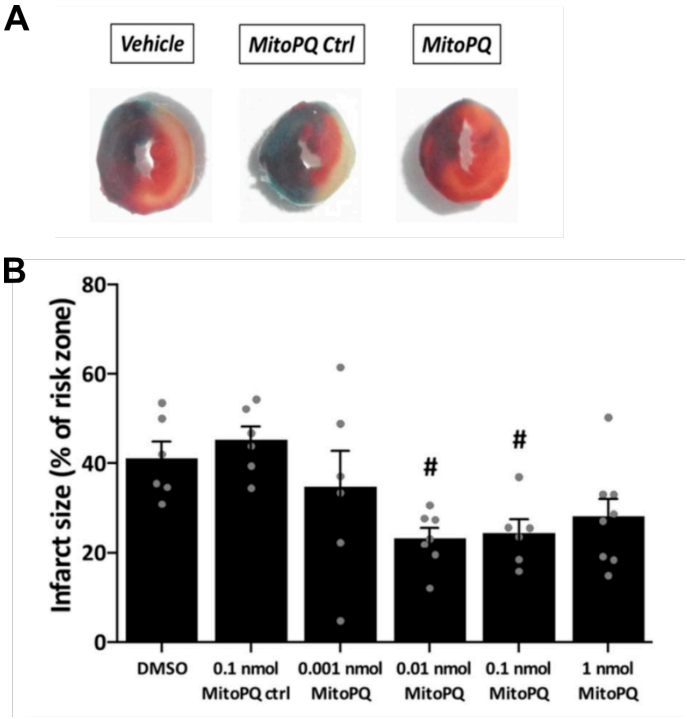

Figure 3.17: Effects of MitoPQ on infarct size after LAD ligation in vivo. The left artery descending (LAD) occlusion model is utilized to investigate the effect of mitochondrial ROS produced by treatment with the mitochondria- targeted compound MitoPQ on ischaemia reperfusion injury in mice. The LAD is occluded in vivo to block blood supply to a part of the left ventricle. Mice were injected with a control compound, a vehicle (ethanol) or MitoPQ at increasing concentrations (in nmol) 10 min before induction of 30 min of ischaemia. (A) Representative infarct slices from hearts treated with vehicle, MitoPQ control compound 0.01 nmol MitoPQ. (B) Infarct size in hearts of mice exposed to acute myocardial I/R, in presence or absence of 0.01 nmol MitoPQ control compound or the indicated dose of MitoPQ. vs DMSO. n=6-8, data are mean ±SEM. #$p < 0.05$. Overall Anova $p=0.0053$. Modified from Antonucci et al., 2019.

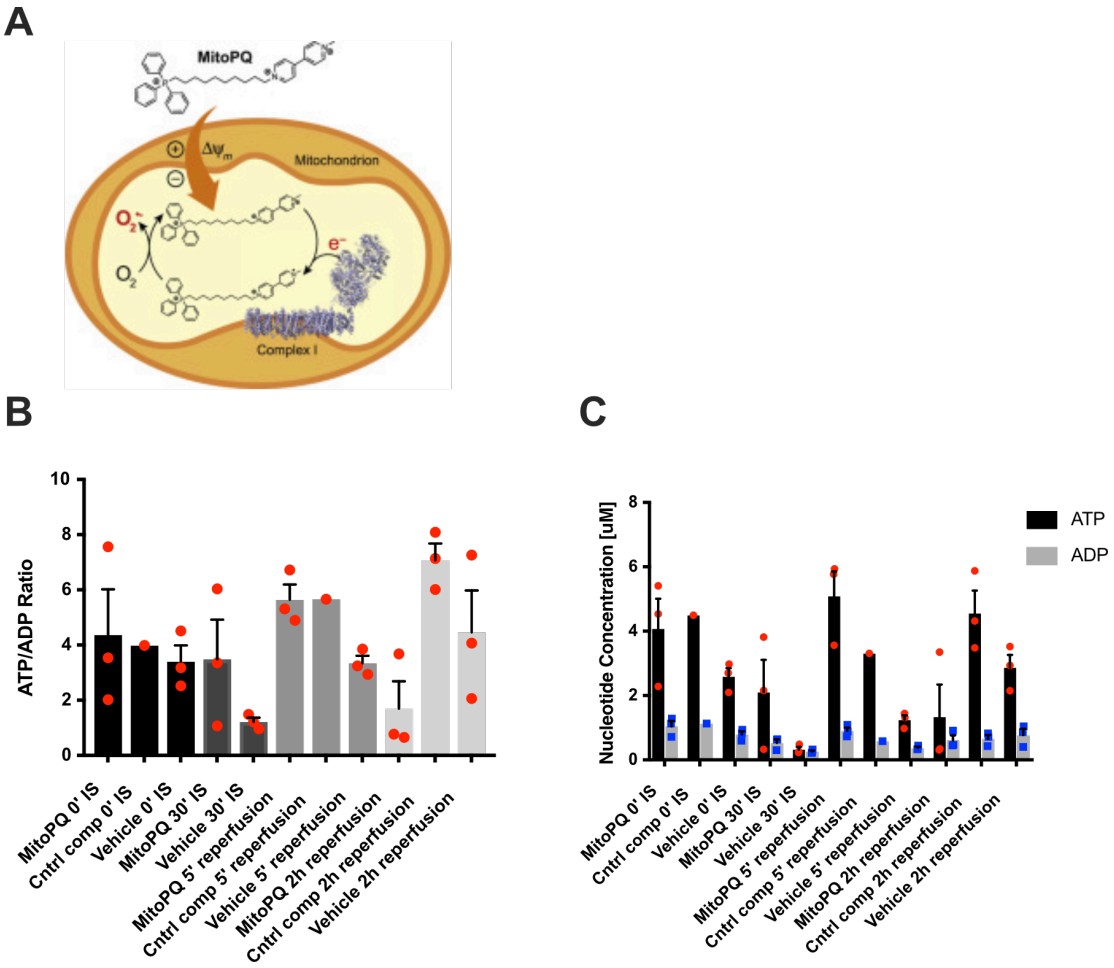

Figure 3.18: Changes in adenosine nucleotide pools after treatment with MitoPQ in the murine LAD occlusion model.(A) Schematic overview of mitochondrial accumulation of MitoPQ modified from Antonucci et a., 2019. Because of its positive charge, TPP- linked paraquat accumulates within mitochondria where it facilitates ROS production at complex I/ with complex I. Adapted from Antonucci et al., 2019. (B- C) The left artery descending (LAD) occlusion model is utilized to investigate the effect of mitochondrial ROS on ischaemia reperfusion injury in mice. The LAD is occluded to block blood supply to a part of the left ventricle. After a normoxic equilibration period of 30 min, ischaemia is subjected for 30 min, before the LAD blockage is removed and the tissue reperfused for up to 2 h. (B) ATP/ADP ratios were determined in murine hearts that underwent mock surgery, were ischaemic for 30 min or reperfused for 5 or 120 min. Mice were injected with a control compound, a vehicle (ethanol) or MitoPQ at 0.01 nmol 10 min before induction of ischaemia/after a 20 min normoxic equilibration period. ATP and ADP concentrations were measured using a Luciferin-based assay and the change in adenosine nucleotides presented as ratio of ATP to ADP. (C) Nucleotide concentrations are measured in nmol/mg. Independent normoxic controls were used for each data sets. Hearts were retrieved and rapidly clamp frozen using Wollenberger clamps. Frozen samples were stored at -80°C and processed within 1 month. n=1- 3 biological replicates, data are mean ±SD, not enough samples for proper statistical analysis.

In order to investigate the impact of mitochondrial ROS on adenosine nucleotides during ischaemia and upon reperfusion, we induced mitochondrial ROS production at various time points before, during and after ischaemia. MitoPQ treatment alone did not affect the ATP/ADP ratios when administered before ischaemia in comparison to control compounds. When administration was started during ischaemia just before reperfusion and continued through reperfusion, it led to an increased ATP/ADP ratio measured 5 min after reperfusion, compared to reperfusion in the absence of MitoPQ (Figure 3.18). Therefore, low levels of ROS seem to be beneficial at this point, but at later reperfusion time points, MitoPQ causes a reduction in the ATP/ADP ratios. The increase or reduction in the ATP/ADP ratios matches the changes in ATP levels. These results present a trend and have to be investigated further in order to understand how mitochondrial ROS affects ischaemic injury.

Altogether, these experiments showed that assessment of adenine nucleotides in the LAD occlusion model in mice is informative to assess the impact of ischaemia and reperfusion during heart attack and opens up the possibility to provide new insights into therapeutic approaches. Further research into ameliorating ATP degradation during ischaemia or improving its recovery upon reperfusion are necessary to elucidate how ischaemia reperfusion injury can be prevented in patients.

3.3.7 Changes in adenosine nucleotides during ischaemia and reperfusion in other organisms

While I could show that changes in adenosine nucleotide pools and the ATP/ADP ratio during ischaemia and reperfusion are conserved among different mammalian species, I also wanted to investigate the changes during ischaemia and reperfusion in non-mammalian species. One important factor for this is that some organisms seem to be far more protected against IR injury than mammals. Thus, investigating how the ATP/ADP ratios and adenosine nucleotides alter under ischaemic conditions in these organisms may shed light on the mechanism that protects them from ischaemia reperfusion injury.

3.3.7.1 Assessment of cardiac adenine nucleotides in the heart of the red-eared slider turtle Trachemys scripta during IR injury

In contrast to mammals, the freshwater red-eared slider turtles *Trachemys scripta* can tolerate anoxia at cold temperatures for weeks and furthermore they do not suffer from reperfusion injury upon reoxygenation. The turtles hibernate under water in winter, cooling down their body temperature from 25°C to 4°C and slowing down their metabolism and heartbeat and this enables them to survive weeks without oxygen. The underlying metabolism occurring during ischaemia includes relying on glycogen reserves for energy production, and exporting lactate, the end product of anaerobic metabolism, to the plasma, where it is buffered by calcium carbonate and released from the shell (Jackson et al., 2007).While most other organs almost completely shut down metabolism during anoxia, the heart keeps beating, which raises questions regarding energy maintenance within this organ during anoxia.

Therefore, we performed a study investigating metabolic changes in turtle hearts during normoxia and ischaemia and analysed how the adenosine nucleotide pools and ATP/ADP ratios respond (Bundgaard et al., 2019). Turtles were gradually acclimated to 5°C over 6 weeks and then exposed to anoxia or normoxia for 9 days. Anoxic turtles were kept submerged in water bubbled with N2, while normoxic turtles were allowed free access to air. The animals were handled by Dr. Amanda Bundgaard at the University of Aarhus, Denmark (further details in Methods), who retrieved and snap froze samples before these were sent on dry ice for analysis to Cambridge.

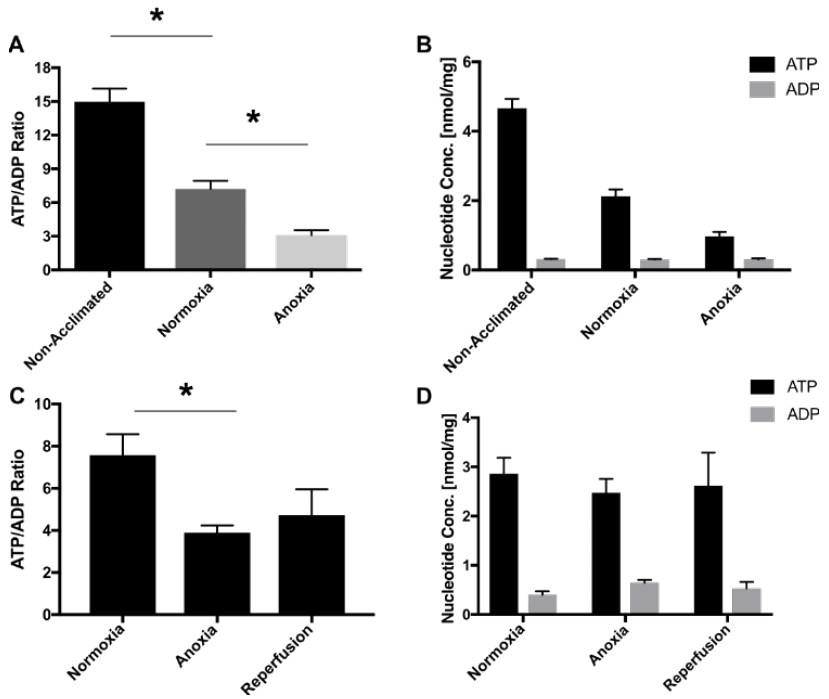

Figure 3.19: ATP/ADP ratios and adenosine nucleotide concentrations in turtle heart during ischaemia and upon reperfusion. Turtle hearts from Trachemys scripta were snap- frozen before acclimatisation from 25°C to 5°C, after acclimatisation when kept at normoxia for 9 days and after anoxia under water for 9 days (Burgaard et al., 2019). (A, B). Furthermore, turtles were reperfused for 1h at 5°C after 3 h of anoxia before hearts were retrieved and snap- frozen and compared to normoxic and anoxic controls at 5°C (C, D). Turtles were handled and samples retrieved by Dr. Amanda Burgaard at the University of Aarhus, Denmark, before samples were send to the MRC MBU and analysed by me. Adenosine nucleotides were measured using a Luciferase luminescence assay and the change in nucleotides presented as ratio of ATP to ADP (A, C). Nucleotide concentrations are measured in nmol/mg (B, D). n= 5 biological replicates, data are mean ±SEM. Statistical analysis via student's t-test. *$p < 0.05$.

Figure 3.19 A- B shows, that the ATP/ADP ratio and ATP content in non-acclimated turtles at 25°C are larger than after acclimatisation to 5°C ("Normoxia"). Even though the turtles are still normoxic and have no oxygen shortage, a decreased body temperature affects the nucleotide pool indicating a metabolic adaptation. During anoxia, the ratios decrease significantly further. Adenosine nucleotide pools prove that the drop in ratios during normoxia as well as anoxia is due to loss of ATP. Upon reperfusion (Figure 3.19 17 C- D) after a short period of anoxia, the ratios that were decreased during anoxia do not recover significantly. Interestingly, the decrease in the ratios is not due to a loss of ATP but due to an increase in ADP during anoxia, which remains unchanged after 1 h of reperfusion.

This study, in parallel with measurements of succinate in tissues and measurements of isolated mitochondria from turtles, gave us interesting insights into the metabolic processes

occurring in non-mammalian animals, that can tolerate ischaemia. Their energy metabolism differs significantly from the mammalian situation and does not show the rapid decrease in ATP concentrations observed in mammals after short anoxic periods. The temperature at which these animals survive anoxia has a big impact on the ATP pool and on the recovery of the ATP/ADP ratio after reperfusion. Thus, our study could show that the animals do lose adenosine nucleotides at cold temperature under conditions that allow them to tolerated prolonged anoxia, but during short phases of anoxia do not lose ATP but accumulate ADP. This high concentration of ADP might prevent reverse electron transfer upon reperfusion and thus ameliorate the burst of ROS that causes IR injury. Therefore, the turtles do not suffer much injury, but can easily survive prolonged anoxia.

3.3.7.2 Assessment of adenosine nucleotides in Drosophila melanogaster during anoxia

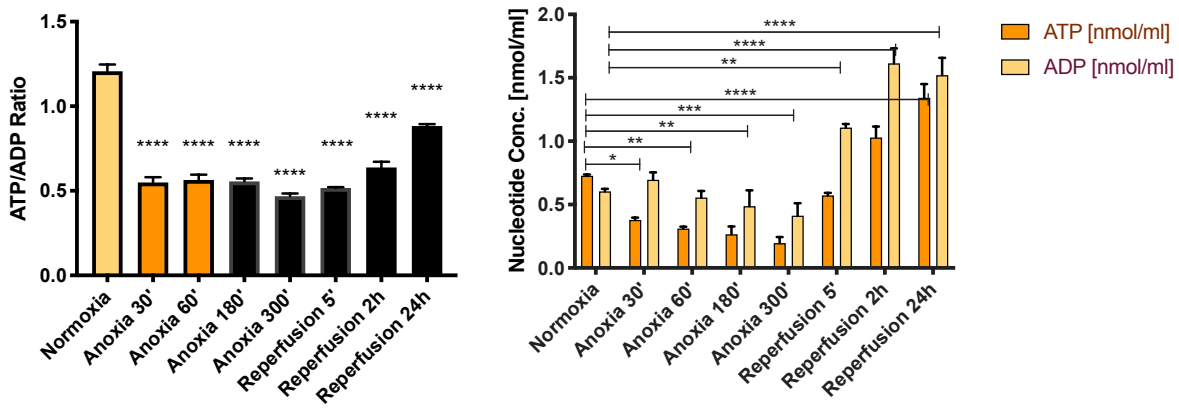

Figure 3.20: ATP/ADP ratios and adenosine nucleotide concentrations in fruit flies during ischaemia and upon reoxygenation. Drosophila melanogaster were either maintained at 27°C in a fly incubator under normoxia or subjected to anoxia at 27°C in an anoxic chamber. For reperfusion experiments, flies were removed from the anoxic chamber and incubated in a fly incubator before lysis. Changes in nucleotides after 1, 3 or 5 h of anoxia or after 60 min anoxia followed by 5 min, 2 or 24 h of reperfusion were determined. These experiments were performed in collaboration with Dr Federica De Lazzari. Adenosine nucleotides were measured using a Luciferase luminescence assay and the change in nucleotides presented as ratio of ATP to ADP (A). Nucleotide concentrations are measured in nmol/mg (B). n= 3 biological replicates, data are mean ±SEM, statistical analysis was performed via one-way ANOVA. *P < 0.05, **P < 0.01, ***P < 0.001, ****P < 0.0001.

One of the most commonly used model organisms in biological research is *Drosophila melanogaster*, the fruit fly. Interestingly, flies are known to be able to survive chronic hypoxia

(5% O_2). During this time, they fall into a stage of paralysis losing the ability to move. Upon reoxygenation it takes them 1-2 h to awake fully from the paralysis. However, this reoxygenation after hypoxia does seem to induce a type of ischaemia reperfusion injury, as the flies so treated have a significantly reduced life span in comparison to animals maintained under normoxic conditions (Zhou et al., 2008). We were intrigued that this widely used model differed from mammals in that they survive prolonged reduced oxygen availability better than wild type flies, showing delayed IR injury. Hence, we hypothesised that the presence of residual oxygen in these hypoxic experimental conditions may prevent the accumulation of the metabolite succinate and is therefore not comparable to the true anoxic conditions as they occur *in vivo* during ischaemia in organ transplantation. Therefore, we utilised an anoxic chamber to maintain flies under conditions of true anoxia (details in methods and following chapters) and then investigated the accumulation of succinate and changes in adenosine nucleotide pools in this model. The fly handling part of this work was performed in collaboration with Dr. Federica De Lazzari, University of Padova, Italy.

As shown in Figure 3.20 B, the concentrations of adenosine nucleotides, especially ATP levels, are much lower than in other animal models in normoxia. However, this might be due to the fact that whole flies were used, rather than just the thoraces which contain the majority of mitochondria in flies. Thus, the extraction includes the chitin, legs, wings, head, abdomen and gut, which is likely to lead to a dilution of the amounts of nucleotides detected. Nevertheless, a clear reduction in ATP/ADP ratios was apparent after 30 min of anoxia (Figure 3.20 A). Interestingly, this ratio was maintained for 3 h of anoxia, before decreasing further after 5 h of anoxia. The ATP/ADP ratios increase again upon reoxygenation, although this does not occur fully until about 2 h after reoxygenation, by which time the flies have largely recovered from the paralysis induced by anoxia. The ATP/ADP ratios increase even more at longer times after reoxygenation, although they do not reach control levels even 24 h later. This phenomenon of depression of the ATP/ADP ratios long after reoxygenation/reperfusion periods is consistent with the other animal models investigated here.

3.4 Discussion

Ischaemia reperfusion injury contributes to many diseases such as heart attack or stroke and also causes damage to the organs used during organ transplantation, increasing the risk of

allograft dysfunction. Characteristic metabolic changes including accumulation of lactate have been known to occur during organ storage for a long time, and more recently other markers such as the accumulation of succinate has been discovered as a driving force for ischaemia reperfusion injury. Our investigations recently have shown that this succinate accumulation is conserved throughout different tissues and species. Even so it is also important to understand the status of the tissue during ischaemia and reperfusion. Analysing the ATP/ADP ratio and assessing the adenosine nucleotide pools in tissues can give an indication of how severe the ischaemia is and whether the adenosine nucleotide pools are large enough to enable rapid regeneration of ATP upon reperfusion and therefore to allow tissue survival. The restoration of the ATP/ADP ratio can only occur as long as the ADP pool is large enough to enable production of ATP. Determining the ATP/ADP ratios in organs before transplantation into a recipient therefore gives a good indication for how severe the ischaemia - the organ was exposed to and also how likely it is to fully recover upon reperfusion. A lot of research has been performed to date into analysing energy availability within ischaemic tissues, but here I could show that any warming of the tissue during ischaemia and also prolonged cooling times can affect the amount of adenosine nucleotides.

Interestingly, different tissues and species contain different absolute amounts of adenosine nucleotides, although the ratios were similar in the same organs among different mammalian species. The data indicate that larger animal species contain more adenosine nucleotides in general. But it is necessary to consider the heterogeneity of the tissue samples as well. The tissue can be contaminated with residual blood or fat tissue, which will contain variable amounts of adenosine nucleotides and could therefore affect the results.

Besides the consistency of the ATP/ADP ratios, the behaviour of ischaemic heart tissue among different mammalian species was similar, with all losing ATP within a few minutes of ischaemia at 37°C, but maintaining a more stable ATP/ADP ratio for several hours at 4°C. This indicates very conserved metabolic mechanisms that occur during ischaemia between different species. The cold temperature slows down ATP consuming and succinate accumulating enzymatic processes, maintaining a more stable adenosine nucleotide component in the tissues. The most translatable results obtained in this study are the ones generated from human samples. These samples show what is happening during human transplant surgery and suggest that mouse experiments do mimic the changes happening in human tissues during ischaemia. They also demonstrate that it is possible to access biopsies from humans and generate useful data of potential translational use. In comparison to animal

species, the human samples result in much more variable results. This is due to the diverse genetic background and life history and the difficulty of gender and age- matching samples.

Another topic addressed in this chapter is ischaemic preconditioning. A huge range of theories have been proposed to explain why short periods of ischaemia and reperfusion are beneficial for the outcome of subsequent severe ischaemia and reperfusion. Our preliminary data suggest, that the effects of preconditioning on ATP/ADP ratios and the maintenance of larger adenine nucleotide pools, may be worth considering as a contributing factor, but far more data are required and the effects seem too small to explain all of the improvements seen in patients and animal models. One possible hypothesis worth exploring is that the benefit occurs due to, or in combination with, other mitochondrial processes, for example the stability of the membrane potential or the induction of MPTP opening.

Understanding all the cellular processes occurring during ischaemia should help in interfering with the damage that occurs upon reperfusion. This accounts for the changes leading to beneficial outcome after preconditioning, but also for understanding the different metabolism of animals that tolerate anoxia. More research is required in order to understand how turtles and flies tolerate hours to weeks of anoxia and also survive reoxygenation better than mammals. Turtles cool down their body temperature, which changes their adenosine nucleotide pools. Flies fall into paralysis, thereby maintaining a decreased ATP/ADP ratio for the hours of anoxia. All this shows, that there are different ways of coping with lack of oxygen. Not all of this will be applicable to mammalian conditions, but still may help better understand the underlying processes of ischaemia reperfusion injury. In general, the data suggest that the more ATP and ADP are still available after ischaemia, the better is the recovery and survival. Thus, monitoring the adenosine nucleotide pools during ischaemia and reperfusion seems to provide useful information about how well the tissue will deal with the ischaemia and the subsequent reperfusion injury.

To summarise, the results obtained in this chapter show how changes in adenosine nucleotide levels during ischaemia and upon reperfusion occur. We now have a more detailed understanding of the rapid, temperature- dependent decrease in ATP/ADP during ischaemia. This characterisation of ATP/ADP ratios during ischaemia and the fact that it is conserved among tissues and species, make it a good marker for ischaemia and recovery upon reperfusion.

Chapter 4

Development of an ischaemia reperfusion model in adult murine cardiomyocytes utilising true anoxia

4.1 Introduction

4.1.1 Hallmarks of ischaemia

In the previous chapter, I generated a detailed analysis of ATP/ADP ratios and the changes in the adenosine nucleotide pools during ischaemia using a murine heart transplantation model plus a number of other transplantation models. This work showed that a decrease in the ATP/ADP ratio and loss of adenosine nucleotide pools are valid markers for the severity of ischaemic insult and subsequently, IR injury. In parallel with these studies, my colleagues investigated the accumulation of succinate in various species and tissues both *ex vivo* and *in vivo* (Chouchani et al., 2014a; Martin et al., 2019).

In our recently published study on the role of succinate accumulation as a driving force for ischaemia reperfusion injury during organ transplantation, we characterised how ATP/ADP ratios, lactate and succinate change during cardiac ischaemia. As depicted in figure 4.1, temperature has a huge impact on changes in these ischemic markers, suggesting the necessity of maintaining a consistent temperature throughout experiments. ATP/ADP ratios (Figure 4.1, A) have been described in detail in the previous chapter and show a rapid decrease within a few minutes of warm ischaemia in heart tissue. Lactate (Figure 4.1, B) as well as succinate (Figure 4.1, C) show a rapid accumulation within 12 min of warm ischaemia at body temperature. As specified in this study, these changes were overall the most striking within ischaemic tissue and therefore represent essential hallmarks of ischaemia.

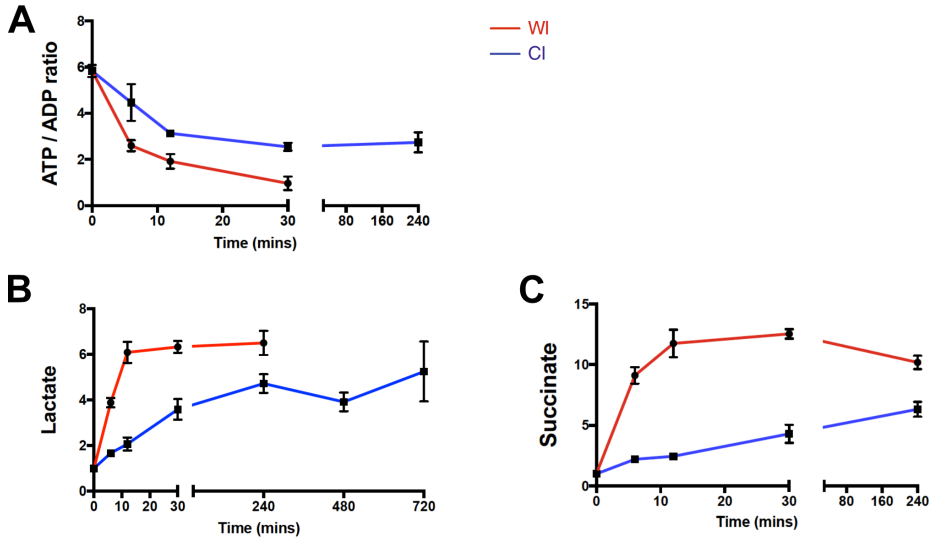

Figure 4.1: Hallmarks of ischaemia in ischaemic heart tissue. Ischaemia was induced in mouse hearts at either 37°C (WI = warm ischaemia) or 4°C (CI = cold ischaemia). At different time points, tissue samples were rapidly clamp frozen and analysed for adenosine nucleotide concentrations and metabolomics. (A) ATP/ADP ratios were determined as described in chapter 3, figure X. (B-C) Lactate and succinate were measured using a mass spectrometry approach and are presented as fold change of control. n= 3-6 biological replicates, data are shown as mean ± S.E.M. (Martin et al., 2019).

4.1.2 Need for *in vitro* models of ischaemia

Although *in vivo* and *ex vivo* models of IRI are physiologically more similar to situations occurring in patients, there is still a significant need to develop simpler cell models of IRI. When studying the underlying molecular processes, these simpler models are easier to understand compared to more complex *in vivo/ex vivo* systems. Additionally, samples from complex interventions are expensive and difficult to access and retrieve, while cell models enable greater control, allow for more types of measurement and enable high-throughput screening of potential therapies at multiple time points. Especially during the development of new therapies to improve IRI outcome, it is useful to be able to screen a range of compounds in a basic cell model first, before investigating the most promising compounds using in *vivo* models to gather evidence to support clinical trials. Because of the limitations of current IRI cell models, many compounds used *in vivo* have so far not been examined in great detail *in vitro*, often making the mechanism of action of the compounds uncertain and rendering compound optimisation challenging.

Cell models have a number of benefits to investigate molecular processes including reproducibility and experimental flexibility as compared to *ex vivo* organ or *in vivo* models. A good example of this is our use of malonate derivatives as malonate pro-drugs. In these experiments, the malonate acts as a complex II inhibitor, to reduce the accumulation of succinate during ischaemia and/or to slow the oxidation of succinate upon reperfusion. Our lab has shown that various malonates are beneficial in a range of models of IRI. However, the complete underlying mechanism of action of these compounds is still unclear, in part because of the difficulty of assessing their efficacy *in vivo*. Additionally, there is still insufficient knowledge about the origin of succinate that accumulates during ischaemia and its metabolism upon reperfusion. All of these points can be investigated in more detail in cell models with the use of different interventions, such as OXPHOS inhibitors, mitochondria-targeted antioxidants or MPTP inhibitors. Furthermore, cellular models open up opportunities for studying metabolic pathways using methods such as tracing metabolism of ^{13}C-labelled precursors using mass spectrometry.

4.1.3 Limitations of current cell models of ischaemia

As discussed above, determining the origin and fate of metabolites during ischaemia and reperfusion, investigating cellular pathway activation and the time course of these processes is difficult in complex organ systems. Over the years, various cardiomyocyte cell models have been developed to mimic hypoxia and reperfusion and to analyse the intracellular responses in detail. While these cell models have provided useful information, working with cell models and hypoxia is associated with limitations which make the comparison to organ and *in vivo* systems problematic. Some of these limitations are described below.

One concern is that the mitochondrial metabolism of cultured cells typically differs considerably from cells found *in vivo*. Most commonly used cultured cell models are cancer cells that grow and divide very rapidly. Their metabolism differs significantly from healthy cells, particularly with regard to mitochondrial metabolism. One way around this is to use primary cells derived from organs, however it is important to note that even primary-derived cells can undergo metabolic remodelling when removed from the supporting structure of an organ and their interaction with other cell types. These interactions enable exchange of metabolites and signalling molecules that are necessary for function of the cell within the organ.

It is also important to note that tissues often rely on mitochondrial energy production which is inhibited by ischaemia. Cardiomyocytes *in vivo* respire primarily on the β-oxidation of fatty acids which drives mitochondrial dependent ATP production. During ischaemia, *in vivo* cells switch to glycolysis based on glycogen breakdown. On the other hand, most isolated cell types rely primarily on glycolysis for energy production, not on their respiratory chain, because they can utilise glucose and glutamine/glutamate supplied in culture media as their primary fuels.

Additionally, the physiological function of most isolated primary cells is suppressed and as a result of that, the cells become glycolytic, shifting away from using OXPHOS for ATP production (Goldberg et al., 2012; Li et al., 2014; Wilson et al., 2014). For example, cardiomyocytes in culture are seldom undergoing contraction as they would in *vivo*. However, they still rely on their mitochondria for other functions, such as calcium buffering and quality control that can lead to, or avoid cell death.

The severity of hypoxia/anoxia in pathological situations may vary. For example, in a heart attack, the location of anoxic and hypoxic zones is dependent on the size and proximity of the blood vessel occlusion and the amount of time tissue is cut off from its blood supply. In comparison, during transplantation, the tissue is completely cut off from its blood supply for extended periods of time, sufficient to achieve a full depletion of oxygen to anoxic levels.

Cell models for IRI which have been developed and published are summarised in Table 4.1. None of them can perfectly mimic IRI in patients and diseases, because of the absence of one or more ischaemic characteristics such as rapid depletion of ATP, accumulation of succinate and lactate, lactic acidosis, glycogen depletion and ROS production upon reperfusion. An additional concern about these models is that they are not good mimics of the true anoxia that occurs during ischaemia *in vivo.* Within tissues, the activity of mitochondria in conjunction with the lack of blood flow will lower the concentration of oxygen to well below the apparent Km for cytochrome oxidase (25 mM), which was confirmed by measurements of true anoxia within ischaemic tissues (Chandel et al., 1996). In contrast, cell models are usually incubated in specialised cell incubators under conditions of hypoxia (0.1 to 5% O_2, table 4.1), not anoxia. Large reservoir of oxygen in the medium and incubation system prevents oxygen-consuming mitochondria from decreasing the oxygen to the anoxic levels seen *in vivo* during ischaemia. In addition, isolated cells are spread out widely over culture dishes in monolayers, often without cell/cell interactions. This might enable easier access to oxygen than in tightly-packed cell structures of tissues. Thus, it is possible that differences in *in vitro* versus *in vivo* models occur due to the residual oxygen in the cell models

in vitro. It is technically difficult to remove all of the oxygen from the environment and especially in isolated cells, even small amounts of residual oxygen can be sufficient to maintain many aerobic pathways and therefore prevent real anoxia.

Table 4.1: List of recent primary cardiomyocyte models for hypoxia and ischaemia reperfusion injury with focus on their ischaemic markers.

Type	Species	Oxygen tension	Hypoxic Time	Temp.	Buffer system	Biomarkers	Reference
embryonic	chicken	1-16%	1-3 h	37°C	M199 (glucose)	ROS	Kulisz2002
embryonic	rat	1 %	1-7 days	37°C	MEM (glucose + serum)	ATP reduction by 30%, apoptotic cell death	Graham et al., 2004
embryonic	rat	1%	6 h	37°C	DMEM (glucose)	Senescence/cell death	Zhang et al., 2007
Comput. analysis	Comput. analysis	Comput. analysis	Comput. analysis	Comput. analysis	Comput. analysis	ATP reduction up to 70%	McDougal et al., 2017
adult	rat	Anoxia, NA	1 h	NA	Tyrode's (glucose free)	Na+ and Ca2+ in- and efflux	Piper et al., 1993
adult	mouse	2%	8 h	NA	DMEM (glucose + serum)	LDH release/cell death	Zhu et al., 2012
adult	rat	0.5%	30 min	37°C	Hypoxic buffer (lactate-based)	pO2 measured	Chouchani et al., 2014
adult	rat	1%	2-12 h	NA	DMEM (glucose)	Cell viability, cytokine production	Shi et al., 2017
adult	mouse	<0.1%	1 h	37°C	DMEM (glucose)+palmitate and pyruvate	Succinate accumulation	Zhang et al., 2018

Table 4.1 summarises some characteristics of a selection of recently published cardiomyocyte models for hypoxia and reperfusion. The high variability between the different models is striking: durations of hypoxia and available nutrients in the buffer systems vary, as well as the

amount of oxygen present. Often, composition of buffers and temperature were not sufficiently controlled in these studies. In addition, in many of these models the hypoxia is not true anoxia. Furthermore, the models have not been evaluated sufficiently, with markers of anoxia/hypoxia such as lactate accumulation and ATP depletion rarely being investigated.

Ischaemia *in vivo* is not characterised only by hypoxia/anoxia but also by the lack of blood flow. This means that ischaemic tissues are no longer supplied with glucose and have to rely on their internal glycogen stores. In isolated cells, however, large volume of incubation medium provides continuous supply of glucose, which can further serve as a primary fuel source. This causes a diversion of the energy metabolism from the *in vivo* scenario, as described above.

Another characteristic consequence of ischaemic lack of blood flow is accumulation of metabolite lactate. Lactate accumulates in ischaemic cells as a product of anaerobic glycolysis when glucose is oxidised to pyruvate which in turn is converted to lactate by the enzyme lactate dehydrogenase in order to oxidise the coenzyme NADH back to NAD^+, which is required for further glycolysis. Lactate is transported out of cells and tissues via membrane transporters of the monocarboxylate transporter (MCT) family. These transporters localise to the plasma membrane and utilise lactate transfer in and out of cells. The proteins contain a substrate binding site in which they bind a proton first followed by a monocarboxylate. It undergoes a conformational change then and releases the bound compounds to the opposite site of the membrane (Halestrap and Meredith, 2004; Halestrap and Price, 1999; Halestrap and Wilson, 2012). The lack of blood supply to tissues *in vivo* and the small amount of extracellular fluid means that they cannot release large amounts of the accumulated lactate. In contrast, isolated cells can release the lactate to their surrounding environment.

Another difficulty with isolated cells is that they are maintained in a highly buffered system. *In vivo*, lactate accumulation is associated with a drop in cytosolic pH. Because cell culture media are highly buffered, there will not be a large a drop in pH of the surrounding cellular environment and cells in culture do not suffer from this aspect of ischaemia.

For all these reasons, the markers of severe ischaemic response we see in the *in vivo* models, such as the depletion of adenosine nucleotides and accumulation of succinate, are rarely observed in the cell models published so far. This highlights the need for development of a cell model that can better mimic these ischaemic changes.

4.1.4 Strategies for improvement of current cell models of ischaemia

One way to address the lack of true anoxia in the cell models may be by the use of an anoxic chamber, rather than the hypoxic chambers usually used. Anoxic chambers are widely used in chemistry for processes that require complete elimination of oxygen. This true anoxic environment might enable us to mimic what occurs in severe ischaemic tissues. Most of the cell models to date have used incubators or hypoxic chambers designed for assessing cells under conditions of low oxygen (down to 0.1% O_2). However, a comparison between anoxic and hypoxic chambers has not been performed in respect to the recent findings of metabolic changes and metabolite accumulation during ischaemia and it is therefore not clear how much oxygen is sufficient for isolated cells to perform sufficient cell respiration to avoid succinate accumulation. A thorough comparison of hypoxic versus anoxic cell model would therefore add important details to the current understanding of cellular processes during ischaemia and reperfusion.

In assessing whether a cell model of IRI mimics the situation *in vivo* we can use the hallmarks of ischaemia discussed above that we have measured in ischaemic tissues. These include the rapid accumulation of lactate and of the TCA cycle metabolite succinate, as well as rapid reduction in the ATP/ADP ratio and loss of the adenine nucleotide pools. However, these have rarely been investigated in the hypoxic cardiomyocyte and cell models described in table 4.1. A comprehensive study of these markers to see if they occur *in vitro* as well as how well they mimic changes occurring in tissues would give important new insights into the molecular mechanisms that occur during IRI.

Cell death is another commonly used endpoint when analysing IRI in cell models, which has been investigated in some of the previously published work. Some of these studies identified necrosis as the main cell death pathway upon reperfusion injury, while others pinpointed apoptosis. As stressed out in the introduction, necrosis leads to plasma membrane permeabilization and consequently to the release of cellular contents. Apoptosis, on the other hand, allows the degradation of most cellular content before membrane permeabilization and therefore utilises different signals towards neighbouring cells and to the adaptive immune system (Honda et al., 2005; Krysko et al., 2008). Both of these scenarios are likely to be involved in IRI. The lack of energy availability will likely cause some cell death by necrosis during ischaemia/anoxia. Then upon reperfusion, the return of oxygen to cells causes the accumulated succinate to drive reverse electron transfer (RET) at complex I, leading to

increased ROS production. This in turn induces the MPTP, damages fatty acids, DNA and proteins and can lead to cell death by necrosis as well as apoptosis. Indeed, *in vivo*, both forms of cell death have been reported, whereby necrosis leads to tissue fibrosis while cell death by apoptosis during IR injury may cause lower levels of damage (Diwan et al., 2008; Dorn, 2008; Gürtl et al., 2009). Thus, assessing cell death by apoptosis *in vitro* is also useful. A number of markers is available to study apoptosis, including caspase activation, DNA laddering assessed by TUNEL staining and exposure of phosphatidyl serine on the cell surface (Wlodkowic et al., 2011).

Altogether, the need for a cellular IRI model is clear, but those developed so far are limited, mainly due to the use of non-physiological cell lines and the lack of true anoxia.

Consequently, results differ significantly from those observed in *in vivo* models, hampering the studies of molecular basis of IRI and evaluation of therapies (Chouchani et al.2014, Pell et al. 2016, Martin et al. 2019). Here, I aim to develop a cardiomyocyte cell model of true anoxia that enables a more detailed analysis of ischaemia reperfusion injury in the heart, as well as the screening of potential therapies. A schematic overview about the workflow of isolating cardiomyocytes (A) and inducing anoxia and reoxygenation (B) is presented in figure 4.2.

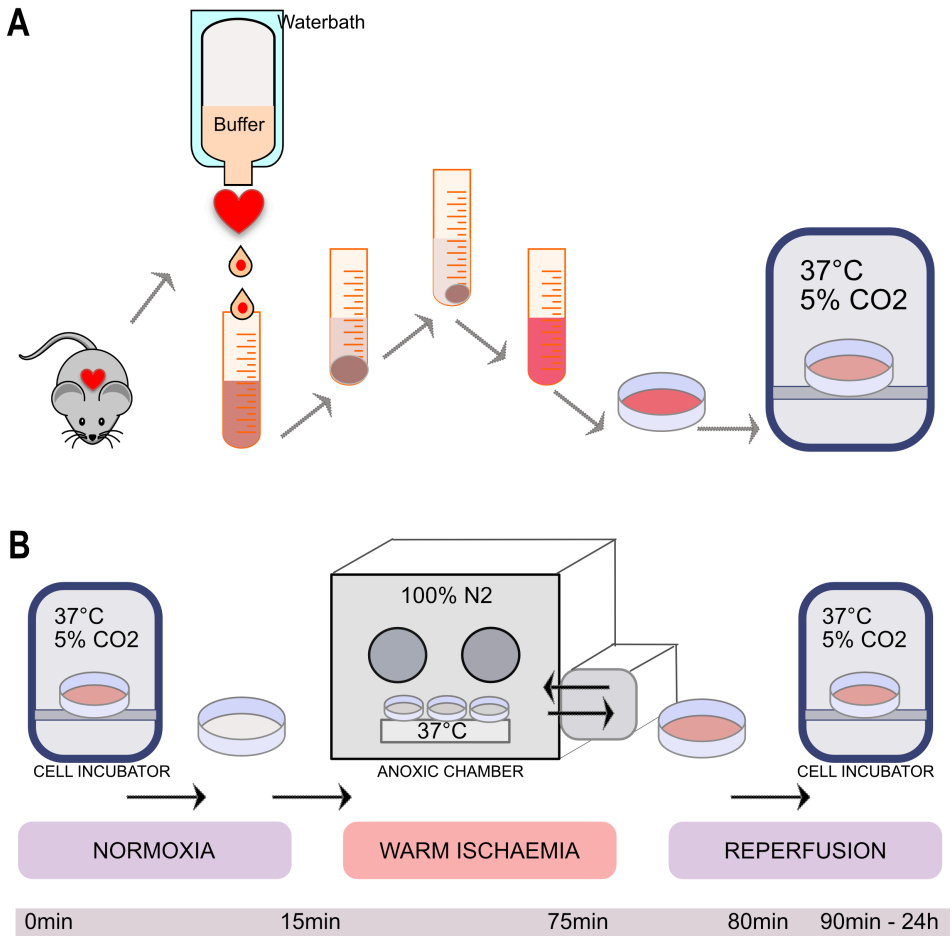

Figure 4.2: Schematic workflow overview. A) Primary murine adult cardiomyocytes were isolated from freshly retrieved hearts and cultured overnight at 37°C, 5% CO_2. B) Anoxia and reperfusion were induced utilising an anoxic chamber. Cells were washed and transferred into experiment buffer, degassed and moved into the anoxic chamber. The samples were either maintained at various time points of anoxia and lysed within the chamber or transferred out of the chamber, put into oxygenated cell medium and kept in a cell incubator for different reperfusion time points.

4.2 Aims

Because no physiologically relevant cardiomyocyte model for ischaemia reperfusion injury that truly mimics *in vivo* conditions as they occur during organ transplantation has been generated so far, the aim of this part of the project was to develop a cell model utilising true anoxia utilising primary adult murine cardiomyocytes. This model was then used to investigate if the hallmarks of ischaemia that have been elucidated in tissues occur *in vitro* as well. Firstly, a true anoxic environment in an anoxic chamber was compared to hypoxic conditions at 0.1%

O_2. Furthermore, different buffer systems were assessed to identify their similarity to the ischaemic environment *in vivo*, by focussing on manipulating the transport of lactate. The novel cell model was assessed using markers of severe ischaemia such as ATP/ADP reduction, lactate and succinate accumulation and oxidative damage upon reperfusion.

4.3 Results

4.3.1 Viability of Cardiomyocytes

Adult cardiomyocytes have a distinct rod-like shape. Their size varies from 50 to 150 µm in length and 20 to 40 µm in diameter. Within cardiac muscle tissue, these cells form fibres linking myocytes via intercalated discs (Wilson et al., 2014). These intercalations enable the transfer of electrical impulses and therefore coordinated, calcium-regulated contraction as a response to the transition of an action potential. Calcium is utilised by cellular sarcomeres to enable muscle contraction (Fearnley et al., 2011). Cardiomyocytes contain bands of myosin and actin that are responsible for the distinct striated structure of cardiac myocytes. Adult primary cardiomyocytes do not adapt easily to cell culture environment and, for example, cannot tolerate serum in their media and are sensitive to antibiotic treatment. Furthermore, *in vivo* they rely on β-oxidation of fatty acids for energy production and to a smaller extent on glycolysis. In order to ensure that the cells remain alive and healthy after isolation and to monitor their behaviour over time during experiments, performing regular cellular viability assessment is crucial. Adult cardiomyocytes are fully differentiated cells which do not undergo cell division and can become senescent when removed from their supporting tissue environment. Alignment of the cells and their contraction due to an electrical current can increase survival of the cells (Stoppel et al., 2016), but this was not possible in my simple cell culture model. For these reasons, experiments have to be performed within a few days of isolation and it is crucial to control the amount of cell death that occurs in cardiomyocyte incubations. To do this, it is important to investigate viability and cell death in these cells over time and to monitor phenotypic changes, as well as understand which cell death pathways are activated. Furthermore, cell death was one of the endpoints used to assess severity of IRI as it is the ultimate outcome of severe ischaemic injury.

4.3.1.1 Cardiomyocyte Incubations

As described in the Methods chapter, the cells were isolated from mouse hearts, counted using a Neubauer chamber and suspended in M199 medium at a density of ~ 10^5 cells/mL. The cell suspension was then transferred to 60 mm diameter glass Petri dishes and incubated for 24 h to allow adhesion of the cells. After experimental treatment, the cells were often directly solubilised in perchloric acid or Triton-X100-containing buffers which made routine protein quantification difficult. Therefore, for most experiments, the number of initially plated cells was used to normalise the samples within and between different experiments.

Healthy, living cardiomyocytes are easily distinguishable from dying ones, due to their distinct rod- like shape, while dying cells collapse, round up and become smaller (figure 4.3). The dead cells also detach from the plate and release their cytosolic content into the surrounding medium, enabling lactate dehydrogenase (LDH) release to be used to measure the amount of cell death. Figure 3 displays cultured cardiomyocytes after isolation. A combination of rod-shaped and round cells is visible in a 4x brightfield microscopy image. The round cells are cardiac myocytes that did not survive the isolation process and their cell membrane collapsed (A, C) while close up pictures of the rod-shaped cells show their distinct striated structure (B, D). The number of rod-shaped vs round cells, or the uptake of dyes that are excluded by healthy cells can also be used to assess viability.

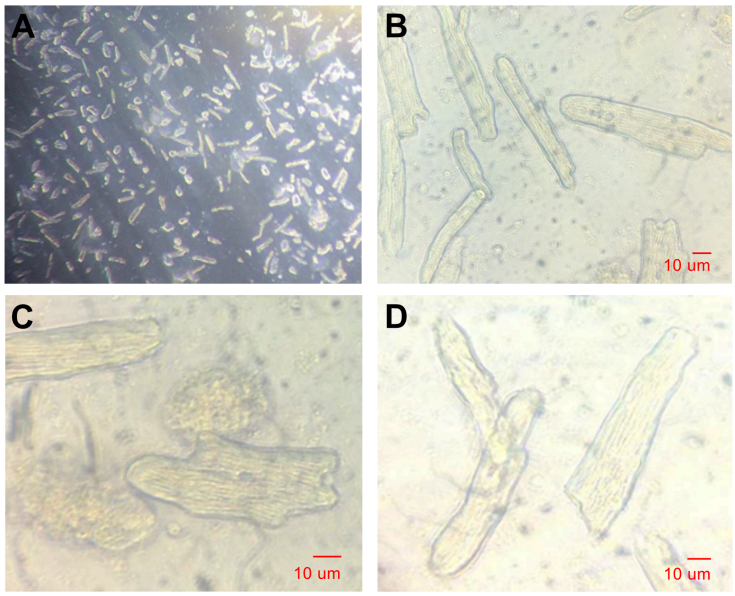

Figure 4.3: Brightfield images of cardiomyocyte culture. Cultured cardiomyocytes 2 h after isolation. A) Brightfield image (4x) of a laminated glass dish containing isolated primary adult cardiomyocytes in M199 medium. B - D) Close up images of rod shaped healthy, or round dying or dead cardiomyocytes.

4.3.1.2 Assessment of Cell Death by Apoptosis vs Necrosis

4.3.1.2.1 Apoptosis

Cardiomyocytes undergo different forms of cell death, with the two main ways being apoptosis and necrosis (Chiong et al., 2011). The literature suggests that both of these pathways may be activated upon IR injury *in vivo* as well as *in vitro*. Therefore, I analysed apoptosis by measuring caspase 3 and 7 activation in these cells (Figure 4.4). I first set out to establish positive controls by inducing apoptosis. This was done by treating the cells with different apoptosis-inducing compounds or UV irradiation. Neither staurosporin nor doxorubicin, which are widely used to induce apoptosis, could elevate caspase activity significantly, in comparison to untreated control cells. However, 9 h of UV irradiation induced a significant amount of apoptosis and was therefore used as positive control in further experiments. This showed that relative rates of apoptosis could be assessed in adult cardiomyocytes. To further investigate cell death pathways, I compared these results to general cell death, measured by LDH release.

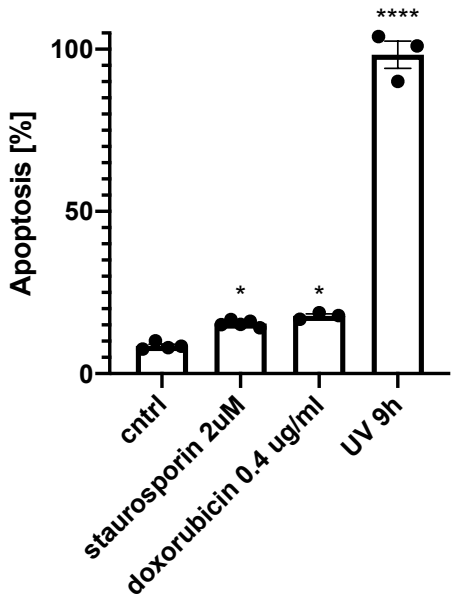

Figure 4.4: Apoptosis in primary murine adult cardiomyocytes. Apoptosis was measured via caspase 3 and 7 activation. Cells were either untreated, treated with staurosporin (2uM), doxorubicin (0.4ug/ml) or 9 h of UV irradiation, which was the positive control used to calculate percentage of total cell death via apoptosis. n= 3-5 biological replicates, data are mean ± S.E.M. Statistical analysis via one-way ANOVA. *P < 0.05, ****P < 0.0001.

4.3.1.2.2 Measurement of cell death by LDH release

The release of LDH is a general marker for cell death by either necrosis or apoptosis, and is therefore a commonly used marker. In order to analyse cell injury, I measured the increase in LDH release from isolated adult cardiomyocytes with increased cell culture time (Figure 4.5). Progressive cell death in control cells in cell medium was monitored over time. A small increase in LDH was detected after 24 h. Furthermore, glucose starvation induced the release of LDH into the cell supernatant. The experimental buffers used, including Tyrode's buffer (glucose-based), addition of the MCT1 inhibitor AR-C141990 (T141990) and Hypoxic buffer (lactate-based) did not alter the release of LDH. Because an increase in LDH release starts to occur within 24 h after initiating culture, all experiments were performed within 1-2 days of isolation of the cardiomyocytes.

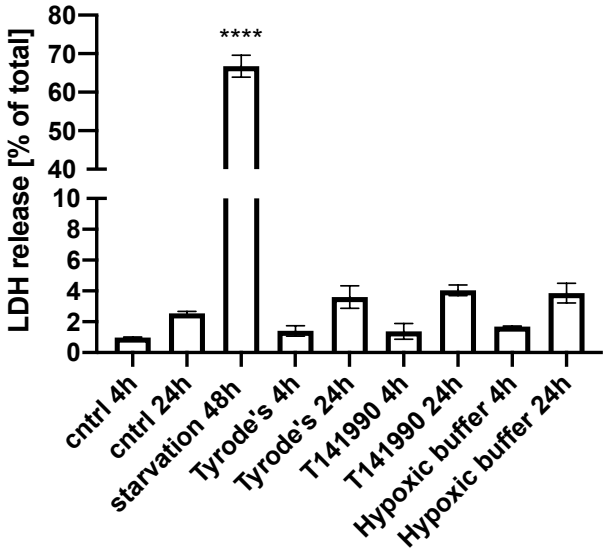

Figure 4.5: LDH release from primary cardiomyocytes. Cardiomyocytes were cultured in a cell incubator at 37°C, 5% CO_2 for different time points and in different buffers. Necrotic cell death was evaluated by measuring the amount of LDH protein released into the cellular supernatant via absorbance at 492 nm. The cells were cultured in M199 medium for 4 or 24 h or starved for 48 h to induce cell death. LDH release was measured as well after cells were cultured in the experiment buffers Tyrode's, Tyrode's + MCT1 inhibitor AR-C141990 (T141990) or Hypoxic Buffer for 4 or 36 h at 37°C, 5% CO_2. Elevated LDH levels indicate increased cell death. Results are presented as percentage of a positive control of cardiomyocytes lysed in 1% Triton. n= 4 biological replicates, data are mean ± S.E.M. Statistical analysis via one-way ANOVA, ****P >0.0001.

Based on these experiments, I concluded that assessment of cell death by LDH release is robust and quantitative, hence this was my main method used to assess cell death during the development of IRI model in isolated cardiomyocytes.

4.3.2 Development of an *in vitro* model of ischaemia

As described in the introduction and in Table 1, several models for hypoxia *in vitro* in primary cardiomyocytes have been described before but none of them can truly replicate results obtained in ischaemic tissues. My hypothesis was that this was in large part due to the *in vitro* systems not establishing true anoxia, as would occur *in vivo* during ischaemia. To develop the physiologically closest cell model to *in vivo* models, I therefore looked at how markers for "true" ischaemia *in vivo* were replicated in various incubation conditions *in vitro*.

4.3.2.1 Comparison of different systems used to mimic ischaemia in vitro

A direct comparison of conventional *in vitro* models with those in which anoxia was confirmed has not been done previously. Figure 4.6 depicts a schematic overview of the different systems I used to induce IRI. Cells were kept either in a plate reader under 0.1% O_2, at 37 °C and 5% CO_2 (hypoxia) or in an anoxic glove box with 0.1 – 10 ppm O_2 under N_2 (anoxia). Furthermore, different buffer systems were also analysed to see how these affected markers of ischaemia: physiological glucose-based buffer (Tyrode's buffer) or lactate-based buffer often used to model chemical hypoxia (Hypoxic buffer).

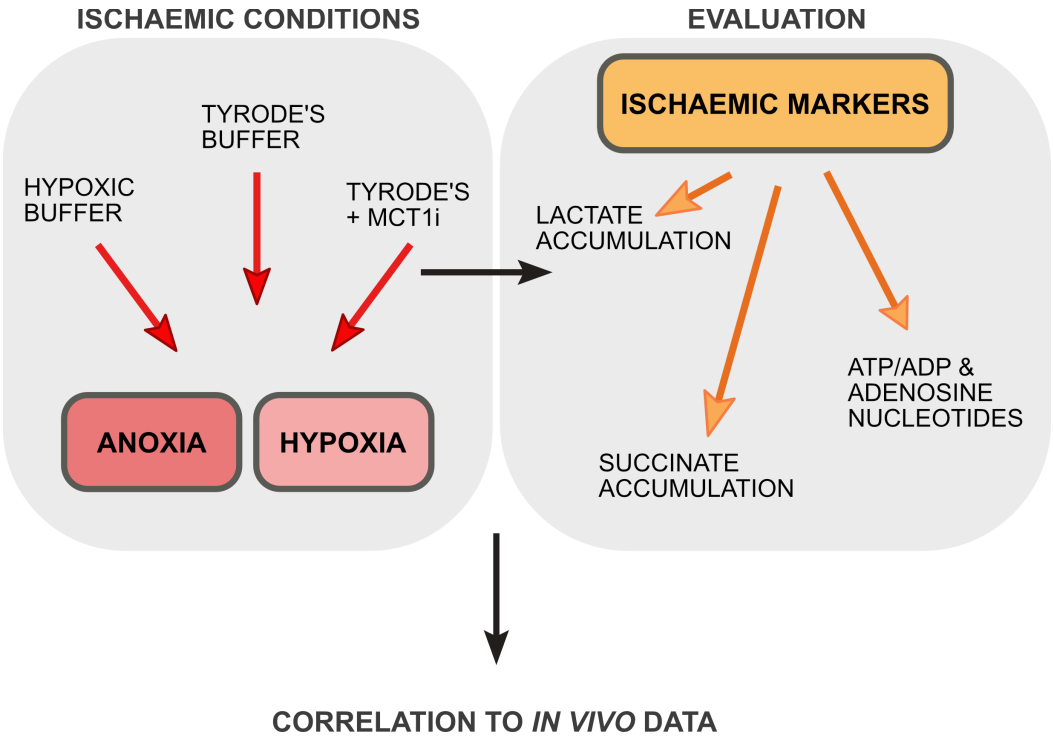

Figure 4.6: Experimental design. Schematic overview of the different ischaemic conditions used and the ischaemic markers that indicated the severity of ischaemia. Ischaemia was either induced in a lactate-based hypoxic buffer or glucose-based Tyrode's buffer in an anoxic chamber with <10 ppm O_2. Or in glucose-based buffer supplemented with MCT1 inhibitor to investigate the effect of metabolite transport inhibition on cellular IRI. Furthermore, the impact of residual oxygen was investigated by comparison of true anoxia to hypoxia. The markers for ischaemia investigated here are lactate and succinate accumulation and loss of adenosine nucleotides. Investigating these different ischaemic conditions and comparing ischaemic markers in an isolated cardiomyocyte system to *in vivo* data enabled the development of a physiologically relevant cell model for ischaemia reperfusion injury.

These different *in vitro* incubation conditions were compared by analysing a number of markers for ischaemia that were determined in the *in vivo* and *ex vivo* systems in the previous chapter where the heart was exposed for genuine ischaemia. As described there, decreases in the size of the adenosine nucleotide pools, and in the ATP/ADP ratio are hallmarks of ischaemia and severe hypoxia in the tissue samples (Chapter 3). Furthermore, as our lab has published before (Martin et al., 2019), this change in the ATP/ADP ratio and size of the adenine nucleotide pools goes hand in hand with an increase in lactate as well as succinate concentrations during ischaemia (Figure 4.1). Therefore, a cell model that successfully replicates the pathological cardiac IRI found in *vivo* would be expected to show similar changes during the phase modelling ischaemia.

4.3.3 Comparison of the effect of *in vitro* anoxia to hypoxia on cardiomyocyte function

4.3.3.1 Assessment of the effect of hypoxia at 0.1% O_2 on cardiomyocyte function

Most hypoxic chambers routinely used for cell incubations cannot control the oxygen tension tightly enough to allow oxygen concentrations below 0.1 - 1%, which is thought to be in excess of the O_2 levels found during ischaemia *in vivo*. To address the extent to which these widely used hypoxic conditions mimicked those occurring in ischaemic tissues *in vivo*, I utilised the ClarioStar plate reader from BMG Labtech. This system has a gas control as well as temperature control unit to incubate cells at 0.1% oxygen. To see how accurately this system reflected *in vivo* ischaemia, I incubated cardiomyocytes under 0.1% oxygen for a range of time points and then measured the effect on the ischaemic markers adenosine nucleotides, lactate and succinate (Figure 4.7).

Analysis of the adenosine nucleotide pools and of the ATP/ADP ratios of cardiomyocytes incubated at 0.1% O_2 for 1 to 5 h shows that there is a small, consistent decrease in both the ATP/ADP ratio and in the magnitude of the adenine nucleotide pools (Figure 4.7, A- B). Interestingly, the levels of nucleotides, especially of ADP, increased after 5 h incubation under hypoxic conditions, pointing to a form of metabolic adaptation to the hypoxia. Lactate did not accumulate within the cells after 2 h of hypoxia, but increased sharply after 5 h incubation, perhaps reflecting an upregulation of glycolysis in response to hypoxia (Figure 4.7, C). Most interestingly, monitoring succinate concentrations within these cells revealed no major increase during the 5 h incubation at 0.1% O_2 (Figure 4.7, D).

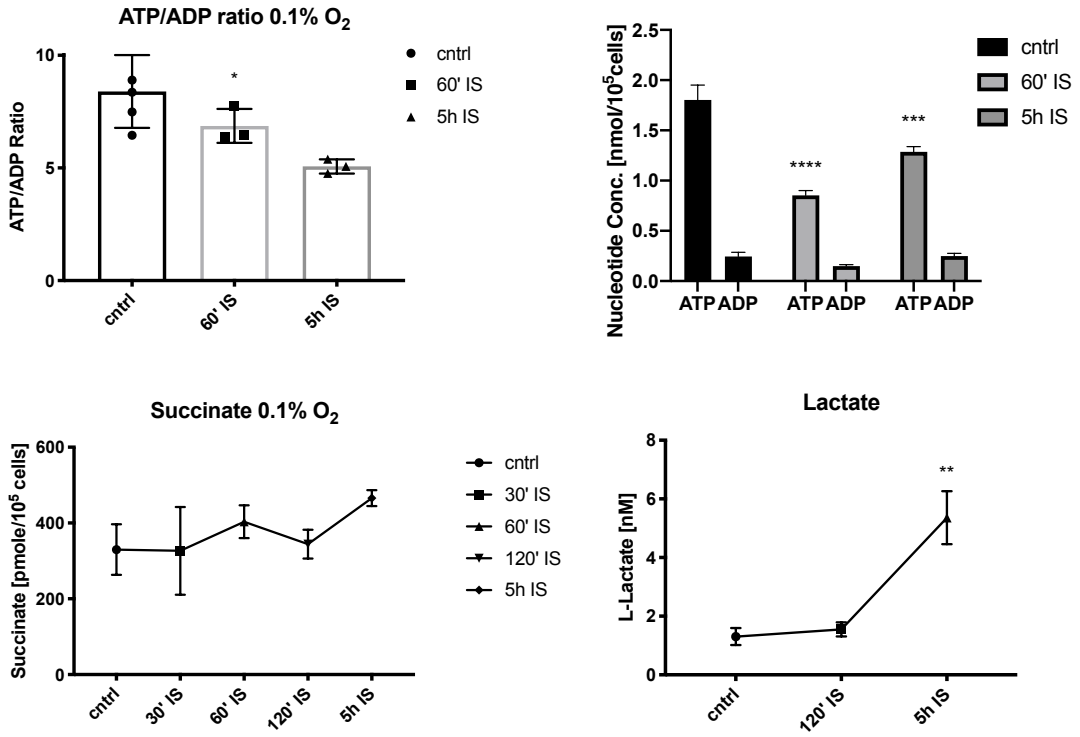

Figure 4.7: Evaluation of cellular changes within cardiomyocytes during hypoxia at 0.1% O_2. Changes in ischaemic markers in primary murine cardiomyocytes were evaluated utilising a hypoxic system at 0.1% O_2, 5% CO_2 at 37°C in a CLARIOStar plate reader. The cells were cultured on laminated 6-well plates 24 h before hypoxia was induced for 1-5 h in Tyrode's supplemented with 10 μM MCT1 inhibitor. Cells were lysed immediately upon retrieval from the plate reader under oxygenated conditions and ATP/ADP ratios (A), adenosine nucleotide pools in form of ATP and ADP as nmol/10 000 cells (B), L-Lactate in nM (C) and Succinate in pmol/10 000 cells were measured via luminescence, absorbance or mass spectrometry approaches. n = 3-5 biological replicates data are mean ± SEM. Statistical analysis via one-way ANOVA, *P =0.01, **P=0.05, ***P=0.001, ****P >0.0001.

Overall, the metabolic changes observed under hypoxia at 0.1 % O_2 were far less pronounced than those seen in tissues during ischaemia *in vivo*, as described in the previous chapter. However, these differences were broadly representative of those published in a range of other cell models utilising similar incubations in biological incubation systems designed to lower O_2 to hypoxic levels (see table 4.1).

4.3.3.2 Comparison of cardiomyocyte incubations under conventional hypoxic conditions to incubation under anoxic conditions

I next set up a system to incubate cardiomyocytes under conditions of true anoxia and compared the changes that occurred in the cardiomyocytes to these occurring during hypoxia. To develop conditions of true anoxia, I used an anoxic chamber that can hold O_2 level below 10 ppm (cf. 0.1% = 1000 ppm) with the temperature controlled at 37°C using a heat block. In addition, to better mimic the situation during ischaemia *in vivo*, I also wanted to imitate the lack of a large amount of extracellular fluid and associated lactate build up in the cell. To do this, all of the experiments shown in Figures 4.6 and 4.7 were performed in Tyrode's buffer containing 10 μM MCT1 inhibitor AR-C141990. The inhibitor will prevent lactate efflux from cells into the excessive supernatant, which does not occur in tissues where extracellular fluid volumes are small and therefore quickly saturated with lactate. Instead intracellular lactate concentration will increase as it does in tissues during anoxia.

I directly compared cells subjected to the hypoxic or anoxic set-up in order to investigate differences between these models. This direct comparison between incubation for 1 h at 0.1% O_2 to that <10 ppm O_2 shows significant differences between the two incubation conditions. The ATP/ADP ratio was significantly decreased after 1 h incubation under anoxic but not hypoxic conditions (Figure 4.8, A). Furthermore, both succinate and lactate increased rapidly after incubation under anoxia, in comparison to hypoxia (Figure 4.8, B- C). Importantly, these changes in ATP, ADP, succinate and lactate under anoxic conditions were far closer to those found in tissues *in vivo* and *ex vivo* (Figure 4.1), compared to those found under hypoxic conditions.

These findings are consistent with my hypothesis that there are striking differences between the severities of the metabolic changes that occur in my *in vitro* anoxic incubations and the systems of hypoxic conditions of low, but not zero, oxygen tension *in vitro*. I concluded, that most commonly used cell models for IRI do not induce the same form of ischaemic damage as seen in pathophysiological conditions *in vivo*. Extensive research has compared various forms of hypoxia and its effect on cells and tissues, but recent findings that include the accumulation of succinate during anoxia have not been confirmed in many cell models yet (Lochner, 1978; Lochner et al., 1979; Piper et al., 1993; Wendt et al., 2009). And especially the efflux of this metabolite that might be facilitated by monocarboxylate transporters (Cortés-Campos et al., 2011; Zhu et al., 2013) has not been investigated so far.

Therefore, for the rest of this study I continued to utilise my new model of true anoxia in conjunction with inhibitors of MCT1.

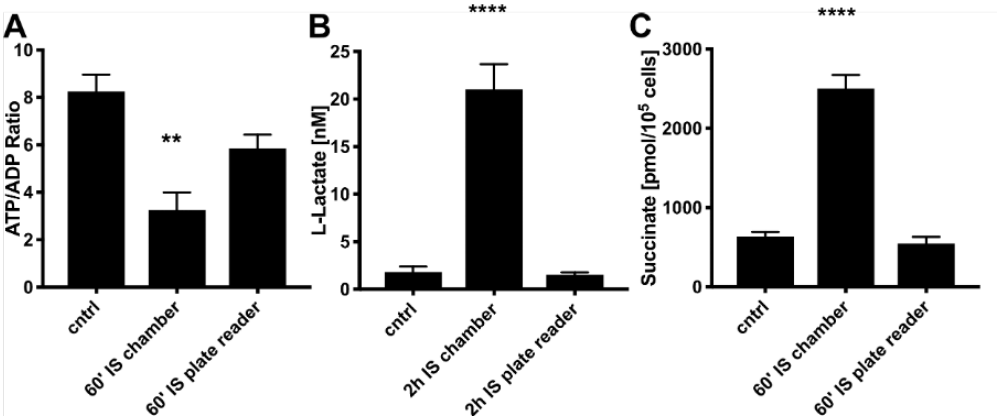

Figure 4.8: Comparison of cellular changes during true anoxia and hypoxia. Cardiomyocytes (in Tyrode's + 10 µM MCT1 inhibitor) were either maintained at 37°C, 5% CO_2 in a cell incubator (control), in an anoxic chamber at 37°C (anoxia) or at 0.1% O_2 at 37°C (hypoxia) for 1 or 2 h. ATP/ADP ratios (A), L-Lactate in nM (B) and succinate in pmol/10 000 cells (C) were evaluated as ischaemic markers and directly compared. n= 3-4 biological replicates, data are mean ± S.E.M., statistical test: one-way ANOVA, **P<0.008, ****P<0.0001.

4.3.4 Comparison between different buffer systems used during true anoxia

For the initial analysis of the effect of anoxia versus hypoxia in cardiomyocytes, I used Tyrode's buffer supplemented with the MCT1 inhibitor AR-C141990. However, in this assessment I did not fully characterise the role of AR-C141990 mimicking ischaemia. Therefore, I next focussed on my model of anoxia (also called ischaemia in this model), but compared the effect of different buffer compositions. First, I compared the effect of Tyrode's and Tyrode's buffer + MCT1 inhibitor AR-C141990 (T141990). Then, I assessed "Hypoxic buffer," which mimics the conditions of ischaemia due to increased lactate concentrations and acidosis. Finally, these three buffer systems were compared to determine which can best mimic ischaemia *in vivo* using a cell model. To investigate the severity of anoxia in primary adult cardiomyocytes incubated with these three buffers, I analysed adenosine nucleotide pools and concentrations of the metabolites lactate and succinate over a time course of anoxia.

4.3.4.1 Adenosine nucleotides in cardiomyocytes with the MCT1 inhibitor AR-C141990

As only one concentration of the MCT1 inhibitor AR-C141990 was used in the initial analysis, I next assessed a range of concentrations to find an effective concentration of AR-C141990 for use during cardiomyocyte incubations. To see at which concentration the inhibitor was efficient in supressing lactate efflux into the excessive supernatant and enhance intracellular lactate so that cellular energy production and viability during anoxia were affected, cells were incubated with Tyrode's buffer supplemented with different concentrations of AR-C141990 and adenosine nucleotide concentrations were determined over a time course of anoxia (Figure 4.9). The lower concentrations of 100 nM or 1 µM AR-C141990 showed no significant effect on decreasing the ATP/ADP ratios, while 10 µM AR-C141990 did decrease the levels and thereby induced a cell phenotype that was closer to ischaemia *in vivo*. Therefore, this concentration of AR-C141990 was used for all further experiments.

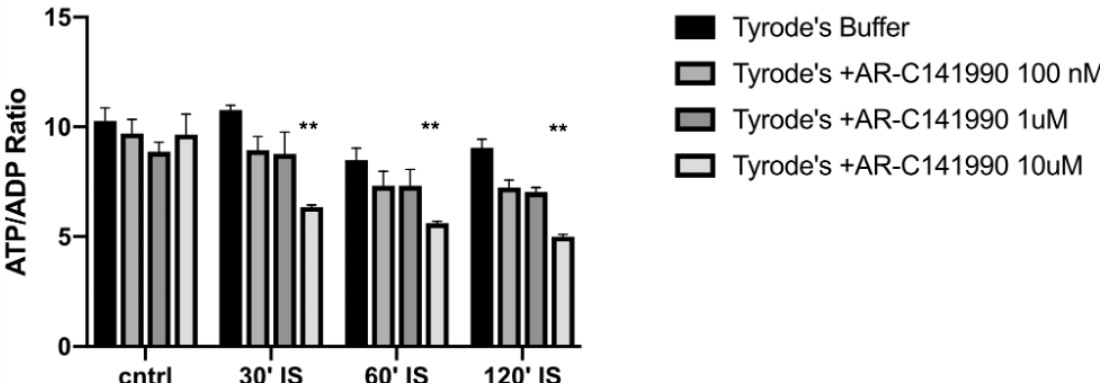

Figure 4.9: The effect of different concentrations of MCT1 inhibitor AR-C141990 on ATP/ADP ratios. Adenosine nucleotides were measured in cardiomyocytes after different periods of anoxia at 37°C in Tyrode's buffer containing 100 nM, 1 µM or 10 µM of the MCT1 inhibitor AR-C141990 and compared to cells maintained in Tyrode's buffer. The change in adenosine nucleotides is presented as ratio of ATP to ADP. n= 3-5 biological replicates, data are mean ± S.E.M., statistical test via two-way ANOVA, **P<0.005.

4.3.4.2 Baseline concentrations of lactate and succinate in the presence of MCT1 inhibition

In order to investigate if MCT1 inhibition affects metabolites in cells even under normoxic conditions, I first compared baseline concentrations of lactate and succinate in the different buffer systems before assessing subsequent changes during anoxia and upon reperfusion. Adult cardiomyocytes were isolated and cultured as described before in Hypoxic buffer, Tyrode's buffer or Tyrode's buffer + AR-C141990 (T141990) and were then subjected to anoxia and reoxygenation before analysis. As shown in Figure 4.10 A-B, the cells incubated in Tyrode's buffer in the presence or absence of AR-C141990 accumulated different amounts of lactate, consistent with its efflux by the MCT1. Cells maintained in T141990 buffer accumulated more lactate than cells in Tyrode's buffer, and consistent with this the latter cells released more lactate into the medium.

There were no significant differences between basal succinate levels when the cells were incubated under normoxic conditions in the different buffers, including Tyrode's buffer and Tyrode's buffer supplemented with MCT1 inhibitor (Figure 4.10 C). Incubation in hypoxic buffer led to a small but non-significant increase in succinate in comparison to cells in Tyrode's buffer (C). However, this could be a response to the high lactate concentration. Because the high concentration of lactate in the hypoxic buffer interferes with the investigation of lactate efflux and also may affect succinate concentration, further experiments focussed on cells incubated in Tyrode's buffer with or without the MCT1 inhibitor AR-C141990.

After determining differences in baseline succinate concentrations in the different buffers, I next investigated the effect of MCT1 inhibition on lactate and succinate accumulation during increasing timepoints of anoxia.

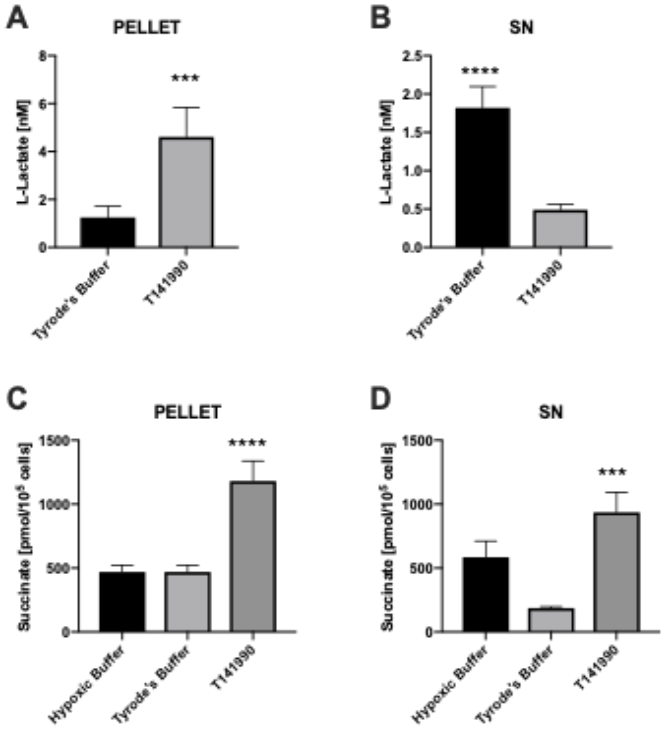

Figure 4.10: Basal levels of intra- and extra- cellular L- lactate and succinate for cardiomyocytes incubated in different buffers. Cardiomyocytes were maintained in Hypoxic buffer, Tyrode's buffer or Tyrode's + AR-C141990 [10 μM] (T141990) for 4 h at 5% CO_2 and 37°C in a cell incubator. L-lactate concentrations in nM were measured utilising absorbance at 450 nm. Succinate concentrations were determined via mass spectrometry in pmol/ 10 000 cells. Intracellular metabolite concentrations were evaluated within cell pellets (A, C), extracellular were extracted from the supernatant (B, D). (A) Cell pellets were collected and the deproteinised using perchloric acid, before lactate was measured. (B) Lactate was directly measured in supernatants retrieved from the cell plates. (C) succinate was extracted from cell pellets or (D) supernatant and basal concentrations determined, n= 4-7 biological replicates, data are mean ± S.E.M, statistical test via one-way ANOVA, ***P<0.001, ***P<0.0001.

4.3.4.3 Effect of the MCT1 inhibitor AR-C141990 on Lactate accumulation by cardiomyocytes during anoxia

I next investigated if the differences between AR-C141990 concentrations were due to the effect of the inhibitor on the ability of cells to excrete lactate into the surrounding media. To assess this, lactate concentrations within the cell pellets and in the surrounding supernatant were determined. The high starting concentration of the lactate concentrations in the supernatant of hypoxic buffer-treated cells made it impossible to assess any further increases in lactate, this buffer was therefore not evaluated in this experiment.

Cells that underwent anoxia in Tyrode's buffer showed only a minor increase in lactate within the cell pellet, but increased concentrations of this metabolite in the supernatant (Figure 4.11), consistent with the export of lactate from the cell by the MCT1 transporter. When cells were exposed to anoxia in Tyrode's buffer containing the MCT1 inhibitor AR-C141990 (T141990), there was a significant increase in lactate concentrations within the cells that occurred after 1 h of anoxia and a further increase after 2 h. A direct comparison between lactate concentrations in the cell's pellets and in supernatant after 1 h of anoxia shows that inhibition of MCT1 with AR-C141990 does decrease lactate concentrations in the supernatant and causes a significant increase in lactate intracellularly (Figure 4.11, A and B). This indicates that inhibition of the lactate transporter decreases the release of lactate from the cell cytosol into the surrounding medium.

Altogether, these data suggest that isolated cardiomyocytes *in vitro* are able to release lactate to the medium during anoxic conditions and thereby avoid accumulation of lactate within the cell pellet. This release of lactate provides a safety valve preventing lactic acidosis within the cells *in vitro*, but this is not available to cells during ischaemia *in vivo*. Therefore, the use of the MCT1 inhibitor AR-C141990 in *vitro* in conjunction with true anoxia provides a better model of ischaemia by inhibiting lactate transport and locking lactate inside the cells via MCT1 inhibition.

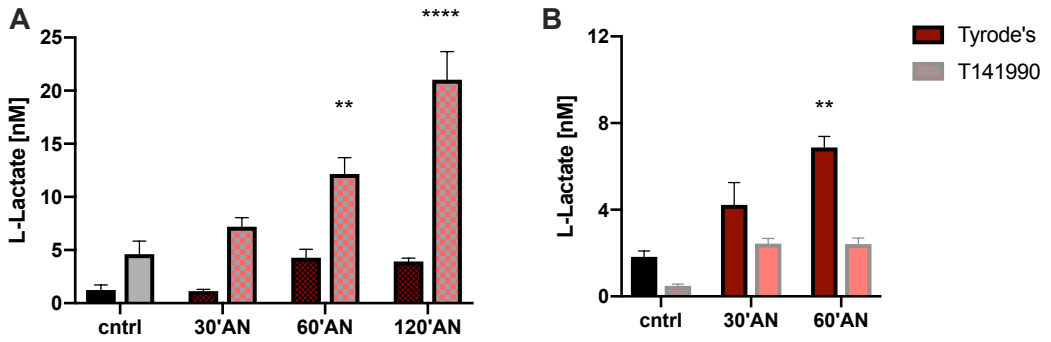

Figure 4.11: Changes in intra- and extra-cellular L-lactate in different buffer systems during anoxia. Cardiomyocytes in Tyrode's buffer or Tyrode's + AR-C141990 [10 µM] were subjected to different periods of anoxia in an anoxic chamber at 37°C. The two buffer systems are displayed in direct comparison. L-lactate concentrations in nM were measured utilising absorbance at 450 nm. (A) Cell pellets were collected and deproteinised using perchloric acid, before lactate was measured. (B) Lactate was directly measured in supernatants retrieved from the cell plates. n= 3-4 biological replicates, data are mean ± S.E.M., statistical analysis via two-way ANOVA. **P<0.01, ****P< 0.0001.

4.3.4.4 Adenosine nucleotide pools in cardiomyocytes during anoxia

I next investigated how the previously demonstrated accumulation of lactate affects the depletion of the adenosine nucleotide pool and the ATP/ADP ratios during anoxia (Figure 4.12). I therefore measured these in the different buffer systems: hypoxic buffer, Tyrode's buffer and Tyrode's with AR-C141990 (T141990).

Cardiomyocytes in the lactate-containing hypoxic buffer lost their ATP over time. After 1 h, the ATP concentrations and ATP/ADP ratios are so low, that it is likely that these cells would not be able to recover upon reoxygenation in comparison to how cardiac tissue behaves as extensively analysed in chapter 3 (Figure 4.12, A- B). Anoxia induced in the glucose-based Tyrode's buffer results in a slight decrease in adenosine nucleotides and ATP/ADP ratios, but stabilises at approximately 66% of control, even after prolonged anoxia (Figure 4.12, C- D). However, after incubating the cells in Tyrode's buffer supplemented with AR-C141990 (T141990), a significant decrease in the ATP/ADP ratios was evident after 30 min of anoxia and the ratios continue to decrease slightly over time (Figure 4.12, E- F).

These results suggest that the combination of excess lactate and anoxia induces a strong ischaemic phenotype in primary cardiomyocytes. In contrast to this, use of the glucose-based Tyrode's buffer alone is not sufficient to deplete the adenosine nucleotide pools during anoxia. Only when lactate efflux from these cells is inhibited with AR-C141990, it is possible to induce an ischaemic phenotype in Tyrode's buffer.

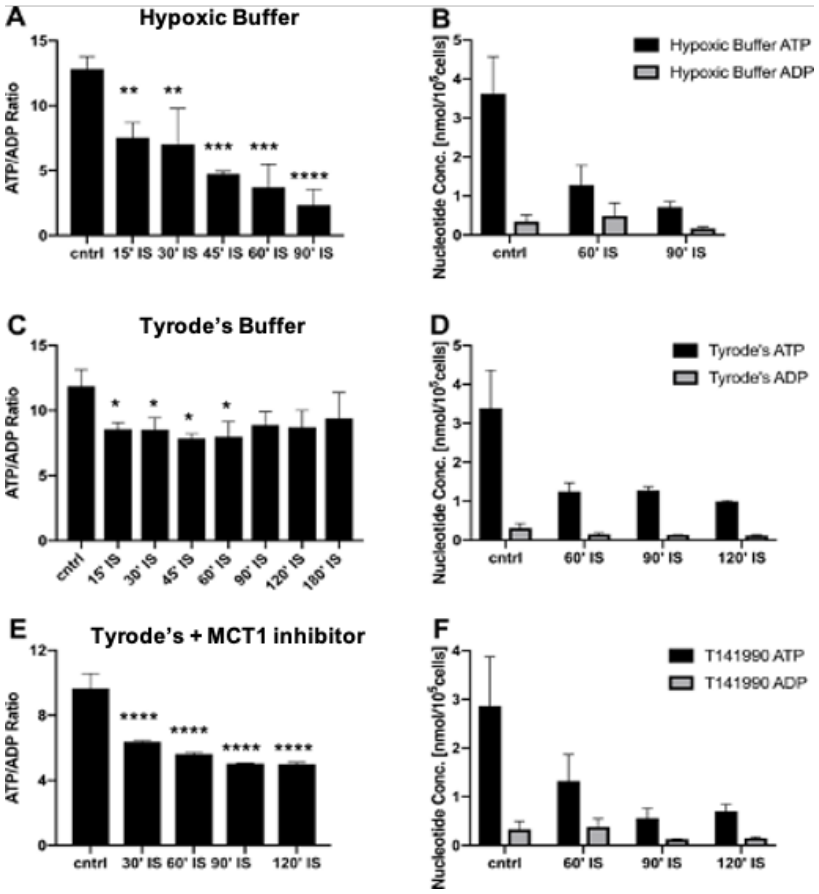

Figure 4.12: ATP/ADP ratios and adenosine nucleotide pools in different buffer systems during anoxia. Adenosine nucleotides were measured in primary murine cardiomyocytes using a Luciferase luminescence assay. Different time points of anoxia at 37°C were induced in either lactate-based Hypoxic Buffer (A + B), glucose- based Tyrode's Buffer (C + D) or Tyrode's + MCT1 inhibitor AR-C141990 (T141990) (E + F). ATP and ADP were measured (B, D, F) and the ATP/ADP ratio calculated (A, C, E). Nucleotide concentrations are measured in nmol/ 10 000 cells. n= 4-6 biological replicates, data are mean ± S.E.M, statistical analysis via one-way ANOVA. *P<0.05, **P<0.01, ***P<0.001, ****P< 0.0001.

4.3.4.5 Succinate accumulation within cardiomyocytes during anoxia

Over the past few years our lab has shown that accumulation of succinate is an important factor in the pathological mechanism of IRI through driving ROS production upon reperfusion (Chouchani et al., 2014a, 2016). Therefore, to validate the ability of cardiomyocytes *in vitro* to mimic *in vivo* ischaemia, I investigated whether succinate accumulates in my isolated cell model of anoxia.

As depicted in Figure 4.12, succinate accumulates within the cardiomyocytes during anoxia in hypoxic buffer (Figure 4.13, A), as well as Tyrode's buffer (Figure 4.13, C) and Tyrode's

+ AR-C141990 (T141990) (Figure 4.13, E). After 1 h without oxygen, there is a significant increase in succinate. Cardiomyocytes that were maintained in Tyrode's buffer plus MCT1 inhibitor show the highest levels of succinate, which indicates that MCT1 inhibition affects the amount of metabolite accumulated in cell pellets.

There is also a clear increase in succinate in the surrounding medium during anoxia (Figure 4.13 B, D, and F). Notably, the biggest increase in extracellular succinate can be detected in the supernatant of cells incubated in Tyrode's buffer. This again underlines the ability of cells to release accumulated metabolites like lactate and succinate out of their cytosol into the supernatant. These data also implicate a potential role of the MCT1 inhibitor in succinate efflux, because higher levels of the metabolite are maintained within the cell and less is released into the supernatant.

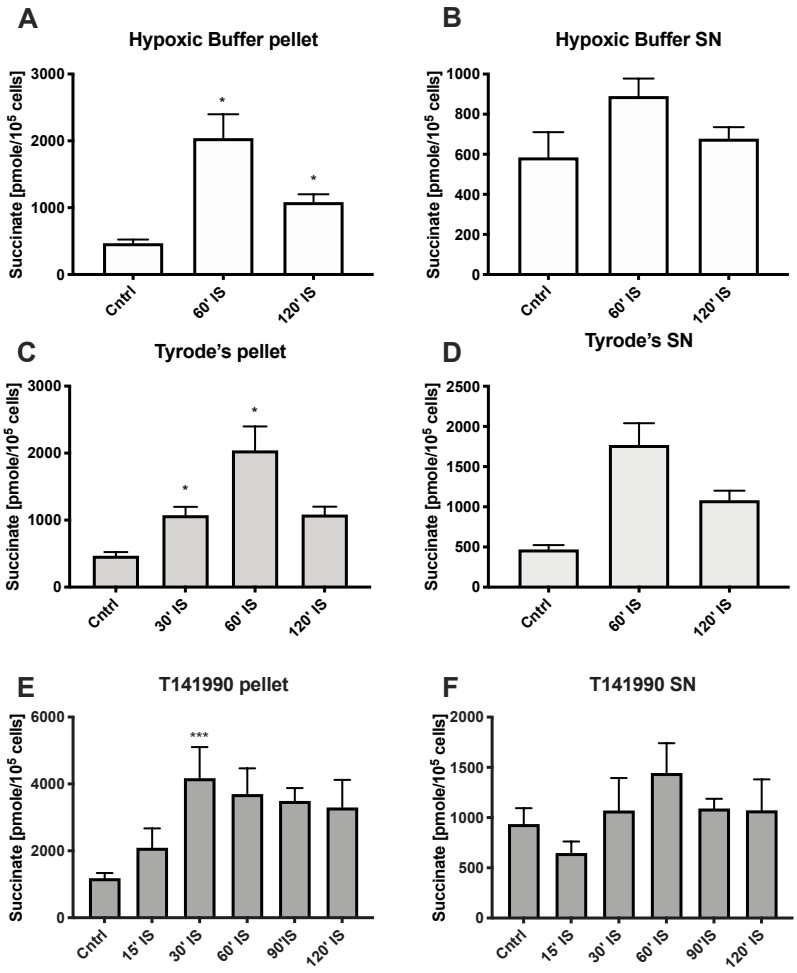

Figure 4.13: Changes in intra- and extra-cellular succinate in different buffer systems during anoxia. Different time points of anoxia at 37°C were induced in primary murine cardiomyocytes in an anoxic chamber in either lactate-based Hypoxic Buffer (A + B), glucose-based Tyrode's Buffer (C + D) or Tyrode's + 10 µM AR-C141990 (E + F). Intracellular succinate was measured in cell pellets (A, C, E) and extracellular succinate in cell supernatants (B, D, F). Succinate concentrations were evaluated in a mass spectrometry assay and are presented in pmol/ 10 000 cells. n= 5-7 biological replicates, data are mean ± S.E.M., statistical analysis was performed via one-way ANOVA, *P< 0.05, ***P< 0.001.

4.3.4.6 Optimisation of buffer composition to best mimic ischaemia in vitro

In order to develop a cell model of IRI closest to *in vivo* models, I performed a direct comparison of changes in ischaemic markers between the three buffer systems to induce a phenotype closest to that of ischaemia *in vivo* (Figure 4.14). The amount of ATP loss (Figure 4.14, A) and lactate accumulation (Figure 4.14, B), as well as cell death (Figure 4.14, D) was the most severe in hypoxic buffer and least in Tyrode's buffer. Interestingly, succinate accumulation was highest in T141990 buffer (Figure 4.14, C). Because I wanted to avoid overloading the cells with lactate which would mask potentially important changes in the metabolite and the role of the MCT1 transporter, the glucose containing Tyrode's buffer supplemented with MCT1 inhibitor AR-C141990 (T141990), which showed comparable results to the hypoxic buffer, in conjunction with true anoxia, was determined to be the best condition to induce ischaemia in cardiomyocytes *in vitro*.

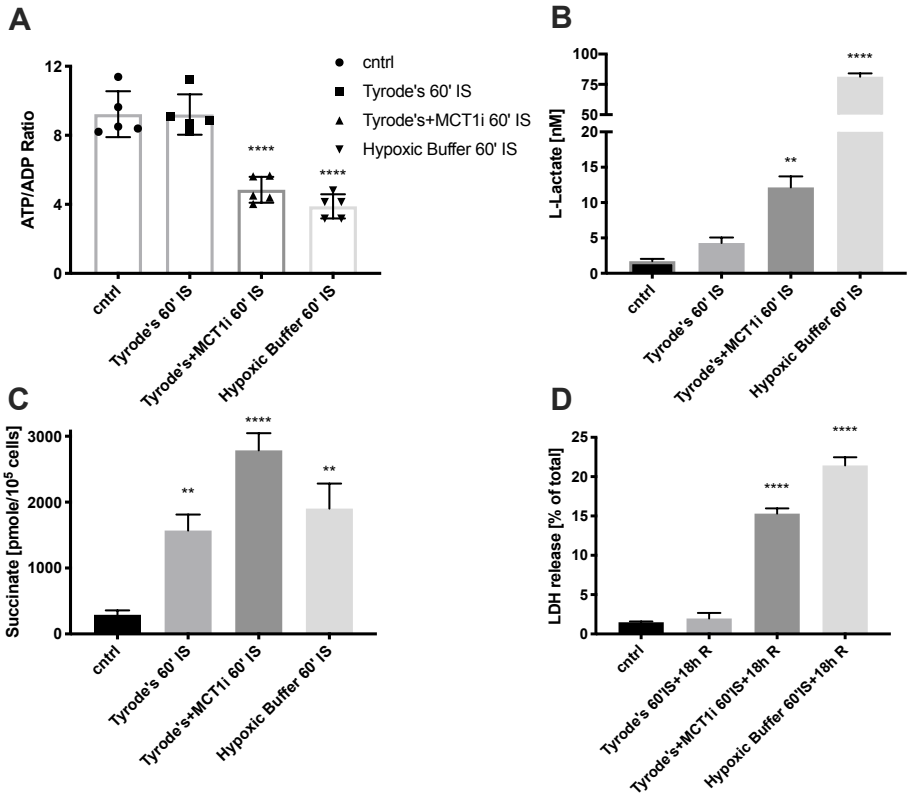

Figure 4.14: Direct comparison of ischaemic markers in different buffer systems during anoxia . Overview over the changes in ischaemic markers in primary cardiomyocytes during true anoxia and upon reperfusion in glucose-based Tyrode's buffer, Tyrode's + 10 µM AR-C141990 (T141990) and lactate-based Hypoxic buffer in comparison to control samples. The evaluated ischaemic markers are (A) ATP/ADP ratios, (B) L-Lactate in nM, (C) succinate in pmol/10 000 cells and (D) LDH release relative to a positive 1% Triton control. n= 5 biological replicates, data are mean ± S.E.M, statistical analysis was performed via one-way ANOVA, **P< 0.01, ****P< 0.0001.

Overall, I have succeeded in developing a cell model that mimics ischaemia *in vivo*. This was done by comparing the effect of different buffer systems and oxygen tensions on the ischaemic markers ATP/ADP ratio, adenine nucleotide pool size and lactate and succinate accumulation, which have been previously evaluated by my lab in *in vivo* and *ex vivo* models. In particular, the data generated in ischaemic mouse heart and published by our lab .(Martin et al., 2019) (Figure 4.1) was compared to the behaviour of cardiomyocytes during anoxia. ATP/ADP ratio decrease, and especially highly increased succinate levels in cardiomyocytes that were kept in Tyrode's buffer supplemented with the MCT1 inhibitor AR-C141990 (T141990) resemble the data generated in ischaemic mouse heart. Thus, I concluded that I have a good model of the ischaemia that occurs *in vivo* and which can be used as a basis to asses IRI further *in vitro*.

4.3.5 Assessment of cell injury upon reoxygenation after anoxia

The results obtained after comparing various cell models for ischaemia above led to the conclusion, that physiologically relevant data can be generated utilising a model of adult primary cardiomyocytes in true anoxia after lactate export has been inhibited. Next, I focused on understanding whether I can use this model to study IRI. To do this, I used the model for ischaemia developed above, I mimicked reperfusion by reoxygenating the ischaemic cells that had undergone up to 1 h of anoxia and then assessed cell function for up to 24 h after reoxygenation. The markers chosen to assess IRI were recovery of adenosine nucleotides pools, ATP/ADP ratio, cell death and oxidative damage.

4.3.5.1 Adenosine nucleotides in cardiomyocytes upon reoxygenation

As depicted in Figure 4.15 (A), ATP/ADP ratios decreased after 1 h of anoxia. Upon reoxygenation, it took 1 h until the ATP/ADP ratio reached a similar level to control samples, although still significantly lower than control samples a gradual increase is detectable, but even after 2 h reoxygenation the cells have still not fully recovered their ATP/ADP ratios. Interestingly, the adenosine nucleotide concentrations increase slowly upon reoxygenation and although ATP is high after 2 h of reperfusion, ADP is increased as well, resulting in a

decreased ATP/ADP ratio (Figure 4.15, B) indicating ongoing energy-dependent pathways and decreased capacity to generate enough ATP. These results are consistent with the delayed recovery of adenosine nucleotide pools in reoxygenated cells after anoxia. Therefore, this cell model is considered to mimic severe ischaemia, which still enables cell recovery.

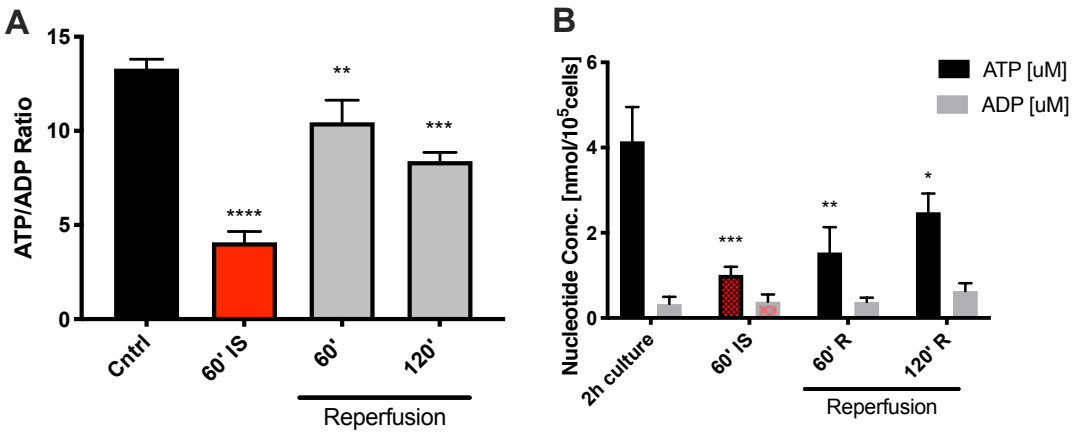

Figure 4.15: ATP/ADP ratios and adenosine nucleotide pools in cardiomyocytes after anoxia and reoxygenation. Cardiomyocytes were maintained in Tyrode's + 10 µM MCT1 inhibitor either at 37°C, 5% CO_2 in a cell incubator as controls, or after induction of anoxia for 1 h in an anoxic chamber at 37°C, before fresh oxygenated buffer was added and the cells were reperfused for 2 h in a cell incubator. Samples were lysed at different time points and adenosine nucleotide pools evaluated using a luciferase assay and measuring luminescence. Changes in (A) ATP/ADP ratios and (B) ATP and ADP nucleotide concentrations in nmol/10^5 cells are displayed to enable direct comparison between anoxia and reperfusion. n= 4 biological replicates, data are mean ± S.E.M, statistical analysis was performed via one-way ANOVA, *P<0.05, **P< 0.01, ***P<0.005, ****P< 0.0001.

4.3.5.2 Cell death after reoxygenation of anoxic cardiomyocytes

To analyse the effect of reoxygenation on cardiomyocytes following anoxia, I next assessed cell death following reoxygenation by counting round/dead cells, measuring apoptosis via caspase3/7 activation or necrosis via LDH release. I counted the total number of Trypan blue stained dead cells after 1 h of anoxia and 24 h of reoxygenation and discovered that in this severe model of IRI more than 50% of the cells die 24 h after reoxygenation (Figure 4.16). However, I also wanted to investigate how much of the cell death that occurs is due to apoptosis and how much due to necrosis.

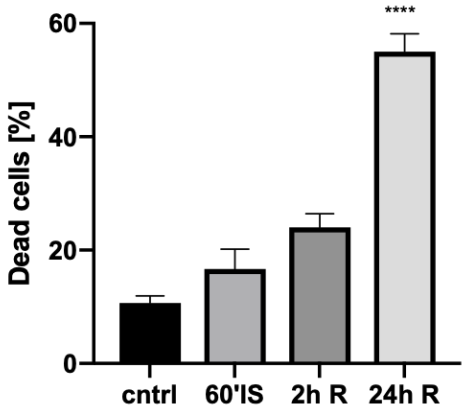

Figure 4.16: Cell death in primary murine adult cardiomyocytes after 1 h anoxia and various times of reoxygenation. The amount of cell death was evaluated in isolated cardiomyocytes. The number of dead cells was counted after 4h incubation in a cell incubator, 1 h of anoxia or 2 and 24 h of reperfusion. Displayed is the percentage of round cells of the total number of cells. n= 5 biological replicates, data are mean ± S.E.M., statistical analysis was performed via unpaired student's t-test, ****P< 0.0001.

4.3.5.2.1 Apoptosis after reoxygenation of anoxic cardiomyocytes

As described before, apoptosis is not easily induced in adult cardiomyocytes. Nevertheless, I investigated caspase 3/7 activity in adult primary cardiomyocyte during 1 h of anoxia followed by up to 18 h of reoxygenation and compared this to a 9 h UV irradiation control. While not much apoptosis was induced during 1 h of anoxia, or upon 30 min reoxygenation, a significant increase in apoptosis was detected 18 h after reoxygenation (Figure 4.17). This increase in apoptosis corresponds to about 20% of the UV positive control, in which total cell death was induced via apoptosis. Because both, apoptosis as well as necrosis are activated upon IRI, I went on to investigating cell death in general via LDH release in further experiments. Thereby, I focussed on establishing cell death as marker for IR injury in this cell model further.

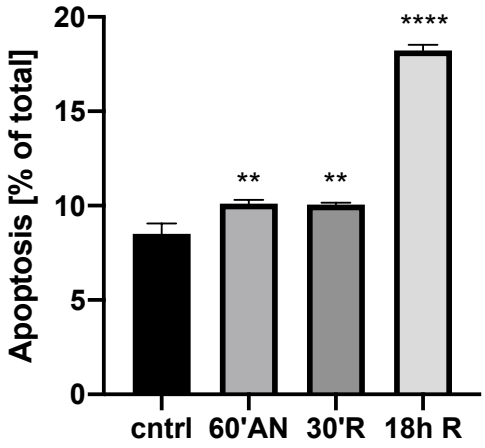

Figure 4.17: Apoptosis in primary murine adult cardiomyocytes upon anoxia and reoxygenation. The amount of apoptosis after anoxia followed by reperfusion was evaluated in isolated cardiomyocytes. Apoptosis was measured via caspase3 and 7 activation. Cells were either untreated or underwent 1 h of anoxia followed by 30 min or 18 h of reperfusion. The data are presented as percentage of positive UV control. n= 3-7 biological replicates, data are mean ± S.E.M., statistical analysis was performed via unpaired student's t-test, *P<0.05, ****P< 0.0001.

4.3.5.2.2 Cell death after reoxygenation of anoxic cardiomyocytes

To investigate how much necrosis occurs upon anoxia and reoxygenation, I utilised the above described experimental setup: Anoxia was induced for up to 1 h (Figure 4.18, A) and the cells were monitored for up to 24 h following reoxygenation after mild (Figure 4.18, C) or severe anoxia (Figure 4.18, A, B, D). The cell incubation supernatant was retrieved at various time points following reoxygenation and the amount of LDH analysed and compared to a positive control of TritonX100-lysed cells, corresponding to 100 % cell death.

This analysis revealed that prolonged anoxia causes increased cell death upon reoxygenation in all of the buffers. Tyrode's buffer (A) induced the east amount of cell death. 60 min of anoxia followed by 24 h of reoxygenation in Hypoxic buffer where comparable to Tyrode's + MCT1 inhibitor AR-C141990 (Figure 4.18, B and D). In general, little LDH release was detectable within 12 h of reoxygenation in all of the buffers. After 18 and 24 h incubation following reoxygenation, cell death occurs, indicating that intra-cellular processes have been initiated which induce cellular death pathways leading to plasma membrane rupture and release of cytosolic content.

Anoxia of 30 min in T141990 buffer showed decreased cell death in comparison to the more severe anoxia of 60 min (Figure 4.18, C and D). This indicates that longer anoxia

leads to elevated injury upon reoxygenation which activates cell death pathways within the cells that can lead to cell death in several hours.

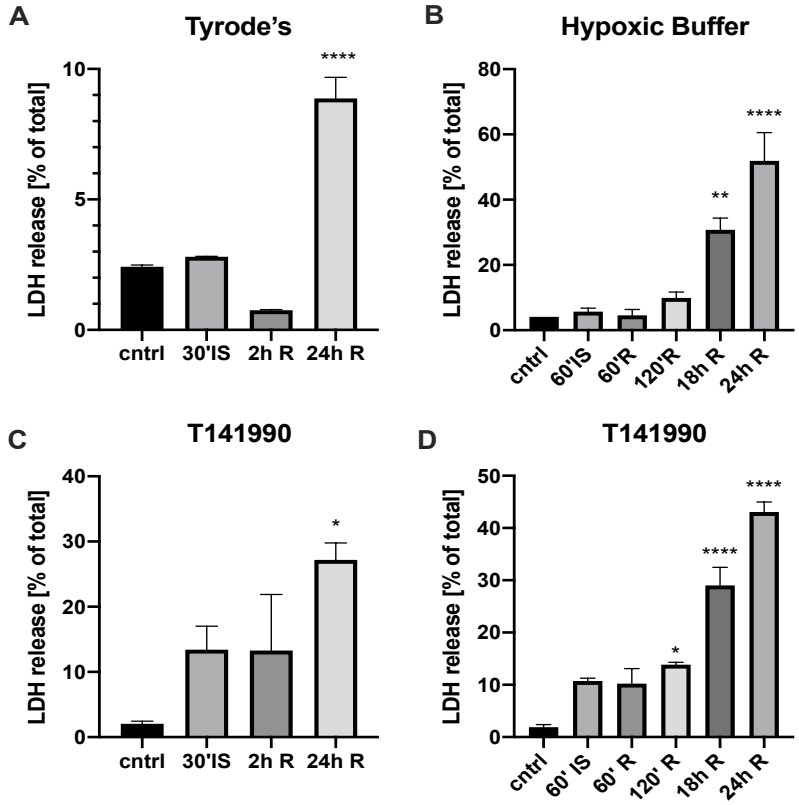

Figure 4.18: LDH release from primary cardiomyocytes upon anoxia and reoxygenation. Primary adult mouse cardiomyocytes were maintained in a cell incubator (controls) or subjected to different time points of anoxia at 37°C in Hypoxic buffer, Tyrode's buffer or Tyrode's + 10 µM AR-C141990. The cells were then reoxygenated in cell medium and cultured in a cell incubator before LDH protein concentrations were measured the cellular supernatant via absorbance at 492 nm. (A) Anoxia and reperfusion in Tyrode's buffer. (B) LDH release after 60 min of anoxia and up to 24 h of reperfusion in Hypoxic buffer. (C) LDH release after 30 min of anoxia and 2-24 h of reperfusion in T141990 buffer. (D) LDH release after 60 min of anoxia and 2-24 h of reperfusion in T141990 buffer. Elevated LDH levels upon prolonged ischaemia and reperfusion indicate increased cell death. Results are presented as percentage of a positive control of cardiomyocytes lysed in 1% Triton. n= 3 biological replicates, data are mean ± S.E.M, statistical analysis was performed via one-way ANOVA, *P<0.05, **P<0.005, ****P< 0.0001.

4.3.5.3 Oxidative damage to mtDNA upon reoxygenation of anoxic cardiomyocytes

Upon reperfusion of ischaemic tissues in disease models, ROS is produced by the mitochondrial respiratory chain. However, it is technically difficult to reliably measure this directly in my *in vitro* model, for example by use of fluorescent probes, due to the necessity to remove cells from the anoxic chamber for the assay, causing their reoxygenation. Instead, I

had to determine the production of ROS indirectly by measuring oxidative damage to mtDNA by quantitative PCR.

To validate this approach, I showed an increase in mtDNA oxidative damage in the model of murine heterotopic heart transplant (Figure 4.19, E). Using the method described in Chapter 3, murine hearts were transplanted into the abdomen of a recipient mouse. 24 h later, the transplanted heart was retrieved and analysed for a range of markers, including mtDNA damage. A decrease in mtDNA amplification was detectable after induction of ischaemia and reperfusion. However, it is not clear at which time point the oxidative damage to the mtDNA occurs, because the heart samples were retrieved 24 h after reperfusion.

I then proceeded to measure mtDNA damage in *in vitro* anoxic cardiomyocytes. After 2 h of reoxygenation, no significant effects were detectable in mtDNA amplification (Figure 4.19, A- B). However, 24 h after reoxygenation, there was decreased mtDNA amplification (B), indicating ongoing damaging processes within the cells after initial anoxia-reoxygenation injury. This indicates that mtDNA is either repaired sufficiently early upon reperfusion damage, or the damage to the mtDNA does not occur immediately.

Another measure of oxidative damage is oxidation of DNA to form the 8OHdG nucleotide and for this, DNA purified from cardiomyocytes after anoxia and reoxygenation was analysed via ELISA to measure 8OHdG base modifications (Figure 4.19). After 2 h of reoxygenation, no significant effects were detectable in whole cell DNA extracts (Figure 4.19, A- B). On the other hand, 24 h after reoxygenation showed elevated 8OHdG (A) indicating ongoing damaging processes within the cells after initial anoxia-reoxygenation injury.

Investigation of the amount of DNA amplification of mtDNA isolated from the supernatant (Figure 4.19, D) or purified from the cytosol (Figure 4.19, C) of reperfused cardiomyocytes shows an elevated number of lesions on this DNA, indicating highly damaged DNA especially in the supernatant. This does not distinguish between fragmented or oxidised DNA and further investigation into this is necessary. Especially because different innate immune response pathways could be activated dependent on the oxidation state of mtDNA, which is addressed further in chapter 6.

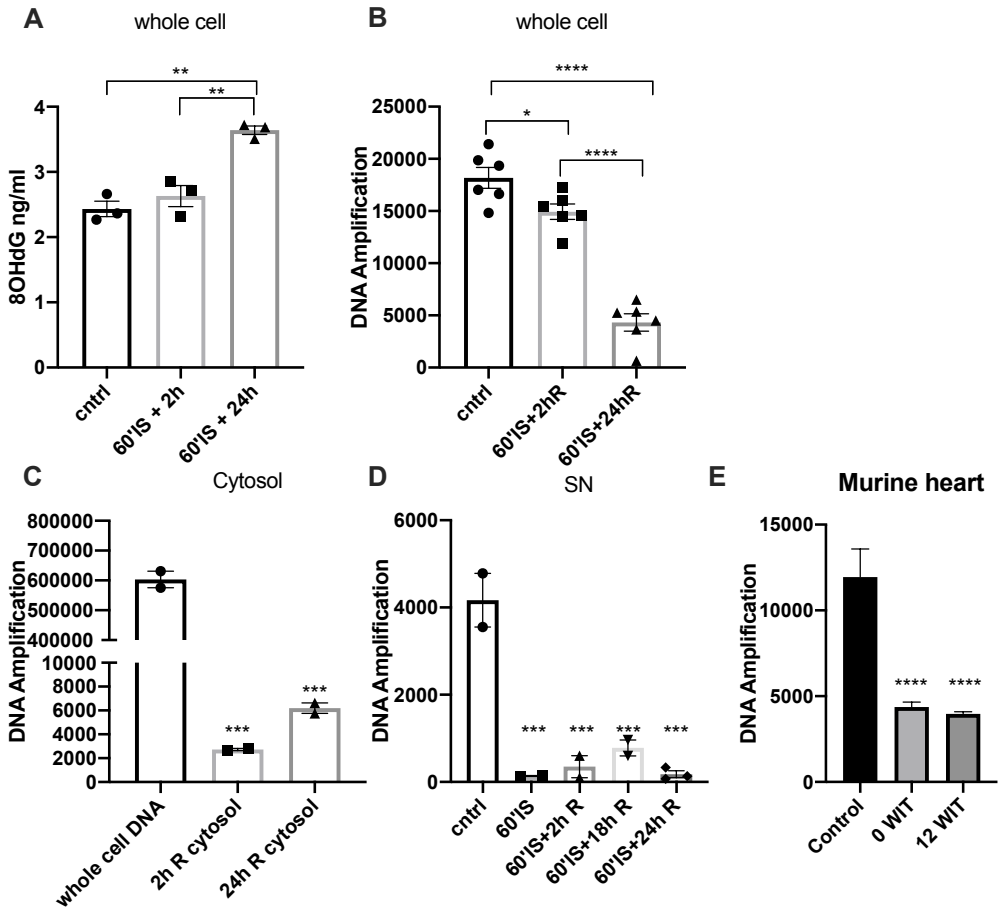

Figure 4.19: Oxidative damage on DNA after anoxia and reoxygenation injury in primary cardiomyocytes. Primary adult mouse cardiomyocytes were maintained as controls in a cell incubator or subjected to 1 h of anoxia at 37°C in Tyrode's + 10 µM AR-C141990. Cells were reperfused in cell medium and maintained in a cell incubator before DNA was extracted and oxidative damage evaluated. (A) The oxidative base modification 8OHdG was measured in ng/mL via ELISA on whole cell DNA. (B-E) mtDNA damage was investigated using qPCR in DNA extracted from whole cell lysates (B), cytosolic fractions (C) or cellular supernatant (D), or (E) from murine heart tissue of control mice, or mice that underwent heterotopic heart transplantation with no (0WIT) or additional 12 min (12WIT) of warm ischaemia. Tissue was retrieved 24 h after reperfusion, DNA extracted and qPCR performed as described for cells. Decreasing amounts of DNA amplification indicate increasing damage on mtDNA. n= 3-6 biological replicates, data are mean ± S.E.M, statistical analysis was performed via one-way ANOVA, *P<0.05, **P<0.005, ***P<0.001, ****P< 0.0001.

To summarise this part of the project, after developing a cell model for heart IRI, I utilised this to investigate how well it modelled IRI *in vivo*. Delayed recovery of the adenosine nucleotide pool as well as increased cell death were the notable results of severe anoxia followed by reoxygenation. Furthermore, anoxia and reoxygenation did result in oxidative damage, which

has been assessed here as oxidation of mtDNA. Further investigation into ROS production and oxidative damage is necessary in order to fully understand the origin and time course of ROS generation.

4.3.6 Anoxia and reoxygenation in embryonic stem cell-derived cardiomyocytes

The model developed above was utilising primary mouse cardiomyocytes and it can be used to assess many aspects of IRI. However, it would also be useful to be able to develop this model for cardiomyocytes from stem cells. Especially utilising induced pluripotent stem cells would open up the possibility of assessing human cells from patients with particular diseases. I therefore investigated how embryonic stem cell (ESC) derived cardiomyocytes respond to anoxia. To do this, I performed a pilot study in collaboration with Dr. Johannes Bargehr (Department of Medicine, University of Cambridge, UK), who is interested in developing regenerative medicine approaches by injecting ESC-derived cardiomyocytes into the ischaemic part of rat hearts to improve healing and reduce fibrosis (Bargehr et al., 2019). Furthermore, although he found some improvement in heart function, the engraftment rates were low and cell death elevated. This may be due to the IRI sustained by the ESC upon engraftment into the recipient heart, which is performed during ischaemia, before reperfusion is induced. Therefore, understanding of how these ESC-derived cardiomyocytes respond to models of IRI *in vitro* may also enable methods to be developed to prevent this cell death and thereby increase the delivery of ESC to repair tissue damage *in vivo*. Therefore, here I investigated how ESC-derived cardiomyocytes behave under anoxia.

4.3.6.1 Anoxic changes in ESC-derived cardiomyocytes

ESC-derived cardiomyocytes were generated in the lab of Dr. Sinha in the Stem Cell Institute Cambridge and cultured by Dr. Johannes Bargehr for 24 h. I then transferred them into Tyrode's buffer supplemented with AR-C141990 and kept them anoxic for up to 6 h. The ischaemic markers, including ATP/ADP ratios and succinate accumulation, were determined (Figure 4.20, A).

The ATP/ADP ratios in these cells decreased early during anoxia but recovered again at the later time points (B). The ATP pool in these cells did not behave as that in adult primary cardiomyocytes during anoxia (C). The ATP concentration was maintained even after prolonged anoxia. This was similar to our hypoxic model where an increase in ATP and ADP was detected after 5 h under low oxygen conditions. Furthermore, the stem cell-derived cardiomyocytes did not accumulate succinate as rapidly (D), instead it took more than 2 h of anoxia to reach a highly increased level of this metabolite. These was also similar to how adult cardiomyocytes behave under hypoxia.

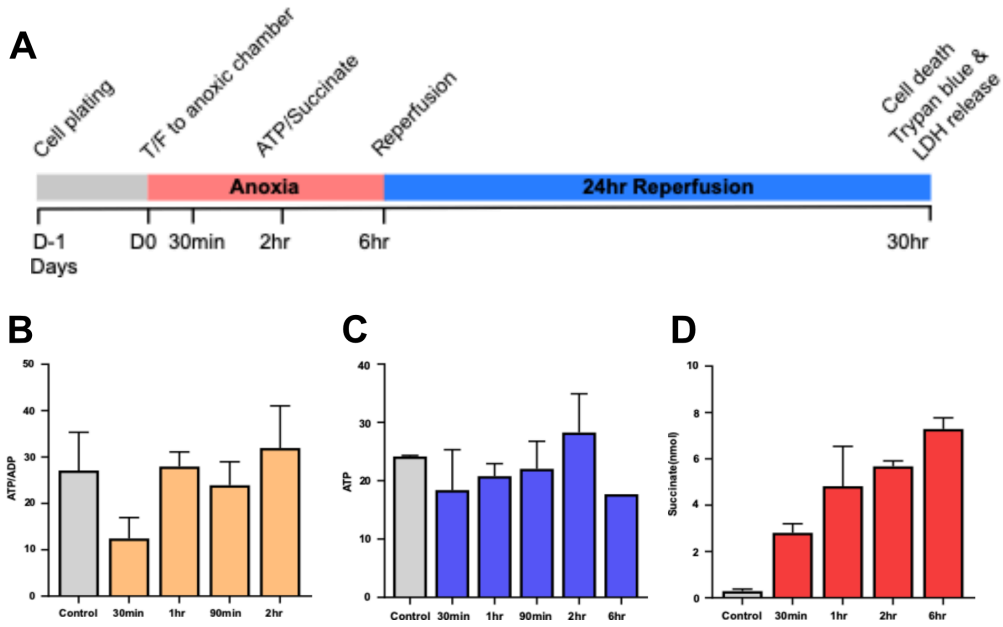

Figure 4.20: Changes during anoxia and reoxygenation in ESC-derived cardiomyocytes. A) Schematic overview of the experimental procedure: ESC-derived cardiomyocytes were maintained in cell culture for 24 h before they were transferred into T141990 buffer into anoxia for up to 6 h. ATP/ADP ratios (B), ATP pools (C) and succinate concentrations (D) were analysed after different anoxic time points using the previously described luciferase assay and mass spectrometry approach. n= 1- 3, data are mean ± S. D.

4.3.6.2 Cell death in ESC-derived cardiomyocytes upon anoxia and reoxygenation

Cell death upon anoxia and reoxygenation was investigated 24 h after 30 min, 2 h or 6 h of anoxia (Figure 4.21). LDH release was determined and a small increase in LDH concentrations detected 24 h after reperfusion when the cells underwent 30 min or 2 h of anoxia. 6 h of anoxia on the other hand caused significantly increased cell death. This is correlating to succinate accumulation and ATP decrease at this time point of anoxia. Further insights into this, such as

changes in lactate and which form of cell death is activated, are necessary in order to disclose why ESC-derived cardiomyocytes behave so differently from adult cardiomyocytes.

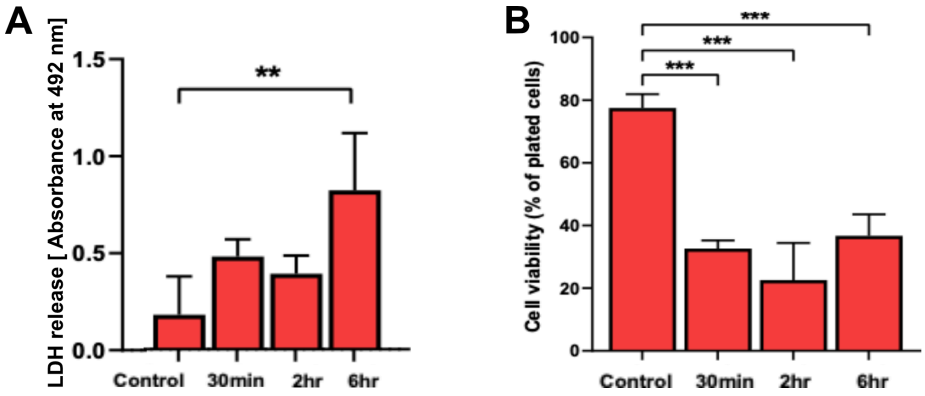

Figure 4.21: Changes during anoxia and reperfusion in ESC-derived cardiomyocytes. ESC-derived cardiomyocytes were maintained in T141990 buffer in anoxia for up to 6 h before cells were reperfused for 24 h with oxygenated medium. (A) LDH release was measured as protein concentrations in the cellular supernatant via absorbance at 492 nm. (B) Cell viability was assessed using Trypan blue staining and is displayed as percentage of the number of cells plated. n= 3, data are mean ± S.E.M

To summarise the effect of anoxia and lactate transport inhibition on ESC-derived cardiomyocytes, these cells can tolerate prolonged hours of anoxia. 6 h of anoxia do induce succinate accumulation resulting in cell death upon reoxygenation. These data improve our understanding of the role ischaemic damage plays in the elevated cell death that has been detected after intramyocardial injection (Bargehr et al., 2019). Even though ischaemic markers like ATP/ADP ratios are maintained stable for prolonged anoxic times, these cells suffer a great hit upon reoxygenation indicating they are very sensitive to IRI.

Further research should aim to develop approaches to ameliorate succinate accumulation during anoxia or prime the cells for the damage using ischaemic preconditioning, so that cell viability upon reperfusion can be increased.

4.4 Discussion

Here, I developed an improved cell model for cardiac ischaemia reperfusion injury by isolating primary adult mouse cardiomyocytes and an anoxic chamber to generate true anoxia. The utilisation of cellular models offers advantages over *in vivo* models for the investigation of disease-underlying molecular processes. However, cellular disease models that mimic the situation *in vivo* are difficult to develop as it is important to maintain the metabolic response of these cells similar to physiological conditions, e.g. the timing and amount of metabolite accumulation during ischaemia, as well as the decrease in ATP/ADP ratios. We have previously determined the detailed metabolic and energetic changes in ischaemic heart tissue (Martin et al., 2019) and discovered that three hallmarks of ischaemia *in vivo* and *ex vivo* in tissues include the rapid depletion of adenosine nucleotides and ATP/ADP ratios, the accumulation of lactate and of succinate. These results were highly conserved among different species, leading to our hypothesis that they are crucial in ischaemic injury and therefore need to be replicated in a cell model.

4.4.1 Comparison of the effect of *in vitro* anoxia and hypoxia on cardiomyocyte function

Although many cardiomyocyte models that investigate IRI have been proposed in recent literature, almost all of these models utilise hypoxic conditions, which differ significantly from anoxic conditions. In order to prove that cellular responses to hypoxia and anoxia vary, I compared the effect of hypoxia at 0.1% O_2 to true anoxia in an anoxic chamber at <10 ppm. While the ischaemic markers lactate, succinate and adenosine nucleotide pools in anoxia changed in a way that is comparable to observations in ischaemic tissue samples, hypoxia had a much slower effect on the cells. Not many changes could be detected within the first 1-2 h of hypoxia, although this would have a big impact on organs *in vivo*.

The striking difference that small amounts of oxygen make on isolated cells during hypoxia implies that a lot of the cell data published so far has to be interpreted carefully because classical ischaemic pathways may not have been activated.

A caveat with the hypoxic cardiomyocyte model used here, is the difficulty in rapid retrieval of samples under hypoxia. While samples can be lysed within the anoxic chamber under anaerobic conditions, this is not doable using the plate reader hypoxic models where plates have to be taken out first before sample lysis is possible in order to not block or destroy

the injector with the harsh lysing solutions used for the experiments performed here. Therefore, sample retrieval in this model takes approximately 30 seconds. ATP and succinate can be rapidly degraded under warm normoxic conditions and it is crucial to freeze samples within seconds. Because of this, these hallmarks of ischaemia are easily lost when being retrieved under normoxia. And it is possible that the results obtained at 0.1% O_2 are affected by the delayed lysis times indicating that the method has to be improved in order to investigate the hypoxic pathways further. A hint as to how crucial lysis under anoxic conditions is, is the difference in detectable succinate after different time points of anoxia in *Drosophila melanogaster*. As described before, flies were kept anoxic for up to 5 h and ATP/ADP ratios as well as succinate levels analysed in collaboration with Dr. Federica De Lazzari and Dr. Hiran Prag. Some of the samples were lysed within the anoxic chamber under anaerobic conditions, the others were transferred to buffer and then moved out of the chamber before snap freezing, a process that took approximately 60 seconds, in order to optimise freezing and lysis methods. As depicted in Figure 4.22, succinate accumulated in anoxic flies, but the amount of detectable metabolite was highly dependent on the type of lysis. Samples that were lysed under anoxia showed more than 3 times the amount of accumulated succinate than those that were snap frozen outside the anoxic chamber first. This indicates that transient exposure to oxygen will support the oxidation of succinate and impact detectable metabolite concentrations.

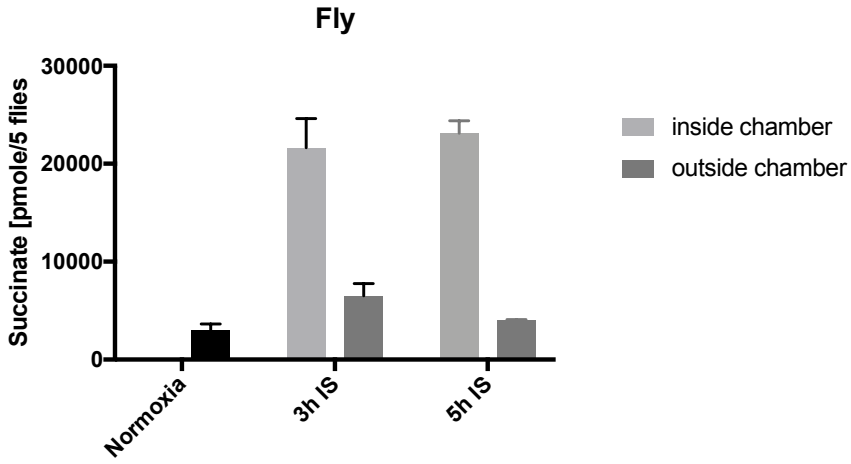

Figure 4.22: Succinate accumulation in anoxic flies. Drosophila melanogaster was maintained under anoxia for up to 5 h and succinate concentration measured using a mass spectrometry approach. Succinate was either extracted from flies within the anoxic chamber under anoxic conditions or after transfer of the flies in extraction buffer, before lysis, into oxygenated environment. Differences in succinate measurements are presented in pmol/5 flies. n= 5, data are mean ± S.E.M.

Therefore, it is possible, that the accumulated succinate is lost during lysis of cells using our hypoxic model. This could explain while even after 5 h of hypoxia, there is just a slight increase in detectable succinate. In this model, the most reliable marker proving that anaerobic metabolism has occurred is lactate. It is more stable and, although it does not increase within 1 h of hypoxia, it does so significantly after 5 h. All of this indicates that hypoxia takes a long time to have its effect. It also shows the importance of developing a system in which handling the samples is easy and tightly controlled, so that loss of succinate due to unwanted reoxidation does not occur.

4.4.2 Comparison between different buffer systems used during true anoxia

Besides oxygen tension, another factor that impacts the system used to induce ischaemia is the buffer composition. Here, I compared a lactate-containing hypoxic buffer to a glucose-containing Tyrode's buffer. Hypoxic buffer introduces changes that resemble the changes in ischaemic tissue, such as pH and lactate concentration. When cardiomyocytes are kept in glucose-based Tyrode's buffer on the other hand, they tolerate prolonged anoxic times without excessive loss of the ATP/ADP ratio or loss of adenosine nucleotides. This may be in part due to the cells excreting excess lactate into the surrounding supernatant, so that they do not experience lactate accumulation within the cells which may block glycolysis. This may also lead to acidosis within their cytosol.

This can be prevented *in vitro* by inhibition of the lactate transporter in the plasma membrane of cardiomyocytes. Supplementing a simple glucose buffer with the MCT1 inhibitor AR-C141990 leads to a significant accumulation of lactate within the cell pellet during anoxia. As shown in this chapter, anoxia alone is not sufficient to induce ischaemic markers like ATP/ADP reduction and succinate accumulation, without inhibition of MCT1. The changes in cardiomyocytes under these conditions are comparable to the ones measured in ischaemic heart tissue. Nevertheless, the addition of an inhibitor of the monocarboxylate transporter may have other, unknown effects on the cardiomyocytes as well.

The family of monocarboxylate transporters has been discovered recently (Halestrap and Wilson, 2012) and a lot is still unknown, for example how many members exists, what the difference is between the different forms and which tissues they are specifically expressed in. A study by Benjamin et al. for example suggests that the transporter MCT1 is mainly responsible for lactate import. But we do see increased lactate accumulation and decreased excretion after inhibition of MCT1 in isolated adult mouse cardiomyocytes indicating that, at least in the model described here, MCT1 is also responsible for lactate export.

MCT2 is a transporter that is structurally so close to MCT1 that it is difficult to investigate them separately. The inhibitor AR-C141990 is as specific as possible for MCT1, but will inhibit MCT2 as well to some extent. Similarly, it has been suggested that MCT2 is expressed in cardiac tissue alongside MCT1 (Cortés-Campos et al., 2011), but it has to be taken into account that antibodies against MCT1 will also detect MCT2 to some extent. Furthermore, the transporter MCT4 produces similar issues. A study by Zhu et al., 2013 claims MCT4 is expressed in rat cardiac tissue, but this could not be confirmed by other groups so far. Benjamin and colleagues published that while MCT1 is responsible for lactate import MCT4 is for lactate export. If MCT4 is expressed in cardiac myocytes, the result we obtain by inhibiting MCT1 is surprising. On the other hand, there is no inhibitor specific to MCT4 available yet. Tocris claims AR-C141990 is specific enough to not influence the activity of MCT4, therefore, it would be interesting to investigate further if MCT4 really is expressed in cardiomyocytes and if so, what the effect would be of specific inhibition of this transporter.

Interestingly, experiments performed in our lab on IRI in murine hearts in a Langendorff model suggest that MCT1 is involved in the export of succinate from ischaemic tissue. The monocarboxylate form of succinate that occurs in the acidic environment in cells during ischaemia could possibly move via this transporter in combination with a proton. Supporting this, inhibition of MCT1 using AR-C141990 decreases the amount of succinate released from the ischaemic heart upon reperfusion (unpublished data, in submission). Experiments in the isolated cardiomyocyte model showed similar trends, as described in the following chapter. If MCT1 is involved in succinate export during IRI, using its inhibition in the cell model described here could affect cellular metabolism in a different way than expected so far.

Although using a glucose-based buffer is in many ways more physiologically relevant than a lactate-based buffer, there are still other factors differing from *in vivo* models, in addition to inhibition of MCT1. There is no source of fatty acids for β-oxidation in the

Tyrode's buffer which is relevant because *in vivo* cardiomyocytes rely mainly on β-oxidation of fatty acids in order to generate ATP by mitochondrial OXPHOS (Goldberg et al., 2012; Stanley, 1989). However, during ischaemia/anoxia the cells are not able to oxidise fatty acids and instead, they use anaerobic glycolysis to produce ATP (McDougal and Dewey, 2017). We therefore concluded, supplementation of Tyrode's with carnitine, as energy donor for fatty acid oxidation, is not necessary and it is sufficient to provide glucose for anaerobic glycolysis.

Altogether, the comparison of lactate- and glucose-based buffers in anoxia shows that cardiomyocytes *in vitro* are capable of excreting excess lactate as well as succinate into the cell incubation medium. Inhibition of this export pathway with an inhibitor of MCT1 promotes the accumulation of lactate and succinate within the cells during anoxia *in vitro* which more closely mimics the changes in ischaemic markers to what we observed *in vivo* before.

4.4.3 Anoxia and reoxygenation in ESC-derived cardiomyocytes

After determining that anoxia and lactate transport inhibition enabled me to better mimic cardiac ischaemia *in vitro*, I wanted to extend this model to embryonic stem cell-derived cardiomyocytes. My data showed that they do not have the same metabolic response as adult cardiomyocytes under anoxia *in vitro* (Figure 4.20). While the ESC-derived cells maintain their ATP/ADP ratio and ATP concentration, they do not accumulate succinate for up to 6 h anoxia. Furthermore, cell death assessed via two different assays, LDH release and Trypan blue staining of the cells, showed variable results. LDH release was increased 24 h after cells had undergone 6 h of anoxia. Cell viability detected via Trypan blue staining indicated loss of cells 24 h after each of the measured anoxic time points. The possible reason might be that the various pipetting steps during Trypan blue staining might have caused excessive cell death and therefore killed the already injured cells upon reoxygenation.

In general, these results are important with regard to using ESC-derived cardiomyocytes in regenerative medicine. As depicted in Figure 4.23, recent research developed a method to improve recovery after heart attack by injecting the stem cell derived cardiomyocytes to replace the lost myocardium. Although the outcome so far is promising (Bargehr et al., 2019), elevated cell death of the injected cells prohibits optimal engraftment. Analysis of ischaemic damage in these cells in my *in vitro* model showed that prolonged anoxia does cause cell death and therefore is a potential explanation for the low engraftment. More information about ischaemic changes is needed in order to fully characterise ESC-

derived cardiomyocytes in ischaemia. Because the cells are resuspended before injection and are therefore isolated, single cells, they might be able to excrete excess lactate without accumulating it, as long as they are not engrafted into the tissue. Therefore, there might be a bigger window without anoxic damage for these cells than expected. Further research into co-culturing adult cardiomyocytes and ESC-derived cells might explain how and in which time frame engraftment occurs.

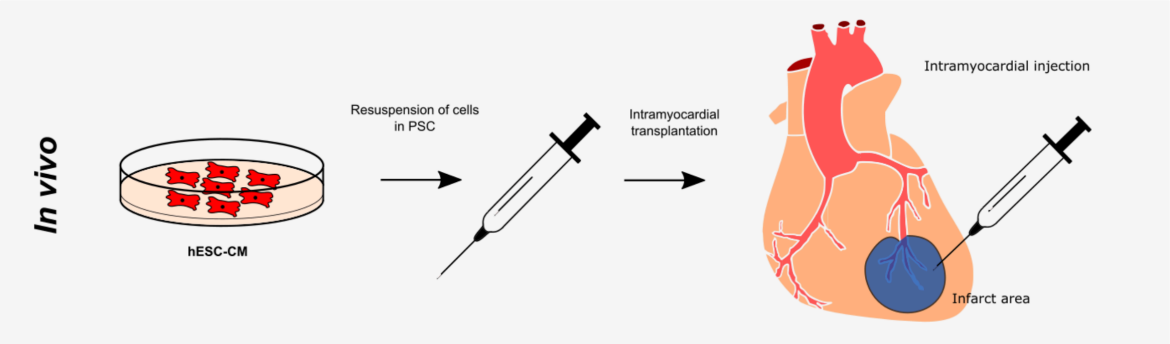

Figure 4.23: Intramyocardial transplantation of ESC- derived cardiomyocytes. Schematic overview of intramyocardial injection of ESC-derived cardiomyocytes into ischaemic heart after heart attack. Cells are generated and cultured before they are resuspended it PBS and injected into the ischaemic area of a heart after infarct. Modified from Dr. Johannes Bargehr.

These pilot experiments have initiated ways of improving approaches in regenerative medicine. In addition, they suggested that stem cell derived cells, may not replicate the ischaemic injury seen by primary adult cardiomyocytes.

4.4.4 Assessment of cardiomyocyte injury upon anoxia and reoxygenation

One of the big problems with using primary adult cardiac myocytes is their inability to survive long-term without the support of sarcomeric heart structure and interconnectivity to other cells such as myoblasts and fibroblasts. Consistent with the literature (Taimor, 2000), I observed that the window of survival of isolated cardiomyocytes is approximately 4 days post-isolation. To be consistent, all my experiments have been initiated at 24 h post-isolation to allow for acclimatisation of the cells to the culture system and the cessation of contractility. Importantly, cell survival was monitored over the course of every experiment via LDH release.

Literature on cell death in cardiomyocytes so far does not distinguish robustly between apoptosis and necrosis (Dorn, 2008; Gürtl et al., 2009; Orogo and Gustafsson, 2013). But given

its relevance in heart failure, further investigation into this is important. Often, the reason is an unclear separation between the different cell types within heart tissue. The heart consists of three different cell types, fibroblasts that maintain the organ structure, mainly on the organ surface, myoblasts, fibroblast-like cells within the heart, connected to myocytes, and cardiomyocytes, the main type of cells within the organ forming the muscle.

Some research has shown apoptosis to be the main pathway that leads to cardiomyocyte death, these studies often did not isolate myoblasts and cardiomyocytes sufficiently. Because of this, it is possible that the mixture of cells, and variable pathways activated in them, falsify the results. A study by Taimor et al. elucidated pathways for cell death in isolated adult rat cardiomyocytes and showed that necrosis is the main form causing more than 40% of all death in these cells after IRI. Apoptosis does occur, but just accounts for ~1.2% according to these experiments. These results are consistent with the data retrieved in the experiments performed here. Using a luciferase-linked assay that is sensitive to the cleavage, and therefore activation, of caspase 3 and 7 showed barely any increase in apoptosis after induction of cell death after anoxia and reperfusion in comparison to a positive UV irradiation control. The assay has been performed with C2C12 cells as positive control as well, which showed a clear significant induction of apoptosis upon UV radiation.

Because of this small amount of apoptotic cell death, I therefore assessed cell death in general by measuring LDH release. The LDH release assay has proven to be an efficient measurement of cell death upon anoxia and reperfusion injury in the model described here. Some literature suggests that apoptosis is the main pathway that leads to cell death in diseased hearts (Diwan et al., 2008; Gürtl et al., 2009) which I did not observe in the isolated cell model utilised here. As elucidated before, this might be a result from other cell types within the heart as well. It is important to investigate cardiac myoblasts as well and also focus on the interaction of myoblasts and myocytes to understand the full picture of processes occurring in the whole organ.

The investigation of anoxia-reoxygenation enabled some insight into the time in which ischaemic damage occurs and importantly, that the recovery of ATP/ADP ratios is rather slow. The ratios do not fully recover upon reoxygenation and the concentrations of ATP and ADP recover only slowly, 2 h after reoxygenation. This slow recovery has to be taken into account when investigating IRI *in vivo*, especially when discovering new biomarkers for IRI. Many of the processes happening after anoxia and upon reoxygenation are slow and will not affect other cells or the organism immediately.

Another result supporting this is the type and especially the timing of cell death after anoxia and reperfusion in cardiomyocytes. Interestingly the main cell death occurs 18 to 24 h after reperfusion. The cells are not releasing LDH before that, indicating that the reperfusion damage either takes time to occur or that intra-cellular pathways are being activated, that will lead to cell death after several hours.

Interestingly, oxidative damage does occur in cardiomyocytes in this model, measured as reduced mtDNA amplification and accumulation of 8OHdG base modification. Surprisingly, the damage occurs late: only minor damage is detectable within 2 h of reoxygenation and it fully manifests after 24 h when cell death already occurred as shown by LDH release. These results can be due to several reasons, one of them being that the PCR assay is not sensitive enough to detect small differences and oxidative damage on mtDNA. Alternatively, oxidative damage might not occur on mtDNA as the first place in mitochondria or it may be immediately repaired. Therefore, it is necessary to investigate the amount and site at which oxidative damage occurs further and analyse further time points in between 2 and 24 h. Other assays, such as protein carbonylation or isoprostane oxidation, allow for further analysis of where the damage occurs. This way, it is possible to distinguish if ROS damage occurs first on proteins, antioxidants or fatty acids, instead of DNA. Understanding the timing of when and where oxidative damage occurs is crucial in order to develop prevention methods and finally therapeutics against IRI in human patients.

In conclusion, primary adult cardiomyocytes do undergo injury after they have been reoxygenated after exposure to severe anoxia. The delayed recovery of the adenosine nucleotide pool is consistent with data retrieved from reperfused tissue as shown in the previous chapter (REF). Interestingly, cell death occurs after 18-24 h. This is also the time point at which oxidative damage to mtDNA could be investigated. Further research has to investigate which cellular pathways are activated during these 24 h and which impact of this form of cell death, that enables the release of mtDAMPs, has in disease models and patients.

4.4.5 Summary

Altogether, the experiments performed here have shown that it is possible to develop an isolated cardiomyocyte model that exhibits the same characteristic markers of ischaemia that have been observed *in vivo*. These hallmarks of ischaemia in tissue are lactate accumulation, succinate accumulation and loss of adenosine nucleotides as investigated in murine, pig and

human heart *ex vivo* and *in vivo* samples under ischaemia (Martin et al., 2019). Although many cell models that have been published before did not investigate these markers of ischaemia, I hypothesise that these models do not resemble tissue ischaemia due to residual oxygen and therefore are unphysiological. Thus, many published cell models for IRI do not mimic the *in vivo* and *ex vivo* situation adequately. Here, I showed that isolated adult cardiomyocytes that are maintained under true anoxia while lactate transport is inhibited, exhibit severe loss of adenosine nucleotides, and accumulation of lactate and succinate. The very low oxygen tension and inhibition of monocarboxylate efflux are crucial for this and implicate a role for MCT1 in exporting lactate and succinate. This model can now be utilised to investigate the cellular pathways that occur during anoxia and immediately upon reperfusion, which is more difficult in whole organs. A major focus of mine in using this model will be in investigating the effect and fate of accumulated succinate, as well as the release of mtDAMPs and other signalling molecules that have been shown to enhance IRI in patients. Furthermore, I am also interested in using this model to develop therapeutic approaches to ameliorate IRI.

Chapter 5

Application of a novel primary cardiomyocyte model to investigate ischaemia reperfusion injury *in vitro*

5.1 Introduction

The hallmarks of ischaemia reperfusion injury in in *vivo* and *ex vivo* models have been characterised and were the focus of chapter 3 of this thesis. These include decreases in the ATP/ADP ratio, loss of adenosine nucleotide pools and accumulation of succinate and lactate. A novel cellular model that better mimics the ischaemic changes found in these *in vivo* and *ex vivo* models has been developed and described in chapter 4. In addition, it was found that reoxygenation of these cells after exposure to conditions that mimicked *in vivo* ischaemia led to damage to the cells and thus this *in vitro* method is a promising model for IR injury. In this chapter I have used this model to explore several aspects of IR injury.

One important aspect that I wished to explore was to build on the recent work in our lab on the role of succinate in ROS generation during IR injury. Previously our lab has shown that succinate builds up during ischaemia and that injury upon reperfusion *in vivo* and *ex vivo* models is due to ROS production (Chouchani et al., 2014a, 2016; Kohlhauer et al., 2019; Martin et al., 2019). The accumulation of this metabolite during ischaemia is highly conserved among different species, however, many detailed aspects of both the source of succinate during ischaemia and its fate upon reperfusion still remain uncertain. Furthermore, an *in vitro* model offers many potential advantages in assessing the ability of potential drugs to interfere with these aspects of succinate metabolism as well as to assess the consequences of ROS production upon succinate oxidation, such as cell death.

As elucidated in detail in the previous chapter of this thesis, a cell model of adult mouse cardiomyocytes and true anoxia mimics *in vivo* ischaemia reperfusion injury. As described there, utilising a cell model opens up many possibilities to investigate the cellular pathways activated upon IR injury in greater detail. Oxygen tension, buffer compositions, as well as sample retrieval time points can be tightly controlled. Furthermore, samples are less contaminated with different cell types, blood or dead tissue which could influence the results of metabolic and related measurements. Understanding which cellular responses are activated in cardiomyocytes during ischaemia or upon reperfusion following ischaemia, at which time points and the downstream pathways activated, are vitally important questions to elucidate and the use of an in vitro model should enable these questions to be addressed more precisely and thus enable us to develop a better understanding of ischaemia reperfusion injury. The data obtained from these in vitro models can then can be used to interpret characteristic markers of ischaemia and of IR injury in humans, and is crucial in order to develop specific and targeted

therapeutics. For example, it is difficult during organ transplantation to deliver drugs to the donor before the organs are retrieved, both because of ethical concerns that constrain current practice in most countries, including the UK, but also because drugs administered systemically, whether they are DBD or DCD donors, could affect other organs differently. Thus, for current organ transplantation it is necessary to develop drugs that can be administered after organ retrieval and which can act at ischaemia during organ storage, and also to act to protect the organ against reperfusion injury when the organ is reperfused within the organ recipient. Furthermore, for the treatment of other diseases, particularly heart attack, the delivery of therapies is constrained to the reperfusion of the ischaemic tissue, for example upon removal of the cardiac artery blockage by primary percutaneous coronary intervention. Therefore, it is important to fully understand each step and cellular change during the anoxic phase, the early reperfusion phase as well as late reperfusion phase, in order to be able to develop drugs that prevent damage.

Succinate accumulation during ischaemia has been shown to be responsible for ROS production and oxidative damage driven by its oxidation by the respiratory chain upon reperfusion. This has been demonstrated in a number of models because amelioration of succinate accumulation and/or oxidation decreases ischaemia reperfusion injury as described before. However, increased succinate in the circulation has also been found in patients after cardiac infarction (Kohlhauer et al., 2018), and upon reperfusion in an ischaemic Langendorff heart (Zhang et al., 2018), indicating that not all succinate is oxidised upon reperfusion, but that a proportion is released and may act as a signalling molecule within the circulation. This signalling may take place via succinate activating the SUCNR1 receptor, a cell-surface G-protein coupled receptor found on many cell types (Wang et al., 2019). Succinate levels decrease to normoxic levels within 2-3 min in reperfused tissue, suggesting rapid oxidation and/or release (Chouchani et al., 2014). In depth analysis of the mechanisms of succinate oxidation and release upon reperfusion can be difficult to investigate in *in vivo* models, where a lot of different factors influence outcomes. I have therefore utilised the previously described *in vitro* cell model that mimics ischaemia reperfusion injury *in vivo*, to analyse the source and fate of accumulated succinate and the mechanism of its release upon reoxygenation after anoxia.

As shown in chapter 4 of this thesis, when lactate transport is inhibited in primary cardiomyocytes, succinate accumulates within 30 min of anoxia. Extending this to 1 h of anoxia induces severe changes that mimic those of ischaemia, as is seen by loss of adenosine nucleotides and cell death 24 h later. The possibility of taking multiple samples during anoxia

and early on during reoxygenation, allows investigation into the first phases of reoxygenation and also enables me to assess the relative amounts of succinate that are released from the cells upon reoxygenation, or oxidised by the electron transport chain. Unpublished data generated by Dr Fay Allen in our lab suggests that succinate is produced during ischaemia within mitochondria but is then rapidly exported into the cytosol, but the mechanism of this transport is unclear. In addition, the mechanism by which this succinate is then released into the circulation is also not known.

The cellular model of IR injury developed in primary adult cardiomyocytes required inhibition of the monocarboxylate transporter MCT1 to be effective. This seems to be because the isolated cells release cytosolic metabolites such as lactate into the surrounding medium. This is not possible in tissues *in vivo* during ischaemia because the extracellular volume is small and the rapid build-up of lactate there prevents further efflux. This efflux of lactate in vitro provides a safety valve by enabling electrons to leave the cell, that both prevents anoxia impacting on cell metabolism and also enables ATP production by glycolysis to continue.

Inhibiting the transport of monocarboxylates may also cause other changes in the cytosolic and extracellular equilibrium of its substrates. It seems that succinate is transported in its monocarboxylate form via MCT1 under anaerobic conditions, when the intracellular pH is lowered. Unpublished data by Drs. Hiran Prag and Dunja Aksentijevic utilising a murine Langendorff heart system for IRI indicates that approximately 40% of the succinate that is accumulated during ischaemia is retained within the tissue, with the rest exported to the circulation upon reperfusion (paper in revision) (Figure 5.1). This export of succinate can be reduced by inhibiting MCT1. In order to understand the molecular basis of this efflux of succinate and the involvement of MCT1 in it further, I will utilise the cell model and buffer systems with or without the addition of the potent and specific MCT1 inhibitor AR-C141990 at various time points before, during or after anoxia or reoxygenation.

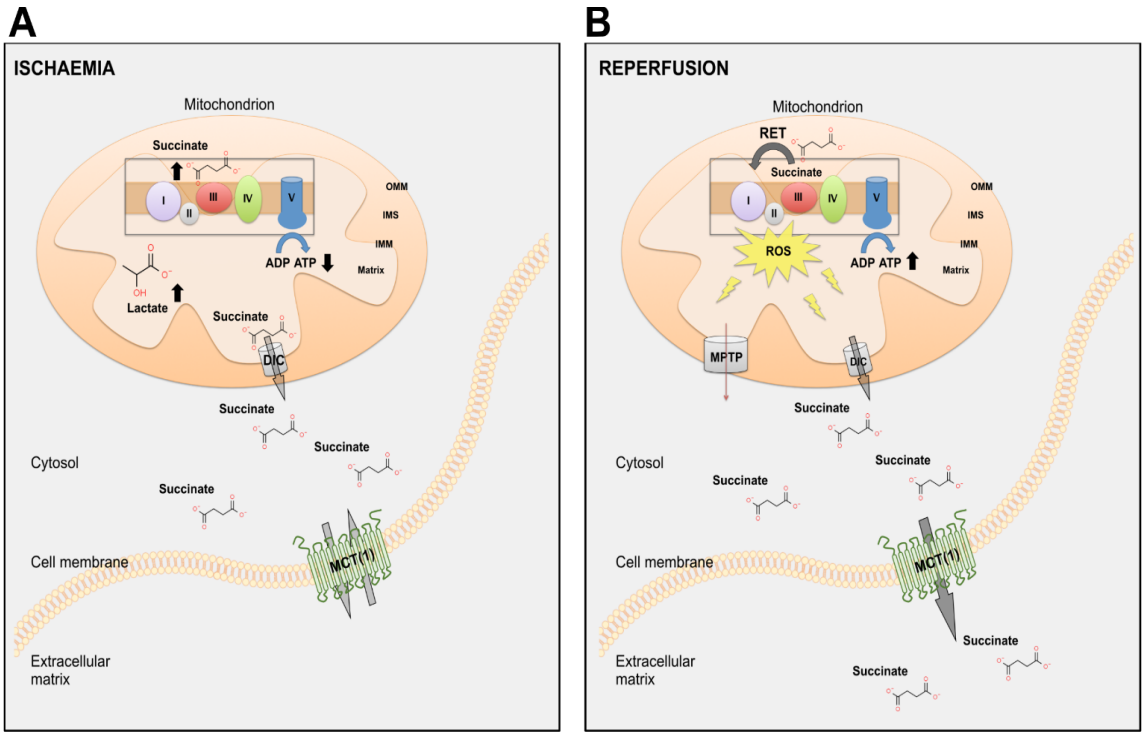

Figure 5.1: Schematic model of succinate accumulation and efflux during ischaemia and upon reperfusion. A) During ischaemia, changes occur in mitochondria including the accumulation of lactate, a decrease in ATP/ADP ratios and a build-up in succinate at complex II of the ETC. Accumulated succinate is transported out of mitochondria into the cellular cytosol via the DIC. And some of it is further effluxed via MCT1 out of the cell into the extracellular environment. B) Upon reperfusion, the succinate retained within mitochondria is oxidised via RET generating a burst of ROS that damages the organelle and leads to MPTP opening and ischaemic injury. The increased level of succinate within the cytosol leads to increased efflux of the metabolite via MCT (1) into the extracellular matrix. I-V= ETC complexes 1-5, OMM= outer mitochondrial membrane, IMS= inter membrane space, IMM= inner mitochondrial membrane, DIC= dicarboxylate carrier, MCT= monocarboxylate carrier, MPTP= mitochondrial permeability transition pore, RET= reverse electron transfer, ROS= reactive oxygen species.

A further advantage of using a cell model for IRI is the possibility of investigating effects on outcome of drugs on anoxic and reoxygenated cells. This cell system may help in understanding the best timing for the drug delivery, the dose and differences in response. Thus, for the novel therapeutics developed by the organic chemists with whom we collaborate, I can assess their uptake and function in cell models, before finally, they are used to treat human organs perfused on an *ex vivo* perfusion system. One of the problems which occurs with screening drugs in cell models is, that the cells often behave quite differently from those *in vivo* in the patient. The IR model developed here that utilises true anoxia in adult primary cardiomyocytes enables a more relevant pathophysiological cell model and therefore should

be a good system to assess drug efficacy and function. This way, compounds that do not affect IRI can be excluded and the timings for drug delivery be optimised before utilising more relevant *ex vivo* and *in vivo* models.

Because a key part of the damage in ischaemia reperfusion injury starts in mitochondria at the respiratory chain, inhibitors of the ETC are potential drug candidates to ameliorate oxidative damage upon reperfusion.

The lack of oxygen during ischaemia results in a blockage in electron transfer onto oxygen molecules as the final acceptor, and as described in detail in the general introduction, this results in a highly reduced CoQ pool driving RET, and with that ROS production, upon reoxygenation. Stopping excess electrons entering the electron transport chain during anoxia or blocking the reversal upon reperfusion might reduce ROS generation (Chouchani et al., 2014, Pell et al., 2016). Therefore, two possible inhibition strategies are to either inhibit complex II and the accumulation of succinate which forces electrons into the ETC upon reperfusion after ischaemia causing RET (Figure 5.2). Alternatively, this can be done by inhibiting complex I upon reperfusion to block RET and therefore ROS generation at complex I, and these approaches are discussed below.

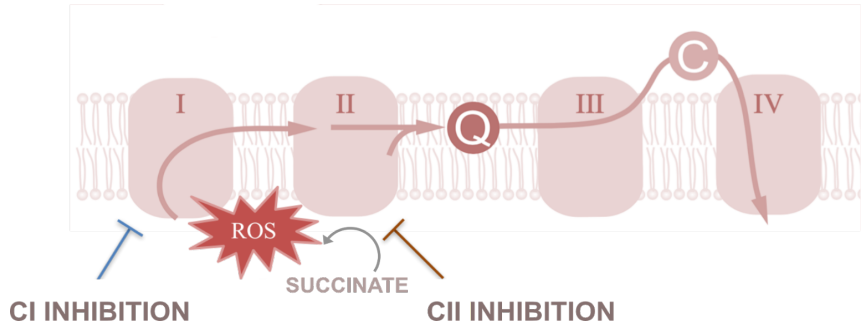

Figure 5.2: ETC inhibition strategy. Schematic overview over the inhibition strategy in order to ameliorate ROS production upon reoxygenation. ROS is generated at complex I via RET during reperfusion. Inhibition of complex I or II might block this and therefore decrease ischaemic damage. ROS= reactive oxygen species, I- IV= ETC complexes, Q= ubiquinone, C= cytochrome c.

Complex I is the main protein complex facilitating electron entry into the respiratory chain. Complex I oxidises the electron donor NADH and utilises this electron to reduce CoQ, hence mutations within its subunits cause severe energetic impairment associated with mitochondrial

diseases. One modulator of complex I is the irreversible inhibitor rotenone, which binds to the quinone binding pocket of the enzyme (Figure 5.3). Under aerobic conditions, this leads to increased ROS production, while under anaerobic conditions, it can block reverse electron transfer (RET). During aerobic conditions, rotenone inhibition can stop forward electron flow and therefore increase ROS generation due to electron saturation at complex I. During anaerobic conditions, as described in detail in the general introduction, the saturated electron transport chain causes a backwards flow of electrons from the fully reduced CoQ pool towards complex I, where this leads to generation of ROS. Blocking complex I could ameliorate this ROS production caused by RET.

Analysis of this inhibition and its effect on succinate accumulation during anoxia, will give rise to a better understanding of the role of the electron transfer chain in ischaemic damage due to its role in succinate accumulation as well as on ROS produced by succinate oxidation via RET at complex I.

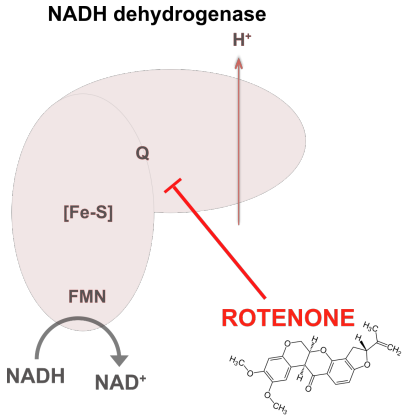

Figure 5.3: Complex I inhibition by rotenone. Schematic overview over inhibition of the NADH dehydrogenase complex I and the rotenone acting site. Complex I receives electrons from NADH at its flavin site, transfers them via iron- sulfur clusters onto ubiquinone enabling proton pumping. The reduction of ubiquinone to ubiquinol at the quinone- binding site can be irreversibly interrupted using the ROS supporting class A inhibitor of complex I rotenone. H^+ = proton pumping, Q = quinone, [FeS]= iron- sulfur clusters, FMN= flavin.

Complex II (succinate dehydrogenase; SDH) oxidises succinate to fumarate utilising electrons from the electron donor $FADH_2$ to reduce ubiquinone in the ETC (Jardim-Messeder et al., 2015; Mowery et al., 1977; Scallet et al., 2003; Valls-Lacalle et al., 2018). This protein complex located in the inner mitochondrial membrane feeds the ETC to produce a proton gradient utilising O_2. Although complex I is the primary source of electrons for oxidative

phosphorylation, complex II contributes as well and inhibition of this complex can impact cellular energy production. Especially during ischaemia and upon reperfusion, complex II and its role in transferring electrons onto CoQ is important, because the reversal of complex II and following succinate accumulation of the metabolite succinate have been shown to drive ischaemia reperfusion injury (Chouchani et al., 2014). Therefore, inhibition of this complex promises therapeutic potential. A range of different compounds is kown to inhibit complex II, as described below.

Thenoyltrifluoroacetone (TTFA) is a reversible inhibitor that binds to the quinone-binding pocket of the SDH complex. 3- nitropropionic acid (3- NPA) on the other hand binds to the substrate- binding site of complex II. Differences in the effect of these two compounds, that inhibit two different sites at complex II, might reveal where detrimental processes occur during anoxia and upon reoxygenation. Additionally, as 3- NPA is an irreversible inhibitor, which might act differently than reversible inhibitors.

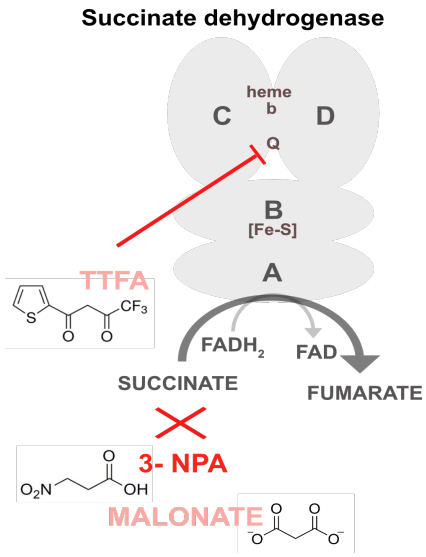

Figure 5.4: Reversible and irreversible inhibition of complex II. Schematic overview over inhibition of the succinate dehydrogenase complex II and the inhibitor acting sites. Complex II receives electrons from succinate onto FAD generating $FADH_2$ at its subunit A which electrons are in turn transferred via iron- sulfur clusters in subunit B onto ubiquinone at the quinone binding-site at subunits C and D. The reversible inhibitor TTFA interrupts SDH activity at this site. The irreversible inhibitor 3-NPA and the competitive inhibitor malonate, which is structurally similar to succinate, inhibit complex II at its substrate binding- site. Q = quinone, [FeS]= iron- sulfur clusters, TTFA = thenoyltrifluoroacetone, 3-NPA= 3- nitropropionic acid.

A reversible and competitive inhibitor of succinate dehydrogenase is malonate, which is structurally similar to succinate and therefore binds in the same binding pocket of the enzyme. It can easily be metabolised allowing normal function of complex II and the respiratory chain (Bowman et al., 2017). *In vivo* experiments showed promising results in ameliorating succinate accumulation during ischaemia when treated with malonate compounds improving outcome after ischaemia reperfusion injury. The cell permeable malonate prodrug dimethyl malonate (DMM) for example prohibited the accumulation of succinate and ischaemia reperfusion injury in mice (Chouchani et al., 2014a; Martin et al., 2019). Disodium malonate (DSM) was protective against IRI in small and large animals (Valls-Lacalle et al., 2018) when administered at reperfusion.

Another therapeutic approach to ameliorate IRI, is the utilisation of hydrogen sulphate (H_2S), and its protein modification S- persulfidation, upon reperfusion. H_2S has been shown to be beneficial in some diseases, mainly linked to inflammatory regulation. Many of the effects of H_2S are thought be due to it modifying protein activity via the formation of persulfides therefore modifying protein thiols (Filipovic, 2015).

Recent research into this has shown promising therapeutic potential: the H_2S-releasing compound AP39 for example has been reported to exert cytoprotective effects by stimulating bioenergetics and by preserving mitochondrial DNA integrity during oxidative stress (Bełtowski, 2015; Citi et al., 2018; Szczesny et al., 2018).

Another way to utilise beneficial effect of H_2S is by directly modifying protein thiols via S- persulfidation. We recently developed the mitochondria-targeted compound MitoSulf, which may S-sulphurate thiols and alter enzyme activity directly. As depicted in Figure 5.5, complex I might be a potential target of persulfidation, inhibiting reactivation of this complex upon reperfusion and therefore blocking RET and ROS production.

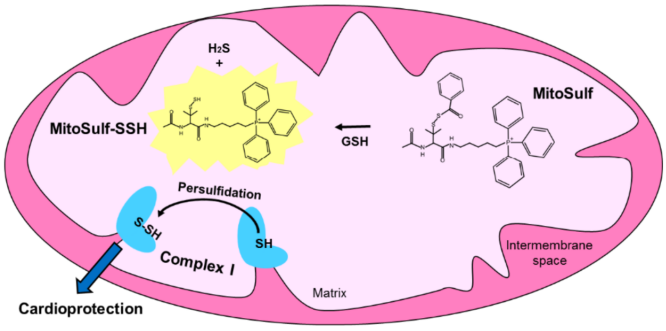

Figure 5.5: Persulfidation as therapeutic approach to ameliorate IRI upon reperfusion. Predicted mechanism of MitoSulf: Upon uptake into the mitochondrial matrix, MitoSulf undergoes GSH-dependent activation to form MitoSulf-SSH which then might catalyse persulfidation of residues on mitochondrial proteins, e.g. Complex I. This persulfidation could inhibit Complex I and protects against RET and therefore ROS production during IR injury. Modified from Joy Shih (unpublished).

Altogether, the analysis of the effect of different ETC inhibitors on succinate accumulation and oxidation and the investigation of cardioprotective compounds might give rise to a better understanding of the pathological processes that occur during ischaemia and upon reperfusion. This will enable the development of better therapeutical compounds as well as elucidate at which point during IRI it is most beneficial to interfere in order to improve patient outcome.

5.2 Aims

After developing a cardiomyocyte model to mimic IRI, I next wanted to utilise this model to focus on two major aspects relevant to understand IRI *in vivo*: discover the fate of accumulated succinate upon reperfusion and test the efficacy of ETC inhibitors as potential therapeutics to ameliorate IRI.

Specifically, one aim is to elucidate how much accumulated succinate is oxidised by the respiratory chain and how much is released from the cells upon reoxygenation and to determine how long it maintains within primary adult murine cardiomyocytes upon reoxygenation, as well as understanding if and how succinate is effluxed into the surrounding medium.

Furthermore, the role of the MCT1 transporter in transporting succinate will be investigated further utilising buffers with or without the inhibitor AR-C141990 at different timepoints.

And finally, one focus of this project is to understand how complexes I and II are affecting succinate accumulation and if inhibition of these complexes may ameliorate the amount of accumulated TCA metabolite and improve IRI outcome in form of cell survival upon reperfusion.

5.3 Results

5.3.1 Succinate efflux from primary cardiomyocytes

Succinate and lactate accumulate in primary adult murine cardiomyocytes during anoxia, as elucidated in the previous chapter. This occurred in a range of different buffer systems, including glucose-based Tyrode's buffer with or without addition of the MCT1 inhibitor AR-C141990. Because I wanted to investigate the putative role of the monocarboxylate transporter in transporting succinate, as well as lactate out of cells, I utilised these different buffer systems to determine how MCT1 inhibition affects intracellular succinate concentrations and further on investigate the mechanism of succinate efflux.

5.3.1.1 Succinate efflux from cardiomyocytes in different buffers upon reoxygenation after anoxia

The efflux of succinate from ischaemic tissue upon reperfusion has been investigated in an *ex vivo* Langendorff models (Zhang et al., 2018) and in addition in human studies (Kohlhauer et al., 2018). In our lab we have further explored the mechanism of this succinate efflux using a Langendorff model. This work suggested a role for MCT1 in this process, as is summarised in (unpublished data, submitted). As part of this work I wished to explore in my cardiomyocyte model the mechanism and time course of this succinate release. Utilising a cell model offers advantages over an *ex vivo* perfused heart with the opportunity to tightly control timings, reoxygenation conditions and buffer composition and was therefore utilised to investigate the mechanism of succinate release from anoxic primary murine cardiomyocytes upon reoxygenation.

As determined in the previous chapter, 1 h of anoxia led to severe ischaemic injury characterised by significant accumulation of succinate within the cardiomyocytes, and was

therefore used in these experiments. To investigate succinate efflux, after 1 h anoxia the cardiomyocytes were washed with anoxic Tyrode`s buffer within the anoxic chamber before fresh Tyrode`s was added and the cells were then transferred to a cell incubator to induce reoxygenation. Then, at various times subsequently the cell pellets and supernatants were isolated and analysed for metabolite concentrations.

I first investigated how intracellular and extracellular lactate concentrations changed upon reoxygenation in the presence or absence of MCT1 inhibition (Figure 5.6). As expected, significantly more lactate accumulates within cardiomyocytes during 60 min anoxia when MCT1 is inhibited. In the supernatant on the other hand, more lactate can be detected in absence of the inhibitor. The inhibitor AR-C141990 was not present in the buffer added just prior to reoxygenation. Assessment 15 min after reoxygenation showed that more lactate was maintained within cells that have undergone anoxia in T141990 buffer, and then transferred to Tyrode`s buffer before reoxygenation than in Tyrode's buffer only. A large release of lactate into the supernatant could be detected 4 h after reoxygenation in both buffer systems, indicating that this metabolite is still generated by the cell after reoxygenation. Furthermore, cells that were made anoxic in both buffers showed an additional increase in intracellular lactate 18 h after reoxygenation, which might be a response to a switch to glycolytic metabolism following mitochondrial damage upon reoxygenation.

Within 5 min of reoxygenation, there was a significant decrease in intracellular succinate (Figure 5.7) returning to baseline levels. 15 min after reoxygenation, an increase within the supernatant was detectable. Calculating the amount of released metabolite in comparison to maintained intracellular succinate shows that after reperfusion, 1300 ± 250 pmol succinate/10^5 cells was released into the extracellular medium. This succinate release was about 60% of that accumulated within the cardiomyocytes during ischaemia.

These data indicate that most of the succinate that accumulated during anoxia is effluxed out of the cells into the incubation medium, with the rest (~40%) being oxidised by the respiratory chain to drive ROS production, consistent with that seen in the Langendorff heart. Even so, further work on succinate oxidation upon re-oxygenation is still required.

Furthermore, my data indicate a role of the MCT1 transporter in succinate efflux upon reoxygenation after anoxia. Cells that were kept in Tyrode's buffer only, accumulated some succinate during anoxia. This succinate concentration within the cell pellet decreases significantly within 15 min of reoxygenation without MCT1 inhibition. If AR-C141990 was

added to the buffer upon reoxygenation, this decrease in intracellular succinate was reduced slightly. However, cells that were incubated in AR-C141990 containing buffer during anoxia, showed a significant accumulation of succinate within the cell pellet after 1 h of anoxia. When these cells were reoxygenated in buffer lacking MCT1 inhibition this led to a return of succinate concentration back to baseline levels, when it was measured 15 min after reoxygenation without the inhibitor. If MCT1 inhibition was maintained during reoxygenation, the amount of succinate retained within the cell pellet was elevated.

The presence of the MCT1 inhibitor AR-C141990 upon reoxygenation did not just affect succinate, but also lactate efflux from cardiomyocytes (Figure 5.8). Cells incubated in Tyrode's buffer during anoxia as well as cells incubated with the MCT1 inhibitor, showed highly decreased amounts of lactate in the surrounding medium 15 min after reoxygenation and higher concentrations were maintained within the cell pellets in comparison to reoxygenation in the absence of MCT1 inhibition.

These data indicate, that inhibition of MCT1 during reoxygenation after anoxia, increases not just the amount of lactate within cells, but also the amount of succinate maintained within the cell pellet and implies a role for MCT1 in succinate efflux upon anoxia and reoxygenation.

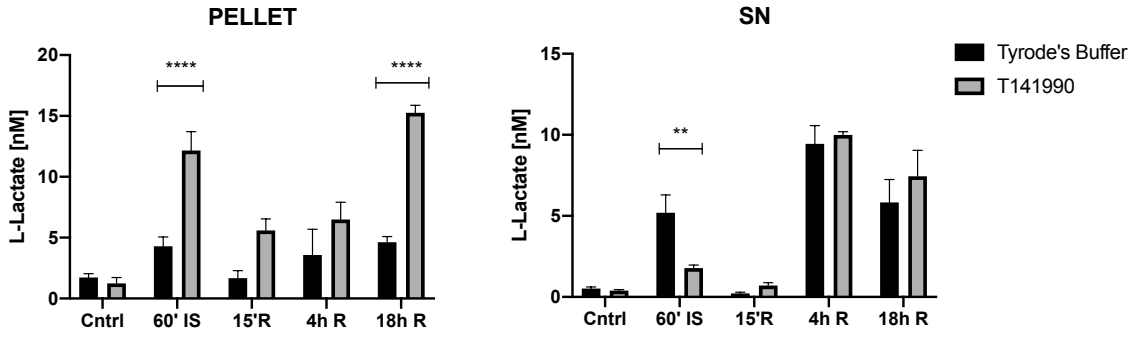

Figure 5.6: Concentrations of intra- and extra- cellular L- lactate in different buffers upon reoxygenation. Cardiomyocytes in Tyrode's buffer or Tyrode's + AR-C141990 [10 µM] (T141990) were subjected to 60 min of anoxia followed by different time points of reperfusion, as described before. L-lactate concentrations [nM] were measured utilising absorbance at 450 nm. Intracellular metabolite concentrations were evaluated within cell pellets (A), extracellular were extracted from the supernatant (B). (A) Cell pellets were collected and the deproteinised using perchloric acid, before lactate was measured. (B) Lactate was directly measured in supernatants retrieved from the cell plates. n= 4 biological replicates, data are mean ±S.E.M. Statistical analysis was performed via two-way ANOVA. **P<0.05, ****<0.0001.

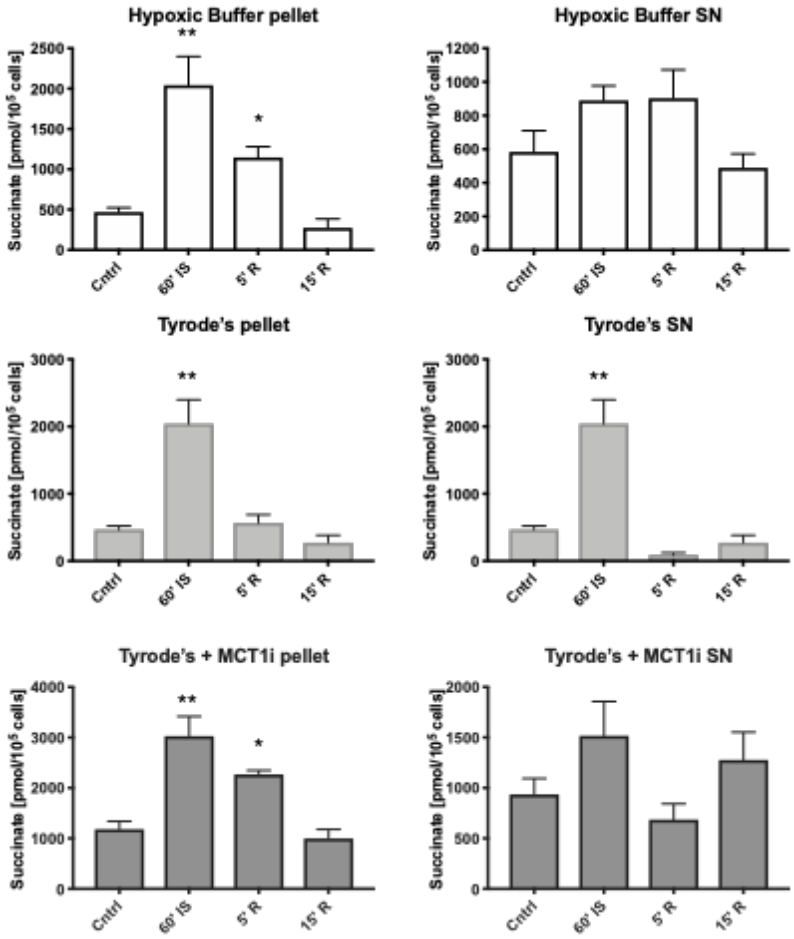

Figure 5.7: Concentrations of intra- and extra- cellular succinate in different buffers upon reperfusion. Cardiomyocytes in hypoxic buffer (A, B). Tyrode's buffer (C, D) or Tyrode's + AR-C141990 [10 μM] (T141990) (E, F) were subjected to 60 min of anoxia followed by different time points of reperfusion, as described before. Succinate concentrations were determined via mass spectrometry in pmol/ 10 000 cells. Intracellular metabolite concentrations were evaluated within cell pellets (A, C, E), extracellular were extracted from the supernatant (B, D, F). (E, F) MCT1 inhibitor AR-C141990 was present at reperfusion. n= 4 biological replicates. Data are mean ± S.E.M. Statistical analysis was performed via unpaired student's t-test. *P<0.05, **<0.01.

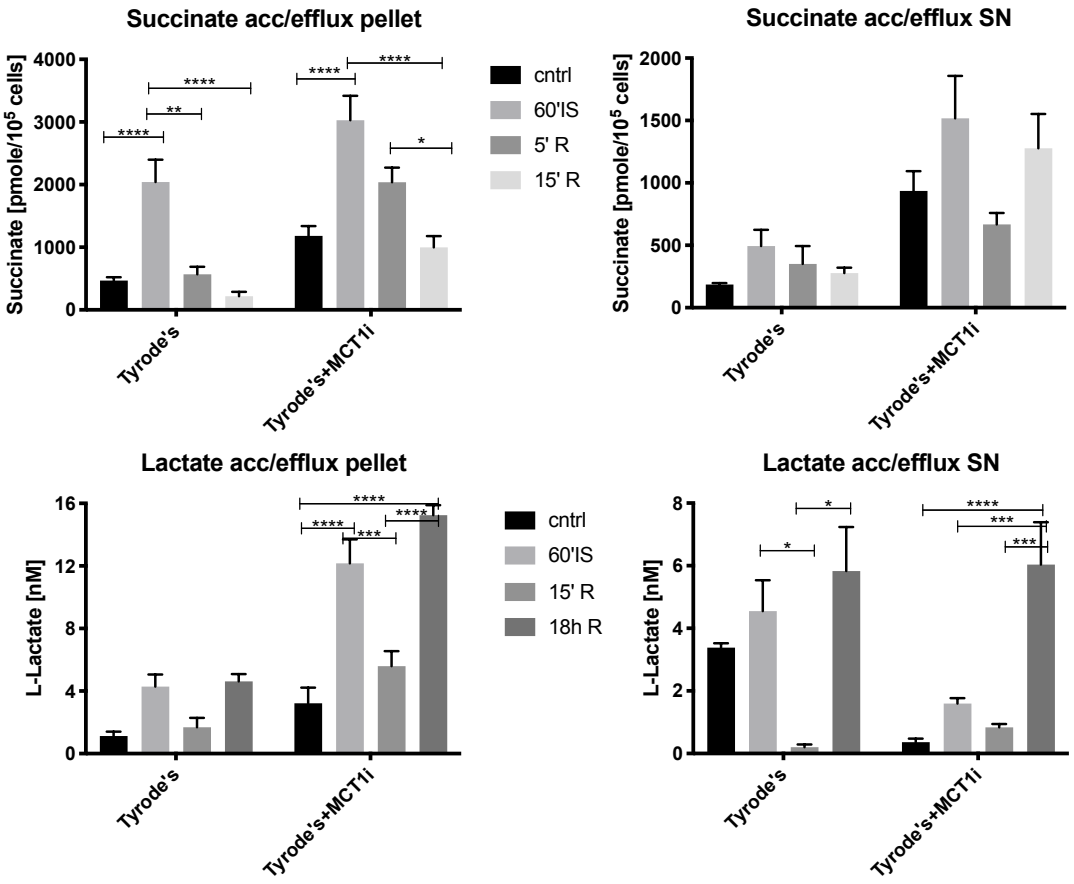

Figure 5.8: Direct comparison of L- lactate and succinate efflux during anoxia and upon reoxygenation in the absence of MCT1 inhibition. Changes in intracellular (A, C) and extracellular (B, D) L-lactate (A, B) and succinate (C, D) concentrations in primary cardiomyocytes that underwent 60 min of anoxia in Tyrode`s buffer or Tyrode`s + AR-C141990 (T141990), followed by up to 15 min of reperfusion in glucose- based Tyrode's buffer. L-Lactate was measured via absorbance at 450 nm in nM, while succinate concentrations were determined via mass spectrometry in pmol/10 000 cells. n= 7 biological replicates for succinate and 3 for lactate concentrations, data are mean ± S.E.M. Statistical analysis was performed via two-way ANOVA. *P<0.05, **<0.01, ***P<0.001, ****P<0.0001.

5.3.2 Inhibition of ETC complexes and its effect on succinate accumulation during ischaemia and reperfusion

In order to assess how succinate accumulation during anoxia, which drives ROS damage upon IRI, was affected by the activity of respiratory chain complexes I looked at the effects of inhibitors. Here, I investigated the effect of inhibition of complex I and SDH on succinate accumulation utilising the cardiomyocyte model.

5.3.2.1 Complex I inhibition during anoxia and upon reoxygenation

To understand how complex I activity affects succinate accumulation and IR injury, the complex was inhibited with rotenone. Anoxia and reoxygenation in primary adult cardiomyocytes was performed as described above. Cardiomyocytes were maintained under normoxia or anoxia for 1 h in T141990 buffer containing 1 μM rotenone throughout the whole procedure (excluding reoxygenation). Or samples were kept in T141990 only during normoxia and anoxia, before rotenone was added 5 min before reoxygenation.

Cell pellets were then analysed for their succinate content, while the supernatants were analysed for succinate, lactate, and also for LDH release as a marker of cell death (Figure 5.9). In comparison to untreated samples, rotenone treated samples seem to accumulate slightly more succinate during 1 h of anoxia, albeit not statistically significant. Strikingly different is the amount of succinate that is released into the supernatant during anoxia as well as upon reoxygenation during rotenone treatment. Although succinate accumulates during anoxia within the cell, it is not significantly effluxed from cells. Upon reperfusion in presence of rotenone, a decrease in intracellular succinate is detectable, but no increase in the supernatant, suggesting that succinate is oxidised within the cell during reperfusion in the presence of rotenone.

Lactate released from the cells during anoxia, or upon reoxygenation did not show any significant difference to untreated samples. Additionally, rotenone treatment did not affect cell viability assessed 2 h after reoxygenation.

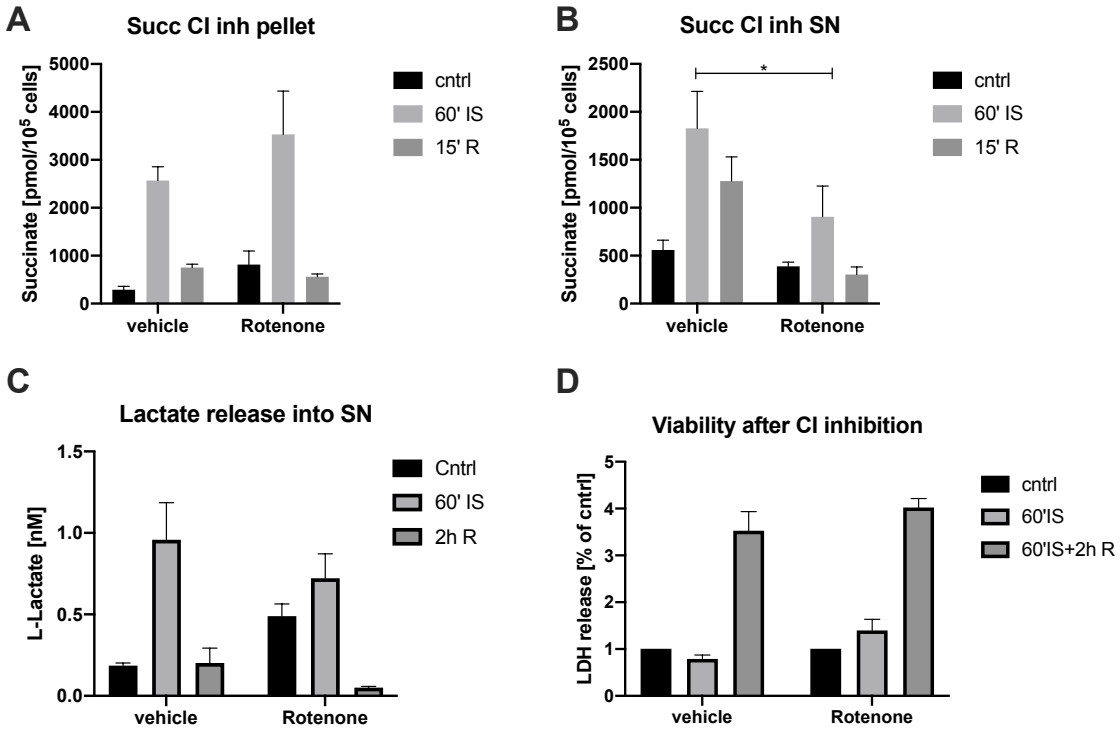

Figure 5.9: Complex I inhibition in primary cardiomyocytes during anoxia and upon reoxygenation Cardiomyocytes in Tyrode's + AR-C141990 [10 µM] (T141990) were subjected to 60 min of anoxia with either DMSO or rotenone [1 μM] followed by 2h reperfusion in Tyrode's buffer, as described before. (A, B) Succinate concentrations were determined via mass spectrometry in pmol/ 10 000 cells in cell pellets and supernatants. (C) Extracellular L-lactate concentrations [nM] were measured utilising absorbance at 450 nm. (D) LDH protein concentrations were measured in the cellular supernatant via absorbance at 492 nm. Elevated LDH levels upon anoxia and reperfusion indicate increased cell death. Results are presented relative to a positive control of cardiomyocytes lysed in 1% Triton. n= 4- 5 biological replicates, data are mean ± S.E.M. Statistical analysis was performed via two-way ANOVA and significance indicated with asterices. *P<0.05.

In summary, inhibition of complex I did not affect succinate accumulation during anoxia, but it decreased the amount of succinate that is effluxed from cells especially upon reoxygenation.

5.3.2.2 SDH inhibition during anoxia and reoxygenation

5.3.2.2.1 Effect of SDH inhibition by 3- NPA and TTFA

I next wanted to elucidate the effect of irreversible complex II inhibition on succinate accumulation, release of metabolites and cell viability upon anoxia and reoxygenation. It has been proposed that during anoxia a highly reduced CoQ pool causes a reversal of SDH and

leads to the reduction of fumarate to succinate. To test this, inhibition of SDH with the three different inhibitors that have been described before, and their effect on succinate accumulation during anoxia has been investigated here (Figure 5.10 & 5.11).

The two irreversible inhibitors TTFA and 3-NPA bind to different sites of SDH. Figure 5.10 shows succinate levels in cell pellets, or released into the supernatant of cardiomyocytes treated with either 3-NPA [500 µM] or TTFA [1 mM] and MCT1 inhibitor AR-C141990 [10 µM] before they were transferred into the anoxic chamber and maintained anoxic for 60 min. The inhibitors were also present in the reoxygenation buffer.

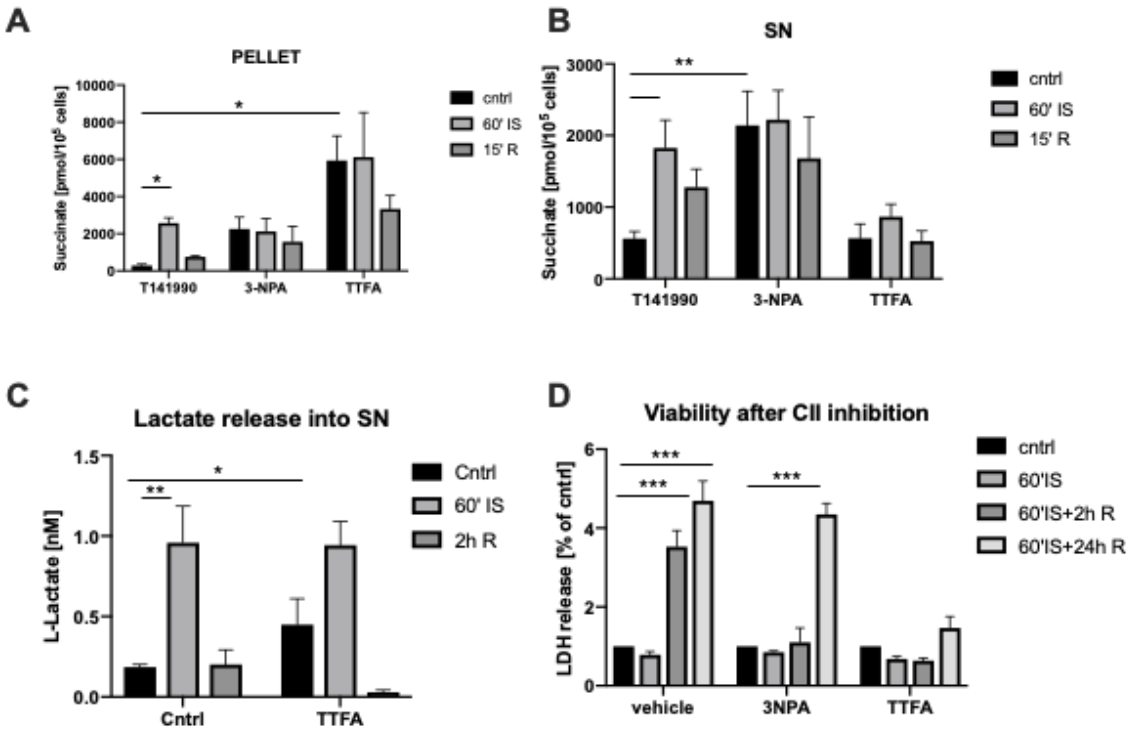

Figure 5.10: Complex II inhibition in primary cardiomyocytes during anoxia and upon reoxygenation. Cardiomyocytes in Tyrode's + AR-C141990 [10 µM] (T141990) were subjected to 60 min of anoxia with either DMSO, 3- nitropropionic acid (3- NPA) [500 µM] or thenoyltrifluoroacetone (TTFA) [1 mM], followed by up to 24h reperfusion in Tyrode's buffer supplemented with the inhibitors. (A, B) Succinate concentrations were determined via mass spectrometry in pmol/ 10 000 cells in cell pellets and supernatants (C) Extracellular L-lactate concentrations [nM] were measured utilising absorbance at 450 nm. (D) LDH protein concentrations were measured in the cellular supernatant via absorbance at 492 nm. Elevated LDH levels upon anoxia and reperfusion indicate increased cell death. Results are presented relative to a positive control of cardiomyocytes lysed in 1% Triton. n= 3-5 biological replicates, data are mean ± S.E.M. Statistical analysis was performed via two-way ANOVA and significance indicated with asterices. *P<0.05, **P<0.01, ***P<0.001.

As expected, both inhibitors cause increased succinate levels in cells maintained in normoxic conditions for 2 h in comparison to untreated cells. While 3- NPA did not significantly affect intracellular succinate during anoxia and upon reoxygenation, TTFA caused a major rise in cellular succinate concentrations at all time points. Release into the supernatant, on the other hand was decreased in all samples treated with TTFA, especially in comparison to 3- NPA treated samples, which showed elevated succinate levels in the extracellular buffer.

Lactate release by the cells was not affected by SDH inhibitors, but cell viability after anoxia/reoxygenation, measured by decreased LDH release, was improved after TTFA treatment. Cardiomyocytes that underwent anoxia and reoxygenation in the presence of 3-NPA did release similar amounts of LDH 24 h upon reoxygenation as untreated samples, but cells treated with TTFA released much less LDH, suggesting decreased cell death.

This shows, that different complex II inhibitors have different effects on succinate accumulation as well as on cell viability. Inhibitors that bind in the substrate binding pocket seem to decrease succinate accumulation, while inhibition of the quinone binding pocket increased intracellular succinate. This might be due to more successful inhibition of succinate production at complex II at the substrate binding pocket, but these different effects of different inhibitors need to be investigated further. Nevertheless, inhibition at this site of the SDH improved cell viability upon IRI.

5.3.2.2.2 Effect of SDH inhibition by Disodium malonate

I next wanted to investigate if the reversible complex II inhibitor disodium malonate, that has been previously shown to be protective again IR injury (Bowman et al., 2017), can affect the succinate accumulation and anoxia-reoxygenation in the cardiomyocyte model. Disodium malonate (DSM, 10 mM) was added before induction of 1 h anoxia in the AR-C141990 containing Tyrode's buffer. Before reoxygenation, cells were washed and transferred into buffer without malonate present. In comparison to control cells without disodium malonate, the amount of succinate within the cell pellet after 1 h of anoxia, but as well in the surrounding supernatant, was reduced. In contrast the membrane permeant malonate prodrug dimethyl malonate (10 mM) did not show any effect on succinate accumulation and was therefore not pursued further in this model, and I focused on DSM for further analysis.

Interestingly, more lactate was released from cells 2 h after reoxygenation when treated with DSM (Figure 5.11, C), perhaps as a consequence of inhibition of mitochondrial respiration. I also found that the ATP/ADP ratios stabilised more quickly at this time point in DSM treated samples, then in untreated samples, consistent with DSM amelioration of the injury caused by anoxia and reoxygenation (Figure 5.11, D).

Most striking are the experiments which involved assessment a long time following reoxygenation after 1 h of anoxia with or without DSM (Figure 5.11, E). Cells that were exposed to anoxia and reoxygenation after inhibition of SDH with DSM show significantly decreased LDH release, consistent with much less cell death after anoxia and reoxygenation. Similar to that investigated *in vivo*, treatment with disodium malonate reduces succinate accumulation and improves cell survival and therefore outcome after anoxia and reoxygenation.

To summarise, these data strengthen our understanding of the therapeutic approach using malonate compounds to ameliorate IR injury in form of cell death. In the future the inhibitor will also be tested upon reperfusion which might have different or additional beneficial effects.

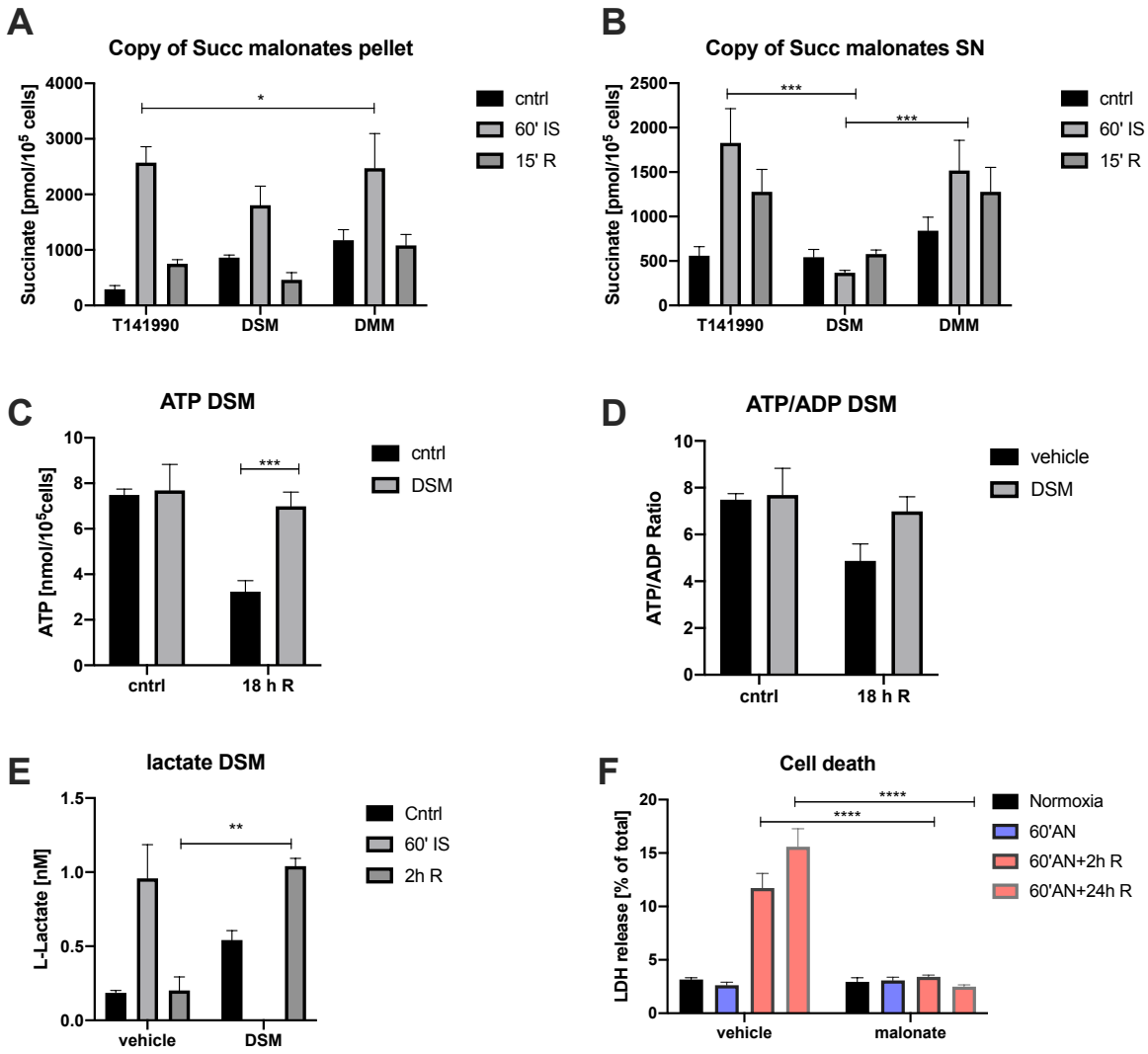

Figure 5.11: Complex II inhibition by disodium malonate in primary cardiomyocytes during anoxia and upon reoxygenation ameliorates IR injury. Cardiomyocytes in Tyrode's + AR-C141990 [10 µM] (T141990) were subjected to 60 min of anoxia with either DMSO or 10 μM disodium malonate (DSM) or (A- B) 10 mM dimethyl malonate (DMM), followed by up to 24h reperfusion in Tyrode's buffer supplemented with the inhibitors. (A, B) Succinate concentrations were determined via mass spectrometry in pmol/ 10 000 cells in cell pellets and supernatants. (C) ATP and (D) ATP/ADP ratios of treated and untreated cells in control samples or anoxic and reoxygenated samples were determined using a luciferase- based luminescence assay. (E) Extracellular L-lactate concentrations [nm.] were measured utilising absorbance at 450 nm. (F) LDH protein concentrations were measured in the cellular supernatant via absorbance at 492 nm. Elevated LDH levels upon anoxia and reperfusion indicate increased cell death. Results are presented relative to a positive control of cardiomyocytes lysed in 1% Triton. n= 3-5 biological replicates, data are mean ± S.E.M. Statistical analysis was performed via two-way ANOVA and significance indicated with asterices. *P<0.05, **P<0.01, ***P<0.001, ****P<0.0001.

5.3.3 Treatment of cardiomyocytes with sulfurylation compounds

As described in the introduction, hydrogen sulphide has been shown to modify protein thiols. It potentially modifies cysteines in complex I and therefore diminishes ROS production upon RET during reperfusion. The mitochondrially- targeted compound MitoSulf can perform these modifications as well and therefore display cardioprotective effects. Here, I tested if MitoSulf can decrease IRI after anoxia and reoxygenation in primary cardiomyocytes

5.3.3.1 Effect of compounds on long- and short- term reperfusion

In order to investigate if MitoSulf can protect cardiomyocytes from injury after anoxia and reoxygenation, I investigated cell viability after both long and short- term treatment. As shown in Figure 5.12, cells treated with 1 µM MitoSulf in T141990 buffer 5 min before reoxygenation did not show any recovery of their ATP/ADP ratios 2 h after reoxygenation but a reduction. However, albeit these results are statistically not yet significant and need to be repeated, when assessed 24 h after reoxygenation, the presence of MitoSulf did decrease LDH release and therefore cell death, while a control compound MitoNAP did not show a similar effect on ameliorating IRI in form of decreased LDH release.

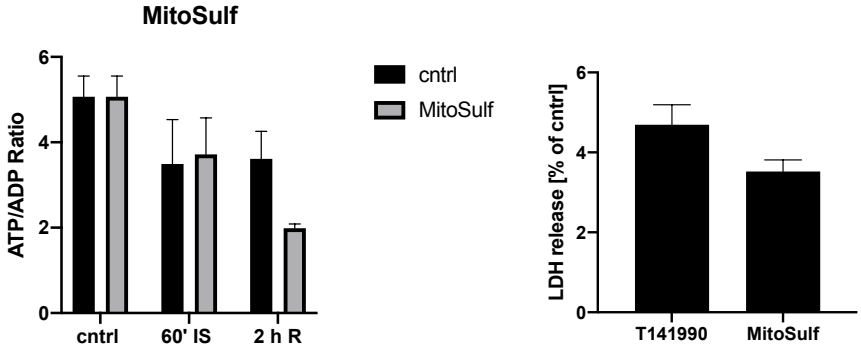

Figure 5.12: The persulfidation agent MitoSulf ameliorates IR injury in form of cell death in primary cardiomyocytes. Cardiomyocytes in Tyrode's + AR-C141990 [10 µM] (T141990) were subjected to 60 min of anoxia, followed by up to 24h reperfusion in Tyrode's buffer supplemented with either DMSO or 1 µM. (A) ATP/ADP ratios of DMSO treated cells in control, anoxic and reoxygenated conditions were determined using a luciferase- based luminescence assay. (F) LDH protein concentrations were measured in the cellular supernatant via absorbance at 492 nm. Elevated LDH levels upon anoxia and reperfusion indicate increased cell death. Results are presented relative to a positive control of cardiomyocytes lysed in 1% Triton. N= 4 biological replicates, data are mean ± S.E.M. Statistical analysis via one-way ANOVA was not significant with p-values of p= 0.1863 and p= 0.0761.

Altogether, treatment with MitoSulf displayed slight protection against the injury caused by anoxia and reoxygenation in primary cardiomyocytes underlying its role as a potential cardioprotective drug. The exact mechanism that leads to amelioration of IRI has to be elucidated and *ex vivo* and *in vivo* models tested to reproduce these results in more complex models. But this shows, that this cardiomyocyte model is useful to screen for potential new therapeutic drugs against IR injury.

5.4 Discussion

The cell model using anoxia-reoxygenation of primary adult mouse cardiomyocytes have been developed in the previous chapter. While cell models published before showed a lower amount of succinate accumulation than *in vivo* models, and not much effect of complex I or II inhibitors on this accumulation (Zhang et al., 2018), our findings here suggest that this might be due to these models using induction of hypoxia, instead of true anoxia as was developed here. Through the use of anoxia followed by reoxygenation, the isolated adult cardiac myocyte model used here, shows a reasonable degree of similarity to *in vivo* heart attack or transplantation models, in particular regarding the loss of adenosine nucleotides, the accumulation of succinate and lactate and the extent of cell damage. The later-onset damage observed here, with cell death occurring 18 to 24 h after reoxygenation, is also often seen in animal disease models. This *in vitro* model is therefore suitable to investigate ischaemia reperfusion injury. It should also be useful to help understand the cellular processes that occur both early and late after reperfusion, to determine how cell death occurs and if it could be ameliorated.

In this chapter, two applications of the cell model were initiated: investigation of the processes occurring during anoxia and upon reoxygenation that cause cell injury; and screening compounds with therapeutic potential. The first goal, focused on succinate accumulation during anoxia and its oxidation or efflux upon reoxygenation. Therefore, the two different buffer systems Tyrode's and Tyrode's containing the MCT1 inhibitor AR-C141990 were utilised and the difference in amount of succinate that accumulates and stays within the cell pellet upon reperfusion investigated. Less succinate accumulates when the cells are kept

in Tyrode's buffer in comparison to Tyrode's + MCT1 inhibition. Furthermore, more succinate is retained within the cell pellet following 5 min as well as 15 min following reoxygenation. This could be due to the higher initial amount of succinate, but in Tyrode's only, the concentration reduces by almost 50% from ~1000 to ~500 pmol/100 000 cells, while in presence of the MCT1 inhibitor the reduction is closer to 33% from ~3000 to ~2000 pmol/100 000 cells. Considering this, we hypothesised, that addition of the MCT1 inhibitor affects the succinate levels that are maintained within the cell pellet upon reperfusion.

It is therefore important to investigate the amount of succinate in the cell surrounding medium, or supernatant, in order to understand if succinate is oxidised within the cell or effluxed into the supernatant and if this is affected by inhibition of the monocarboxylate transporter. Unfortunately, measurement of succinate in the large volume of medium in which the cells are kept is not comparable to the number of cells. 1 ml of buffer is used for 100, 000 cells, which is a huge volume for a small succinate concentration in comparison to the concentrated cell pellets. The large volume of the supernatant could dilute the metabolite and cover small changes in succinate making it more difficult to determine how much succinate is released. But after assessing the amount of metabolite retained within cells and comparing it to baseline levels makes it possible to accurately calculate percentages of the intracellular succinate that is oxidised within the cell pellet and the amount that is released out of the cell.

This comparison of changes in succinate release upon reoxygenation between the two different buffer systems showed intriguing data. In general, more succinate is released in the inhibitor containing buffer, which could be due to the much higher amount of the metabolite within the cell pellet during anoxia. In both systems, the MCT1 inhibitor was not added to the reoxygenation buffer, but the cells are washed, and the buffer was changed upon reoxygenation. While barely any succinate is released within 5 min of reoxygenation from cells incubated in Tyrode's buffer, even though a significant amount did accumulate during the 1 h of anoxia, and a bit more is released within the next 10 min, it is not more than ~500 pmol/100 000 cells succinate release. From cells that were anoxic in presence of the inhibitor, more than this is already released within 5 min and double the amount in the following 10 min. 15 min after reoxygenation, approximately the same amount of succinate is retained within the cells in both buffers under the condition that MCT1 was not inhibited upon reoxygenation.

Regarding release into the supernatant, cells in both buffer systems behave the same. The addition of AR-C141990 to the reoxygenation buffer decreases succinate efflux. Within 15 min of reoxygenation, less of the metabolite can be found in the supernatant than after 5

min in a buffer without this inhibitor. This can be discovered in both buffers, but due to the small amounts of succinate present in the Tyrode's only buffer system, these results are clearer in Tyrode's + MCT1 inhibition.

These observations might indicate that MCT1 inhibition decreases the release of succinate. In a next step, it would be interesting to analyse membrane potential and complex II activity in this cell model early upon reoxygenation, to add more insight into the fate of succinate.

It is possible that inhibiting MCT1 in the cardiomyocytes affects their metabolism or membrane potential and therefore influences metabolite efflux and/ or oxidation during reperfusion. Further and more detailed analysis into this is necessary. Earlier time points might give more insight as well, and genetic knockouts could elucidate how the monocarboxylate transporter is involved in metabolite release, especially succinate release, further.

The second application of the anoxic cell model, screening compounds and pathways with therapeutic potential, focused mainly on complex I and II inhibitors, because both of these complexes are involved in electron entry into the respiratory chain, which leads to a maximally reduced CoQ pool, and the possibility for ROS production at complex I via RET. Succinate is thought to be generated at complex II during ischaemia, which upon reperfusion pushes electrons into the ETC driving RET and therefore ROS production at complex I. Furthermore, succinate is transported out of the ischaemic cell and functions as a signalling molecule that activates immune cells. This makes the ETC complexes especially interesting as potential therapeutic targets in order to ameliorate succinate accumulation and with that ROS generation.

The inhibitor rotenone was used to help understand the role of complex I during anoxia and reoxygenation. Here, we could show a slight increase in succinate accumulation during anoxia, while before a slight reduction has been observed by Zhang and colleagues. Upon reoxygenation, the succinate within the cell pellet is reduced within 15 min and is not released into the supernatant, where no increase in succinate could be detected upon reperfusion. This indicates that succinate that accumulates is oxidised within the cell. It is not clear if the succinate stays within mitochondria and is oxidised at complex II, and utilised for the TCA metabolic pathway, or if it is rapidly transported into the cytosol. The fate of accumulated succinate during reperfusion in cells inhibited with rotenone has to be investigated further. Complex II inhibitors on the other hand enable the investigation of the source of succinate and its role in causing damage upon reoxygenation. The inhibitors TTFA, 3-NPA and disodium

malonate all target complex II. TTFA at a CoQ binding pocket, the other two at the substrate binding pocket. 3-NPA is irreversible, in contrast to malonate. Comparison of these inhibitors shows some differences in their effect on succinate accumulation and release during anoxia and reperfusion. 3-NPA caused increased succinate release into the supernatant, while TTFA treatment resulted in increased intracellular levels of the metabolite and lower levels in the extracellular medium. While neither disodium nor dimethyl malonate showed differences in intracellular succinate concentrations, DSM lead to less succinate release into the supernatant during anoxia and upon reoxygenation.

An important marker in order to investigate therapeutic potential of the inhibitors is cell death. Especially assessing LDH release 24 h after 1 h of anoxia followed by reoxygenation in the presence of the inhibitor. Interestingly, not all of the complex II inhibitors showed the same effect. 3-NPA could not rescue cell death, while TTFA but most prominently disodium malonate did rescue cell survival. TTFA is an irreversible complex II inhibitor and therefore not suitable for therapeutic approaches, but cell- penetrating/permeable malonate compounds has already been shown to be beneficial in murine IRI models (Chouchani et al., 2014a; Martin et al., 2019). Data gained from animal models in our lab indicate that DMM given only at reperfusion or DSM only during ischaemia did not protect against IR injury (unpublished data). This indicates potentially slow malonate release from DMM and poor cellular accumulation of DSM during anoxia.
A crucial future experiment involves investigating malonate release and uptake within cells and supernatant concentrations of this compound. These experiments can be performed by analysing cardiomyocytes that were treated with DSM or DMM during anoxia and reperfusion in a mass spectrometry approach analysing malonate concentrations.

The mitochondria-targeted compound MitoSulf ameliorated IRI as well, decreasing cell death upon reperfusion. These experiments prove that it is easy to screen therapeutic drugs in the cell system for their efficacy before utilising more complex and expensive *ex* or *in vivo* models. Further experiments into the exact mechanism of this protection are needed focusing on screening for the protective protein modification.

To summarise this chapter, the cardiomyocyte model can be utilised to investigate underlying IRI processes like the oxidation or efflux of succinate in detail, as well as proving the efficacy of therapeutic compounds. Here, I could reproduce the therapeutic effect of

malonate, precisely disodium malonate, after IRI on cardiac cells. We can now utilise this to understand how and when malonate ameliorates ischaemic damage and then improve the timing of when this compound has to be given to the organ or patient in order to be most beneficial. Therefore, more detailed analyses of succinate oxidation versus efflux are needed to understand if it is better to maintain succinate within the cell or release it, where it could subsequently act as a signalling molecule. Therefore, the fate of intracellular, not effluxed succinate has to be elucidated: is it used to induce RET and ROS at complex I or is it involved in other cellular pathways, possibly causing further damage. I have not measured ROS production in the presence or absence of the inhibitors and can therefore not reveal how and where the damage occurs that leads to cell death upon reperfusion. It is crucial to investigate in detail where ROS is produced and oxidative damage occurs and then further which cellular pathways are activated to rescue the cell or induce cell death respectively and which role succinate in particular plays in this. Thus, utilising a cell model allows detailed in-depth analysis of molecular pathways that are too complex to reliably be disclosed in *in vivo* models.

Chapter 6

mtDNA release after ischaemia reperfusion injury

6.1 Introduction

Our model of ischaemia reperfusion injury is that IR injury is initiated by a burst in ROS production at complex I upon reperfusion. This damages mitochondria first, before affecting other cellular compartments, thereby causing cell dysfunction and finally cell death. The various stages of damage can take place over several hours and days after IR injury. However, these processes are initiated by the changes that occur upon the first few minutes of reperfusion, or after reoxygenation in our cardiomyocyte model. From the moment ROS is produced upon reperfusion, until cell death, several pathways may contribute. Furthermore, in many of the cells that survive the injury, their function is still altered in various ways that contribute to the increased inflammation and tissue remodelling that have long-term impacts on recovery from IR injury.

In this chapter my particular interest is in how acute mitochondrial damage can activate inflammatory pathways. Acute damage to tissues can lead to the release of mtDAMPs that can lead to the activation of inflammation against the damaged tissue. The three main pathways that relate to the mitochondrial DAMP mtDNA have been described in detail the introduction. Briefly, cytokines are produced either after activation of Toll like receptors, or the assembly of an inflammasome complex, or via interferon signalling. Recent studies have implicated the release of mitochondrial DNA from mitochondria into the cytosol in activating cellular immune responses (Gao et al., 2019; Kanneganti et al., 2015; Mills et al., 2017; Vringer and Tait, 2019). Some innate immune response pathways are sensitive to the release of mtDNA, for example the cytosolic dsDNA sensor cGAS, that activates the ER-localised protein STING and results in IFNβ production, has gained interest recently (Liu et al., 2016a; Maekawa et al., 2019). It is possible that different pathways are activated dependent on the type of released mtDNA (Figure 6.1): oxidised DNA has been shown to be involved in NLRP3 inflammasome activation; unmethylated, single stranded CpG motifs, which are primarily found on bacterial and mitochondrial DNA, can be recognised by the TLR9 receptor; and double stranded DNA is recognised by cytosolic cGAS, which activates an inflammatory cascade via STING. All of this implies that released DNA could sensitively modulate what type of response is activated upon mitochondrial dysfunction and damage. This furthermore could have impact on the activation of the immune response upon IR injury in patients that underwent organ transplantation. The role of free mtDNA in ischaemia reperfusion injury has never been investigated before, but increased IL-6 levels upon TLR9 stimulation have been shown (Oka et al., 2012; Ueda et al., 2019). Additionally, cyclosporin A has been shown to protect against

IR injury after organ transplantation, but as elucidated in the general introduction this might be due to a number of effects cyclosporin A has on the innate and adaptive immune response (Hausenloy et al., 2012; Nakagawa et al., 2005; Nighoghossian et al., 2016).

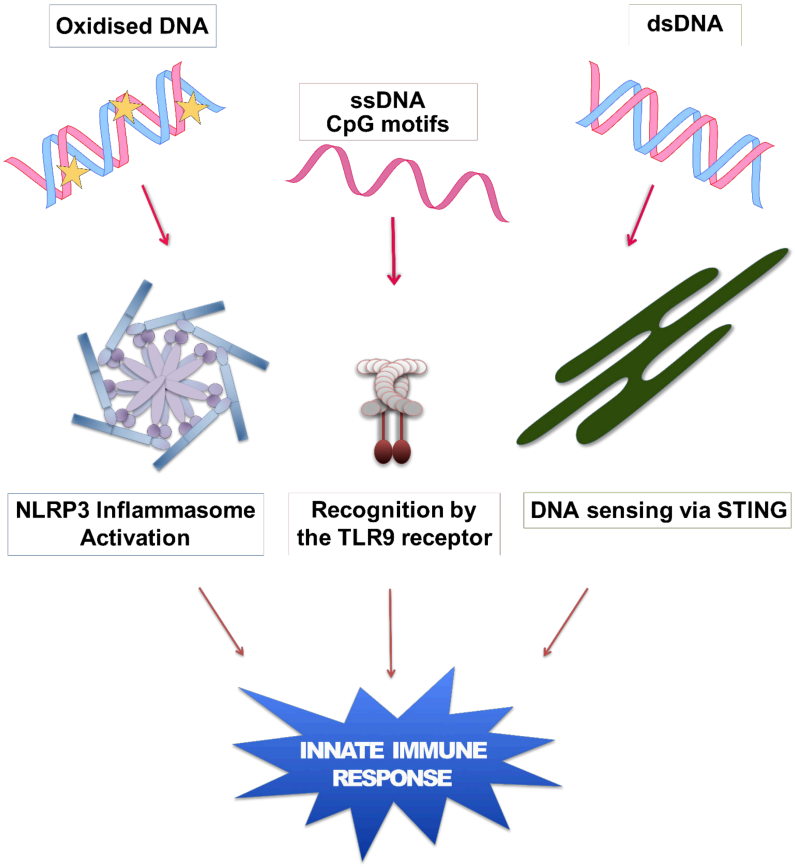

Figure 6.1: DNA can activate innate immune pathways. Schematic model of the involvement of DNA in activating the immune response. DNA has been known to be able to activate different innate immune response pathways. Oxidised DNA molecules can cause NLRP3 inflammasome activation, while CpG motifs on single stranded DNA are recognised by and activate the toll like receptor 9 (TLR9). Double stranded DNA molecules within the cytosol can activate the ER- linked cGAS/STING pathway. All of these pathways activate different transcription factors, which all result in an immune response cascade that results in the production of cytokines and other immune signalling molecules.

So far, these pathways have mainly been investigated in cell models (Liu et al., 2016a; McArthur et al., 2018; Riley et al., 2018). mtDAMPs such as mtDNA are known to be released

upon mitochondrial damage in many diseases, as well as during aging and exercise (Pinti et al., 2014; Stawski et al., 2017). Despite the large amount of data on the implication of mtDNA in inflammation in various diseases (Gan et al., 2015; Nakahira et al., 2013; Tsuji et al., 2016; Wang et al., 2011; Wenceslau et al., 2014), the role of mtDNA release in IR injury is unclear. It may be that the release of mtDNA may contribute to an inflammatory response in patients following IR injury. Therapies may then be developed to shut down the damaging aspects of the adaptive immune response in patients after IRI. However, which of these pathways - TLR9, NLRP3 or cGAS/STING – could be activated upon IRI is not known.
I am therefore interested in investigating if the mtDAMP is released upon IRI and via which mechanism this release occurs.

One possible way of release of mtDNA after oxidative damage is following induction of the permeability transition pore (MPTP). Other possible DNA release mechanisms have been described as well such as herniation (Kim et al., 2019; McArthur et al., 2018; Riley et al., 2018). Related to this, is the possibility that mtDNA is oxidised upon reperfusion and then the oxidised mtDNA is released from the mitochondria to the cytosol, where it initiates the activation of one or more of the innate immune pathways depicted in Figure 6.2.

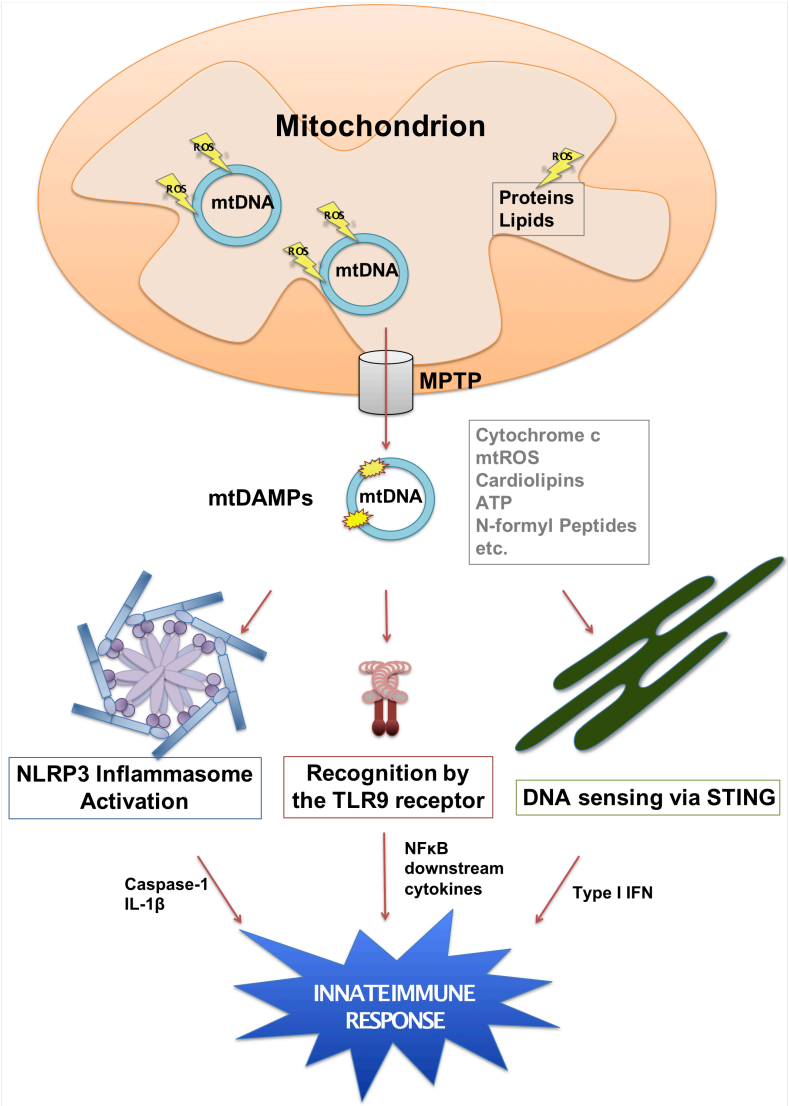

Figure 6.2: Schematic model of mtDAMP release upon ischaemia reperfusion injury and the role of mtDNA in activating the innate immune response. Schematic hypothesis of the role of mtDNA as mtDAMP in activating the innate immune response. Upon ischaemia reperfusion injury, reverse electron transport causes a burst in ROS, which damages mitochondrial content like lipids, proteins and mtDNA. It is possible that the mitochondrial permeability transition pore opens and releases mitochondrial damage associated molecular patterns into the cytosol. One of them is mtDNA, which in the cytosol could potentially be involved in activating immune pathways. As described earlier, three pathways are known to be activated by DNA molecules: the NLRP3 inflammasome that leads to caspase-1 activation and IL1β production; the toll like receptor 9, located primarily at endosomes, activating the NfκB response; or the ER- linked cGAS/STING pathway leading to interferon type 1 production.

The cardiomyocyte model of IR injury that I have developed earlier offers an opportunity to investigate this process in detail. I will also investigate a range of *ex vivo* and *in vivo* models which are already in place.

6.2 Aim

Here, I aimed to investigate the mechanism and the extent of mtDNA release into the cytosol and form there into the circulation. Then, I was also keen to explore the role of circulating mtDNA in ischaemia reperfusion injury using various models for organ transplantation. I focused on four main aims: 1) Is mtDNA released upon anoxia and reoxygenation *in vitro*; 2) is the release of mtDNA into the cytosol occurring in response to the permeability transition pore; 3) is this release of mtDNA followed by an activation of the inflammatory response; 4) is mtDNA then released from the cell into the circulation. In order to determine these, different experimental models have been utilised: an *in vitro* model of anoxic primary adult murine cardiomyocytes, and different *ex* and *in vivo* setups for mouse IRI disease models.

6.3 Results

6.3.1 Time course of mtDNA release upon anoxia and reoxygenation in primary adult cardiomyocytes

The release of mtDNA from mitochondria into the cytosol has been reported in various cell models (Kim et al., 2019; McArthur et al., 2018; Riley et al., 2018). To see whether mtDNA is released from mitochondria into the cytosol upon ischaemia reperfusion injury, I first used the primary adult cardiac myocytes model utilising true anoxia and inhibition of the monocarboxylate transporter 1.

6.3.1.1 Time course of mtDNA release into the cytosol

Cardiomyocytes were subjected to 60 min of anoxia in Tyrode's buffer supplemented with MCT1 inhibitor AR-C141990. After washing, the incubation medium was replaced with

culture medium and the cells were incubated under normoxic conditions for 15 min, 2 h or 24 h. Cells were then scraped from the plate, transferred to 1.5 mL Eppendorf tubes and pelleted by centrifugation for 1 min at 300 x g. The pellets were incubated with digitonin (30 µg/mL) for 10 min at room temperature before the cytosolic fraction was extracted in several centrifugation steps as described in the methods. Total DNA was isolated from 200 µL of this cytosolic fraction using a QIAmp DNA Blood Mini Kit (QIAGEN, UK) and 1 ng DNA analysed via droplet digital PCR (ddPCR), a novel PCR approach utilising the distribution of single DNA molecules into oil droplets allowing accurate quantification of minimal amounts of DNA amplicons. To do this, the mitochondrial gene ND5 and the nuclear gene β-actin were amplified in the presence of primer-specific probes and the amount of DNA quantified on the basis of droplets positive for the respective probes. DNA quantification was performed using the BIORAD Quantilife programme. The results depicted in Figure 6.3 present ddPCR results as mtDNA to nuclear (nDNA) ratio.

First of all, in control cell samples that were not exposed to anoxia and reoxygenation, there is a baseline amount of both mt and nDNA detectable in the cytosol. This is expected and is likely to result from either background levels in the cytosol or release due to damage to mitochondria and nuclei upon isolation. The mtDNA/nDNA ratio increases 15 min after reoxygenation and continues to increase significantly until 2 h after the onset of reoxygenation. However, 24 h after reoxygenation, a striking reduction in mtDNA/nDNA ratios is detectable compared to that after reoxygenation.

Together, these data indicate that mtDNA might be released from mitochondria into the cytosol upon anoxia reoxygenation injury in cells.

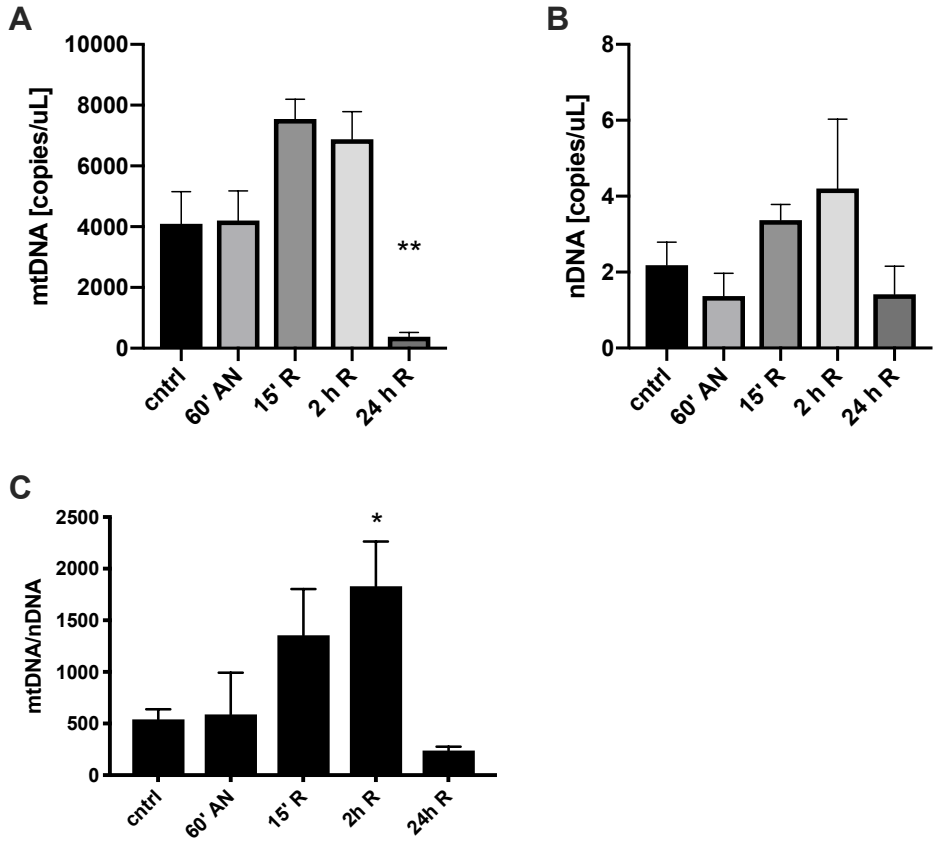

Figure 6.3: mtDNA is released into the cardiomyocyte cytosol upon anoxia reoxygenation injury Adult primary cardiomyocytes were isolated and anoxia and reoxygenation injury induced as previously described. Cells underwent 60 min of anoxia, before reperfusion was induced and samples were retrieved at different time points. A) Cytosolic fractions were retrieved after digitonin treatment as described in the method. DNA was purified from these fractions and the mitochondrial gene ND5 as well as the nuclear gene β- actin amplified via ddPCR. DNA was quantified in copies per μL using the BIORAD Quantilife software. Results are presented as mtDNA copies/μL (A), nDNA copies/µL (B) or mtDNA to nDNA ratios. n= 4-5 biological replicates, data are mean ± S.E.M. Statistical analysis was performed via unpaired student's t-test. *P< 0.05, **P<0.01.

6.3.1.2 Time course of mtDNA release into the extracellular matrix

I was intrigued by the fact that cytosolic mtDNA/nDNA ratios decrease after 24 h of reoxygenation. In particular, I was interested in the finding from other labs that an elevation in circulating free mtDNA has been found in patient studies following IR injury (Harrington et al., 2019; Hu et al., 2018; Nakahira et al., 2013). Thus, I next wanted to investigate if mtDNA is released from the cytosol into the extracellular environment of cardiomyocytes that

underwent anoxia and reoxygenation. Furthermore, I wanted to analyse if the decrease in cytosolic mtDNA after 2 h reoxygenation was due in part to mtDNA release from the cell, or whether it could be accounted for by degradation of this mtDNA within the cell.

To do this, primary adult cardiomyocytes were subjected to 60 min of anoxia in Tyrode's buffer + MCT1 inhibitor AR-C141990, before being reoxygenated in culture medium. The cell medium was then collected at different time points after reoxygenation and analysed for DNA release via ddPCR as described before (Figure 6.5 5A-D). In parallel, I also assessed whether anoxia reoxygenation injury led to cell death, measured via LDH release (Figure 6.5 E). Interestingly, as shown in Figure 6.5 A, the mtDNA/nDNA ratio shows a release of mtDNA into the cytosol after 18 h of reoxygenation. Investigating mtDNA copy number in comparison to nDNA copy number (Figure 6.5 B) indicates a continual increase in released mtDNA, notably 18 h after reoxygenation, followed by an increase in nDNA 24 h after reoxygenation which causes the decrease in the ratio seen in Figure 6.5 A. The rise in mtDNA release occurs in parallel with increased LDH release, which is also significantly decreased after 18 h of reoxygenation (Figure 6.5 E). Therefore, I conclude, that mtDNA is released into the extracellular environment from cells that underwent anoxia-reoxygenation, but that this release does not occur immediately upon reoxygenation, but more than 12 h later.

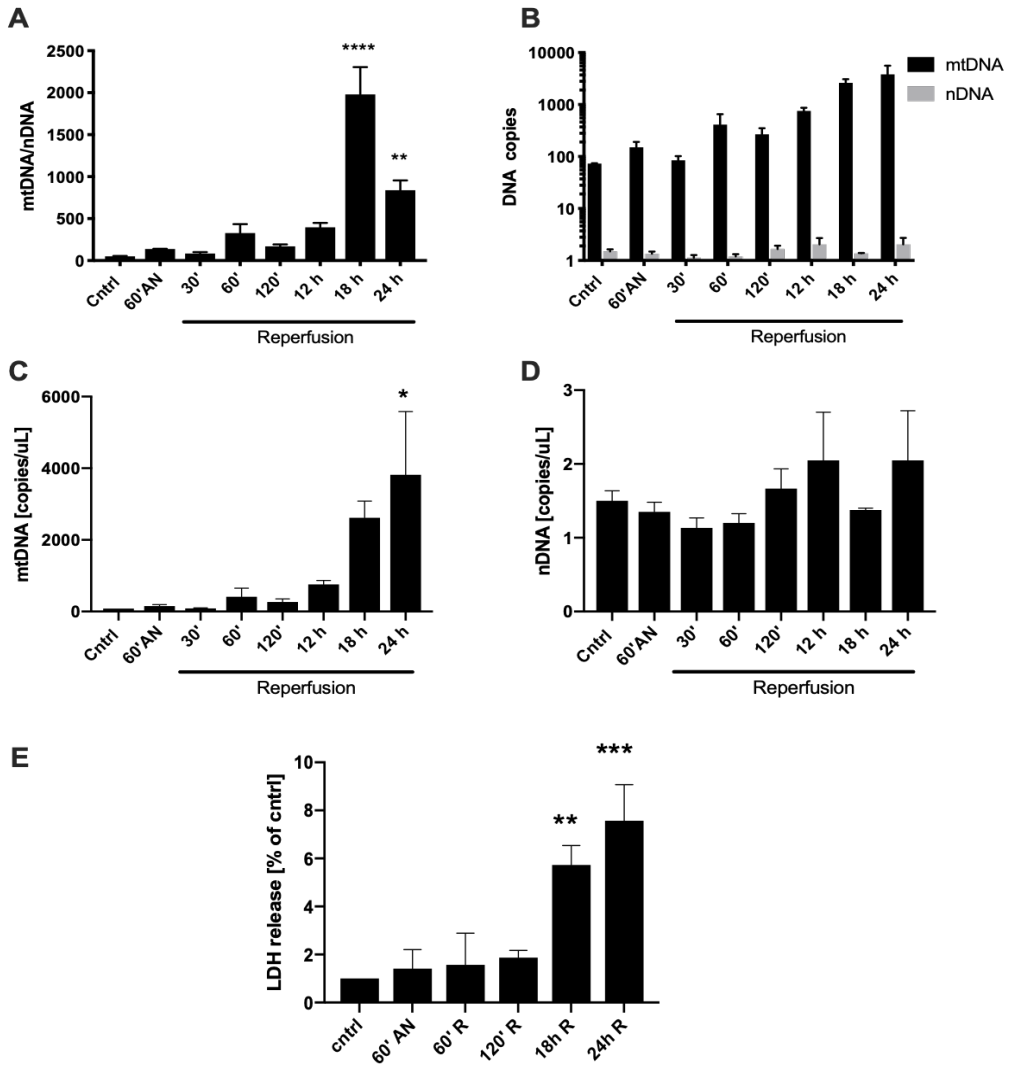

Figure 6.4: mtDNA is released from cardiomyocytes upon anoxia reoxygenation injury. Supernatants from cardiomyocytes that underwent 60 min of anoxia and different timepoints of reperfusion were analysed for mtDNA release (A, B) and for cell death (C). (A, B) DNA was extracted from cellular supernatants and analysed via ddPCR (ND5 as mitochondrial and β- actin as nuclear gene) as described in detail in the methods. DNA was quantified in copies per μL using the BIORAD Quantilife software. (A) data are presented as ratio of mtDNA to nDNA or (B) copies of DNA per μL, (C) mtDNA [copies/μL], (D) nDNA [copies/μL]. (E) Cell death was evaluated by measuring the amount of LDH protein released into the cellular supernatant via absorbance at 492 nm. Elevated LDH levels indicate increased cell death. Results are presented relative to a positive control of cardiomyocytes lysed in 1% Triton. n= 4-7 biological replicates, data are mean ± S.E.M. Statistical analysis was performed via one-way ANOVA. *P< 0.05, **P<0.01, ***P<0.0005, ****P<0.0001.

6.3.2 Inhibition of mtDNA release in primary adult cardiomyocytes upon anoxia and reoxygenation

After demonstrating that mtDNA is released from mitochondria into the cytosol upon anoxia and reoxygenation in primary cardiomyocytes, I next wanted to investigate how this release occurred. As a major factor in mitochondrial damage in IR injury is the induction of the MPTP (Hausenloy et al., 2012; Ong et al., 2015), which can lead to permeabilisation of the mitochondrial inner membrane, I first assessed if the release of mtDNA into the cytosol was associated with induction of the MPTP.

6.3.2.1 Release of mt DNA is associated with induction of the MPTP

To see if this mtDNA release occurred upon induction of the MPTP, I used Cyclosporin A (CsA), which is well established to inhibit induction of the MPTP by binding to the protein Cyclophilin D. I therefore treated primary cardiomyocytes with CsA at 200 nM, a concentration which is known to prevent the MPTP (Karch and Molkentin, 2014), during the 60 min of anoxia and upon reoxygenation. As shown in Figure 6.7 A, mtDNA release is decreased by CsA. However, increased mtDNA can be found in cells 24 h after reoxygenation if MPTP opening was inhibited. This may be because the mtDNA being released into the cell 24 h after reoxygenation is retained in the cell when MPTP opening is interrupted, rather than being released into the cell incubation medium upon cell death (Figure 6.7 B). This finding is consistent with decreased LDH release 24 h after reoxygenation for cells treated with CsA (Figure 6.7 D). Furthermore, qPCR analysis on DNA extracted from whole cell lysates showed increased damage to mtDNA 24 h after reoxygenation in control, but not in CsA treated cells (Figure 6.7 C).

In summary, inhibition of MPTP opening with Cyclosporin A decreased mtDNA release into the cytosol from mitochondria upon reoxygenation following anoxia. These findings suggest that induction of the MPTP facilitates the release of mtDNA. In parallel, blocking MPTP opening ameliorates cell death and also decreases the overall damage to mtDNA.

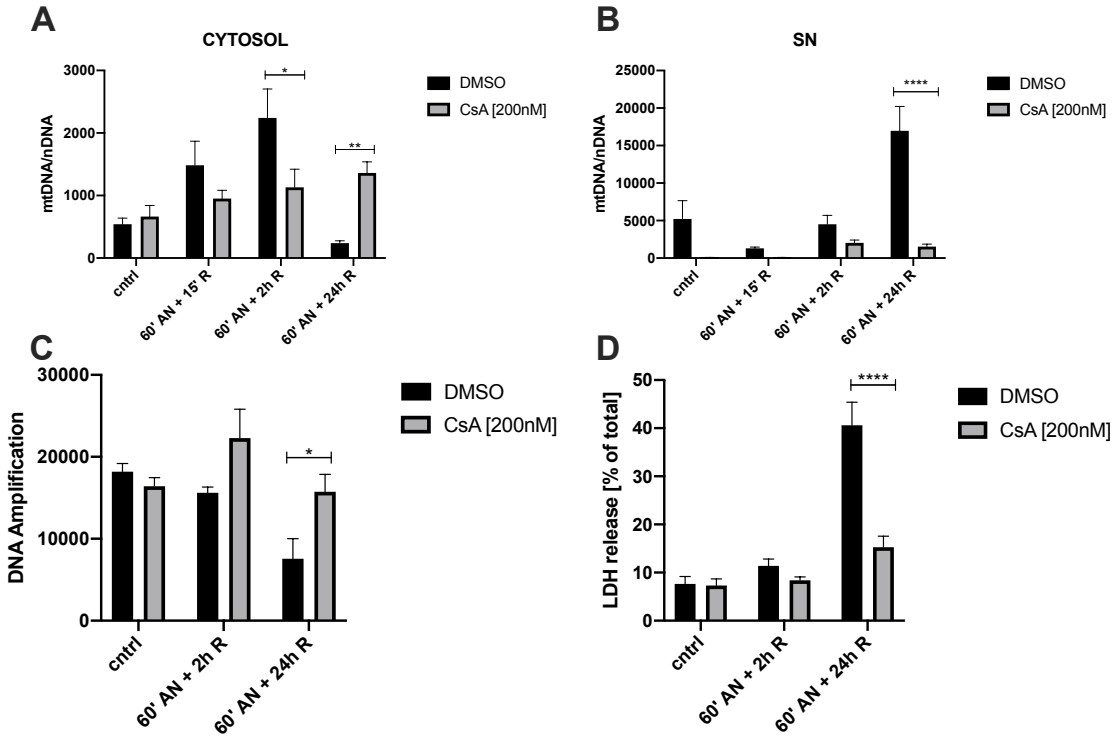

Figure 6.5: Cyclosporin A inhibits mtDNA release and ameliorates anoxia reoxygenation injury. Cardiomyocytes were treated with either DMSO or Cyclosporin A (CsA) at 200 mM throughout the whole experiment. Cells were anoxic for 60 min before being reperfused for different time points as described before. DNA was isolated from (A) cytosolic extracts, (B) extracellular supernatant or (C) whole cell lysates. (A, B) released DNA was quantified via ddPCR as described before and the amount of released DNA from CsA treated cells compared to that from DMSO treated ones. Data are presented as ratio of mtDNA to nDNA. (C) whole cell DNA was extracted form DMSO and CsA treated control or anoxia reperfused cells and mtDNA damage assessed via qPCR as described before. The less amplification was possible, the more damage occurred. (D) Anoxia reoxygenation injury in form of cell death was evaluated by measuring the amount of LDH protein released into the cellular supernatant via absorbance at 492 nm. Elevated LDH levels indicate increased cell death. Results are presented relative to a positive control of cardiomyocytes lysed in 1% Triton. N= 6- 10 biological replicates, data are mean ± S.E.M. Statistical analysis was performed via two-way ANOVA. *P< 0.05, **P<0.01, ****P<0.0001.

6.3.3 Activation of the innate immune response in primary adult cardiomyocytes upon anoxia and reoxygenation

After showing that mtDNA is released from mitochondria in to the cytosol of cardiomyocytes, I next wanted to investigate whether the mtDNA activated different innate immune pathways.

6.3.3.1 Activation of an immune response

As mtDNA is released by cardiomyocytes, I first investigated if the supernatant of cardiomyocytes that underwent 60 min of anoxia followed by reoxidation, could activate an immune response. To do this, macrophage activation assays were performed. RAW264.7 murine macrophages were cultured with 1:10 in culture medium diluted supernatant of the anoxic and reoxygenated cardiomyocytes. After 24 h, cell activation was measured as nitrite formation from nitric oxide, using the Griess assay. As shown in Figure 6.8, the supernatant of untreated control and anoxic or short-time reoxygenated cardiomyocytes did not activate macrophages. An increase in macrophage activity is detectable after incubation with supernatant from 30 min to 2 h reoxygenated cardiomyocytes with a major increase after 18 h of reoxygenation and less increase after 24 h. This indicates that the innate immune response can be activated by DAMPs released from injured cardiomyocytes. The increase in macrophage activation by cardiomyocyte supernatant after 30 min of reoxygenation occurs before mtDNA release into the supernatant was detectable, suggesting that other, earlier activators exist in the supernatant other than mtDNA. The large rise in macrophage activation upon incubation with supernatant from cardiomyocytes after 18 h reoxygenation fits the time course of cell death, as well as mtDNA release observed before.

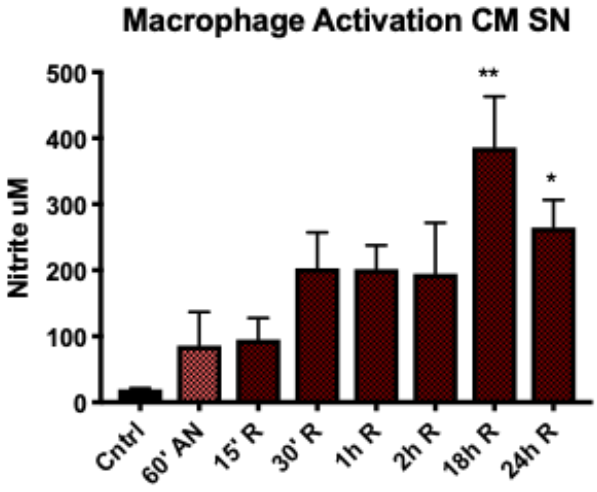

Figure 6.6: Supernatant from anoxic and reoxygenated cardiomyocytes activates macrophages. Cardiomyocytes were subjected to anoxia and reoxygenation as described before. The supernatant of these cells was collected at different time points. Macrophage activation was assessed via the Griess assay. Therefore, murine RAW264.7 were cultured and incubated in 1:10 diluted cardiomyocyte supernatant. After addition of Griess reagent to RAW264.7 supernatant, the formation of nitrite from nitric oxide was measured in a colorimetric change via absorbance at 540 nm. Results were compared to a nitrite standard curve in the μM range. Increased nitrite indicates elevated macrophage activity. N= 4- 7 biological replicates, data are mean ± S.E.M. Statistical analysis was performed via one-way ANOVA. *P< 0.05, **P<0.01.

6.3.3.2 Activation of the Toll-like receptor TLR9

Next, the role of DAMPs released after anoxia reoxygenation injury on activating the TLR9 receptor was investigated. The receptor is activated by unmethylated CpG motifs and could therefore be activated by mtDNA that enters the cytosol. I utilised the HEK-BLUE TLR9 cell line which transiently express plasma membrane-localised TLR9 as well as a phosphatase that is expressed under a promotor that will be activated by NfκB stimulation. Therefore, activation of TLR9, which leads to NfκB stimulation, will cause expression of this phosphatase, whose activity can be measured.

HEK- BLUE TLR9 cells were incubated with 1:10 diluted cardiomyocyte supernatant for 24 h. The supernatant was retrieved from untreated cardiomyocytes or those that underwent anoxia for 60 min and different times of reoxygenation. As a positive control, HEK-BLUE TLR9 cells were incubated with an oligonucleotide known to activate TLR9 (2006) and also an antagonistic oligonucleotide (Figure 6.9). Incubation with activator oligonucleotide 2006 caused a significant increase in phosphatase activity. This could be reduced by approximately 50% in presence of an antagonist oligonucleotide (both p<0.0001 via one- way ANOVA).

Activation of TLR9 is much lower in samples incubated with cardiomyocyte supernatant in all conditions and at all time points following reoxygenation in comparison to the control compound. A significant increase, although much smaller than the positive control, is detectable after incubation with supernatant of cardiomyocytes after 18 h or more reperfusion time (one- way ANOVA, 18h p= 0.0011 and 24 h p= 0.0003). This indicates that the molecules released late after reperfusion from anoxic and reoxygenated cardiomyocytes can activate the innate immune pathway via TLR9 activation, but just to a minor amount.

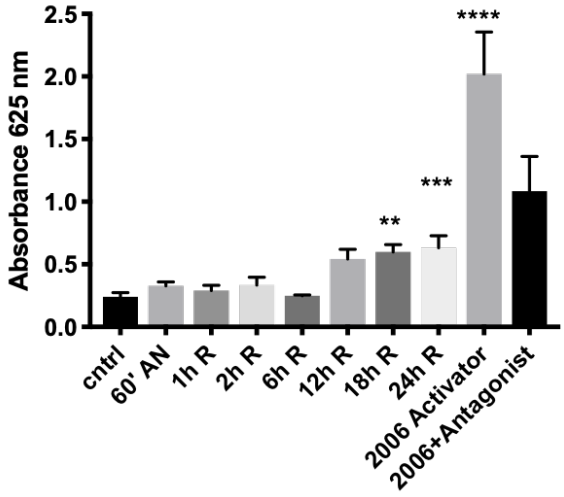

Figure 6.7: Supernatant from anoxic and reoxygenated cardiomyocytes activates toll like receptor 9. Cardiomyocytes were subjected to anoxia and reoxygenation as described before. The supernatant of these cells was collected at different time points. TLR9 activation was assessed using the InvivoGen HEK-BLUE TLR9 cell line, that expresses TLR9. Incubated in a reaction medium, TLR9 activation will cause a colorimetric change that can be assessed by measuring changes in absorbance at 625 nm. Therefore, InvivoGen TLR9 HEK 293 cells were cultured and incubated with 1:10 diluted cardiomyocyte supernatant. After addition of the reaction medium, TLR9 activation was measured. Results were compared to cells treated with the TLR9 activator oligonucleotide number 2006 as well as 2006 + an antagonist oligonucleotide (both at 100 ug/mL). Increased absorbance indicates elevated TLR9 activation. n= 2- 6 biological replicates, data are mean ± S.E.M, statistical analysis was performed via one-way ANOVA as specified in the text. *P < 0.05, **P < 0.01, ***P < 0.001, ****P < 0.0001.

6.3.3.3 Activation of the cGAS/STING pathway and INF type 1 signalling

I next investigated if the cytosolic dsDNA-sensing cGAS/STING pathway could contribute to response to anoxia reoxygenation injury and mtDNA release in cardiomyocytes. To do this I assessed the production of the type 1 interferonβ (IFNβ), which is increased upon stimulation

of cGAS. Cardiomyocytes were subjected to 60 min of anoxia followed by reoxygenation and cytosolic and cell medium fractions were retrieved as described before at various time points.

An early product of the activation of this pathway is 2'3'cGAMP, which is generated by cGAS after it senses dsDNA. Its levels were assessed via ELISA in cytosolic and cell medium samples (Figure 6.10 C). After reoxygenation, there was a significant increase within the cytosol. Especially after 2 h of reoxygenation, cardiomyocytes show elevated 2'3'cGAMP levels. These decreased again upon 24 h of reoxygenation. There was no 2'3'cGAMP release into the cell medium.

The levels of IFNβ within cardiomyocyte cytosol increased following anoxia and 2 h of reoxygenation, assessed by ELISA (Figure 6.10 A). The levels of IFNβ then decreased after 24 h of reoxygenation, while IFNβ concentrations in the cell medium increased with time (Figure 6.10 B). Elevated IFNβ concentrations were found in the medium 18 h after reoxygenation and increases further after 24 h of reperfusion.

These data indicate that the cGAS/STING dsDNA-sensing pathway in the cytosol is activated upon anoxia and reoxygenation in a time course consistent with the release of mtDNA from mitochondria into the cytosol. This leads to the production of IFNβ within the cytosol and release into the surrounding supernatant, until cell death occurs, as measured via LDH release.

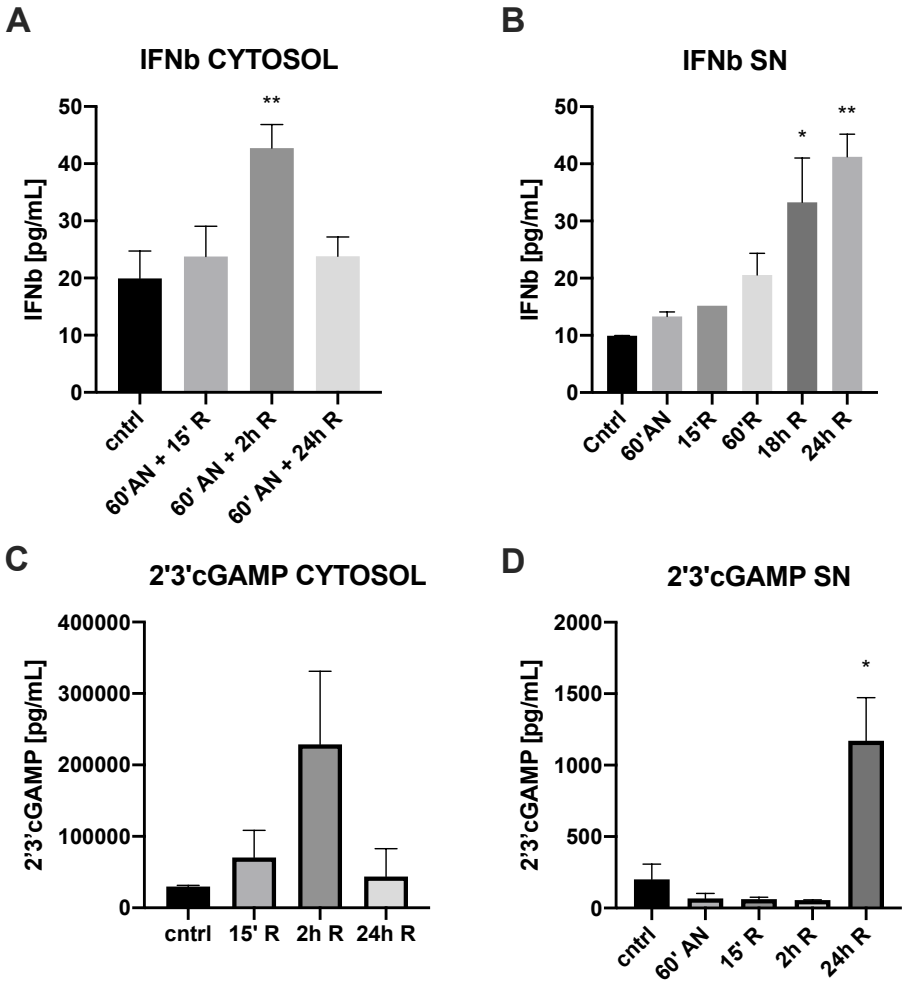

Figure 6.8: INF type 1 signalling via the cGAS/STING pathways is activated upon mtDNA release after anoxia and reoxygenation in cardiomyocytes. Cardiomyocytes were subjected to anoxia and reoxygenation as described before. Cells were anoxic for 60 min before being reperfused for several time points as described before. (A, C) Cytosolic fractions were extracted after digitonin treatment as described in detail in the methods. (B, C) Supernatant samples were retrieved from samples at different time points after reperfusion. (A, B) IFNβ, a type 1 interferon, was measured using enzyme-linked immunosorbent assays (ELISA) on cytosolic extract (A) or supernatant samples (B). Concentrations were determined in pg/mL using an IFNβ standard curve. (C) Concentrations of the cGAS product 2'3'cGAMP were determined in cytosolic and supernatant fractions via ELISA and quantified using a standard curve in pg/mL. n= 4- 7 biological replicates, data are mean ± S.E.M, statistical analysis was performed via student's t-test. *P < 0.05, **P < 0.01.

6.3.3.4 Pharmacological inhibition of the cGAS/STING pathway

I next wanted to see if the cGAS pathway activation was due to mtDNA release from mitochondria, or if the mtDNA release occurred as a downstream consequence of the activation of this pathway by other factors. To assess this, primary adult cardiomyocytes were incubated with a small molecule inhibitor of the cGAS pathway (Ru.521, InvivoGen) during anoxia and upon reoxygenation. Cytosolic fractions and cell incubation medium samples were retrieved at different time points following reoxygenation after 60 min of anoxia and mtDNA release, LDH release and IFNβ production was determined.

As depicted in Figure 6.11 A, mtDNA release into the cytosol was lower in cells that were treated with Ru.521 early after reoxygenation, significant after 2h of reoxygenation, but then largely increased after 24 h, perhaps suggesting a slight delay in release. The mtDNA/nDNA ratios detected in the cell medium show no significant release of mtDNA into the extracellular medium, indicating that 24 h after reperfusion, released mtDNA is maintained within the cytosol (Figure 6.11 B). This may imply that there was less cell death in cells treated with the cGAS inhibitor (Figure 6.11 C). Furthermore, IFNβ production is decreased within cardiomyocytes treated with the cGAS inhibitor Ru.521 at all time points following reoxygenation. This was also the case for cells treated with Cyclosporin A, which ameliorated mtDNA release into the cytosol, as described previously in Figure 6.7. These data show, mtDNA release occurs upstream of cGAS activation and furthermore, that IFNβ production and cell death upon anoxia and reoxygenation in primary adult cardiomyocytes are dependent on cGAS activity. IFNβ production can be ameliorated either by inhibiting cGAS or mtDNA release via MPTP opening.

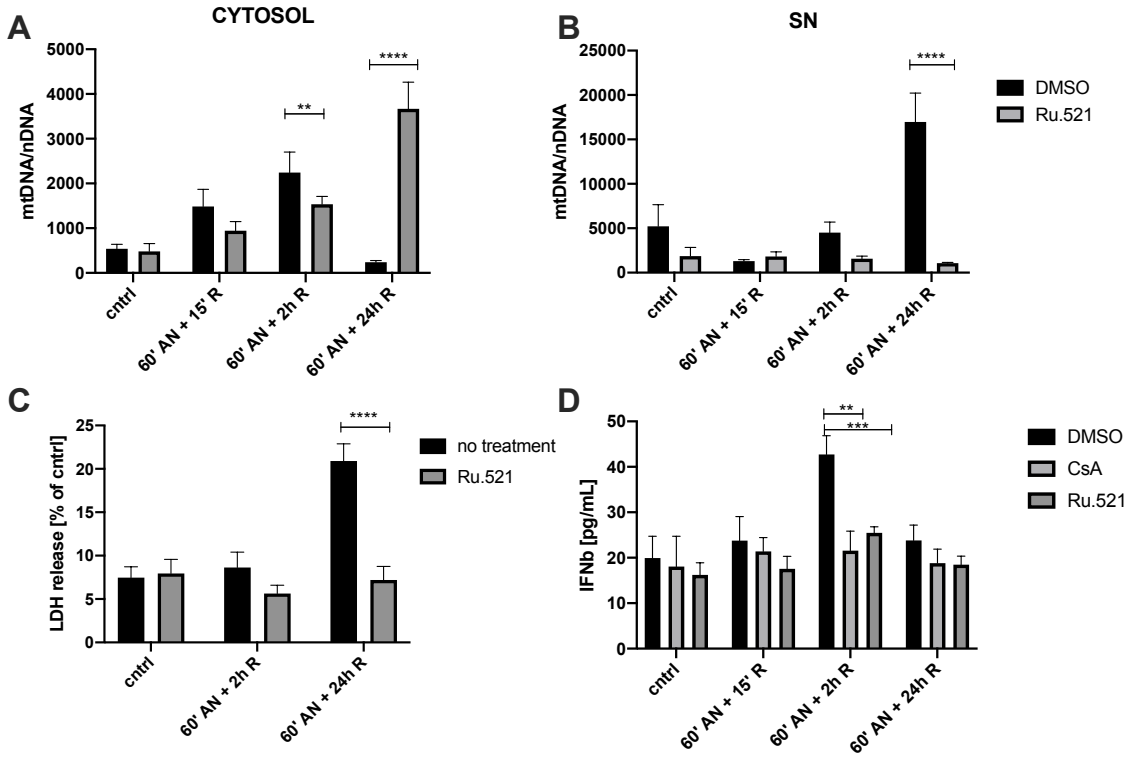

Figure 6.9: Inhibition of INF type 1 signalling via the cGAS/STING pathways ameliorates anoxia and reoxygenation injury in cardiomyocytes. Cardiomyocytes were treated with either DMSO (200 nM) or the cGAS inhibitor Ru.521 from InvivoGen at 2 ug/mL throughout the whole experiment. Cells were anoxic for 60 min before being reperfused for different time points as described before. (A, D) Cytosolic fractions were extracted after digitonin treatment as described in detail in the methods. (B, C) Supernatant samples were retrieved from samples at different time points after reperfusion. DNA was isolated from (A) cytosolic extracts or (B) extracellular supernatant and released mitochondrial and nuclear DNA quantified via ddPCR as described before/in the methods. (C) Anoxia reoxygenation injury in form of cell death was evaluated by measuring the amount of LDH protein released into the cellular supernatant via absorbance at 492 nm. Elevated LDH levels indicate increased cell death. Results are presented relative to a positive control of cardiomyocytes lysed in 1% Triton. (D) IFNβ concentrations were measured using enzyme-linked immunosorbent assays (ELISA) on cytosolic sample extract from cells treated with DMSO, Ru.521 or CsA (200 nM). IFNβ was quantified in pg/mL using a standard curve. n= 5 biological replicates, data are mean ± S.E.M, statistical analysis was performed via two-way ANOVA. **P < 0.01, ****P<0.0001.

To summarise, mtDNA is released from adult primary cardiomyocytes upon anoxia and reoxygenation. The DNA is thereby released into the cytosol first, where it remains until 18-24 h later. At this time, mtDNA release into the extracellular medium can be detected in parallel to plasma membrane rupture, investigated in form of LDH release. Inhibition of the MPTP upon reoxygenation could block mtDNA release from mitochondria.

Within the cytosol, mtDNA stimulates innate immune responses. notably the cGAS/STING pathway Altogether these findings make mtDNA an interesting immune activator molecule.

6.3.4 mtDNA release in mouse models of ischaemia reperfusion injury

It is important to understand if these findings in cells extrapolate to more complex disease models. I therefore next used different *ex vivo* and *in vivo* mouse models of IR injury to assess whether there was also mtDNA release during IR injury.

6.3.4.1 mtDNA release from the murine heart in a Langendorff system

I analysed mtDNA release from mouse hearts that were equilibrated (EQ) and then were subjected to 20 min of global ischaemia before being reperfused for up to 6 min while perfusate was collected. These Langendorff procedures were performed by Dr. Dunja Aksentijevic at Queen Mary University, London. I extracted DNA from the perfusates and analysed it via ddPCR as described before. Figure 6.12 A presents DNA levels in the perfusate as mtDNA/nDNA ratios. The ratios are highly variable and are already high at the end of the equilibration phase (EQ). They remain similar 1 min after reperfusion was initiated, but there is a trend to decrease after 6 min of reperfusion albeit not significantly (2-way ANOVA). MtDNA copies (Figure 6.12 B) within the perfusate increase slightly upon reperfusion after 1 min and decrease in the following minutes. This suggests that mtDNA is released from the ischaemic mouse heart upon reperfusion, even during the equilibration period. Initially, more mtDNA is released and the circulating DNA levels decrease then with prolonged reperfusion for up to 6 min. Unfortunately, so far, we only had access to early reperfusion time points and this preliminary experiment will be extended with longer reperfusion times in the future. However, these results show, that a Langendorff system is suitable to assess mtDNA release *ex vivo*.

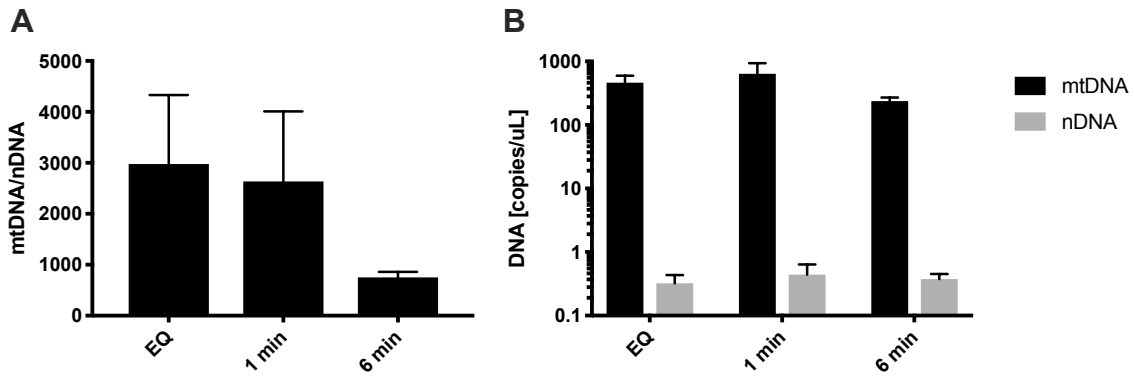

Figure 6.10: mtDNA is released from ex vivo murine hearts after ischaemia reperfusion injury Bl6 wild type mice underwent global ischaemia reperfusion injury ex vivo in a Langendorff perfusion model. After a 20 min equilibration period (EQ), hearts were subjected to 20 min ischaemia before being reperfused for 6 min. Perfusate samples were collected during reperfusion. (A, B) DNA was extracted from perfusate samples and analysed via ddPCR (ND5 as mitochondrial and β- actin as nuclear gene) as described in detail in the methods. DNA was quantified using the BIORAD Quantilife software. (A) data are presented as ratio of mtDNA to nDNA or (B) copies of DNA per μL. n= 4 biological replicates, data are mean ± S.E.M., statistical analysis via 2-way ANOVA showed no significant results, p=0.1347.

6.3.5 mtDNA release in *in vivo* mouse models of ischaemia reperfusion injury

I next investigated if mtDNA was released during IRI *in vivo* using mouse models of heart and kidney IR injury

6.3.5.1 mtDNA release and damage after heterotopic heart transplantation in mice

The murine heterotopic heart transplant model has been described in chapter 2 and 3. As depicted in Figure 6.13 A, donor mice were anaesthetised and their hearts retrieved and either transplanted immediately (0´WI) subjected to additional warm ischaemia (12´WI) or treated with dimethyl malonate (DMM) to block succinate accumulation or acetoxymethyl succinate (AMS) to induce succinate accumulation. The hearts were then transplanted into the abdomen of a recipient mouse which recovered for 24 h before abdominal blood serum samples were collected from the carcass after exsanguination. DNA was extracted, analysed and quantified via ddPCR as described before (Figure 6.13 B) 12 min of additional warm ischaemia (12´WI)

induced a rise in mtDNA/nDNA ratios, while DMM treatment ameliorated this. Treatment with AMS on the other resulted in elevated mtDNA/nDNA ratios. MtDNA copies showed a similar trend to the ratios (Figure 6.13 C). DNA damage analysis via qPCR of these samples (Figure 6.13 D) showed lowest DNA amplification and therefore most damage in samples after 12 min of additional ischaemia. DMM treatment resulted in elevated DNA amplification indicating less DNA damage. Finally, Figure 6.13 E shows serum troponin levels, a heart damage marker (as published in Martin et al., 2019. These levels show increased damage upon 12 min of additional ischaemia as well as AMS treatment, underlining the results obtained from analysis of circulating mtDNA.

Altogether this shows that mtDNA is released upon cardiac IRI *in vivo* and that this can be ameliorated via malonate treatment or elevated by increased succinate. Importantly, mtDNA levels in the circulation correlate with the damage marker troponin.

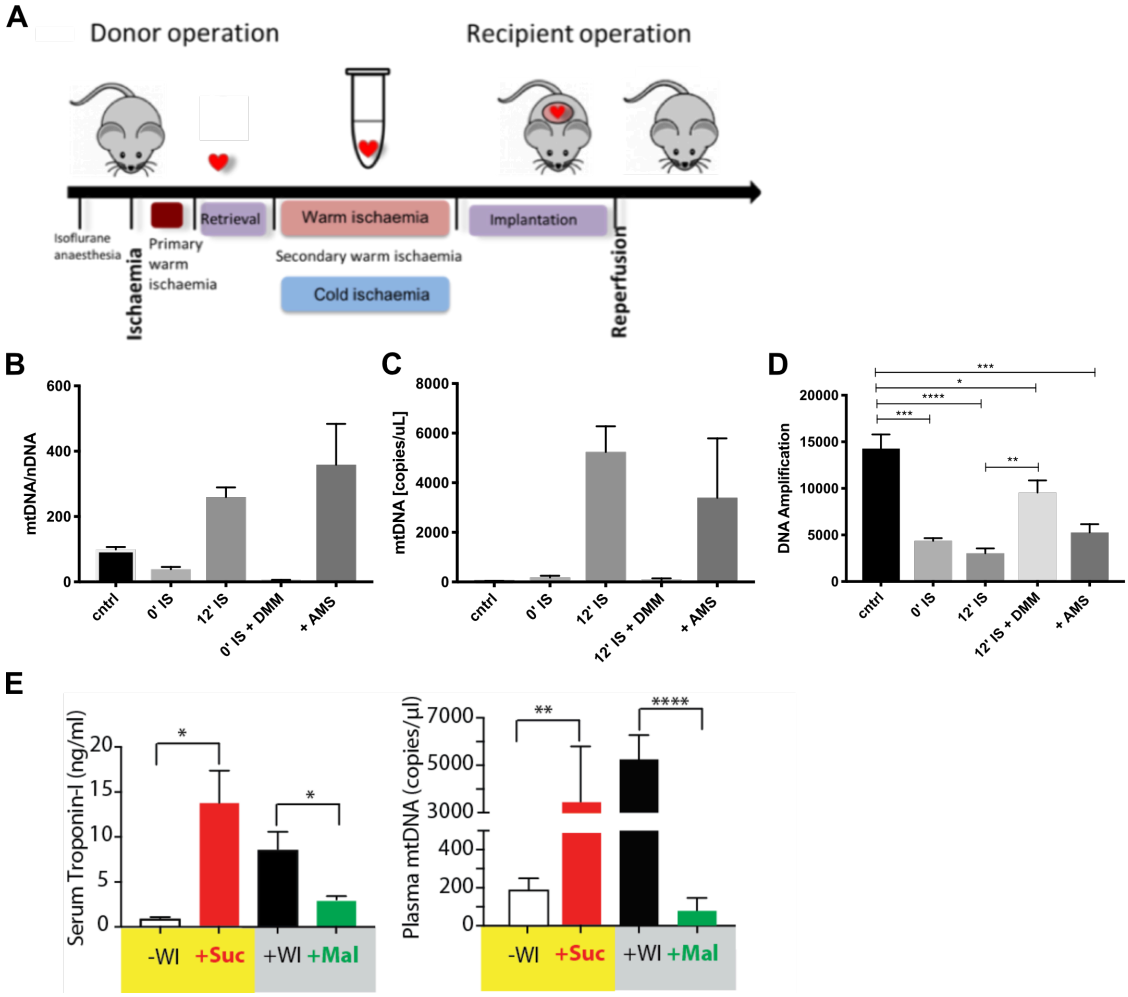

Figure 6.11: mtDNA is released upon IRI after murine heterotopic heart transplantation and can be ameliorated upon malonate treatment BL6 wild type mice were subjected to ischaemia reperfusion injury during heterotopic heart transplantation. (A) Schematic overview: anaesthetised donors were either treated with an infusion of dimethyl malonate (DMM), acetoxymethyl succinate (AMS) or saline control 10 minutes prior to retrieval. Donor hearts were retrieved following IVC administration of cardioplegia and exposed to either 12 minutes of warm ischaemia or no additional warm ischaemia. Donor hearts were then transplanted heterotopically into the abdomen of recipient animals and compared to control transplants. Recipient serum and donor hearts were retrieved after 24 h and DNA release, damage and troponin levels assessed. (B- C) DNA isolated and analysed via ddPCR (ND5 as mitochondrial and β- actin as nuclear gene) as described in detail in the methods. DNA was quantified in copies per μL using the BIORAD Quantilife software. (B) Data are presented as mtDNA to nDNA ratio, (C) mitochondrial DNA is presented as copies per μL. (D) DNA was extracted from tissue samples and DNA damage assessed via qPCR as described before: amplification of a long fragment of mtDNA was compared to a short one to determine damage on mtDNA. The less amplification the more damage occurred. (E) Troponin was measured in serum samples using ELISA and quantified on a standard curve in ng/mL. This is directly compared to the mtDNA values in the same samples (same samples as in B-D). (E) is adapted from Martin et al., 2019. n= 4-12 biological replicates per group, data are mean ± S.E.M., statistical analysis was performed using unpaired student's t-test with Welsh correlation. *P < 0.05, **P < 0.01, ****P < 0.0001.

6.3.5.2 mtDNA release in a mouse model of renal IRI

I next investigated if mtDNA occurs *in vivo* upon IR injury to the kidney. To do this, Dr. Timothy Beach developed a murine renal IRI model, in which he clamps off the blood-supplying artery to one kidney in BL6 wild type mice for 25 min, before reperfusing the organ again and allowing animal recovery for 24 h before the kidneys, as well as abdominal blood were retrieved. This surgical procedure was compared to control sham surgery without any induced ischaemia. Serum was isolated and DNA extracted followed by ddPCR analysis and quantification as described before. As presented in Figure 6.14, the mtDNA/nDNA ratio (Figure 6.14 A) as well as copies of mtDNA (Figure 6.14 B) are elevated in the circulation of mice that underwent ischaemia in comparison to sham surgery. nDNA is elevated in IRI samples, too. This indicates that renal IRI does result in increased release of both mtDNA and nDNA into the circulation leading to elevated mtDNA/nDNA ratios.

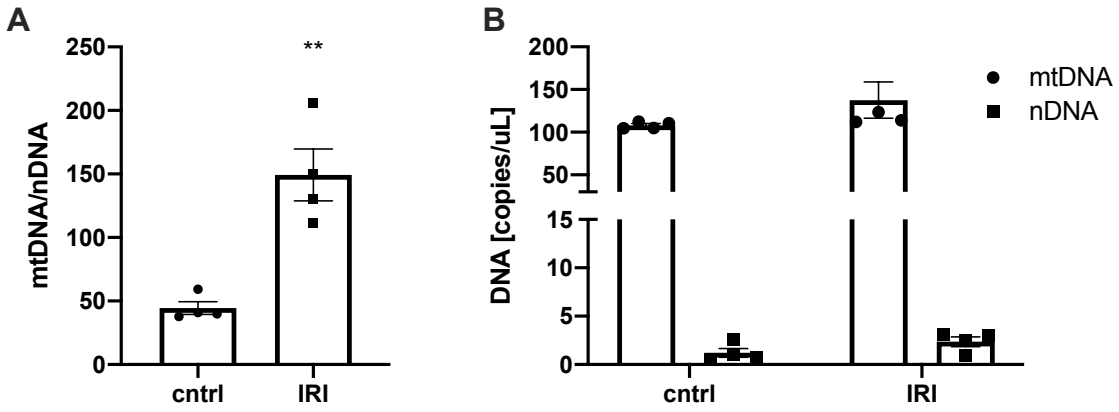

Figure 6.12: mtDNA is released upon murine renal IRI. BL6 wild type mice were subjected to a renal model of ischaemia reperfusion injury. The mice were anaesthetised and the artery to one of the kidneys clamped to stop blood supply to the organ. Ischaemia was induced for 25 min before the clamps were opened and blood supply re-established. Control mice underwent anaesthesia and sham surgery without clamping of the kidney artery. The mice recovered for 24 h before abdominal blood was retrieved. DNA was then isolated and analysed via ddPCR (ND5 as mitochondrial and β- actin as nuclear gene) as described in detail in the methods. DNA was quantified in copies per μL using the BIORAD Quantilife software. (A) Data are presented as mtDNA to nDNA ratio, (B) mitochondrial and nuclear DNA presented as copies per μL. n= 4 biological replicates per group (Cntrl or IRI), data are mean ± S.E.M, statistical analysis was performed using unpaired student's t-test, **P < 0.01.

6.4 Discussion

In this part of my project, I analysed the release of mtDNA as a potential mtDAMP upon ischaemia reperfusion injury. Using the previously described cardiomyocyte model in true anoxia under MCT1 inhibition, it was possible to determine the time course of mtDNA release from mitochondria into the cytosol and further on from cells into the surrounding medium. This showed, that mtDNA is released upon anoxia and reoxygenation starting within 15 min of reperfusion and continuing until 2 h of reperfusion. Interestingly, this mtDNA remains within the cellular cytosol for almost 24 h, before the DNA is further released from the cell. This release into the supernatant occurs after plasma membrane rupture, as shown by LDH release. These data suggest that mtDNA is not actively released from injured cells.

Interestingly, treatment with Cyclosporin A, which among other effects inhibits MPTP opening, inhibits mtDNA release from mitochondria in isolated cardiomyocytes and ameliorates IRI. This indicates that the mitochondrial permeability transition pore contributes to mtDNA release upon IRI. Recently published cellular mtDNA release models reported different, tightly controlled release mechanism (Kim et al., 2019; McArthur et al., 2018) upon apoptosis. This possibility has not been investigated in our anoxia reoxygenation system but might also contribute. Cyclosporin A is already used as immunosuppressant in organ transplantation, due to its function as a T-cell proliferation inhibitor, but its beneficial effects upon ischaemia reperfusion injury may also be worth exploring.

Besides the need for further investigation into which mtDNA release pathways occurs during IRI, the oxidative state of this released DNA has to be investigated in more detail. Possibly, different release pathways are responsible for the efflux of undamaged versus fragmented or oxidised mtDNA. Several pathways are known which are activated by different types of DNA, single stranded or double stranded or oxidised.

Here, I focused on two innate immune pathways: TLR9 activation and cGAS/STING dsDNA- sensing. TLR9 was activated by supernatant from cardiomyocytes as well as by serum after ischaemia and reperfusion. The pattern of TLR9 activation correlates with mtDNA release, which in turn occurs upon cell membrane breakdown. More interestingly, I showed activation of cGAS within cardiomyocytes as indicated by increased 2’3’cGAMP as well as IFNβ production. The latter could be inhibited by cGAS inhibition and ameliorate anoxia reoxygenation injury. It was unclear why there was a delay in the increase in cytosolic mtDNA after treatment with the Ru.521 inhibitor. This opens up the question if this treatment has other effects than blocking cGAS, which might lead to stabilised mitochondria and less initial

mtDNA release and therefore decreased IRI. It is likely, that anoxia and reoxygenation induces major mitochondrial injury, so that fragmented, oxidised DNA as well as undamaged mtDNA is released into the cytosol. This may be part of an immune cascade in response to severe ischaemia reperfusion injury *in vivo*. In addition, there are other pathways in addition to the ones investigated here, including the dsDNA sensors IFI-16, DDX41 and LRRFIP1**,** and AIM2, which upon activation forms another inflammasome leading to the secretion of IL-1β.

Additionally, to discovering mtDNA release upon anoxia reoxygenation in isolated cardiomyocytes, this study also presents data on mtDNA release upon IRI in *ex vivo* and *in vivo* models. Strikingly, the time frame of DNA release in these models correlated to the one discovered in cells, indicating that mtDNA is released late upon reperfusion, after death of the affected cells. A baseline level of circulating mtDNA and initial release of mitochondrial as well as nuclear DNA from ischaemic organs upon reperfusion could be found in all the models. Strikingly, this release could be ameliorated by SDH inhibition with malonate in a murine heart transplant model, while increasing succinate concentrations in the animals increased the levels of circulating mtDNA. This suggests, that succinate is the driving force for ischaemia reperfusion injury and inhibiting succinate accumulation ameliorates IR injury in *in vivo* models.

Altogether, the findings obtained in this part of my thesis show that mtDNA is indeed released upon IR injury, but remains within the cellular cytosol where it activates innate immune pathways like the cGAS/STING pathway causing IFNβ production. Just after cell death, mtDNA is released into the extracellular matrix. This release of mtDNA can also be found upon IR injury in murine *ex vivo* and *in vivo* models, where levels of circulating DNA are elevated 24 h after reperfusion. And most interestingly, this amount of circulating mtDNA can be reduced *in vivo* after SDH inhibition which decreases ischaemia reperfusion injury.

Chapter 7

mtDNA release upon IRI in human models

7.1 Introduction

The demonstration of mtDNA release upon IR injury in murine models of organ transplantation led to the question if this is a conserved mechanism in human patients. Due to my affiliation with the Department of Surgery at the University of Cambridge, I was able to collaborate with surgeons overseeing patients that underwent some form of ischaemia reperfusion injury, such as organ transplantation, where controlled and significant ischaemia and reperfusion occurs. Therefore, I next investigated if circulating DNA levels were elevated in human models of IR injury.

In the last chapter, I used murine *ex vivo* and in *vivo* models to assess mtDNA release, but often, findings in mouse experiments do not translate to patients. This can be due to a range of reasons. For example, animals used for biomedical research are usually genetically identical, while the genetic background in humans is very different. Further environmental factors like lifestyle are highly variable in patients and can impact the condition of the patient and their underlying pathologies. Thus, it is crucial to assess human samples in combination with other models to confirm underlying pathological pathways.

To begin assessing mtDNA release in human tissues, I first utilised organ perfusion systems available through the Department of Surgery such as an ex *vivo* normothermic perfusion system. This model offers an experimental setup that is more complex and physiologically relevant than a cell model, but experimental conditions can be easily controlled and modified. Therefore, these models can function as an intermediate between *in vitro* and *in vivo* data. In addition, I also utilised *in vivo* IR systems, such as samples from transplantation surgery and partial nephrectomy surgery in which part of the kidney is removed and consequently undergoes IRI. All of these offer the possibility to study mtDNA release upon ischaemia reperfusion injury in patients.

MtDNA release into the circulation has been proposed as a potential biomarker for IR injury, and for mitochondrial dysfunction in general. Biomarkers specific for mitochondrial dysfunction might open up the possibility of detecting disease on-set in patients. MtDNA has been detected in patient blood samples (Pinti et al., 2014; Stawski et al., 2017; Zhang et al., 2010), and is easy to isolate and analyse using PCR and related methods. These molecules are potential markers for mitochondrial damage, but their release into the circulation and the time course of degradation or persistence within the body are not known. Thus, it would be interesting to compare and correlate established biomarkers to circulating mtDNA.

Some operations can lead to secondary organ damage and failure, for example recipients of liver transplants often develop acute kidney injury (AKI), the reason for which remains to be fully elucidated. While liver biomarkers, like AST and ALT, and general inflammation markers, like IL1β or leucocyte numbers, are constantly monitored, AKI cannot be distinguished specifically via these markers. A study by our collaborator Dr. Ina Jochmans in Leuven, Belgium revealed that patients who developed AKI upon liver transplantation exhibited increased liver damage markers AST and ALT in their circulation unlike patients that did not develop AKI (Jochmans et al., 2017). This opens up the question whether other biomarkers, for example mtDNA released after ischaemia reperfusion injury due to liver transplantation, could indicate the severity of primary organ damage and the likelihood for developing secondary organ damage.

In order to understand if IR injury and released mtDNA correlate with each other and with organ damage and inflammation, a number of different outcome measurements in the same samples have to be compared. Ideally, it would be good to determine whether circulating mtDNA levels could provide a diagnostic or prognostic marker in patients undergoing surgery of various types. Research into mtDNA as both a clinical biomarker and as a mtDAMP is therefore of great interest for surgeons.

7.2 Aim

The main aim of this chapter was to assess mtDNA release into circulation in a range of human patients who are undergo various modes of ischaemia reperfusion injury during operations. I first utilised *ex vivo* normothermic perfusion of discarded human kidneys. Then I investigated mtDNA release in patients that underwent liver transplantation and subsequently developed acute kidney injury, as well as patients that underwent kidney ischaemia and reperfusion injury during nephrectomy surgery. I then explored if this release of mtDNA correlated with established biomarkers for organ damage in these patients.

7.3 Results

7.3.1 mtDNA release from human kidneys during *Ex Vivo* Normothermic Perfusion

Having shown that mtDNA is released from perfused murine organs, I next wanted to investigate if this is also the case in human organs. Dr. Mazin Hamid retrieved human kidneys that could not be used for organ transplantation, but were donated for research purposes. These organs underwent the normal transplantation procedure as depicted schematically in Figure 7.1 A. Kidneys were subjected to an initial period of warm ischaemia in the donor body during organ retrieval, before they are transferred onto ice. There, they were flushed with cold storage solution and cooled down rapidly entering cold ischaemia. During this study, we investigated the effect of treatment with the mitochondria-targeted antioxidant MitoQ on IR injury. Therefore, the cold flushing solution was supplemented with 50 or 100 µM of MitoQ and compared to untreated kidneys. The organs were then subjected to an additional 4 h of cold ischaemia before reperfusion for 6 h with leucocyte-depleted blood using an *ex vivo* normothermic perfusion (EVNP) machine. Samples of the circulating blood and of urine produced by the perfused kidney were collected at different time points.

Levels of mtDNA and nDNA were then assessed via ddPCR and quantified using the BIORAD Quantilife software. Figure 7.1 B-D show DNA levels circulating after reperfusion of untreated kidneys, or organs treated with different amounts of MitoQ extracted from the blood and normalised to the level of DNA in the blood before perfusion. An increase in mtDNA/nDNA ratios in plasma is detectable after 6 h of EVNP reperfusion (Figure 7.1 B) and can be ameliorated with MitoQ treatment. Detailed analysis of mtDNA release (Figure 7.1 C) shows that the DNA is released after 1 and 6 h of reperfusion from untreated kidneys, but not from MitoQ treated ones. Nuclear DNA, on the other hand increases more in the circulation of MitoQ treated kidneys than untreated organs (Figure 7.1 D). DNA levels in the urine produced by the perfused kidneys did not parallel those measured in plasma samples. Although an increase in mtDNA/nDNA ratios was detectable in the circuit of MitoQ treated kidneys after 6 h of reperfusion (Figure 7.1 E), overall mtDNA levels do not change significantly (Figure 7.1 F) and nDNA levels are generally low (Figure 7.1 G). These data show that DNA is released from *ex vivo* perfused kidneys and that the mtDNA/nDNA ratio in the perfusate can be reduced by MitoQ treatment. More mtDNA than nDNA is cleared into the urine, but no significant changes are detectable over perfusion time and between different treatments.

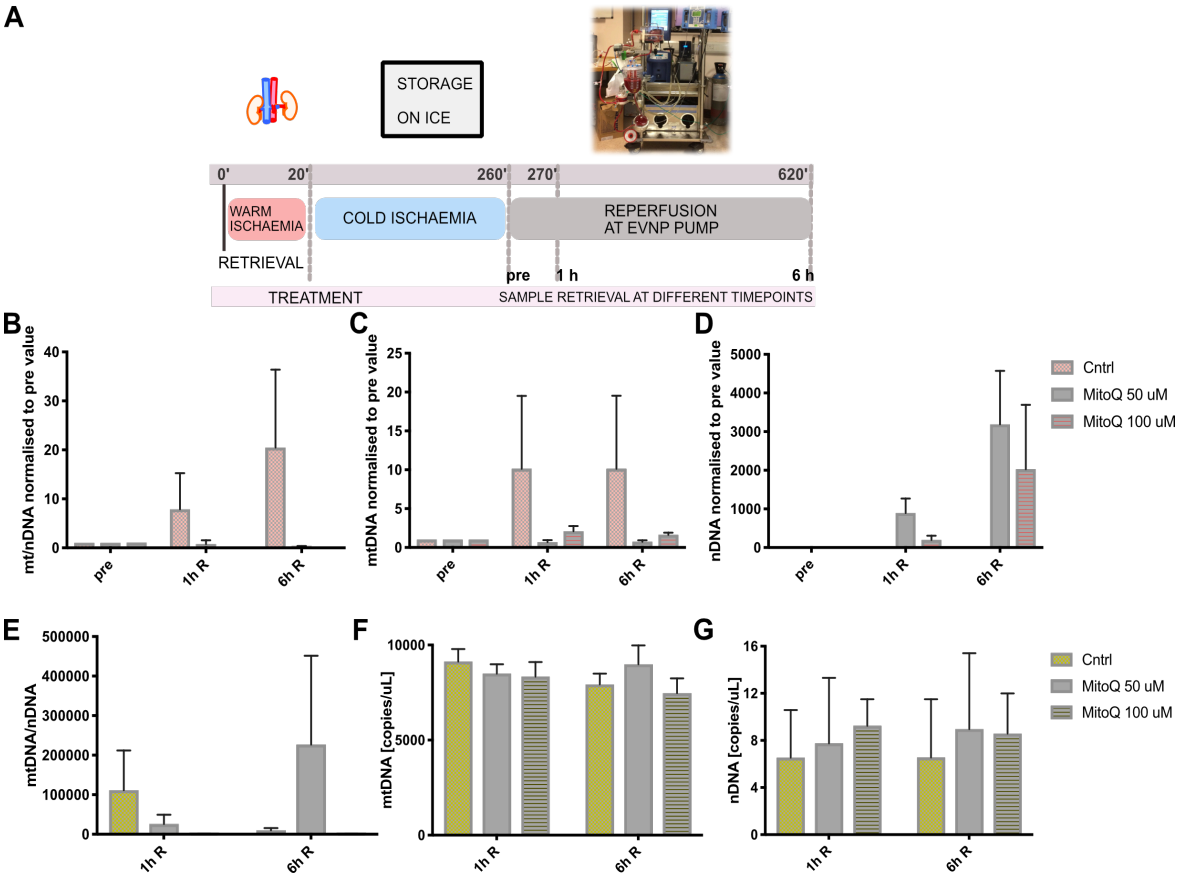

Figure 7.1: mtDNA is released from human kidneys that are perfused ex vivo. Human kidneys that were rejected for transplantation but cleared for scientific usage were retrieved, treated with the mitochondria- targeted antioxidant MitoQ, subjected to ischaemia and reperfused at an ex vivo normothermic perfusion (EVNP) machine and DNA release was investigated. (A) Schematic workflow overview: Human kidneys that were discarded for transplantation were retrieved for scientific purpose. During the transplantation surgery procedure, the kidneys were subjected to approximately 20 min of warm ischaemia. Upon retrieval, the organs were transferred to ice and flushed with a cold saline solution supplemented with MitoQ at 50 or 100 µM. After additional 4 h of ischaemia on ice, the kidneys were perfused with leucocyte depleted blood on an ex vivo normothermic perfusion pump for 6 h. Perfusate samples were retrieved during this perfusion period at different time points. (B-G) DNA was extracted from perfusate and urine samples and analysed via ddPCR (ND1 as mitochondrial and RNaseP as nuclear gene) as described in detail in the methods. DNA was quantified in copies per μL using the BIORAD Quantilife software. (B-D) DNA release analysis in blood perfusate samples. (B) Data are presented as mtDNA to nDNA ratio and normalised to each kidney's "pre" baseline DNA level. (C-D) Data are presented as DNA copies per μL and normalised to each kidney's "pre" baseline DNA level. (E-G) DNA release in urine samples collected 1 h and 6 h after starting reperfusion. (E) Data are presented as mtDNA to nDNA ratio. (F) Data are presented as mtDNA copies per μL. (G) Data are presented as nDNA copies per μL. n= 2-5 biological replicates, data are mean ± S.E.M. Statistical analysis was performed using 2-way ANOVA, but did not show significant results.

7.3.2 The role of circulating mtDNA in human liver transplantation

As ischaemia reperfusion injury occurs during transplantation, we next collaborated with Dr. Ina Jochmans at the University Hospital in Leuven, Belgium, who performed a series of liver transplantation on patients. In particular, she focussed on a cohort of these patients who developed secondary acute kidney injury (AKI). Ina and her colleagues collected plasma and urine samples from patients at different times before, during and after liver transplantation in the recipients (Figure 7.2 A). In their publication (Jochmans et al., 2017) they describe a significant difference in peak AST levels, a marker of liver damage, between patients that developed AKI or patients with normal renal function (NRF) upon receiving a liver graft (Figure 7.2 B). A subset of 10 of these patients (5 NRF, 5 AKI), which were selected by Dr. Jochmans to investigate the development of AKI upon liver transplantation, were analysed further for DNA release into the recipient after liver transplantation. Donor and recipient demographics are presented in table 7.1.

Table 7.1: Demographics of the cohort of patients that retrieved liver transplants, as published in Jochmans et al., 2017. AKI= acute kidney injury, AST= aspartate transaminase, ALT= alanine aminotransferase, Bil= bilirubin, gGT= gamma glutamyl-transferase, CIT= cold ischaemic time.

ID	AKI	Donor Age	AST (peak)	ALT (peak)	Tot Bil (peak)	Creatinine (peak)	gGT (peak)	Recipient Age	CIT (h)	Implantation time (min)
007	yes	45	51.00	38.00	3.97	2.24	59.00	39	8.75	76
023	yes	28	198.00	136.00	2.80	1.30	615.00	63	9.02	47
034	no	77	37.00	19.00	0.68	0.90	28.00	63	9.63	50
039	no	36	72.00	43.00	0.29	0.7	135.00	42	7.83	55
051	yes	42	91.00	76.00	0.40	1.68	60.00	26	9.62	44
057	yes	56	8.00	13.00	2.46	0.78	73.00	70	5.17	46
062	no	22	89.00	240.00	1.10	1.30	19.00	25	9.85	45
064	no	49	144.00	216.00	0.52	1.10	20.00	70	4.38	43
070	yes	76	15.00	15.00	0.34	1.16	34.00	57	11.20	44
075	no	22	118.00	146.00	0.59	6.99	57.00	61	10.97	39

DNA was extracted from the plasma and urine samples and quantified via ddPCR. The patient samples were compared to mtDNA and nDNA values in samples obtained from the NHS blood bank. The plasma mtDNA/nDNA ratios, as shown in Figure 7.2 D, indicate increased mtDNA release after 5 days of reperfusion in the recipient. Actual mtDNA copy numbers in these plasma samples are slightly increased during the surgery procedure but are maintained at this level until at least 5 days after surgery, when a significant increase in mtDNA in the circulation is still detectable (Figure 7.2 E). Interestingly, nDNA values behave differently. Nuclear DNA levels in the plasma samples increase during the surgery procedure, after hepatectomy and early on after reperfusion and stay elevated for the next 5 h, but start decreasing 24 h after reperfusion (Figure 7.2 E). Analysis of DNA release into the urine of these patients revealed increasing levels of mtDNA post-surgery (Figure 7.2 F) that stay increased even 6 h after transplantation. There is no increase in nDNA, but only in mtDNA in the urine (Figure 7.2 G). Altogether, these data show that mtDNA is released into the circulation of patients that had undergone liver transplantation. Some of the mtDNA is cleared into the urine early after transplantation, and a significant increase in mtDNA can still be detected within blood samples 5 days after reperfusion.

Next, I investigated if the released mtDNA can activate the innate immune response via TLR9 activation. TLR9 activation was determined utilising the InvivoGen HEK- BLUE TLR9 cell line. As presented in Figure 7.2 C, plasma samples collected after reperfusion can activate TLR9, especially the latest time point, 5 days after surgery, results in activation to a similar level as the control oligonucleotide.

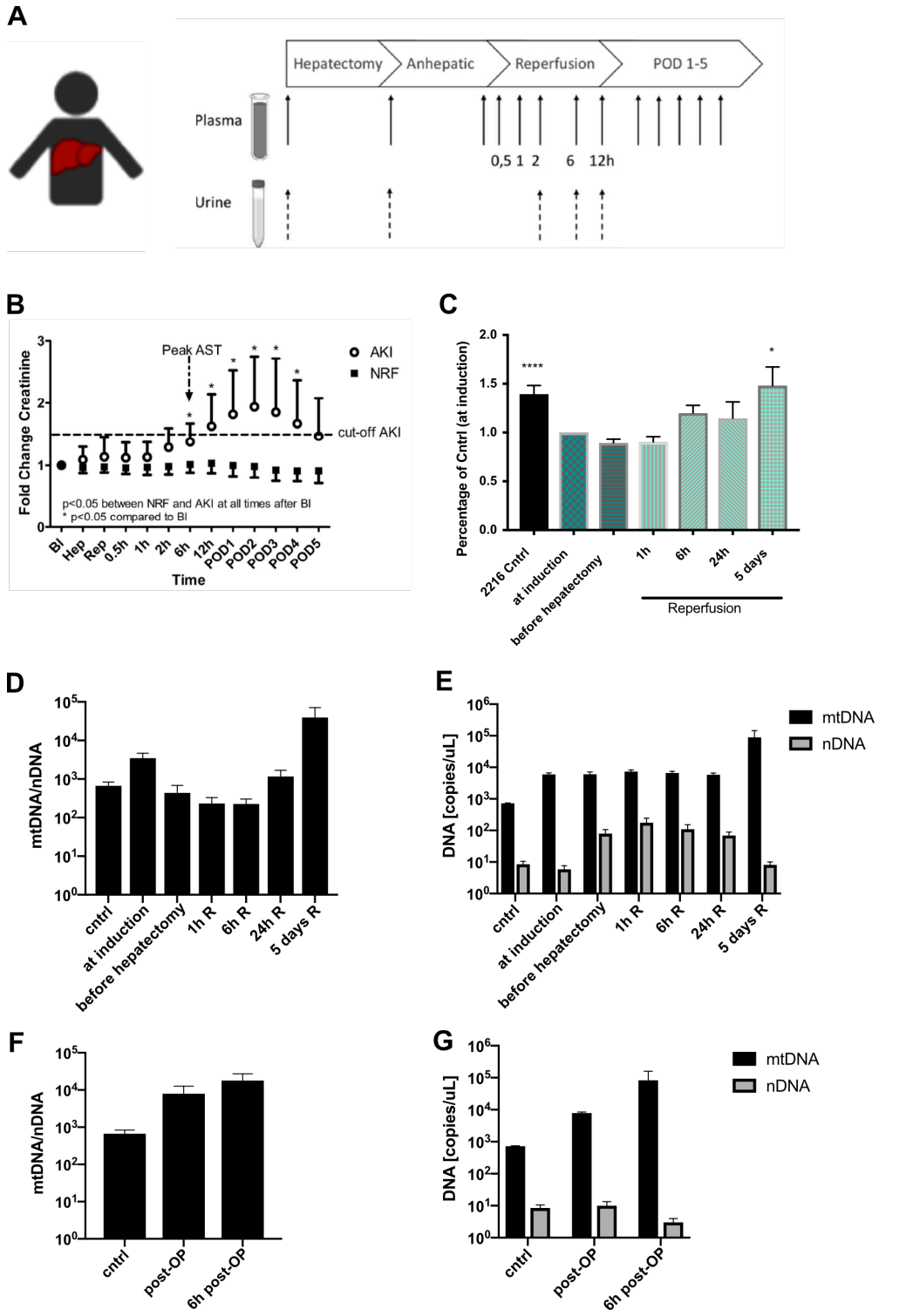

Figure 7.2: mtDNA is released upon IRI after human liver transplantation. Figure legend on the next page.

Figure 7.3: mtDNA is released upon IRI after human liver transplantation. Liver transplantation was performed by our collaborator Dr. Ina Jochmans in Leuven, Belgium. They investigated organ damage biomarkers in plasma and urine samples of patients that underwent liver transplantation and developed subsequent acute kidney injury (AKI). A cohort of 10 patients from the study (5 with normal renal function (NRF), 5 that developed AKI) was analysed further. (A) Schematic overview of sample retrieval during the transplantation process and patient recovery. POD = post operation day. (B) Comparison of AST peak values between patients with NRF or AKI depicted as fold change of creatinine values. (A&B) modified from Jochmans et al., 2018 (C) TLR9 activation was assessed using the InvivoGen TLR9 HEK293 cell line that expresses TLR9 as described before. Therefore, InvivoGen TLR9 HEK 293 cells were cultured and incubated with 1:10 diluted plasma or urine samples. After addition of the reaction medium, TLR9 activation was measured via absorbance at 625 nm. Results were compared to cells treated with the TLR9 activator 2218 and normalised to values at induction of transplantation. (D- G) DNA was isolated from plasma and urine samples and analysed via ddPCR (ND1 as mitochondrial and RNaseP as nuclear gene) as described in detail in the methods. DNA was quantified in copies per μL using the BIORAD Quantilife software. Data are plotted as logarithmic values. (D- E) DNA release from patient plasma. (D) Data are presented as mtDNA to nDNA ratio, (E) mitochondrial and nuclear DNA presented as copies per μL. (F- G) DNA release from patient urine. (F) Data are presented as mtDNA to nDNA ratio, (G) mitochondrial and nuclear DNA presented as copies per μL. n= 10 biological replicates, data are mean ± S.E.M., statistical analysis was performed via one-way ANOVA. *P < 0.05, ****P < 0.0001.

7.3.2.1 mtDNA release in patients that developed acute kidney injury upon liver transplantation

I next investigated differences between the patients who developed acute kidney injury versus the control group with normal renal function, with a further comparison to blood bank control samples. MtDNA/nDNA ratios do behave differently in the NRF versus AKI cohort (Figure 7.3 A). Patients with normal renal function have increased ratios, which is significant 5 days after transplantation. An overview (Figure 7.3 B) shows that mtDNA levels are relatively stable until at least 5 days after surgery, while nDNA only increases early on upon reperfusion. Detailed analysis of this, as presented in Figure 7.3 C, underlines again that transplant patients in general have slightly increased circulating mtDNA levels but are not changed between AKI and NRF cohort throughout surgery. Nuclear DNA on the other hand is significantly higher in the circulation of patients that developed AKI upon liver transplantation (Figure 7.3 D). More nDNA is released already 1 h upon reperfusion and continues to be elevated up to 24 h after transplantation. mtDNA/nDNA ratios in urine of these patients behave similarly and are increased in NRF patients (Figure 7.4 A). This is due to both the increased mtDNA in the urine of NRF patients 6 h after surgery (Figure 7.4 B, C) but especially the increased nDNA values in AKI patients (Figure 7.4 B, D). However, urine values could not be normalised to volume and are therefore difficult to interpret. These data show that there are differences in

DNA release in patients that developed AKI from patients with normal renal function.

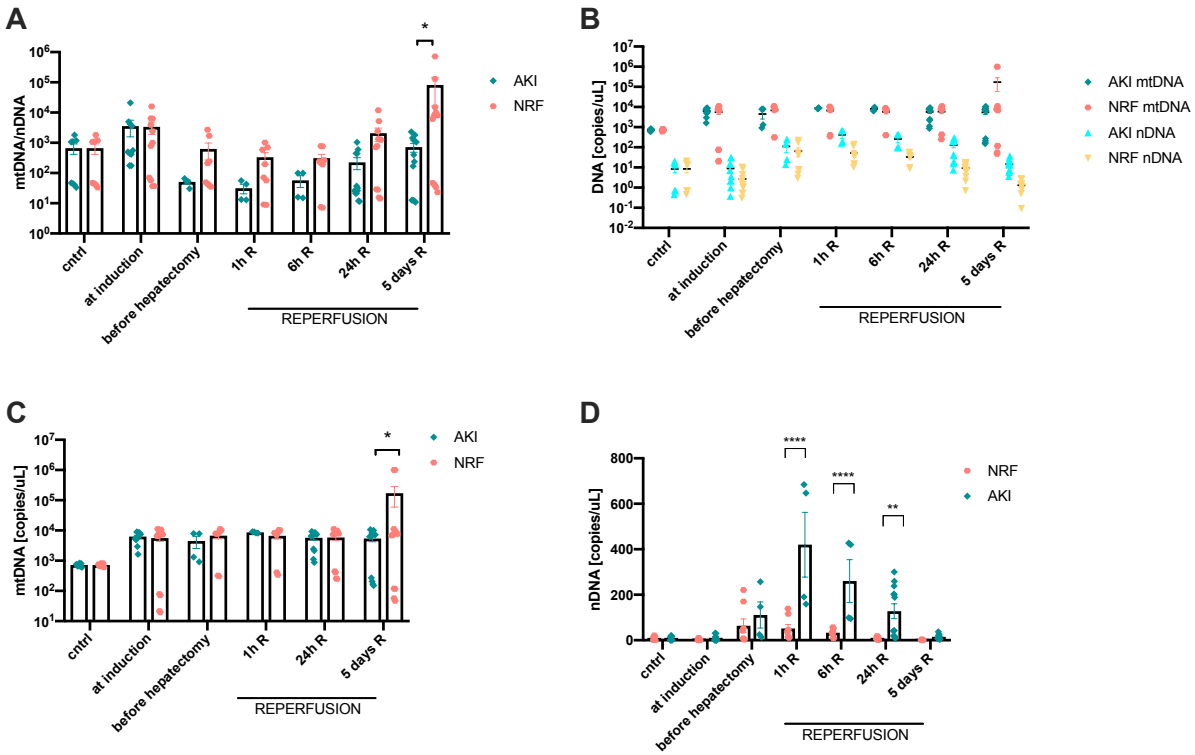

Figure 7.4: Less mtDNA circulates in patients that developed subsequent AKI after liver transplantation. A cohort of 10 patients from the study described in Jochmans et al, 2018 (5 with normal renal function (NRF), 5 that developed AKI) was analysed further and differences in DNA release between the cohorts investigated. DNA was isolated from plasma samples and analysed via ddPCR (ND1 as mitochondrial and RNaseP as nuclear gene) as described in detail in the methods. DNA was quantified in copies per μL using the BIORAD Quantilife software. (A) A comparison between the AKI and the NRF cohort is presented as mtDNA to nDNA ratio, (B) mitochondrial and nuclear DNA presented as copies per μL. (C) mtDNA release from AKI or NRF patients is presented as mtDNA copies per μL. (D) nDNA release from AKI or NRF patients is presented as mtDNA copies per μL. n= 5 biological replicates per group (AKI or NRF), data are mean ± S.E.M., statistical analysis via 2- way ANOVA, *P < 0.05, **P < 0.01, ***P < 0.001, ****P < 0.0001.

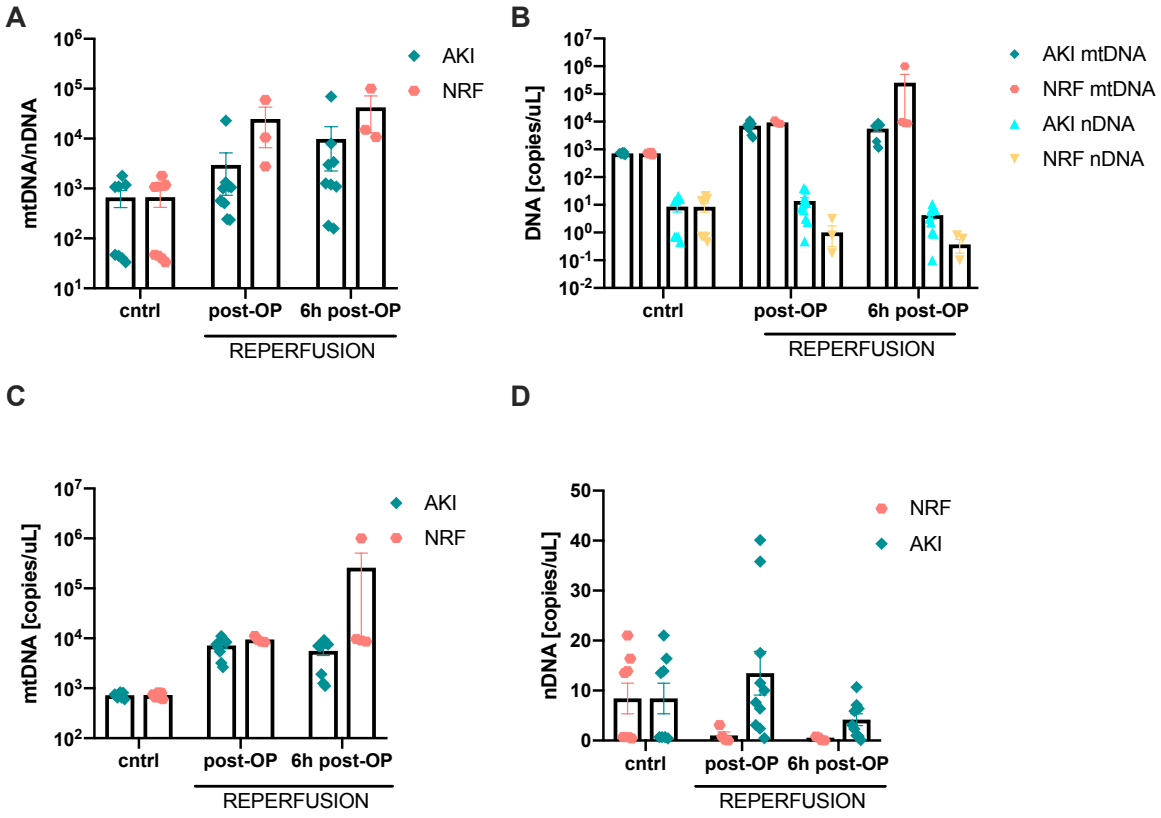

Figure 7.5: Less mtDNA is cleared from patients that developed subsequent AKI after liver transplantation. A cohort of 10 patients from the study described in Jochmans et al., 2018 (5 with NRF, 5 that developed AKI) was analysed further and differences in DNA clearance into urine between the cohorts investigated. DNA was isolated from urine samples and analysed via ddPCR (ND1 as mitochondrial and RNaseP as nuclear gene) as described in detail in the methods. DNA was quantified in copies per μL using the BIORAD Quantilife software. (A) A comparison between the AKI and the NRF cohort is presented as mtDNA to nDNA ratio, (B) mitochondrial and nuclear DNA presented as copies per μL. (C) mtDNA release from AKI or NRF patients is presented as mtDNA copies per μL. (D) nDNA release from AKI or NRF patients is presented as mtDNA copies per μL. n= 5 biological replicates per group (AKI or NRF), data are mean ± S.E.M., statistical analysis via 2- way ANOVA, which did not show significant results.

7.3.2.2 Correlation analysis of released mtDNA as potential biomarker for organ damage

I next assessed whether the levels of circulating mtDNA correlated with other organ damage markers. Because AST values have been shown by Dr. Ina Jochmans to correlate to AKI, I investigated if AST correlates to other outcome markers as well. As shown in Figure 7.5 A, no correlation can be detected in this limited cohort of 10 patients between peak AST values and ALT, bilirubin, gGT and AST. Donor age, cold ischaemic time and warm ischaemic implantation time also do not correlate with peak AST (Figure 7.5 B).

Creatinine does correlate with the log of peak AST in this cohort of patients (Figure 7.5 C) as assessed via linear regression analysis, while mtDNA/nDNA ratios do not correlate (Figure 7.5 D). The ratios do not correlate with donor age either (Figure 7.5 E).

To summarise, clinical biomarkers commonly used to predict organ damage, do not correlate with mtDNA values, possibly due to the limited number of patients investigated.

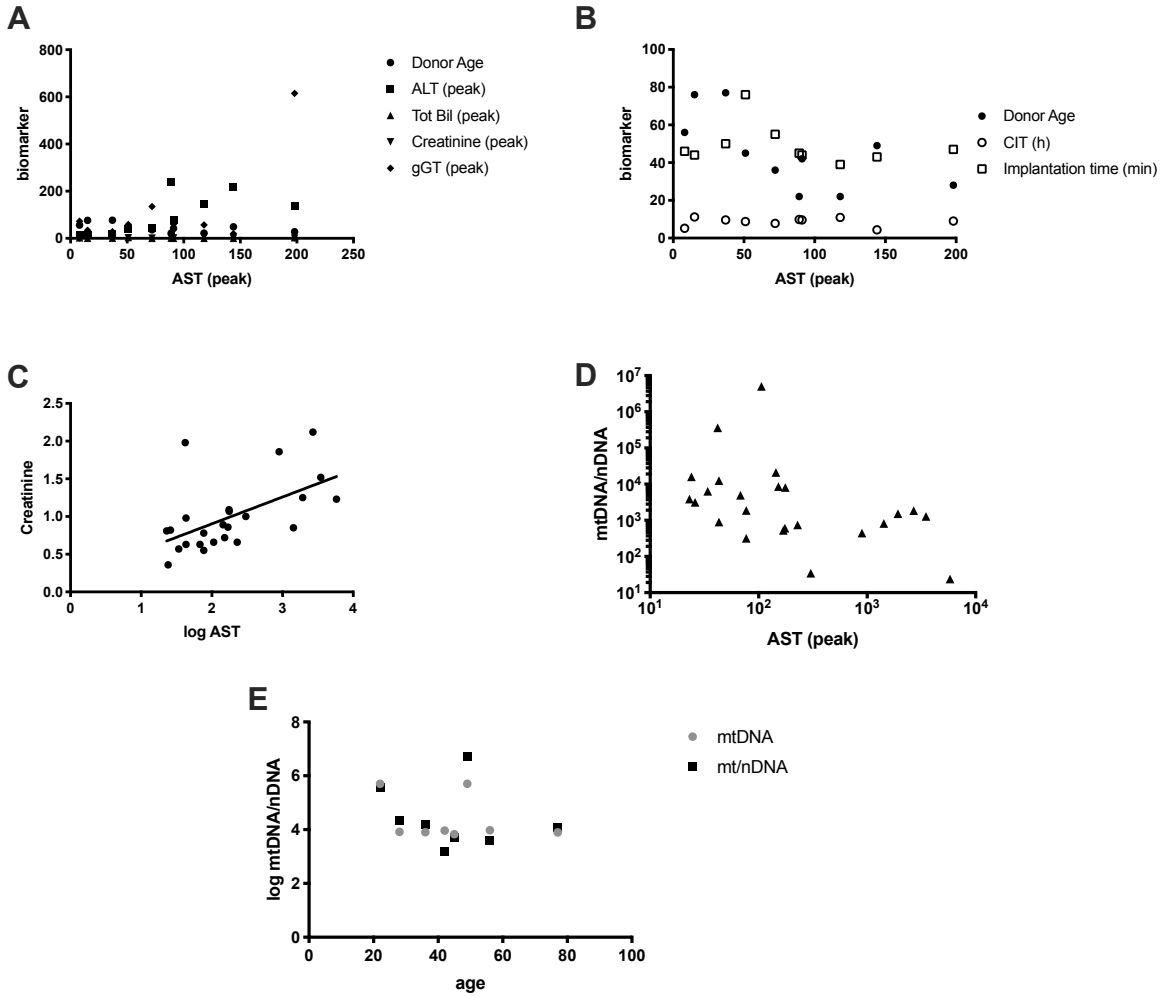

Figure 7.6: Correlation analysis of biomarkers for organ damage after human liver transplantation. Organ damage biomarkers were investigated in plasma and urine samples of a cohort of 10 patients that underwent liver transplantation. Here, correlation analysis was performed between different markers of damage. (A) The different biomarkers donor age, peak ALT, peak levels of total bilirubin, peak creatinine and peak gamma- glutamyl transferase (gGT) levels are correlated to peak AST values. (B) Donor age, cold ischaemic time (CIT) and implantation time are correlated to peak AST values. (C) Creatinine shows correlation to logarithm of peak AST evaluated via linear regression analysis. (D) mt/nDNA ratios do not correlate to peak AST values. (E) Logarithm of mt/nDNA or mtDNA does not correlate to donor age. n= 10, data are mean ± S.E.M., statistical analysis via linear regression analysis.

As published (Jochmans et al., 2017), peak AST values are significantly different in patients that developed AKI from patients with normal renal function. This can also be displayed in the analysis of creatinine to log AST, which does correlate as shown via linear regression

analysis in Figure7.6 A. In- depth analysis of this shows differences between this correlation in the cohort of patients that developed AKI to the NRF patients (Figure7.6 B & C), with a stronger correlation in AKI patients. Released mtDNA levels in the AKI patients do not correlate with creatinine (Figure7.7A), while mtDNA/nDNA ratio shows a weak correlation (Figure7.7 C). The ratios do also show a weak correlation to peak AST values in AKI patients, while the data in NRF patients did not show any correlation (see appendix, additional data to chapter7).

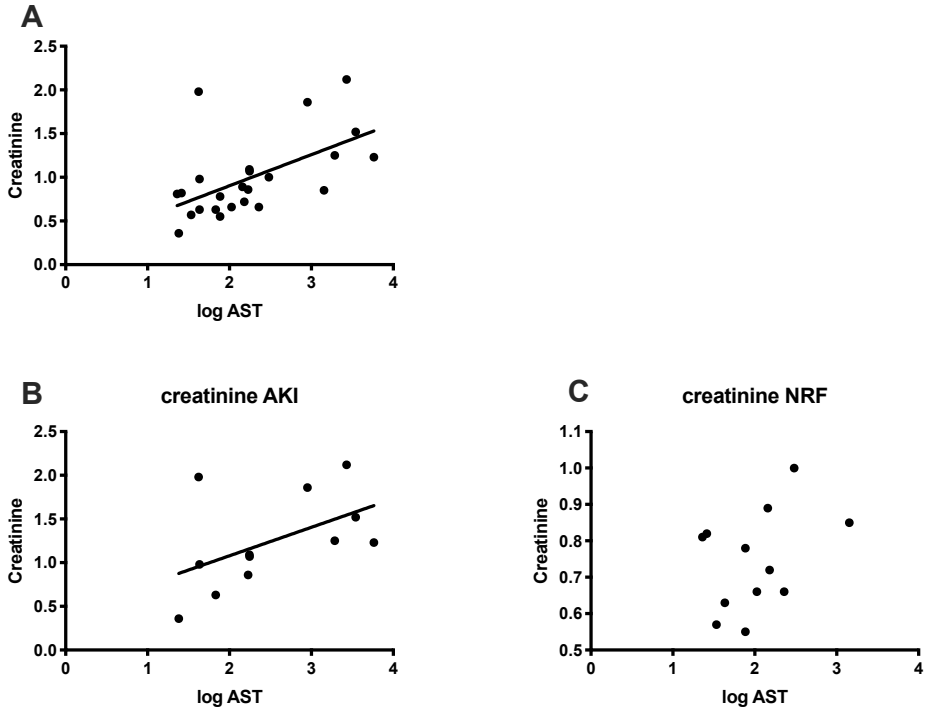

Figure 7.7: Correlation analysis of organ damage biomarkers in patients that developed AKI after human liver transplantation. Organ damage biomarkers were investigated in plasma and urine samples of a cohort of 10 patients that underwent liver transplantation, 5 of this with NRF and 5 that developed AKI. Here, correlation analysis was performed between creatinine and log peak AST in the different groups. (A) Summary of correlated creatinine to peak AST as depicted in Figure 18. (B) Correlation of creatinine and peak AST in AKI patients only. (C) Correlation of creatinine and peak AST in NRF patients only n= 5 biological replicates per group (AKI or NRF), data are mean ± S.E.M., statistical analysis via linear regression analysis. no significant result, R^2 always < 0.5.

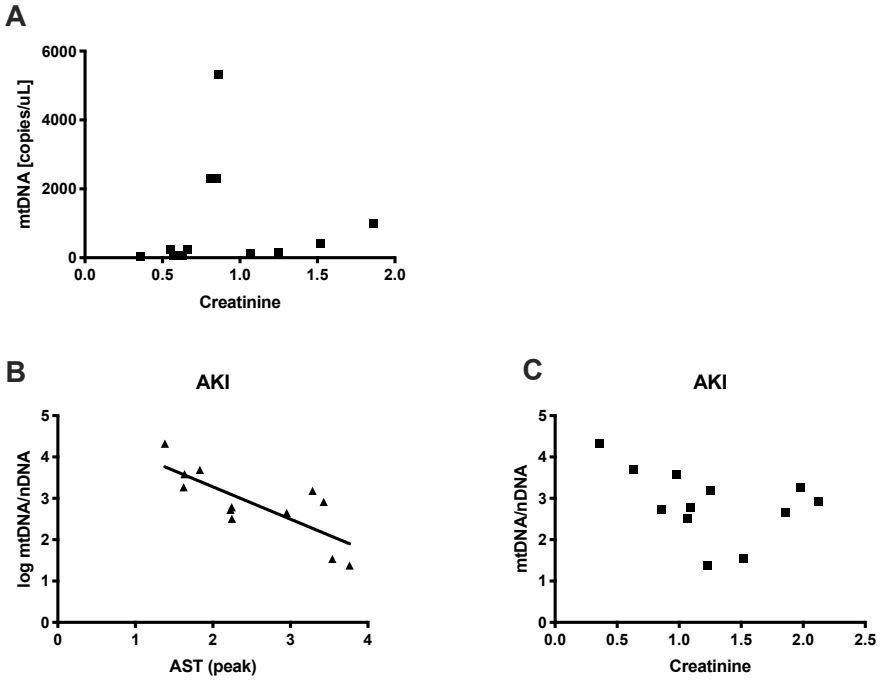

Figure 7.8: Correlation analysis of mtDNA release to damage biomarkers in patients that developed AKI after human liver transplantation. mtDNA release and damage biomarkers were investigated in plasma and urine samples of a cohort of 10 patients that underwent liver transplantation, 5 of this with NRF and 5 that developed AKI. Here, correlation analysis was performed between creatinine and log peak AST in the different groups. (A) Summary of correlated mtDNA to creatinine in the whole patient cohort. (B) Correlation of mtDNA/nDNA ratios to peak AST in AKI patients only. (C) Correlation of mtDNA/nDNA ratios to creatinine in AKI patients only, n= 5 biological replicates per group (AKI or NRF), data are mean ± S.E.M., statistical analysis via linear regression analysis.

All of this indicates that there are differences between AKI and NRF patients and the different biomarkers correlate with secondary organ damage. However, the number of patients analysed in this pilot study here is too small to gain relevant conclusions and further analysis with larger groups is necessary.

7.3.3 The role of circulating mtDNA in patients after partial nephrectomy surgery

As shown in *ex vivo* and *in vivo* models, renal IR injury results in the release of DNA into the circulation, as well as into the urine. A human model for renal ischaemia reperfusion injury occurs during partial nephrectomy. This surgery is performed to remove a part of the organ, often a tumour, and includes a period of ischaemia followed by reperfusion. As depicted in Figure 7.8 A, during surgery the blood supply to the kidney is cut off by clamping the renal artery, before the tumour is removed. The residual tissue is stitched back together, before the clamps are removed and the organ is reperfused. This procedure induces approximately 20 min of ischaemia. Nephrologists perform this surgery in two different ways, dependent on the accessibility of the tumour, they either perform laparoscopic surgery with minimal trauma to the patient, or they perform open surgery. In the latter case, the surgeons cool down the ischaemic kidney with ice during the procedure, but it is not known if this has beneficial effects on surgery outcome. I therefore collaborated with Prof. Grant Stuart from the Department of Surgery, Cambridge, who performed a series of partial nephrectomies on a cohort of 18 patients, 9 that underwent open surgery and 9 that were treated via laparoscopy, their demographics can be found in table 7.2. Plasma and urine samples were retrieved at different time points before, during and after surgery, following the patients' recovery for up to 12 months.

Table 7.2: Demographics of patients that underwent partial nephrectomy surgery. Patients were anonymised and given an identification number. They underwent either laparoscopic (robotic) surgery inducing warm ischaemia, or open surgery while the kidney was cooled with ice for cold ischaemia. N/A=data not available, TKI=tyrosine kinase inhibitor treatment/cancer treatment.

DIAMOND No	Age	Gender	Open or Robotic Surgery	Ischaemia Type	Ischaemia Time	Surgical Notes
6304	67	Male	Robotic	Warm	31 Mins	Hilar dissection challenging due to no mono/bipolar diathermy as patient has pacemaker
7027	45	Male	Robotic	Warm	30 Mins	
7028	61	Male	Robotic	Warm	22 Mins	
7035	55	Female	Robotic	Warm	34 Mins	
7044	65	Male	Robotic	Warm	27 Mins	
7056	50	Male	Robotic	Warm	19 Mins	
7058	55	Male	Robotic	Warm	22 Mins	
7069	64	Female	Robotic	Warm	15 Mins	
7061	68	Male	Robotic	Warm	8 Mins	
6284	54	Female	Open	Cold	42 Mins	
6291	56	Male	Open	Cold	36 Mins	Neoadjuvant TKI prior to surgery - Patient also has solitary kidney
7029	49	Male	Open	Cold	40 Mins	
7023	51	Male	Open	Cold	36 Mins	Neoadjuvant TKI prior to surgery - Patient also has solitary kidney
7037	33	Male	Open	Cold	43 Mins	Von Hippel Lindau Patient
7137	71	Male	Open	Cold	32 Mins	
7095	76	Male	Open	Cold	N/A	
7148	47	Male	Open	Cold	N/A	
7114	67	Male	Open	Cold	25 Mins	

I first investigated if circulating DNA levels increased after surgery in the above patients. Figure 7.8 B shows mtDNA/nDNA ratios in partial nephrectomy patients before, during and up to 12 months after surgery. No increase in the ratios is detectable, but the highest values occur before and at the beginning of surgery and decrease constantly from then on. Investigating mtDNA levels in detail (Figure 7.8 C) show that these levels increase 1 day after surgery and remain elevated for 6 months before they decrease and are barely detectable 12 months after surgery. The ratios are therefore decreasing due to elevated nDNA after partial nephrectomy. A similar trend can be detected in urine. mtDNA/nDNA ratios (Figure 7.8 D) are elevated before, during and up to 6 weeks after surgery but decrease after that, while mtDNA copies in urine (Figure 7.8 E) remain elevated for up to 6 months.

I further analysed these samples to investigate other renal damage markers. We tested if the release of the renal proteins Neutrophil Gelatinase-Associated Lipocalin (NGAL) and Kidney Injury Molecule-1 (KIM-1) was elevated upon renal damage after partial nephrectomy (Figure 7. 9). While levels of the epithelial protein NGAL does not change in serum samples (Figure 7. 9 A), levels of the renal proximal tubule protein KIM-1 does increase slightly 1 day after reperfusion (Figure 7. 9 B). NGAL levels in urine remain elevated even 6 months after surgery (Figure 7. 9 C), while KIM-1 levels are reduced after surgery (Figure 7. 9 D). The commonly used urine marker creatinine is only slightly, but not significantly, elevated shortly after the surgical procedure.

To summarise, mtDNA is released upon IR injury after partial nephrectomy and remains elevated n the circulation for several months. The renal damage marker NGAL does not increase within serum samples, while KIM-1 indicates early damage upon reperfusion.

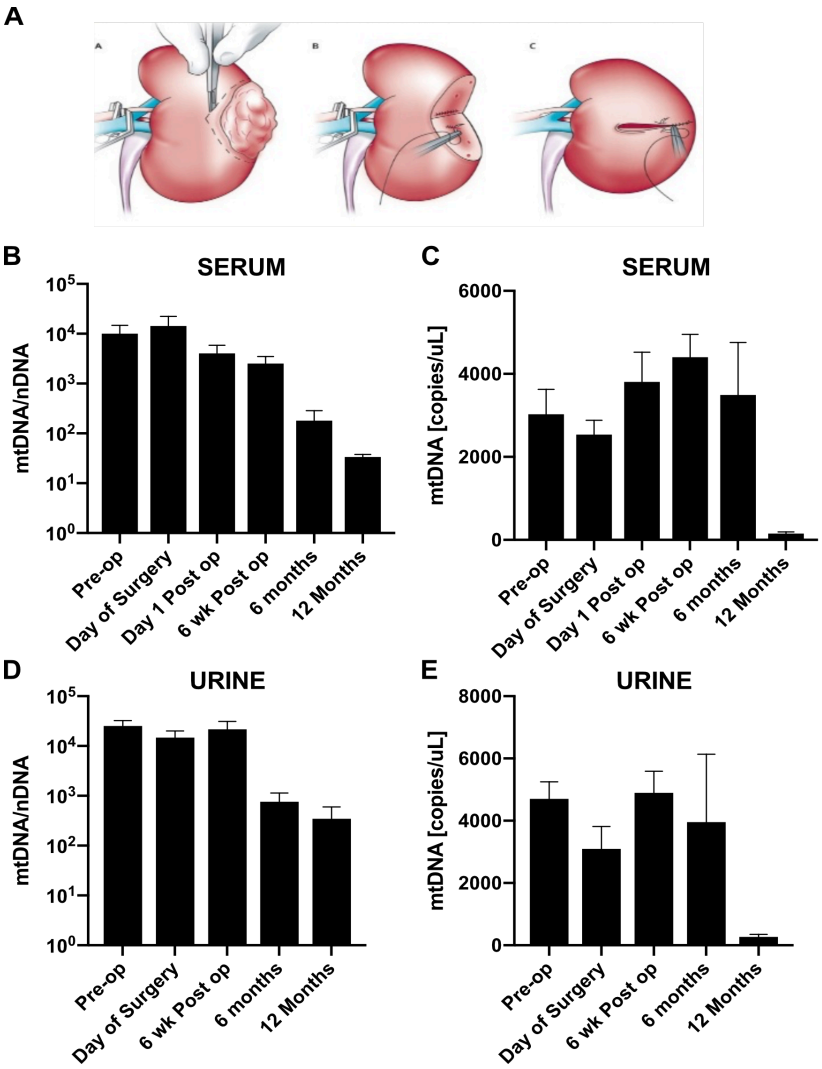

Figure 7.9: mtDNA is released after renal ischaemia reperfusion injury in patients that underwent partial nephrectomy. A cohort of 18 patients underwent partial nephrectomy performed by Dr. Grant Stuart and colleagues at the Department of Surgery, Cambridge. Serum and urine samples were retrieved at different time points before, during and after surgery. (A) Schematic overview over partial nephrectomy surgery: If tumour has to be removed from a kidney, first, the blood- supplying artery is clamped and interrupted. Next, the tumour is removed, before the injured organ is stitched. Finally, after approximately 20 min of ischaemia, the clamps are released and the organ reperfused. (B- C) DNA was isolated from serum samples and analysed via ddPCR (ND1 as mitochondrial and RNaseP as nuclear gene) as described in detail in the methods. DNA was quantified in copies per μL using the BIORAD Quantilife software. (B) Data are presented as mtDNA to nDNA ratio, (C) Data are presented as mitochondrial DNA copies per μL. (D- E) DNA was isolated from urine samples and analysed via ddPCR as described before. (D) Data are presented as mtDNA to nDNA ratio, (E) Data are presented as mitochondrial DNA copies per μL. n= 4-18 biological replicates, data are mean ± S.E.M., statistical analysis via 2- way ANOVA. No significant results were obtained.

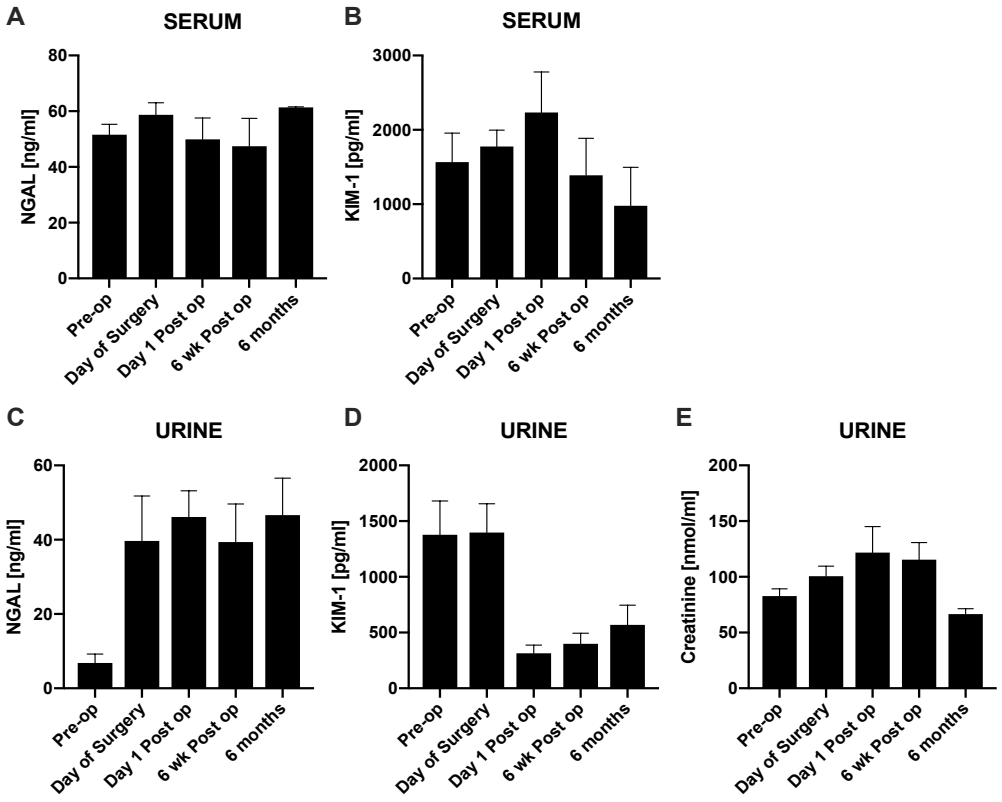

Figure 7.10: Potential organ damage markers after renal ischaemia reperfusion injury in serum and urine samples of patients that underwent partial nephrectomy. A cohort of 18 patients underwent partial nephrectomy inducing 20 min of renal ischaemia performed by Dr. Grant Stuart and colleagues at the Department of Surgery, Cambridge. Serum and urine samples were retrieved at different time points before, during and after surgery and the potential biomarkers NGAL and KIM-1 investigated. (A&B) Analysis of serum samples. (A) NGAL was quantified via ELISA in ng/mL. (B) KIM-1 was quantified via ELISA in pg/mL. (C-E) Analysis of urine samples. (C) NGAL was quantified via ELISA in ng/mL. (D) KIM-1 was quantified via ELISA in pg/mL. (E) Creatinine levels in urine were determined via ELISA in nmol/mL. n= 4-18 biological replicates, data are mean ± S.E.M., statistical analysis via 2- way ANOVA. No significant results were obtained.

7.3.3.1 Comparison of the effect of laparoscopic surgery and open surgery on mtDNA release

The partial nephrectomy was performed either as open surgery or as laparoscopic surgery. Although the amount of ischaemic time is the same, the impact on the body is greater in open surgery than laparoscopy. On the other hand, surgeons try to cool down the ischaemic organ during open surgery attempting to induce cold instead of warm ischaemia. This is not possible during laparoscopic surgery. Comparison of DNA release into the blood of patients that underwent laparoscopy did show some differences from patients that underwent open surgery.

As shown in Figure 7.10 A and B, mtDNA/nDNA ratios and mtDNA levels are not significantly different between the two groups until 6 months after surgery, when open surgery results in increased ratios. NGAL levels in serum are increased in open surgery patients on the day of surgery, while KIM-1 is significantly elevated 1 day after open surgery (Figure 7.10 C &D). In patients' urine samples, elevated mtDNA/nDNA ratios (Figure 7.11 A) as well as mtDNA copies (Figure 7.11 B) are detectable from 6 months after open surgery in comparison to laparoscopy. NGAL values (Figure 7.11 C) are highly variable but show a tendency to be increase in the urine of open surgery patients after the operation. KIM-1 levels (Figure 7.11 D) do not show a significant difference between the two groups, but a small increase in KIM-1 6 months after operation in laparoscopy patients in comparison to open surgery patients. Creatinine values are elevated in patient urine from the day of surgery onwards until 6 weeks after operation in open surgery patients (Figure 7.11 E).

These data show that overall damage markers are more elevated in blood as well as urine samples of patients that underwent open surgery in comparison to laparoscopy, indicating more damage, even though the ischaemic kidney was cooled down during open surgery.

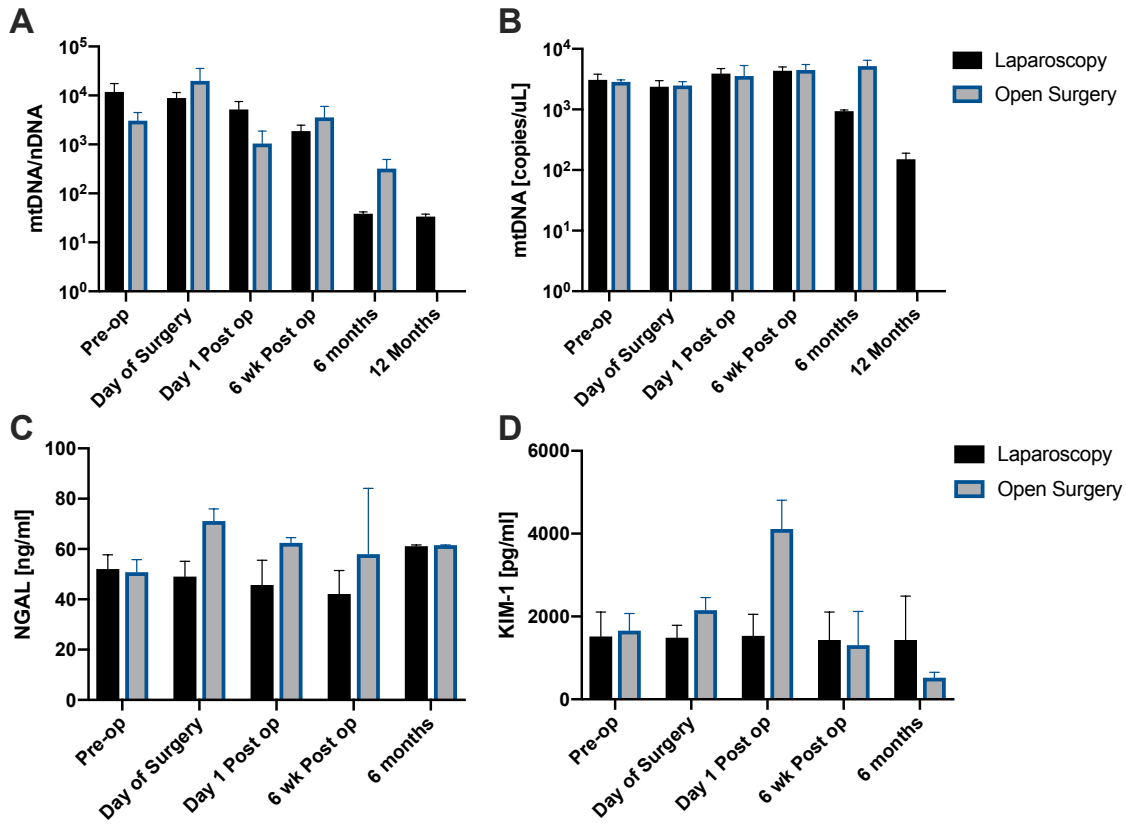

Figure 7.11: Differences in serum markers of patients that underwent laparoscopic or open partial nephrectomy surgery. A cohort of 18 patients underwent partial nephrectomy inducing 20 min of renal ischaemia performed by Dr. Grant Stuart and colleagues at the Department of Surgery, Cambridge. Surgery was either performed laparoscopic at body temperature, or as open abdomen surgery with ice surrounding the organ with 9 patients in each group. Serum samples were retrieved at different time points before, during and after surgery and the potential biomarkers mtDNA, NGAL and KIM-1 investigated. (A- B) DNA was isolated from serum samples and analysed via ddPCR (ND1 as mitochondrial and RNaseP as nuclear gene) as described in detail in the methods. DNA was quantified in copies per μL using the BIORAD Quantilife software. (A) Data are presented as mtDNA to nDNA ratio, (B) Data are presented as mitochondrial DNA copies per μL. (C) NGAL was quantified via ELISA in ng/mL. (D) KIM-1 was quantified via ELISA in pg/mL. n= 4-9 biological replicates per group, data are mean ± S.E.M., statistical analysis 2- way ANOVA. No significant results were obtained.

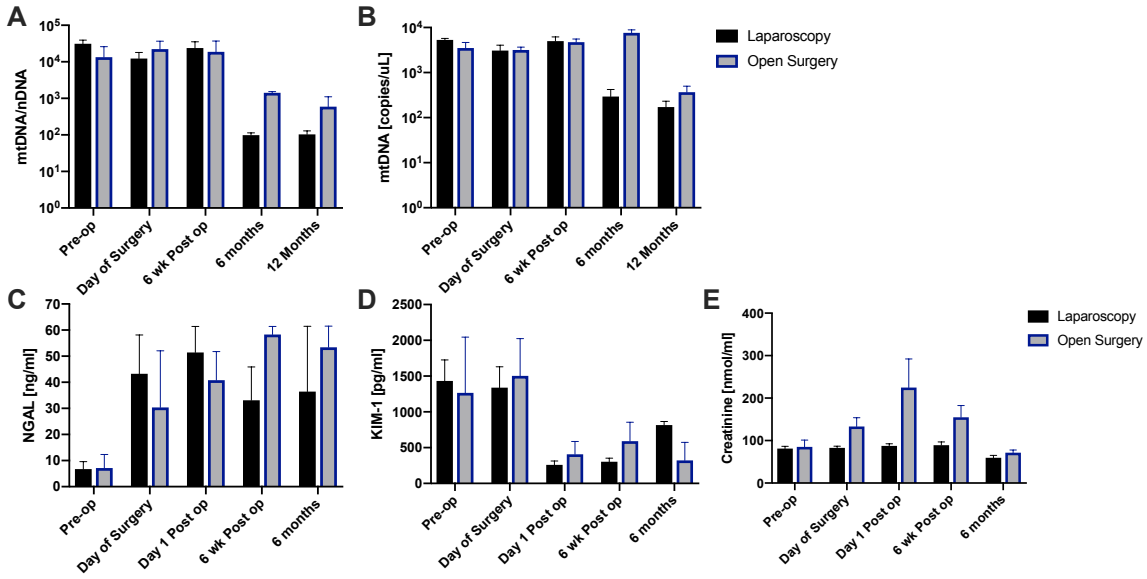

Figure 7.12: Differences in urine markers of patients that underwent laparoscopic or open partial nephrectomy surgery A cohort of 18 patients underwent partial nephrectomy inducing 20 min of renal ischaemia performed by Dr. Grant Stuart and colleagues at the Department of Surgery, Cambridge. Surgery was either performed laparoscopic at body temperature, or as open abdomen surgery with ice surrounding the organ with 9 patients in each group. Urine samples were retrieved at different time points before, during and after surgery and the potential biomarkers mtDNA, creatinine, NGAL and KIM-1 investigated. (A- B) DNA was isolated from urine samples and analysed via ddPCR (ND1 as mitochondrial and RNaseP as nuclear gene) as described in detail in the methods. DNA was quantified in copies per μL using the BIORAD Quantilife software. (A) Data are presented as mtDNA to nDNA ratio, (B) Data are presented as mitochondrial DNA copies per μL. (C) NGAL was quantified via ELISA in ng/mL. (D) KIM-1 was quantified via ELISA in pg/mL. (E) Creatinine levels in urine were determined via ELISA in nmol/mL n= 2-9 biological replicates per group, data are mean ± S.E.M., statistical analysis via 2- way ANOVA. No significant results were obtained.

7.3.3.1.1 Correlation analysis of released mtDNA as a potential biomarker for organ damage

To see if NGAL and KIM-1 could be potential clinical biomarkers for kidney damage, I performed correlation analysis between the previously assessed levels of these proteins in urine and serum of partial nephrectomy patients and urine creatinine values. As depicted in Figure 7.12, neither NGAL (Figure 7.12 A), nor KIM-1 (Figure 7.12B) show a correlation to creatinine, mtDNA (Figure 7.12 C)
or mtDNA/nDNA (Figure 7.12 D) in blood. The functional kidney damage marker estimated glomerular filtration rate (eGFR), does correlate with creatinine values analysed via linear regression (Figure 7.12 E) with an R^2 value <0.90. However, there was no correlation with KIM-1 (Figure 7.12 F) nor NGAL (Figure 7.12 G) in urine of the 18 patients that underwent partial nephrectomy. Furthermore, mtDNA (F Figure 7.12 H), and mtDNA/nDNA (Figure 7.12 I) levels did not correlate.

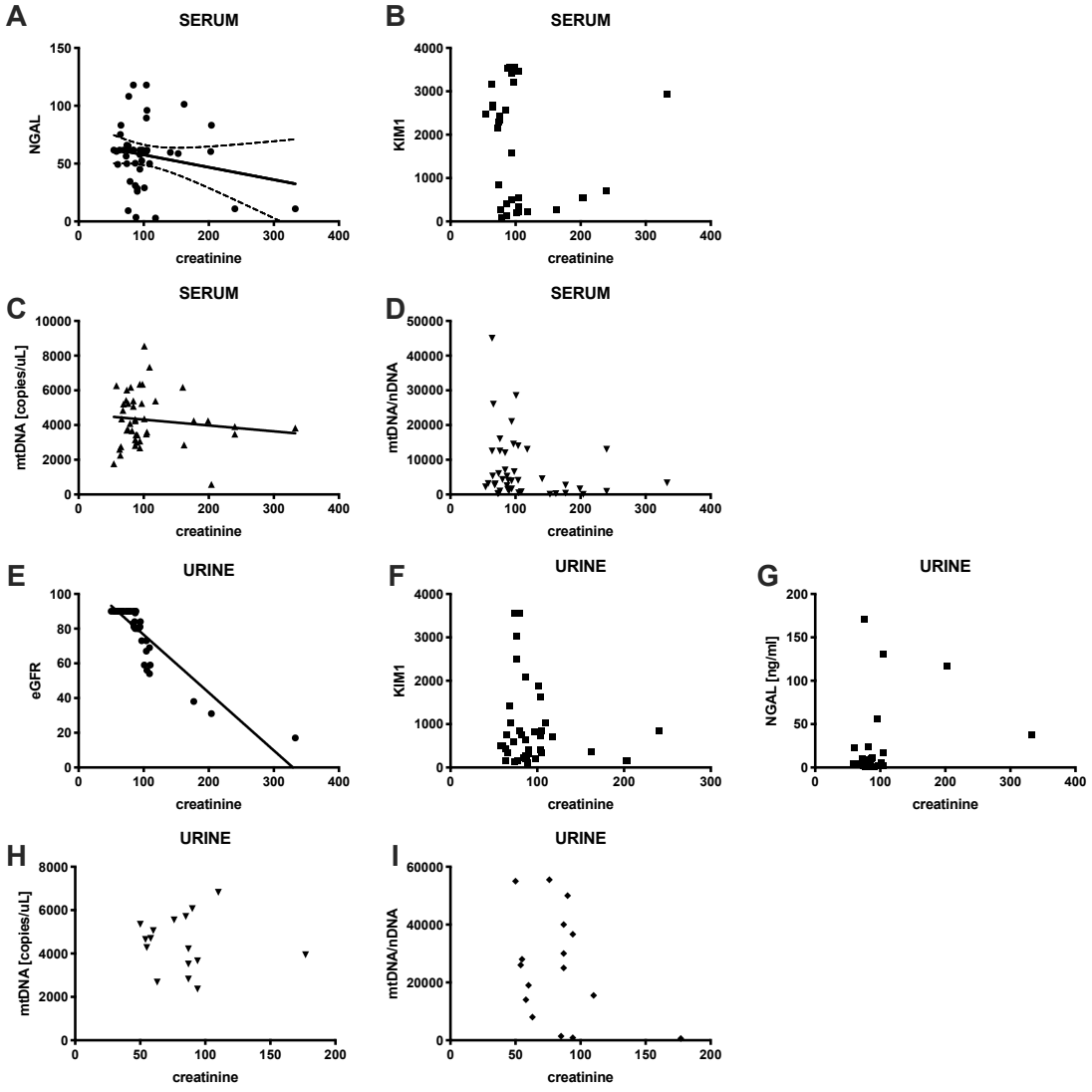

Figure 7.13: Correlation analysis of biomarkers for organ damage after human liver transplantation. Organ damage biomarkers were investigated in serum and urine samples of a cohort of 18 patients that underwent partial nephrectomy. Correlation analysis was performed between different markers of damage and creatinine levels. (A-D) Correlation analysis in combined patient serum samples. (A) Correlation of NGAL and creatinine analysed via linear regression analysis. (B) Correlation of KIM-1 and creatinine. (C) Correlation of mtDNA copies and creatinine analysed via linear regression analysis. (D) Correlation of mtDNA/nDNA ratio and creatinine. (E-I) Correlation analysis in combined patient urine samples. (E) Correlation of estimated glomerular filtration rate (eGFR) and creatinine analysed via linear regression analysis. (F) Correlation of KIM-1 and creatinine. (G) Correlation of NGAL and creatinine. (H) Correlation of mtDNA copies and creatinine. (I) Correlation of mtDNA/nDNA ratio and creatinine. n= 4-18 biological replicates, data are mean ± S.E.M., statistical analysis via linear regression analysis.

As we detected differences in DNA release between laparoscopic and open surgery, I next wanted to investigate if circulating mtDNA or released renal protein correlate to the urine renal damage marker creatinine. Neither NGAL (Figure 7.12 A & B), nor mtDNA/nDNA (Figure 7.13 C & D) in serum samples correlate to the patients' creatinine values. NGAL in patients that underwent open surgery (Figure 7.13 B) shows a tendency to correlate with creatinine than in patients that underwent laparoscopy (Figure 7.13 A) mtDNA/nDNA ratios in open surgery patients (Figure 7.13 D) are more scattered when plotted against creatinine values than laparoscopy patients (Figure 7.13 C), but do not correlate. Analysis of damage markers in urine from these patients reveals a stronger correlation of eGFR to creatinine in laparoscopic patients (Figure 7.13 E) than open surgery patients (Figure 7.13 F). mtDNA/nDNA ratios in laparoscopic (Figure 7.13 G) as well as open surgery (Figure 7.13 H) are too low in numbers to make robust conclusions.

Altogether, these data suggest that the renal damage markers tested here, including mtDNA/nDNA ratios do not correlate to commonly used clinical biomarkers. However, this result may have arose due to a cohort of 18 patients, 9 per surgery group, being relatively small, thus making a true statement on the correlation between these markers difficult.

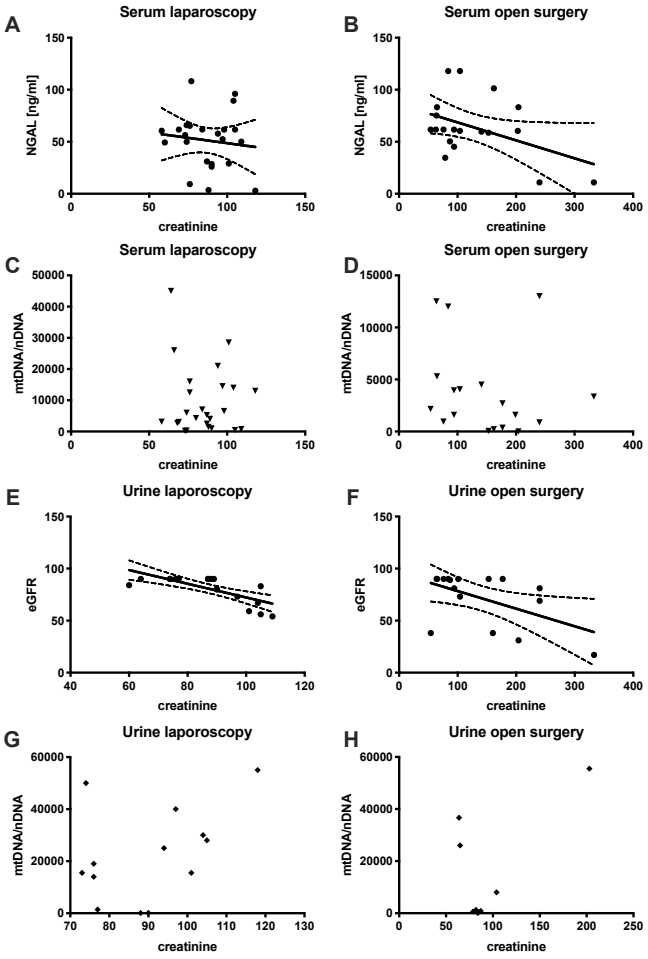

Figure 7.14: Correlation analysis of biomarkers for organ damage in patients that underwent laparoscopic or open partial nephrectomy. A cohort of 18 patients underwent partial nephrectomy inducing 20 min of renal ischaemia performed by Dr. Grant Stuart and colleagues at the Department of Surgery, Cambridge. Surgery was either performed laparoscopic at body temperature, or as open abdomen surgery with ice surrounding the organ with 9 patients in each group. Organ damage biomarkers were investigated in serum and urine samples of these patients. Correlation analysis was performed between different markers of damage and creatinine levels. (A-D) Correlation analysis in serum samples of patients that underwent laparoscopy or open surgery. (A) Correlation of NGAL and creatinine analysed via linear regression analysis in laparoscopy patients. (B) Correlation of NGAL and creatinine analysed via linear regression analysis in open surgery patients. (C) Correlation of mtDNA/nDNA ratio and creatinine in laparoscopy patients. (D) Correlation of mtDNA/nDNA ratio and creatinine in open surgery patients. (E-H) Correlation analysis in urine samples of patients that underwent laparoscopy or open surgery. (E) Correlation of eGFR and creatinine analysed via linear regression analysis in laparoscopy patients. (F) Correlation of eGFR and creatinine analysed via linear regression analysis in open surgery patients. (G) Correlation of mtDNA/nDNA ratio and creatinine in laparoscopy patients. (H) Correlation of mtDNA/nDNA ratio and creatinine in open surgery patients. n= 2-9 biological replicates per group, data are mean ± S.E.M., statistical analysis via linear regression analysis.

7.4 Discussion

These findings show that mtDNA is released into circulation by patients that experienced ischaemia reperfusion injury. This was demonstrated in EVNP perfused kidneys, as well as in blood and urine samples from patients that underwent surgery that induced IRI, either liver transplantation, or partial nephrectomy. In comparison to the results in the isolated cardiomyocyte model as well as in murine cardiac and renal ischaemia-reperfusion injury models, the human data was less definitive. This may be due in part to the small numbers of patients analysed in this pilot study to investigate if mtDNA is released at all upon IRI in humans. However, an increase in mtDNA levels in circulation late after reperfusion was detected in both human and mouse studies. We therefore conclude that mtDNA release does occur in patients upon IR injury.

Decreased mtDNA/nDNA ratios detected in patients with severe organ damage (e.g. the cohort that developed AKI after liver transplantation) is likely due to increased nuclear DNA after cell death. This decreases the mtDNA/nDNA ratio and makes it necessary to investigate DNA copies in parallel. However, neither mtDNA/nDNA ratios, nor mtDNA copy number alone correlated with common organ damage markers. The number of patients the two human studies are not large enough to achieve statistical significance, but even so no tendencies were detected making it unlikely that circulating mtDNA is a good biomarker for severe mitochondrial damage upon IRI in patients.

But interestingly, circulating mtDNA has been associated recently with AKI in clinical studies (Tsuji et al., 2016; Whitaker et al., 2015). The latest study links mitochondrial damage upon tubular inflammation in AKI and following this, mtDNA release to the activation of the cGAS/STING pathway and subsequent development of acute kidney injury (Maekawa et al., 2019). Our data of elevated mtDNA levels in AKI patients support these findings.

Thus, despite the limited number of samples analysed, the investigation of mtDNA release in these human patient studies gave rise to a better understanding of the time course of ischaemia reperfusion injury and its impact on the patient's immune response. The partial nephrectomy model was particularly informative, as just one of the two kidneys in a patient was ischaemic and still results in detectable increase of free mtDNA. The level of circulating mtDNA is strikingly elevated in patients that underwent more severe open surgery in comparison to laparoscopy, even though the ischaemic times were identical and the organ was

cooled during the open operation. This underlines the impact surgical procedures have on the body and that improving surgical techniques is as important as reducing ischaemia. Especially interesting is the fact that mtDNA was found circulating in patients for a long time after reperfusion. While nuclear DNA is released early upon reperfusion and is no longer significantly elevated in the circulation 24 h after reperfusion, mtDNA levels maintain elevated. Further research into this is necessary to explore if this is this due to a primary release of mtDNA from the damaged organ.

In summary, we discovered that mtDNA is released upon reperfusion in human models of ischaemia reperfusion injury. The pathology and the severity of a surgical procedure induce cell death, and cause elevated nuclear DNA levels in the blood together with increased mtDNA levels, but strikingly high mtDNA values can be detected even months after ischaemia/reperfusion. This work results in several novel research questions: where is the mtDNA coming from? How stable is mtDNA in the circulation? What does it do within the circulation? These and other questions will be addressed in the future.

Chapter 8:

General discussion and future directions

8.1 General discussion and future directions

The overall aim of this thesis was to investigate the role of mitochondria in ischaemia reperfusion injury in clinical and experimental models of organ transplantation. To do this I utilised and developed a series of complex *in vivo*, as well as simpler *ex vivo* and *in vitro* models. Using these I was able to analyse the underlying mitochondrial processes occurring during ischaemia and upon reperfusion, which contribute to IR injury. In order to understand the long-term impact of mitochondrial IR injury, I also investigated the role of release of mtDNA during IR injury as a mtDAMP in activating the innate immune response. Detailed discussions of the experiments and findings have been outlined at the end of each chapter. In this section, the limitations of the different models, the major implications of the findings and future experiments will be discussed in detail.

8.2 Understanding energy metabolism in tissues during ischaemia

The first aim I addressed in this thesis, was to investigate the changes in energy availability in the form of ATP/ADP ratios and adenosine nucleotide pools during ischaemia in different organisms and organs. I could thereby show that rapid freezing and no long-term storage of the samples is crucial to obtain accurate results about adenosine nucleotide concentrations in tissue samples. This may explain, why some of the previously published values seem to be surprisingly low.

I could show that even a few minutes of warm ischaemia causes loss of the majority of adenosine nucleotide species, and that cooling the organ can prevent this rapid loss. Strikingly, this process is conserved not just in different organs, but also in different mammalian species. For this I compared mouse, pig and human samples (and further rabbit sample analysis can be found in the appendix chapter of this thesis). I also analysed fruit fly and turtle tissue samples and could show that there was also ATP loss during anoxia in non-mammalian species, but that this was less than in mammals. Probably the most translatable data set I generated, was from the retrieval of human heart samples from rejected donated organs. Control samples from these organs were retrieved from the still beating, non-ischaemic heart, which has not been done before. Retrieving these controls very rapidly is crucial in order to investigate small changes that occur subsequently. This is especially important when analysing ischaemic samples, because of the rapid changes that occur within a few minutes and lead to ATP degradation and succinate accumulation. Therefore, slow sample retrieval

and freezing will generate misleading results. Furthermore, the differences in human lifestyle, age and health will all impact the quality of the samples. To extend this in future work, we recently started a collaboration with Dr. Sanjay Prasad and Dr. Richard Jones on investigating the energetic status of the hibernating human heart. Building on our knowledge of the time course of changes in adenosine nucleotide pools during ischaemia in the human heart, we are now going to investigate how these nucleotides behave in the chronically hibernating heart. Patients that have to undergo by-pass surgery in order to restore reperfusion of the heart have been recruited for this study. In this the surgeon will retrieve a sample from the hibernating part of the beating heart during the surgery. In addition to that, another sample is retrieved from a non-hibernating part of the patient's heart. Both of these samples are rapidly clamp-frozen and metabolomic analysis will be performed, including measurement of the ATP/ADP ratios. This offers the unique opportunity to compare hibernating tissue to normoxic tissue from the same patient.

To summarise, I could show that adenosine nucleotide degradation is rapid during warm ischaemia and is a highly conserved and characteristic hallmark of ischemia. My work has contributed to a number of publications, which are listed in an appendix to this thesis.

8.3 Establishment of a cellular model for ischaemia and reperfusion injury

The next aim during my thesis work, was to analyse cellular processes and their impact on ischaemia reperfusion injury in more detail. Therefore, I developed a cardiomyocyte model that was designed to better resemble physiological IRI, as it occurs in the heart during transplantation. For this I used primary adult mouse cardiomyocytes and utilised an anoxic incubator, rather than just a hypoxic incubator. I then confirmed the induction of anoxia and reperfusion injury by analysing hallmarks of ischaemia and IRI, including the accumulation of succinate, a reduction in the ATP/ADP ratios and increased cell death upon reperfusion. Most interesting, in developing this model were the striking differences between hypoxia at 0.1% oxygen in comparison to true anoxia. This distinction has so far been somewhat neglected in literature and has a significant impact on the interpretation of results and discrepancies between different studies utilising cardiomyocytes.

Building on this development, I could show that different inhibitors affect IRI by affecting succinate accumulation and ameliorated cell death upon reoxygenation.

Furthermore, I also investigated succinate efflux upon reoxygenation and the role of the monocarboxylate transporter in this. Although this work is so far preliminary, it has opened up new working hypotheses and research questions, which I will address in future work. The efflux of succinate from the cell is of particular interest as it could point to a further role of this metabolite in IR injury, as a signalling molecule and activator of succinate receptor SUCNR1, a receptor located in the plasma membrane of many cell types, especially immune cells, that is stimulated by extracellular succinate and sensitively regulates cell metabolism and therefore activates immunological responses to IRI (Ariza et al., 2012).

One further interesting finding achieved using the cardiomyocyte model, was that cell death upon reoxygenation is detectable after 18- 24 h. This underlines that we need to know more about the timings of the processes that occur between reperfusion and cell death, which may also enable us to develop new therapeutic targets. While we have just recently started to reveal the underlying mitochondrial processes, such as succinate accumulation and oxidation, that drive IR injury, we still lack understanding about many aspects of what is going on upon reperfusion and how cellular damage is caused. While we know understand better which processes occur during ischaemia, in isolated cells and tissues, we cannot just assume that oxidative damage alone causes cell death upon reperfusion. Direct ROS measurements are difficult and have therefore not fully clarified the time course of cell damage. The cell model developed here will enable analysis of these, however this model also has limitations. One of the biggest is that these cells are postmitotic and do not last more than a few days after isolation and are changing continually from isolation onwards. Other cell models, such as immortalised HEK cells, have some advantages, as they are less variable, easier to maintain and do not require animals for each preparation. I was able to induce anoxia in HEK cells in the same way as it in cardiomyocytes, and could detect decrease in ATP/ADP ratios and succinate accumulation (Appendix). These changes were delayed in comparison to cardiomyocytes and most importantly, IR injury upon reoxygenation in the form of cell death was not elevated. Therefore, while this cell model can be utilised to determine experimental conditions, is not suitable to investigate the injury that occurs upon reperfusion. In general, the primary cardiomyocyte model is more physiologically relevant than other cell models to investigate cellular IRI. However, findings achieved from this model need to be interpreted carefully and tested in other, more complex *in vivo* models.

8.3.1 Future directions

The work performed so far on cardiomyocytes is relatively preliminary and more in-depth analysis needs to be performed to fully understand how these cells respond to anoxia and reoxygenation.

Further interesting experiments would be to analyse gene expression changes in these cells under normoxia, anoxia and different reperfusion time points. This could elucidate which cellular response pathways are activated and when and this could be confirmed with proteomics. Another set of experiments that will be performed is metabolomic analysis of these cells during normoxia and anoxia. As we have detailed information about the metabolic changes in ischaemic heart tissue, it would be interesting to compare these to cardiomyocytes and to intervene pharmacologically, and with ^{13}C-labelled metabolite tracers which is far easier in cells than in organs.

Furthermore, oxidative damage as a result of IRI has only been investigated by assessing mtDNA damage. This damage was only detectable 24 h after reoxygenation. Perhaps this method is not sensitive enough, or other damage occurs prior to this. I would therefore want to investigate other possible markers of damage over a series of time points. I was also able to show that succinate accumulates during anoxia, and that some of it effluxed from cells upon reperfusion via the MCT1. Further analysis into how this occurs is necessary, for example in utilising mice with genetically knocked out MCT1. Further possible future experiments could focus on investigating the status of the CoQ pool and changes in the mitochondrial membrane potential to understand, if these are the driving force for ROS production at complex I.

Future work also needs to determine how ischaemia reperfusion injury leads to cell death 24 h later. This might be due to ROS damage accumulating slowly. Potentially, cellular antioxidant and repair pathways are maintaining the cell alive for a while, before they fail. Altogether, the cardiomyocyte model developed here has so far not been investigated in detail and many more aspects of cellular IR injury need to be investigated.

8.4 Investigation of mtDNA release and its role as mtDAMP upon IRI *in vitro*, *ex vivo* and *in vivo*

The final aim of my thesis, was to investigate the role of mtDNA as a damage associated molecular pattern upon ischaemia reperfusion injury. First, I assessed whether mtDNA was

released from mitochondria upon anoxia and reoxygenation in cardiomyocytes. Interestingly, I could show that mtDNA is released into the cytosol early upon reoxygenation and remains there, before it is released from the cell. This release of mtDNA could be blocked by inhibiting the MPTP with cyclosporin A. I also generated preliminary data for a role of mtDNA in activating the innate immune response via TLR9 or cGAS stimulation. Not much is known about how mitochondria involved in activating the immune response and understanding how mitochondria influence ischaemia reperfusion injury and recovery in this way is an important area to investigate.

Throughout this work, I was able to collaborate with surgeons and retrieve clinical samples which enabled me to assess mtDNA release into the circulation upon IRI. I showed that mtDNA is released upon IRI, in a time course comparable to what we have seen in cells before. Interestingly, mtDNA levels remained elevated within patients for days after transplantation. Additionally, circulating mtDNA levels were correlated with other, known organ damage markers in order to provide insight into mtDNA as biomarker for pathological IR injury. While the increase in circulating mtDNA upon reperfusion was clear, it was difficult to obtain significant results from patient subgroups and correlation analysis, due to their variability. Bigger data sets will be necessary to discover trends and correlations between for example ischaemic times and mtDNA release or secondary organ damage. Therefore, the work accomplished on this here is just a starting point and much more work has to done.

To sum up this part of my work, we could show that mtDNA is released into the cytosol upon IR injury, and is maintained there where it activates innate immune response pathways. Upon cell death mtDNA is released into the circulation where it may function as mtDAMP. It is important to note that this analysis of mtDNA release was only possible due to access to ddPCR technology. Before, when I performed initial experiments on circulating DNA using “traditional” RT-PCR, the low amounts of DNA in the samples lead to results that were unreliable.

8.4.1 Future directions

Investigation into mtDNA release upon IRI initiated some interesting finding, but many open questions remain. Now that we know that mtDNA remains within the cytoplasm for several hours following IR injury, further research is needed to determine which cellular pathways are activated by this mtDNA. The dsDNA- sensor cGAS is one such pathway, but another

abundant immune response occurs via the NLRP3 inflammasome. Building on this, one missing link in our understanding of the innate immune response to cytosolic DNA, is investigation into the different DNA species, such as fragmented DNA, specific DNA sequences, or oxidised DNA. It is possible that IR injury causes a certain type of mtDNA to be released, while other pathologies result in different mtDNA species. Preliminary results suggest that the cGAS/STING pathway is activated in cardiac myocytes, but further experiments need to be performed for example using the STING-inhibitor Ru.521.

Finally, another crucial question to be addressed is whether the circulating mtDNA released from the donated organ after organ transplantation is recognised as foreign by the recipient. In order to answer this question, we set up experiments involving the previously described heterotopic heart transplant model in mice between two mouse strains with different mtDNA haplotypes. This conplastic mouse strain (Latorre-Pellicer et al., 2016) contains mtDNA that is different from commonly used BL6 wild type mice, but has the same nuclear DNA. We will transplant the heart from one mouse line into the abdomen of a recipient from the other strain (Figure 8.1). Upon reperfusion, we will retrieve blood samples, extract DNA and analyse the amount of circulating DNA as performed already in the normal heterotopic heart transplant model. I already set up a pyrosequencing approach to distinguish which type of mtDNA is circulating in the recipients and I have investigated the time course of mtDNA release upon transplant surgery. Thus, these experiments will provide information on the origin and effect of the circulating mtDNA after ischaemia reperfusion injury. Furthermore, we can utilise these samples as well to investigate if different mitochondrial haplotypes affect the severity of IR injury upon organ transplantation, which might give interesting insights into donor-recipient matching in clinic.

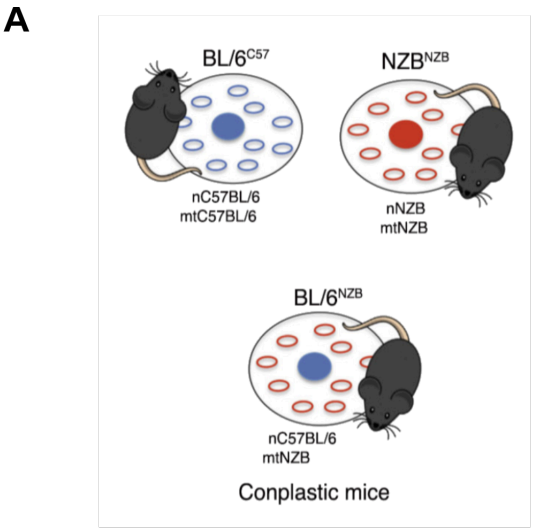

B

Position	C57BL/6	NZB	Gen	Category	Position	C57BL/6	NZB	Gen	Category
55	G	A	tRNA Phe	non-coding	8858	T	C	COIII	silent
716	A	G	rRNA 16S	non-coding	8864	C	T	COIII	silent
1353	A	G	rRNA 16S	non-coding	9137	A	G	COIII	silent
1519	G	A	rRNA 16S	non-coding	9152	T	C	COIII	silent
1590	G	A	rRNA 16S	non-coding	9391	A	G	tRNA Gly	non-coding
1822	T	C	rRNA 16S	non-coding	9461	T	C	ND3	silent
2201	T	C	rRNA 16S	non-coding	9530	C	T	ND3	silent
2340	G	A	rRNA 16S	non-coding	9581	C	T	ND3	silent
2525	C	T	rRNA 16S	non-coding	9599	A	G	ND3	silent
2766	A	G	ND1	missense	9829*	T	AA	tRNA Arg	non-coding
2767	T	C	ND1	missense	9985	G	A	ND4l	missense
2798	C	T	ND1	silent	10547	C	T	ND4	silent
2814	T	C	ND1	silent	10583	A	G	ND4	silent
2840	C	T	ND1	silent	10952	C	A	ND4	missense
2934	C	T	ND1	missense	11843	G	A	ND5	silent
3194	T	C	ND1	silent	11846	C	T	ND5	silent
3260	A	G	ND1	silent	11933	A	C	ND5	silent
3422	T	C	ND1	silent	12353	C	T	ND5	silent
3467	T	C	ND1	silent	12575	T	A	ND5	silent
3599	T	C	ND1	silent	12695	A	G	ND5	silent
3692	A	G	ND1	silent	12835	T	C	ND5	missense
3932	G	A	ND2	missense	12890	A	G	ND5	silent
4123	C	T	ND2	silent	13004	G	A	ND5	silent
4276	G	A	ND2	silent	13444	C	T	ND5	missense
4324	T	C	ND2	silent	13612	T	C	ND6	silent
4408	G	A	ND2	silent	13689	C	T	ND6	missense
4706	A	G	ND2	missense	13781	A	G	ND6	missense
4732	C	T	ND2	silent	13780	T	C	ND6	missense
4771	T	C	ND2	silent	13837	A	G	ND6	silent
4885	A	C	ND2	silent	13983	A	G	ND6	silent
4903	T	G	ND2	silent	14186	T	C	CYTB	silent
5204	A	AG	tRNA Cys	non-coding	14211	G	A	CYTB	missense
5463	G	A	COI	missense	14363	A	G	CYTB	silent
5552	T	C	COI	silent	14642	G	A	CYTB	silent
5930	G	A	COI	silent	14738	C	T	CYTB	silent
6041	T	C	COI	silent	15499	T	A	D-Loop	intergenic
6407	C	T	COI	silent	15549	C	T	D-Loop	intergenic
6470	A	G	COI	silent	15578	A	T	D-Loop	intergenic
6575	C	T	COI	silent	15588	C	T	D-Loop	intergenic
6620	G	A	COI	silent	15603	C	T	D-Loop	intergenic
6785	G	A	COI	silent	15657	T	C	D-Loop	intergenic
7411	A	G	COII	silent	15916	C	T	D-Loop	intergenic
7870	G	A	ATP8	silent	16017	A	C	D-Loop	intergenic
8439	A	G	ATP6	silent	16268	A	G	D-Loop	intergenic
8467	T	C	ATP6	silent	16272	T	C	D-Loop	intergenic
8568	C	T	ATP6	silent					

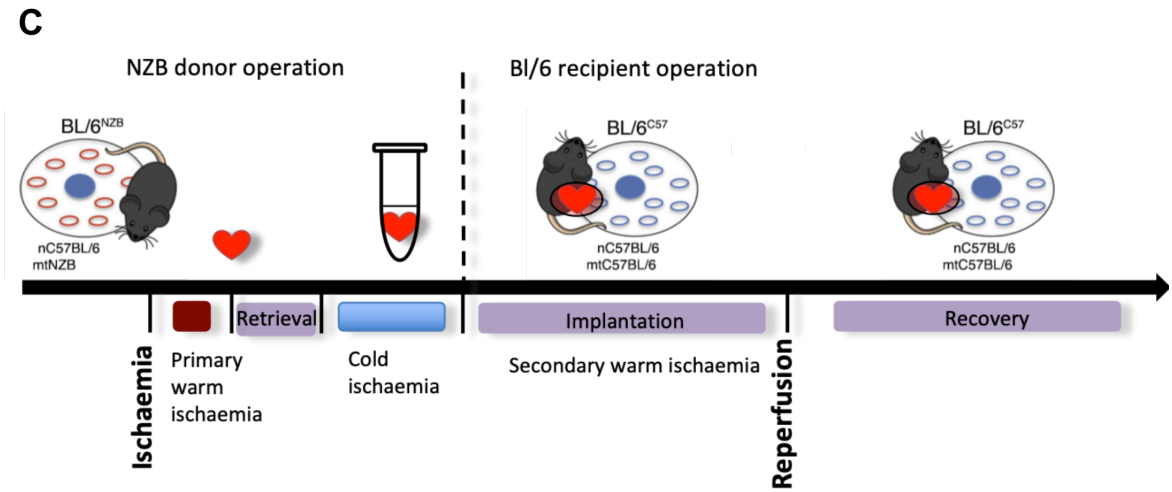

Figure 8.1: Investigating mtDNA release after heterotopic heart transplantation in a conplastic mouse model. The conplastic mouse model has been described by Latorre-Pelicer et al., 2015. BL/6 wildtype mice and NZB mice have been backcrossed over many generations to retrieve a conplastic mouse line, that contains a BL/6 nuclear DNA haplotype and NZB mitochondrial DNA (A). (B) A list of variances between BL/6 wildtype mtDNA and NZB mtDNA. (C) Schematic overview over the experimental procedure: The heart of a conplastic mouse donor is retrieved and transplanted into the abdomen of a wildtype recipient mouse. Additional ischaemia can be induced to cause severe IR injury upon reperfusion. 24 h after surgery, samples are retrieved, processed and analysed.

In summary, the findings achieved in this part of my work have provided insights into the involvement of mitochondria in IR injury during transplantation, while opening up many more questions that will have to be addressed in future work. Especially interesting will be the utilisation of the conplastic mouse model to investigate the interplay between the donated organ and the recipient.

8.5 Final summary

The insights provided in this thesis into the complex cellular pathways activated upon IR injury, have contributed to our understanding of ischaemia reperfusion injury. This will help us to develop methods to prevent it and to translate our knowledge to patients. The translation from bench work to clinical practice is difficult but my collaborations and communication with both basic researchers and clinicians has helped me understand how to do this. Understanding the molecular basis of ischaemia reperfusion injury in cells, followed by analysis of subsequent damage to tissues, and finally decoding the complex pathways occurring in in patients, is challenging. To do this we developed experimental systems from cells to *in vivo* models. With this, we aim to develop effective therapeutics which will one day be applicable in the clinic. The clinical relevance of my research initiated a number of important collaborations that enabled us to investigate IR injury in human organs and patients directly. Throughout the course of my work, I realised how beneficial such collaborations are. While my background is in genetic and mitochondrial research, collaborating with surgeons helped me to understand the complexity of medical research and the necessity to apply our *in vitro* research to *in vivo* models and to human patient studies.

Altogether, the work in this thesis has helped our understanding of the role of mitochondria in ischaemia reperfusion injury. This work will form the basis, for future projects. While some of this research has already contributed to publications, other findings shown here will have to be refined and further experiments performed before they can be published.

References

Akira, S., and Hemmi, H. (2003). Recognition of pathogen-associated molecular patterns by TLR family. Immunol. Lett. *85*, 85–95.

Akram, M. (2014). Citric Acid Cycle and Role of its Intermediates in Metabolism. Cell Biochem. Biophys. *68*, 475–478.

Alavian, K.N., Beutner, G., Lazrove, E., Sacchetti, S., Park, H.-A., Licznerski, P., Li, H., Nabili, P., Hockensmith, K., Graham, M., et al. (2014). An uncoupling channel within the c-subunit ring of the F1FO ATP synthase is the mitochondrial permeability transition pore. Proc. Natl. Acad. Sci. *111*, 10580–10585.

Alegre, M.-L., Goldstein, D.R., and Chong, A.S. (2008). Toll-like receptor signaling in transplantation: Curr. Opin. Organ Transplant. *13*, 358–365.

Andrienko, T.N., Pasdois, P., Pereira, G.C., Ovens, M.J., and Halestrap, A.P. (2017). The role of succinate and ROS in reperfusion injury – A critical appraisal. J. Mol. Cell. Cardiol. *110*, 1–14.

Ariza, A.C., Deen, P.M.T., and Robben, J.H. (2012). The succinate receptor as a novel therapeutic target for oxidative and metabolic stress-related conditions. Front. Endocrinol. *3*, 22.

Arnoult, D., Soares, F., Tattoli, I., and Girardin, S.E. (2011). Mitochondria in innate immunity. EMBO Rep. *12*, 901–910.

Baines, C.P., Kaiser, R.A., Purcell, N.H., Blair, N.S., Osinska, H., Hambleton, M.A., Brunskill, E.W., Sayen, M.R., Gottlieb, R.A., Dorn, G.W., et al. (2005). Loss of cyclophilin D reveals a critical role for mitochondrial permeability transition in cell death. Nature *434*, 658–662.

Bargehr, J., Ong, L.P., Colzani, M., Davaapil, H., Hofsteen, P., Bhandari, S., Gambardella, L., Le Novère, N., Iyer, D., Sampaziotis, F., et al. (2019). Epicardial cells derived from human embryonic stem cells augment cardiomyocyte-driven heart regeneration. Nat. Biotechnol. *37*, 895–906.

Barker, C.F., and Markmann, J.F. (2013). Historical Overview of Transplantation. Cold Spring Harb. Perspect. Med. *3*, a014977–a014977.

Bass, T.M., Grandison, R.C., Wong, R., Martinez, P., Partridge, L., and Piper, M.D.W. (2007). Optimization of Dietary Restriction Protocols in Drosophila. J. Gerontol. A. Biol. Sci. Med. Sci. *62*, 1071–1081.

Beck, S.J., Guo, L., Phensy, A., Tian, J., Wang, L., Tandon, N., Gauba, E., Lu, L., Pascual, J.M., Kroener, S., et al. (2016). Deregulation of mitochondrial F1FO-ATP synthase via OSCP in Alzheimer's disease. Nat. Commun. *7*, 11483.

Beecher, H.K. (2007). A Definition of Irreversible Coma: Int. Anesthesiol. Clin. *45*, 113–119.

Bełtowski, J. (2015). Hydrogen sulfide in pharmacology and medicine – An update. Pharmacol. Rep. *67*, 647–658.

Bernardi, P. (2018). Why F-ATP Synthase Remains a Strong Candidate as the Mitochondrial Permeability Transition Pore. Front. Physiol. *9*, 1543.

Bernardi, P., and Di Lisa, F. (2015). The mitochondrial permeability transition pore: molecular nature and role as a target in cardioprotection. J. Mol. Cell. Cardiol. *78*, 100–106.

Bernardi, P., and von Stockum, S. (2012). The permeability transition pore as a Ca2+ release channel: New answers to an old question. Cell Calcium *52*, 22–27.

Bernardi, P., Rasola, A., Forte, M., and Lippe, G. (2015). The Mitochondrial Permeability Transition Pore: Channel Formation by F-ATP Synthase, Integration in Signal Transduction, and Role in Pathophysiology. Physiol. Rev. *95*, 1111–1155.

Bickler, P.E., and Buck, L.T. (2007). Hypoxia Tolerance in Reptiles, Amphibians, and Fishes: Life with Variable Oxygen Availability. Annu. Rev. Physiol. *69*, 145–170.

Bond, M., Pitt, M., Akoh, J., Moxham, T., Hoyle, M., and Anderson, R. (2009). The effectiveness and cost-effectiveness of methods of storing donated kidneys from deceased donors: a systematic review and economic model. Health Technol. Assess. *13*.

Boros, P., and Bromberg, J.S. (2006). New Cellular and Molecular Immune Pathways in Ischemia/Reperfusion Injury: Pathways in Ischemia/Reperfusion Injury. Am. J. Transplant. *6*, 652–658.

Bowman, C.E., Rodriguez, S., Selen Alpergin, E.S., Acoba, M.G., Zhao, L., Hartung, T., Claypool, S.M., Watkins, P.A., and Wolfgang, M.J. (2017). The Mammalian Malonyl-CoA Synthetase ACSF3 Is Required for Mitochondrial Protein Malonylation and Metabolic Efficiency. Cell Chem. Biol. *24*, 673-684.e4.

Brealey, D., Brand, M., Hargreaves, I., Heales, S., Land, J., Smolenski, R., Davies, N.A., Cooper, C.E., and Singer, M. (2002). Association between mitochondrial dysfunction and severity and outcome of septic shock. The Lancet *360*, 219–223.

Briston, T., Roberts, M., Lewis, S., Powney, B., M. Staddon, J., Szabadkai, G., and Duchen, M.R. (2017). Mitochondrial permeability transition pore: sensitivity to opening and mechanistic dependence on substrate availability. Sci. Rep. *7*, 10492.

Brooks, C., Wei, Q., Cho, S.-G., and Dong, Z. (2009). Regulation of mitochondrial dynamics in acute kidney injury in cell culture and rodent models. J. Clin. Invest. *119*, 1275–1285.

Bruinsma, B.G., Sridharan, G.V., Weeder, P.D., Avruch, J.H., Saeidi, N., Özer, S., Geerts, S., Porte, R.J., Heger, M., van Gulik, T.M., et al. (2016). Metabolic profiling during ex vivo machine perfusion of the human liver. Sci. Rep. *6*, 22415.

Bundgaard, A., James, A.M., Gruszczyk, A.V., Martin, J., Murphy, M.P., and Fago, A. (2019). Metabolic adaptations during extreme anoxia in the turtle heart and their implications for ischemia-reperfusion injury. Sci. Rep. *9*, 2850.

Burnette, W.N. (1981). "Western Blotting": Electrophoretic transfer of proteins from sodium dodecyl sulfate-polyacrylamide gels to unmodified nitrocellulose and radiographic detection with antibody and radioiodinated protein A. Anal. Biochem. *112*, 195–203.

Campbell, C.T., Kolesar, J.E., and Kaufman, B.A. (2012). Mitochondrial transcription factor A regulates mitochondrial transcription initiation, DNA packaging, and genome copy number. Biochim. Biophys. Acta BBA - Gene Regul. Mech. *1819*, 921–929.

Cavaillé-Coll, M., Bala, S., Velidedeoglu, E., Hernandez, A., Archdeacon, P., Gonzalez, G., Neuland, C., Meyer, J., and Albrecht, R. (2013). Summary of FDA Workshop on Ischemia Reperfusion Injury in Kidney Transplantation: FDA IRI Workshop. Am. J. Transplant. *13*, 1134–1148.

Chandel, N.S. (2015). Evolution of Mitochondria as Signaling Organelles. Cell Metab. *22*, 204–206.

Chandel, N.S., Budinger, G.R.S., and Schumacker, P.T. (1996). Molecular Oxygen Modulates Cytochrome *c* Oxidase Function. J. Biol. Chem. *271*, 18672–18677.

Chen, R., Hu, Z., Chen, R.-L., Zhang, D., Xu, L., Wang, J., and Wei, L. (2015). Socioeconomic deprivation and survival after stroke in China: a systematic literature review and a new population-based cohort study. BMJ Open *5*, e005688–e005688.

Chiao, H., Kohda, Y., McLeroy, P., Craig, L., Housini, I., and Star, R.A. (1997). Alpha-melanocyte-stimulating hormone protects against renal injury after ischemia in mice and rats. J. Clin. Invest. *99*, 1165–1172.

Chiong, M., Wang, Z.V., Pedrozo, Z., Cao, D.J., Troncoso, R., Ibacache, M., Criollo, A., Nemchenko, A., Hill, J.A., and Lavandero, S. (2011). Cardiomyocyte death: mechanisms and translational implications. Cell Death Dis. *2*, e244–e244.

Chouchani, E.T., Pell, V.R., Gaude, E., Aksentijević, D., Sundier, S.Y., Robb, E.L., Logan, A., Nadtochiy, S.M., Ord, E.N.J., Smith, A.C., et al. (2014a). Ischaemic accumulation of succinate controls reperfusion injury through mitochondrial ROS. Nature *515*, 431–435.

Chouchani, E.T., Pell, V.R., Gaude, E., Aksentijević, D., Sundier, S.Y., Robb, E.L., Logan, A., Nadtochiy, S.M., Ord, E.N.J., Smith, A.C., et al. (2014b). Ischaemic accumulation of succinate controls reperfusion injury through mitochondrial ROS. Nature *515*, 431–435.

Chouchani, E.T., Pell, V.R., James, A.M., Work, L.M., Saeb-Parsy, K., Frezza, C., Krieg, T., and Murphy, M.P. (2016). A Unifying Mechanism for Mitochondrial Superoxide Production during Ischemia-Reperfusion Injury. Cell Metab. *23*, 254–263.

Citi, V., Piragine, E., Testai, L., Breschi, M.C., Calderone, V., and Martelli, A. (2018). The Role of Hydrogen Sulfide and H2S-donors in Myocardial Protection Against Ischemia/Reperfusion Injury. Curr. Med. Chem. *25*, 4380–4401.

Collins, L.V., Hajizadeh, S., Holme, E., Jonsson, I., and Tarkowski, A. (2004). Endogenously oxidized mitochondrial DNA induces in vivo and in vitro inflammatory responses. J. Leukoc. Biol. *75*, 995–1000.

Collins, Y., Chouchani, E.T., James, A.M., Menger, K.E., Cochemé, H.M., and Murphy, M.P. (2012). Mitochondrial redox signalling at a glance. J. Cell Sci. *125*, 801–806.

Corry, R.J., Winn, H.J., and Russell, P.S. (1973). PRIMARILY VASCULARIZED ALLOGRAFTS OF HEARTS IN MICE: THE ROLE OF H-2D, H-2K, AND NON-H-2 ANTIGENS IN REJECTION. Transplantation *16*, 343–350.

Cortés-Campos, C., Elizondo, R., Llanos, P., Uranga, R.M., Nualart, F., and García, M.A. (2011). MCT Expression and Lactate Influx/Efflux in Tanycytes Involved in Glia-Neuron Metabolic Interaction. PLoS ONE *6*, e16411.

Dare, A.J., Logan, A., Prime, T.A., Rogatti, S., Goddard, M., Bolton, E.M., Bradley, J.A., Pettigrew, G.J., Murphy, M.P., and Saeb-Parsy, K. (2015). The mitochondria-targeted anti-oxidant MitoQ decreases ischemia-reperfusion injury in a murine syngeneic heart transplant model. J. Heart Lung Transplant. *34*, 1471–1480.

Di Meo, S., Reed, T.T., Venditti, P., and Victor, V.M. (2016). Role of ROS and RNS Sources in Physiological and Pathological Conditions. Oxid. Med. Cell. Longev. *2016*, 1–44.

Diwan, A., Wansapura, J., Syed, F.M., Matkovich, S.J., Lorenz, J.N., and Dorn, G.W. (2008). Nix-Mediated Apoptosis Links Myocardial Fibrosis, Cardiac Remodeling, and Hypertrophy Decompensation. Circulation *117*, 396–404.

Dorn, G.W. (2008). Apoptotic and non-apoptotic programmed cardiomyocyte death in ventricular remodelling. Cardiovasc. Res. *81*, 465–473.

Downey, J.M., Davis, A.M., and Cohen, M.V. (2007). Signaling pathways in ischemic preconditioning. Heart Fail. Rev. *12*, 181–188.

D'Souza, A.R., and Minczuk, M. (2018). Mitochondrial transcription and translation: overview. Essays Biochem. *62*, 309–320.

Eefting, F. (2004). Role of apoptosis in reperfusion injury. Cardiovasc. Res. *61*, 414–426.

Eltzschig, H.K., and Collard, C.D. (2004). Vascular ischaemia and reperfusion injury. Br. Med. Bull. *70*, 71–86.

Eltzschig, H.K., and Eckle, T. (2011). Ischemia and reperfusion—from mechanism to translation. Nat. Med. *17*, 1391–1401.

Farahani, R., and Haddad, G.G. (2003). Understanding the molecular responses to hypoxia using Drosophila as a genetic model. Respir. Physiol. Neurobiol. *135*, 221–229.

Fearnley, C.J., Roderick, H.L., and Bootman, M.D. (2011). Calcium Signaling in Cardiac Myocytes. Cold Spring Harb. Perspect. Biol. *3*, a004242–a004242.

Ferrigno, A., Di Pasqua, L., Berardo, C., Siciliano, V., Rizzo, V., Mannucci, B., Richelmi, P., Croce, A., and Vairetti, M. (2017). Liver Graft Susceptibility during Static Cold Storage and Dynamic Machine Perfusion: DCD versus Fatty Livers. Int. J. Mol. Sci. *19*, 109.

Filipovic, M.R. (2015). Persulfidation (S-sulfhydration) and H2S. In Chemistry, Biochemistry and Pharmacology of Hydrogen Sulfide, P.K. Moore, and M. Whiteman, eds. (Cham: Springer International Publishing), pp. 29–59.

Fink, S.L., and Cookson, B.T. (2005). Apoptosis, pyroptosis, and necrosis: mechanistic description of dead and dying eukaryotic cells. Infect. Immun. *73*, 1907–1916.

Finkel, T. (2012). Signal Transduction by Mitochondrial Oxidants. J. Biol. Chem. *287*, 4434–4440.

Frey, T.G., and Mannella, C.A. (2000). The internal structure of mitochondria. Trends Biochem. Sci. *25*, 319–324.

Galluzzi, L., Vitale, I., Abrams, J.M., Alnemri, E.S., Baehrecke, E.H., Blagosklonny, M.V., Dawson, T.M., Dawson, V.L., El-Deiry, W.S., Fulda, S., et al. (2012). Molecular definitions of cell death subroutines: recommendations of the Nomenclature Committee on Cell Death 2012. Cell Death Differ. *19*, 107–120.

Gan, L., Chen, X., Sun, T., Li, Q., Zhang, R., Zhang, J., and Zhong, J. (2015). Significance of Serum mtdna Concentration in Lung Injury Induced by Hip Fracture. Shock *44*, 52–57.

Gao, Y., Xu, W., Dou, X., Wang, H., Zhang, X., Yang, S., Liao, H., Hu, X., and Wang, H. (2019). Mitochondrial DNA Leakage Caused by Streptococcus pneumoniae Hydrogen Peroxide Promotes Type I IFN Expression in Lung Cells. Front. Microbiol. *10*, 630.

García, N., and Chávez, E. (2007). Mitochondrial DNA fragments released through the permeability transition pore correspond to specific gene size. Life Sci. *81*, 1160–1166.

García, N., García, J.J., Correa, F., and Chávez, E. (2005). The permeability transition pore as a pathway for the release of mitochondrial DNA. Life Sci. *76*, 2873–2880.

Goldberg, I.J., Trent, C.M., and Schulze, P.C. (2012). Lipid Metabolism and Toxicity in the Heart. Cell Metab. *15*, 805–812.

Gottlieb, R.A. (2011). Cell Death Pathways in Acute Ischemia/Reperfusion Injury. J. Cardiovasc. Pharmacol. Ther. *16*, 233–238.

Graham, E.L., Balla, C., Franchino, H., Melman, Y., del Monte, F., and Das, S. (2013). Isolation, Culture, and Functional Characterization of Adult Mouse Cardiomyoctyes. J. Vis. Exp. 50289.

Gray, M.W. (2012). Mitochondrial Evolution. Cold Spring Harb. Perspect. Biol. *4*, a011403–a011403.

Great Britain, and Department of Health & Social Care (2018). NHS Blood and Transplant Annual Report and Accounts 2017-18.

Green, D.R. (2004). The Pathophysiology of Mitochondrial Cell Death. Science *305*, 626–629.

Groß, C.J., Mishra, R., Schneider, K.S., Médard, G., Wettmarshausen, J., Dittlein, D.C., Shi, H., Gorka, O., Koenig, P.-A., Fromm, S., et al. (2016). K + Efflux-Independent NLRP3 Inflammasome Activation by Small Molecules Targeting Mitochondria. Immunity *45*, 761–773.

Grynberg, A., and Demaison, L. (1996). Fatty Acid Oxidation in the Heart: J. Cardiovasc. Pharmacol. *28*, 11–17.

Gürtl, B., Kratky, D., Guelly, C., Zhang, L., Gorkiewicz, G., Das, S.K., Tamilarasan, K.P., and Hoefler, G. (2009). Apoptosis and fibrosis are early features of heart failure in an animal model of metabolic cardiomyopathy: Animal model of metabolic cardiomyopathy. Int. J. Exp. Pathol. *90*, 338–346.

Halestrap, A. (2004). Mitochondrial permeability transition pore opening during myocardial reperfusion—a target for cardioprotection. Cardiovasc. Res. *61*, 372–385.

Halestrap, A.P., and Meredith, D. (2004). The SLC16 gene family from monocarboxylate transporters (MCTs) to aromatic amino acid transporters and beyond. Pfl□gers Arch. Eur. J. Physiol. *447*, 619–628.

Halestrap, A.P., and Price, N.T. (1999). The proton-linked monocarboxylate transporter (MCT) family: structure, function and regulation. Biochem. J. *343 Pt 2*, 281–299.

Halestrap, A.P., and Wilson, M.C. (2012). The monocarboxylate transporter family-Role and regulation. IUBMB Life *64*, 109–119.

Hanson, M.A., Hamilton, P.T., and Perlman, S.J. (2016). Immune genes and divergent antimicrobial peptides in flies of the subgenus Drosophila. BMC Evol. Biol. *16*, 228.

Harper, S.J.F., Hosgood, S.A., Waller, H.L., Yang, B., Kay, M.D., Goncalves, I., and Nicholson, M.L. (2008). The Effect of Warm Ischemic Time on Renal Function and Injury in the Isolated Hemoperfused Kidney: Transplantation *86*, 445–451.

Harrington, J.S., Huh, J.-W., Schenck, E.J., Nakahira, K., Siempos, I.I., and Choi, A.M.K. (2019). Circulating Mitochondrial DNA as Predictor of Mortality in Critically Ill Patients. Chest *156*, 1120–1136.

Hausenloy, D., Boston-Griffiths, E., and Yellon, D. (2012). Cyclosporin A and cardioprotection: from investigative tool to therapeutic agent: CsA and cardioprotection. Br. J. Pharmacol. *165*, 1235–1245.

He, Y., Hara, H., and Núñez, G. (2016). Mechanism and Regulation of NLRP3 Inflammasome Activation. Trends Biochem. Sci. *41*, 1012–1021.

Hessheimer, A.J., Billault, C., Barrou, B., and Fondevila, C. (2015). Hypothermic or normothermic abdominal regional perfusion in high-risk donors with extended warm ischemia times: impact on outcomes? Transpl. Int. *28*, 700–707.

Hinchy, E.C., Gruszczyk, A.V., Willows, R., Navaratnam, N., Hall, A.R., Bates, G., Bright, T.P., Krieg, T., Carling, D., and Murphy, M.P. (2018). Mitochondria-derived ROS activate AMP-activated protein kinase (AMPK) indirectly. J. Biol. Chem. *293*, 17208–17217.

Hodgson, R., Young, A.L., Attia, M.A., and Lodge, J.P.A. (2017). Impact of a National Controlled Donation After Circulatory Death (DCD) Program on Organ Donation in the United Kingdom: A 10-Year Study. Am. J. Transplant. *17*, 3172–3182.

Holmström, K.M., and Finkel, T. (2014). Cellular mechanisms and physiological consequences of redox-dependent signalling. Nat. Rev. Mol. Cell Biol. *15*, 411–421.

Honda, H.M., Korge, P., and Weiss, J.N. (2005). Mitochondria and Ischemia/Reperfusion Injury. Ann. N. Y. Acad. Sci. *1047*, 248–258.

Horton, K.L., Stewart, K.M., Fonseca, S.B., Guo, Q., and Kelley, S.O. (2008). Mitochondria-Penetrating Peptides. Chem. Biol. *15*, 375–382.

Hosgood, S.A., and Nicholson, M.L. (2010). The Role of Perfluorocarbon in Organ Preservation: Transplantation *89*, 1169–1175.

Hosgood, S.A., Mohamed, I.H., Bagul, A., and Nicholson, M.L. (2011). Hypothermic machine perfusion after static cold storage does not improve the preservation condition in an experimental porcine kidney model. Br. J. Surg. *98*, 943–950.

Hosgood, S.A., Hunter, J.P., and Nicholson, M.L. (2012). Early Urinary Biomarkers of Warm and Cold Ischemic Injury in an Experimental Kidney Model. J. Surg. Res. *174*, e85–e90.

Hosgood, S.A., Shah, K., Patel, M., and Nicholson, M.L. (2015). The effect of prolonged of warm ischaemic injury on renal function in an experimental ex vivo normothermic perfusion system. J. Transl. Med. *13*, 207.

Houten, S.M., and Wanders, R.J.A. (2010). A general introduction to the biochemistry of mitochondrial fatty acid β-oxidation. J. Inherit. Metab. Dis. *33*, 469–477.

Hu, Q., Ren, H., Ren, J., Liu, Q., Wu, J., Wu, X., Li, G., Wang, G., Gu, G., Guo, K., et al. (2018). Released Mitochondrial DNA Following Intestinal Ischemia Reperfusion Induces the Inflammatory Response and Gut Barrier Dysfunction. Sci. Rep. *8*, 7350.

Iliodromitis, E.K., Lazou, A., and Kremastinos, D.T. (2007). Ischemic preconditioning: protection against myocardial necrosis and apoptosis. Vasc. Health Risk Manag. *3*, 629–637.

Jackson, D.C., and Heisler, N. (1982). Plasma ion balance of submerged anoxic turtles at 3°C: The role of calcium lactate formation. Respir. Physiol. *49*, 159–174.

Jackson, D.C., Taylor, S.E., Asare, V.S., Villarnovo, D., Gall, J.M., and Reese, S.A. (2007). Comparative shell buffering properties correlate with anoxia tolerance in freshwater turtles. Am. J. Physiol.-Regul. Integr. Comp. Physiol. *292*, R1008–R1015.

Jardim-Messeder, D., Caverzan, A., Rauber, R., de Souza Ferreira, E., Margis-Pinheiro, M., and Galina, A. (2015). Succinate dehydrogenase (mitochondrial complex II) is a source of

reactive oxygen species in plants and regulates development and stress responses. New Phytol. *208*, 776–789.

Jochmans, I., Meurisse, N., Neyrinck, A., Verhaegen, M., Monbaliu, D., and Pirenne, J. (2017). Hepatic ischemia/reperfusion injury associates with acute kidney injury in liver transplantation: Prospective cohort study: Jochmans et al. Liver Transpl. *23*, 634–644.

Kane, A.B., Petrovich, D.R., Stern, R.O., and Farber, J.L. (1985). ATP depletion and loss of cell integrity in anoxic hepatocytes and silica-treated P388D1 macrophages. Am. J. Physiol.-Cell Physiol. *249*, C256–C266.

Kang, P., Liu, Y., Zhu, H., Zhang, J., Shi, H., Li, S., Pi, D., Leng, W., Wang, X., Wu, H., et al. (2018). The effect of dietary asparagine supplementation on energy metabolism in liver of weaning pigs when challenged with lipopolysaccharide. Asian-Australas. J. Anim. Sci. *31*, 548–555.

Kanneganti, T.-D., Kundu, M., and Green, D.R. (2015). Innate Immune Recognition of mtDNA—An Undercover Signal? Cell Metab. *21*, 793–794.

Karch, J., and Molkentin, J.D. (2014). Identifying the components of the elusive mitochondrial permeability transition pore. Proc. Natl. Acad. Sci. *111*, 10396–10397.

Karmazyn, M. (1999). [No title found]. J. Thromb. Thrombolysis *8*, 33–38.

Kausar, S., Yang, L., Abbas, M.N., Hu, X., Zhao, Y., Zhu, Y., and Cui, H. (2020). Mitochondrial DNA: A Key Regulator of Anti-Microbial Innate Immunity. Genes *11*, 86.

Kay, M.D., Hosgood, S.A., Harper, S.J.F., Bagul, A., Waller, H.L., and Nicholson, M.L. (2011). Normothermic Versus Hypothermic Ex Vivo Flush Using a Novel Phosphate-Free Preservation Solution (AQIX) in Porcine Kidneys. J. Surg. Res. *171*, 275–282.

Kim, J., Gupta, R., Blanco, L.P., Yang, S., Shteinfer-Kuzmine, A., Wang, K., Zhu, J., Yoon, H.E., Wang, X., Kerkhofs, M., et al. (2019). VDAC oligomers form mitochondrial pores to release mtDNA fragments and promote lupus-like disease. Science *366*, 1531–1536.

Kohlhauer, M., Dawkins, S., Costa, A.S.H., Lee, R., Young, T., Pell, V.R., Choudhury, R.P., Banning, A.P., Kharbanda, R.K., Oxford Acute Myocardial Infarction (OxAMI) Study, et al. (2018). Metabolomic Profiling in Acute ST-Segment–Elevation Myocardial Infarction Identifies Succinate as an Early Marker of Human Ischemia–Reperfusion Injury. J. Am. Heart Assoc. *7*.

Kohlhauer, M., Pell, V.R., Burger, N., Spiroski, A.M., Gruszczyk, A., Mulvey, J.F., Mottahedin, A., Costa, A.S.H., Frezza, C., Ghaleb, B., et al. (2019). Protection against cardiac ischemia-reperfusion injury by hypothermia and by inhibition of succinate accumulation and oxidation is additive. Basic Res. Cardiol. *114*, 18.

Krysko, D.V., Vanden Berghe, T., D'Herde, K., and Vandenabeele, P. (2008). Apoptosis and necrosis: Detection, discrimination and phagocytosis. Methods *44*, 205–221.

Kuznetsov, A.V., Schneeberger, S., Seiler, R., Brandacher, G., Mark, W., Steurer, W., Saks, V., Usson, Y., Margreiter, R., and Gnaiger, E. (2004). Mitochondrial defects and heterogeneous

cytochrome *c* release after cardiac cold ischemia and reperfusion. Am. J. Physiol.-Heart Circ. Physiol. *286*, H1633–H1641.

Kwong, J.Q., and Molkentin, J.D. (2015). Physiological and pathological roles of the mitochondrial permeability transition pore in the heart. Cell Metab. *21*, 206–214.

L, L., and X, W. (2016). Ischemia-reperfusion Injury in the Brain: Mechanisms and Potential Therapeutic Strategies. Biochem. Pharmacol. Open Access *5*.

Land, W., Schneeberger, H., Schleibner, S., Illner, W.-D., Abendroth, D., Rutili, G., Arfors, K.E., and Messmer, K. (1994). THE BENEFICIAL EFFECT OF HUMAN RECOMBINANT SUPEROXIDE DISMUTASE ON ACUTE AND CHRONIC REJECTION EVENTS IN RECIPIENTS OF CADAVERIC RENAL TRANSPLANTS: Transplantation *57*, 211–217.

Lane, N., and Martin, W. (2010). The energetics of genome complexity. Nature *467*, 929–934.

Large, S., Tsui, S., and Messer, S. (2017). Clinical and ethical challenges in heart transplantation from donation after circulatory determined death donors: Curr. Opin. Organ Transplant. *22*, 251–259.

Latorre-Pellicer, A., Moreno-Loshuertos, R., Lechuga-Vieco, A.V., Sánchez-Cabo, F., Torroja, C., Acín-Pérez, R., Calvo, E., Aix, E., González-Guerra, A., Logan, A., et al. (2016). Mitochondrial and nuclear DNA matching shapes metabolism and healthy ageing. Nature *535*, 561–565.

Leemkuil, M., Lier, G., Engelse, M.A., Ploeg, R.J., de Koning, E.J.P., 't Hart, N.A., Krikke, C., and Leuvenink, H.G.D. (2018). Hypothermic Oxygenated Machine Perfusion of the Human Donor Pancreas: Transplant. Direct *4*, e388.

Lemasters, J.J., Theruvath, T.P., Zhong, Z., and Nieminen, A.-L. (2009). Mitochondrial calcium and the permeability transition in cell death. Biochim. Biophys. Acta BBA - Bioenerg. *1787*, 1395–1401.

Li, D., Wu, J., Bai, Y., Zhao, X., and Liu, L. (2014). Isolation and Culture of Adult Mouse Cardiomyocytes for Cell Signaling and in vitro Cardiac Hypertrophy. J. Vis. Exp. 51357.

Li, H., Satriano, J., Thomas, J.L., Miyamoto, S., Sharma, K., Pastor-Soler, N.M., Hallows, K.R., and Singh, P. (2015). Interactions between HIF-1α and AMPK in the regulation of cellular hypoxia adaptation in chronic kidney disease. Am. J. Physiol.-Ren. Physiol. *309*, F414–F428.

Li, S., Hu, Q., Huang, J., Wu, X., and Ren, J. (2019). Mitochondria-Derived Damage-Associated Molecular Patterns in Sepsis: From Bench to Bedside. Oxid. Med. Cell. Longev. *2019*, 1–9.

Lindberg, B., and Hansen, K. (1967). Some Properties of Partially Purified Mammalian Adenosine Kinase. 8.

Liu, S., Feng, M., and Guan, W. (2016a). Mitochondrial DNA sensing by STING signaling participates in inflammation, cancer and beyond: mtDNA in inflammation, cancer and beyond. Int. J. Cancer *139*, 736–741.

Liu, X., Jie, C., Zhang, Z., Yan, S., Wang, J.-J., Wang, X., Kurian, S., Salomon, D.R., Abecassis, M., and Hummel, M. (2016b). Transplant-induced reactivation of murine cytomegalovirus immediate early gene expression is associated with recruitment of NF-κB and AP-1 to the major immediate early promoter. J. Gen. Virol. *97*, 941–954.

Lochner, A. (1978). Mitochondrial oxidative phosphorylation in low-flow hypoxia: Role of free fatty acids. J. Mol. Cell. Cardiol. *10*, 857–875.

Lochner, A., Kotzé, J.C.N., Gevers, W., and Benade, A.J.S. (1979). Substrate effects on mitochondrial function and tissue lipids in low-flow hypoxia of isolated perfused rat hearts. Basic Res. Cardiol. *74*, 303–312.

Luongo, T.S., Lambert, J.P., Yuan, A., Zhang, X., Gross, P., Song, J., Shanmughapriya, S., Gao, E., Jain, M., Houser, S.R., et al. (2015). The Mitochondrial Calcium Uniporter Matches Energetic Supply with Cardiac Workload during Stress and Modulates Permeability Transition. Cell Rep. *12*, 23–34.

Maekawa, H., Inoue, T., Ouchi, H., Jao, T.-M., Inoue, R., Nishi, H., Fujii, R., Ishidate, F., Tanaka, T., Tanaka, Y., et al. (2019). Mitochondrial Damage Causes Inflammation via cGAS-STING Signaling in Acute Kidney Injury. Cell Rep. *29*, 1261-1273.e6.

Maida, K., Akamatsu, Y., Hara, Y., Tokodai, K., Miyagi, S., Kashiwadate, T., Miyazawa, K., Kawagishi, N., and Ohuchi, N. (2016). Short Oxygenated Warm Perfusion With Prostaglandin E1 Administration Before Cold Preservation as a Novel Resuscitation Method for Liver Grafts From Donors After Cardiac Death in a Rat In Vivo Model: Transplantation *100*, 1052–1058.

Marí, M., Morales, A., Colell, A., García-Ruiz, C., and Fernández-Checa, J.C. (2009). Mitochondrial Glutathione, a Key Survival Antioxidant. Antioxid. Redox Signal. *11*, 2685–2700.

Martin, J.L., Costa, A.S.H., Gruszczyk, A.V., Beach, T.E., Allen, F.M., Prag, H.A., Hinchy, E.C., Mahbubani, K., Hamed, M., Tronci, L., et al. (2019). Succinate accumulation drives ischaemia-reperfusion injury during organ transplantation. Nat. Metab. *1*, 966–974.

Matesanz, R., Coll, E., Domínguez-Gil, B., de la Rosa, G., Marazuela, R., Arráez, V., Elorrieta, P., Fernández-García, A., Fernández-Renedo, C., Galán, J., et al. (2012). Benchmarking in the Process of Donation After Brain Death: A Methodology to Identify Best Performer Hospitals: Benchmarking in Donation After Brain Death. Am. J. Transplant. *12*, 2498–2506.

McArthur, K., Whitehead, L.W., Heddleston, J.M., Li, L., Padman, B.S., Oorschot, V., Geoghegan, N.D., Chappaz, S., Davidson, S., San Chin, H., et al. (2018). BAK/BAX macropores facilitate mitochondrial herniation and mtDNA efflux during apoptosis. Science *359*, eaao6047.

McDougal, A.D., and Dewey, C.F. (2017). Modeling oxygen requirements in ischemic cardiomyocytes. J. Biol. Chem. *292*, 11760–11776.

Merrill, J.P. (1956). SUCCESSFUL HOMOTRANSPLANTATION OF THE HUMAN KIDNEY BETWEEN IDENTICAL TWINS. J. Am. Med. Assoc. *160*, 277.

Methner, C., Chouchani, E.T., Buonincontri, G., Pell, V.R., Sawiak, S.J., Murphy, M.P., and Krieg, T. (2014). Mitochondria selective *S* -nitrosation by mitochondria-targeted *S* -nitrosothiol protects against post-infarct heart failure in mouse hearts: MitoSNO protects from post-infarct heart failure. Eur. J. Heart Fail. *16*, 712–717.

Mills, E.L., Kelly, B., Logan, A., Costa, A.S.H., Varma, M., Bryant, C.E., Tourlomousis, P., Däbritz, J.H.M., Gottlieb, E., Latorre, I., et al. (2016). Succinate Dehydrogenase Supports Metabolic Repurposing of Mitochondria to Drive Inflammatory Macrophages. Cell *167*, 457-470.e13.

Mills, E.L., Kelly, B., and O'Neill, L.A.J. (2017). Mitochondria are the powerhouses of immunity. Nat. Immunol. *18*, 488–498.

Mitchell, P. (1961). Coupling of Phosphorylation to Electron and Hydrogen Transfer by a Chemi-Osmotic type of Mechanism. Nature *191*, 144–148.

Monbaliu, D., Vekemans, K., Hoekstra, H., Vaahtera, L., Libbrecht, L., Derveaux, K., Parkkinen, J., Liu, Q., Heedfeld, V., Wylin, T., et al. (2009). Multifactorial Biological Modulation of Warm Ischemia Reperfusion Injury in Liver Transplantation From Non–Heart-Beating Donors Eliminates Primary Nonfunction and Reduces Bile Salt Toxicity: Ann. Surg. *250*, 808–817.

Morris, P.J. (2004). Transplantation — A Medical Miracle of the 20th Century. N. Engl. J. Med. *351*, 2678–2680.

Mowery, P.C., Steenkamp, D.J., Ackrell, B.A.C., Singer, T.P., and White, G.A. (1977). Inhibition of mammalian succinate dehydrogenase by carboxins. Arch. Biochem. Biophys. *178*, 495–506.

Murphy, M.P. (2009). How mitochondria produce reactive oxygen species. Biochem. J. *417*, 1–13.

Murphy, M.P. (2016). Understanding and preventing mitochondrial oxidative damage. Biochem. Soc. Trans. *44*, 1219–1226.

Murphy, E., and Steenbergen, C. (2008). Mechanisms Underlying Acute Protection From Cardiac Ischemia-Reperfusion Injury. Physiol. Rev. *88*, 581–609.

Murry, C.E., Jennings, R.B., and Reimer, K.A. (1986). Preconditioning with ischemia: a delay of lethal cell injury in ischemic myocardium. Circulation *74*, 1124–1136.

Nagata, S. (2018). Apoptosis and Clearance of Apoptotic Cells. Annu. Rev. Immunol. *36*, 489–517.

Nakagawa, T., Shimizu, S., Watanabe, T., Yamaguchi, O., Otsu, K., Yamagata, H., Inohara, H., Kubo, T., and Tsujimoto, Y. (2005). Cyclophilin D-dependent mitochondrial permeability transition regulates some necrotic but not apoptotic cell death. Nature *434*, 652–658.

Nakahira, K., Kyung, S.Y., Rogers, A.J., Gazourian, L., Youn, S., Massaro, A.F., Quintana, C., Osorio, J.C., Wang, Z., Zhao, Y., et al. (2013). Circulating Mitochondrial DNA in Patients in the ICU as a Marker of Mortality: Derivation and Validation. PLoS Med. *10*, 1–12.

Nelson, K.K., and Melendez, J.A. (2004). Mitochondrial redox control of matrix metalloproteinases. Free Radic. Biol. Med. *37*, 768–784.

NHS Blood and Transplant (2015a). Annual report on cardiothoracic transplantation. *2015*, 131–131.

NHS Blood and Transplant (2015b). Organ Donation and Transplantation Activitity Report. Glob. Obs. Donation Transplant. GODT.

Nicholls, D.G., and Crompton, M. (1980). Mitochondrial calcium transport. FEBS Lett. *111*, 261–268.

Nicholls, D.G., and Ferguson, S.J. (2013). Bioenergetics (Amsterdam: Academic Press, Elsevier).

Nighoghossian, N., Ovize, M., Mewton, N., Ong, E., and Cho, T.-H. (2016). Cyclosporine A, a Potential Therapy of Ischemic Reperfusion Injury. A Common History for Heart and Brain. Cerebrovasc. Dis. *42*, 309–318.

O'Callaghan, J.M., Knight, S.R., Morgan, R.D., and Morris, P.J. (2012). Preservation Solutions for Static Cold Storage of Kidney Allografts: A Systematic Review and Meta-Analysis: Preservation Solutions for Kidney Allografts. Am. J. Transplant. *12*, 896–906.

Oka, T., Hikoso, S., Yamaguchi, O., Taneike, M., Takeda, T., Tamai, T., Oyabu, J., Murakawa, T., Nakayama, H., Nishida, K., et al. (2012). Mitochondrial DNA that escapes from autophagy causes inflammation and heart failure. Nature *485*, 251–255.

O'Neill, L.A.J., Bryant, C.E., and Doyle, S.L. (2009). Therapeutic Targeting of Toll-Like Receptors for Infectious and Inflammatory Diseases and Cancer. Pharmacol. Rev. *61*, 177–197.

Ong, S.-B., Samangouei, P., Kalkhoran, S.B., and Hausenloy, D.J. (2015). The mitochondrial permeability transition pore and its role in myocardial ischemia reperfusion injury. J. Mol. Cell. Cardiol. *78*, 23–34.

Opelz, G., and D??hler, B. (2007). Multicenter Analysis of Kidney Preservation: Transplantation *83*, 247–253.

Orogo, A.M., and Gustafsson, Å.B. (2013). Cell death in the myocardium: My heart won't go on: Cell Death in the Myocardium. IUBMB Life *65*, 651–656.

Pan, X., Liu, J., Nguyen, T., Liu, C., Sun, J., Teng, Y., Fergusson, M.M., Rovira, I.I., Allen, M., Springer, D.A., et al. (2013). The physiological role of mitochondrial calcium revealed by mice lacking the mitochondrial calcium uniporter. Nat. Cell Biol. *15*, 1464–1472.

Pegg, D.E., Calne, R.Y., Pryse-davies, J., and Brown, F.L. (2006). canine renal preservation using surface and perfusion cooling techniques*. Ann. N. Y. Acad. Sci. *120*, 506–523.

Pell, V.R., Spiroski, A.-M., Mulvey, J., Burger, N., Costa, A.S.H., Logan, A., Gruszczyk, A.V., Rosa, T., James, A.M., Frezza, C., et al. (2018). Ischemic preconditioning protects against

cardiac ischemia reperfusion injury without affecting succinate accumulation or oxidation. J. Mol. Cell. Cardiol. *123*, 88–91.

Perico, N., Cattaneo, D., Sayegh, M.H., and Remuzzi, G. (2004). Delayed graft function in kidney transplantation. The Lancet *364*, 1814–1827.

Pickard, J.M.J., Burke, N., Davidson, S.M., and Yellon, D.M. (2017). Intrinsic cardiac ganglia and acetylcholine are important in the mechanism of ischaemic preconditioning. Basic Res. Cardiol. *112*, 11.

Pinti, M., Cevenini, E., Nasi, M., De Biasi, S., Salvioli, S., Monti, D., Benatti, S., Gibellini, L., Cotichini, R., Stazi, M.A., et al. (2014). Circulating mitochondrial DNA increases with age and is a familiar trait: Implications for "inflamm-aging": Innate immunity. Eur. J. Immunol. *44*, 1552–1562.

Pinton, P., Giorgi, C., Siviero, R., Zecchini, E., and Rizzuto, R. (2008). Calcium and apoptosis: ER-mitochondria Ca2+ transfer in the control of apoptosis. Oncogene *27*, 6407–6418.

Piper, H.M., Siegmund, B., Ladilov, Yu.V., and Schl□ter, K.-D. (1993). Calcium and sodium control in hypoxic-reoxygenated cardiomyocytes. Basic Res. Cardiol. *88*, 471–482.

Planker, M., Schnurr, E., and Schneider, W. (1983). Elevated ATP levels in the red cells of patients with renal failure. Klin. Wochenschr. *61*, 709–713.

Prime, T.A., Blaikie, F.H., Evans, C., Nadtochiy, S.M., James, A.M., Dahm, C.C., Vitturi, D.A., Patel, R.P., Hiley, C.R., Abakumova, I., et al. (2009). A mitochondria-targeted S-nitrosothiol modulates respiration, nitrosates thiols, and protects against ischemia-reperfusion injury. Proc. Natl. Acad. Sci. *106*, 10764–10769.

Pryde, K.R., and Hirst, J. (2011). Superoxide is produced by the reduced flavin in mitochondrial complex I: A single, unified mechanism that applies during both forward and reverse electron transfer. J. Biol. Chem. *286*, 18056–18065.

Quinlan, C.L., Perevoschikova, I.V., Goncalves, R.L.S., Hey-Mogensen, M., and Brand, M.D. (2013). The Determination and Analysis of Site-Specific Rates of Mitochondrial Reactive Oxygen Species Production. In Methods in Enzymology, (Elsevier), pp. 189–217.

Ren, J., Sherry, A.D., and Malloy, C.R. (2015). ^{31} P-MRS of healthy human brain: ATP synthesis, metabolite concentrations, pH, and T_1 relaxation times: BRAIN ATP SYNTHESIS BY BAND INVERSION TRANSFER. NMR Biomed. *28*, 1455–1462.

Riley, J.S., Quarato, G., Cloix, C., Lopez, J., O'Prey, J., Pearson, M., Chapman, J., Sesaki, H., Carlin, L.M., Passos, J.F., et al. (2018). Mitochondrial inner membrane permeabilisation enables mt DNA release during apoptosis. EMBO J. *37*.

Robb, E.L., Gawel, J.M., Aksentijević, D., Cochemé, H.M., Stewart, T.S., Shchepinova, M.M., Qiang, H., Prime, T.A., Bright, T.P., James, A.M., et al. (2015). Selective superoxide generation within mitochondria by the targeted redox cycler MitoParaquat. Free Radic. Biol. Med. *89*, 883–894.

Röhrig, F., and Schulze, A. (2016). The multifaceted roles of fatty acid synthesis in cancer. Nat. Rev. Cancer *16*, 732–749.

Roth, G.M., Bader, D.M., and Pfaltzgraff, E.R. (2014). Isolation and Physiological Analysis of Mouse Cardiomyocytes. J. Vis. Exp. 51109.

Rottenberg, H., and Hoek, J.B. (2017). The path from mitochondrial ROS to aging runs through the mitochondrial permeability transition pore. Aging Cell *16*, 943–955.

Salehi, A. (2004). Effects of ghrelin on insulin and glucagon secretion: a study of isolated pancreatic islets and intact mice. Regul. Pept. *118*, 143–150.

Sazanov, L.A. (2015). A giant molecular proton pump: structure and mechanism of respiratory complex I. Nat. Rev. Mol. Cell Biol. *16*, 375–388.

Scallet, A.C., Haley, R.L., Scallet, D.M., Duhart, H.M., and Binienda, Z.K. (2003). 3-Nitropropionic Acid Inhibition of Succinate Dehydrogenase (Complex II) Activity in Cultured Chinese Hamster Ovary Cells. Ann. N. Y. Acad. Sci. *993*, 305–312.

Schott, R.J., Rohmann, S., Braun, E.R., and Schaper, W. (1990). Ischemic preconditioning reduces infarct size in swine myocardium. Circ. Res. *66*, 1133–1142.

Schultz, V., Sussman, I., Bokvist, K., and Tornheim, K. (1993). Bioluminometric Assay of ADP and ATP at High ATP/ADP Ratios: Assay of ADP After Enzymatic Removal of ATP. Anal. Biochem. *215*, 302–304.

Schwartz, W. (1982). L. Margulis, Symbiosis in Cell Evolution. Life and its Environment on the Early Earth. XXII + 479 S., 104 Abb., 59 Tab. San Francisco 1981. W. H. Freeman and Co. £ 16.40 (Board), £ 9.20 (Paper). Z. Für Allg. Mikrobiol. *22*, 427–427.

Seong, S.-Y., and Matzinger, P. (2004). Hydrophobicity: an ancient damage-associated molecular pattern that initiates innate immune responses. Nat. Rev. Immunol. *4*, 469–478.

Shimada, K., Crother, T.R., Karlin, J., Dagvadorj, J., Chiba, N., Chen, S., Ramanujan, V.K., Wolf, A.J., Vergnes, L., Ojcius, D.M., et al. (2012). Oxidized Mitochondrial DNA Activates the NLRP3 Inflammasome during Apoptosis. Immunity *36*, 401–414.

Smith, R.A.J., and Murphy, M.P. (2010). Animal and human studies with the mitochondria-targeted antioxidant MitoQ: Smith and Murphy. Ann. N. Y. Acad. Sci. *1201*, 96–103.

Soboll, S., Sholz, R., and Heldt, H.W. (1978). Subcellular Metabolite Concentrations. Dependence of Mitochenodrial and Cytosolic ATP Systems on the Metabolic STate of Perfuse Rat Liver. Eur. J. Biochem. *87*, 377–390.

Stanley, P.E. (1989). A review of bioluminescent ATP techniques in rapid microbiology. J. Biolumin. Chemilumin. *4*, 375–380.

Stawski, R., Walczak, K., Kosielski, P., Meissner, P., Budlewski, T., Padula, G., and Nowak, D. (2017). Repeated bouts of exhaustive exercise increase circulating cell free nuclear and mitochondrial DNA without development of tolerance in healthy men. PLOS ONE *12*, e0178216.

Stehlik, J., Edwards, L.B., Kucheryavaya, A.Y., Aurora, P., Christie, J.D., Kirk, R., Dobbels, F., Rahmel, A.O., and Hertz, M.I. (2010). The Registry of the International Society for Heart and Lung Transplantation: Twenty-seventh official adult heart transplant report—2010. J. Heart Lung Transplant. *29*, 1089–1103.

Stettner, A.I., and Segre, D. (2013). The cost of efficiency in energy metabolism. Proc. Natl. Acad. Sci. *110*, 9629–9630.

Stoppel, W.L., Kaplan, D.L., and Black, L.D. (2016). Electrical and mechanical stimulation of cardiac cells and tissue constructs. Adv. Drug Deliv. Rev. *96*, 135–155.

Strehler, B.L. (1974). Adenosine-5′-triphosphate and Creatine Phosphate Determination with Luciferase. In Methods of Enzymatic Analysis (Second English Edition), (Academic Press), pp. 2112–2126.

Summers, D.M., Johnson, R.J., Allen, J., Fuggle, S.V., Collett, D., Watson, C.J., and Bradley, J.A. (2010). Analysis of factors that affect outcome after transplantation of kidneys donated after cardiac death in the UK: a cohort study. The Lancet *376*, 1303–1311.

Szczesny, B., Marcatti, M., Ahmad, A., Montalbano, M., Brunyánszki, A., Bibli, S.-I., Papapetropoulos, A., and Szabo, C. (2018). Mitochondrial DNA damage and subsequent activation of Z-DNA binding protein 1 links oxidative stress to inflammation in epithelial cells. Sci. Rep. *8*, 914.

Taimor, G. (2000). Apoptosis induction by nitric oxide in adult cardiomyocytes via cGMP-signaling and its impairment after simulated ischemia. Cardiovasc. Res. *45*, 588–594.

Takeda, E., Terao, J., Nakaya, Y., Miyamoto, K., Baba, Y., Chuman, H., Kaji, R., Ohmori, T., and Rokutan, K. (2004). Stress control and human nutrition. J. Med. Invest. *51*, 139–145.

Tang, D., Kang, R., Coyne, C.B., Zeh, H.J., and Lotze, M.T. (2012). PAMPs and DAMPs: signals that spur autophagy and immunity. Immunol. Rev. *249*, 158–175.

Tormos, K.V., Anso, E., Hamanaka, R.B., Eisenbart, J., Joseph, J., Kalyanaraman, B., and Chandel, N.S. (2011). Mitochondrial Complex III ROS Regulate Adipocyte Differentiation. Cell Metab. *14*, 537–544.

Tsuji, N., Tsuji, T., Ohashi, N., Kato, A., Fujigaki, Y., and Yasuda, H. (2016). Role of Mitochondrial DNA in Septic AKI via Toll-Like Receptor 9. J. Am. Soc. Nephrol. JASN *27*, 2009–2020.

Ueda, H., Yamaguchi, O., Taneike, M., Akazawa, Y., Wada-Kobayashi, H., Sugihara, R., Yorifuji, H., Nakayama, H., Omiya, S., Murakawa, T., et al. (2019). Administration of a TLR9 Inhibitor Attenuates the Development and Progression of Heart Failure in Mice. JACC Basic Transl. Sci. *4*, 348–363.

Ultsch, G.R. (1989). ECOLOGY AND PHYSIOLOGY OF HIBERNATION AND OVERWINTERING AMONG FRESHWATER FISHES, TURTLES, AND SNAKES. Biol. Rev. *64*, 435–515.

Ultsch, G.R. (2006). The ecology of overwintering among turtles: where turtles overwinter and its consequences. Biol. Rev. *81*, 339.

Umland, S.P., Shah, H., Jakway, J.P., Shortall, J., Razac, S., Garlisi, C.G., Falcone, A., Kung, T.T., Stelts, D., Hegde, V., et al. (1999). Effects of Cyclosporin A and Dinactin on T-Cell Proliferation, Interleukin-5 Production, and Murine Pulmonary Inflammation. Am. J. Respir. Cell Mol. Biol. *20*, 481–492.

Valls-Lacalle, L., Barba, I., Miró-Casas, E., Ruiz-Meana, M., Rodríguez-Sinovas, A., and García-Dorado, D. (2018). Selective Inhibition of Succinate Dehydrogenase in Reperfused Myocardium with Intracoronary Malonate Reduces Infarct Size. Sci. Rep. *8*, 2442.

van der Vliet, J.A., Warlé, M.C., Cheung, C.L.S., Teerenstra, S., and Hoitsma, A.J. (2011). Influence of prolonged cold ischemia in renal transplantation: Cold ischemia in renal transplantation. Clin. Transplant. *25*, E612–E616.

de Vries, D.K., Kortekaas, K.A., Tsikas, D., Wijermars, L.G.M., van Noorden, C.J.F., Suchy, M.-T., Cobbaert, C.M., Klautz, R.J.M., Schaapherder, A.F.M., and Lindeman, J.H.N. (2013). Oxidative Damage in Clinical Ischemia/Reperfusion Injury: A Reappraisal. Antioxid. Redox Signal. *19*, 535–545.

Vringer, E., and Tait, S.W.G. (2019). Mitochondria and Inflammation: Cell Death Heats Up. Front. Cell Dev. Biol. *7*, 100.

Wang, C., and Youle, R.J. (2009). The role of mitochondria in apoptosis*. Annu. Rev. Genet. *43*, 95–118.

Wang, T., Xu, Y., Yuan, Y., Xu, P., Zhang, C., Li, F., Wang, L., Yin, C., Zhang, L., Cai, X., et al. (2019a). Succinate induces skeletal muscle fiber remodeling via SUNCR 1 signaling. EMBO Rep. *20*.

Wang, X., O'Brien, M.E., Yu, J., Xu, C., Zhang, Q., Lu, S., Liang, L., An, X., McDyer, J.F., and Mallampalli, R.K. (2019b). Prolonged Cold Ischemia Induces Necroptotic Cell Death in Ischemia–Reperfusion Injury and Contributes to Primary Graft Dysfunction after Lung Transplantation. Am. J. Respir. Cell Mol. Biol. *61*, 244–256.

Wang, Y.-C., Lee, W.-C., Liao, S.-C., Lee, L.-C., Su, Y.-J., Lee, C.-T., and Chen, J.-B. (2011). Mitochondrial DNA copy number correlates with oxidative stress and predicts mortality in nondiabetic hemodialysis patients. J. Nephrol. *24*, 351–358.

Warren, D.E., Reese, S.A., and Jackson, D.C. (2006). Tissue Glycogen and Extracellular Buffering Limit the Survival of Red-Eared Slider Turtles during Anoxic Submergence at 3°C. Physiol. Biochem. Zool. *79*, 736–744.

Watson, C.J.E., and Dark, J.H. (2012). Organ transplantation: historical perspective and current practice. Br. J. Anaesth. *108*, i29–i42.

Watt, I.N., Montgomery, M.G., Runswick, M.J., Leslie, A.G.W., and Walker, J.E. (2010). Bioenergetic cost of making an adenosine triphosphate molecule in animal mitochondria. Proc. Natl. Acad. Sci. *107*, 16823–16827.

Weinberg, S.E., Sena, L.A., and Chandel, N.S. (2015). Mitochondria in the Regulation of Innate and Adaptive Immunity. Immunity *42*, 406–417.

Wenceslau, C.F., McCarthy, C.G., Szasz, T., Spitler, K., Goulopoulou, S., and Webb, R.C. (2014). Mitochondrial damage-associated molecular patterns and vascular function. Eur. Heart J. *35*, 1172–1177.

Wendt, I.R., Mellor, K.M., Barclay, C., Bell, J.R., and Delbridge, L.M.D. (2009). Achieving Cardiomyocyte Hypoxia in an in vitro Simulated Ischemic Environment. Heart Lung Circ. *18*, S312.

West, A.P., Shadel, G.S., and Ghosh, S. (2011). Mitochondria in innate immune responses. Nat. Rev. Immunol. *11*, 389–402.

West, A.P., Khoury-Hanold, W., Staron, M., Tal, M.C., Pineda, C.M., Lang, S.M., Bestwick, M., Duguay, B.A., Raimundo, N., MacDuff, D.A., et al. (2015). Mitochondrial DNA stress primes the antiviral innate immune response. Nature *520*, 553–557.

Whitaker, R.M., Stallons, L.J., Kneff, J.E., Alge, J.L., Harmon, J.L., Rahn, J.J., Arthur, J.M., Beeson, C.C., Chan, S.L., and Schnellmann, R.G. (2015). Urinary mitochondrial DNA is a biomarker of mitochondrial disruption and renal dysfunction in acute kidney injury. Kidney Int. *88*, 1336–1344.

Wiesner, R.J., Rüegg, J.C., and Morano, I. (1992). Counting target molecules by exponential polymerase chain reaction: Copy number of mitochondrial DNA in rat tissues. Biochem. Biophys. Res. Commun. *183*, 553–559.

Williams, B.C., Gatti, M., and Goldberg, M.L. (1996). Bipolar spindle attachments affect redistributions of ZW10, a Drosophila centromere/kinetochore component required for accurate chromosome segregation. J. Cell Biol. *134*, 1127–1140.

Wilson, A.J., Schoenauer, R., Ehler, E., Agarkova, I., and Bennett, P.M. (2014). Cardiomyocyte growth and sarcomerogenesis at the intercalated disc. Cell. Mol. Life Sci. *71*, 165–181.

Wlodkowic, D., Telford, W., Skommer, J., and Darzynkiewicz, Z. (2011). Apoptosis and beyond: cytometry in studies of programmed cell death. Methods Cell Biol. *103*, 55–98.

Wood, K.J., Bushell, A., and Hester, J. (2012). Regulatory immune cells in transplantation. Nat. Rev. Immunol. *12*, 417–430.

Wu, F., Jeneson, J.A.L., and Beard, D.A. (2007). Oxidative ATP synthesis in skeletal muscle is controlled by substrate feedback. Am. J. Physiol.-Cell Physiol. *292*, C115–C124.

Xia, P., Wang, S., Gao, P., Gao, G., and Fan, Z. (2016). DNA sensor cGAS-mediated immune recognition. Protein Cell *7*, 777–791.

Yang, X., Cohen, M.V., and Downey, J.M. (2010). Mechanism of cardioprotection by early ischemic preconditioning. Cardiovasc. Drugs Ther. *24*, 225–234.

Yellon, D.M., and Downey, J.M. (2003). Preconditioning the myocardium: from cellular physiology to clinical cardiology. Physiol. Rev. *83*, 1113–1151.

Zager, R.A., Foerder, C., and Bredl, C. (1991). The influence of mannitol on myoglobinuric acute renal failure: functional, biochemical, and morphological assessments. J. Am. Soc. Nephrol. JASN *2*, 848–855.

Zhai, Y., Petrowsky, H., Hong, J.C., Busuttil, R.W., and Kupiec-Weglinski, J.W. (2013). Ischaemia–reperfusion injury in liver transplantation—from bench to bedside. Nat. Rev. Gastroenterol. Hepatol. *10*, 79–89.

Zhang, F., Chen, M., Shan, Q., Zou, J., Chen, C., Yang, B., Xu, D., Jin, Y., and Cao, K. (2007). Hypoxia reoxygenation induces premature senescence in neonatal SD rat cardiomyocytes. Acta Pharmacol. Sin. *28*, 44–51.

Zhang, J., Wang, Y.T., Miller, J.H., Day, M.M., Munger, J.C., and Brookes, P.S. (2018). Accumulation of Succinate in Cardiac Ischemia Primarily Occurs via Canonical Krebs Cycle Activity. Cell Rep. *23*, 2617–2628.

Zhang, Q., Raoof, M., Chen, Y., Sumi, Y., Sursal, T., Junger, W., Brohi, K., Itagaki, K., and Hauser, C.J. (2010a). Circulating mitochondrial DAMPs cause inflammatory responses to injury. Nature *464*, 104–107.

Zhang, Q., Raoof, M., Chen, Y., Sumi, Y., Sursal, T., Junger, W., Brohi, K., Itagaki, K., and Hauser, C.J. (2010b). Circulating Mitochondrial DAMPs Cause Inflammatory Responses to Injury. Nature *464*, 104–107.

Zhao, H.W., and Haddad, G.G. (2011). Review: Hypoxic and oxidative stress resistance in Drosophila melanogaster. Placenta *32 Suppl 2*, S104-108.

Zhao, H., Alam, A., Soo, A.P., George, A.J.T., and Ma, D. (2018). Ischemia-Reperfusion Injury Reduces Long Term Renal Graft Survival: Mechanism and Beyond. EBioMedicine *28*, 31–42.

Zhou, D., Xue, J., Lai, J.C.K., Schork, N.J., White, K.P., and Haddad, G.G. (2008). Mechanisms Underlying Hypoxia Tolerance in Drosophila melanogaster: hairy as a Metabolic Switch. PLoS Genet. *4*, e1000221.

Zhu, Y., Wu, J., and Yuan, S.-Y. (2013). MCT1 and MCT4 Expression During Myocardial Ischemic-Reperfusion Injury in the Isolated Rat Heart. Cell. Physiol. Biochem. *32*, 663–674.

(2009). Organ Donation and Transplantation after Cardiac Death (Oxford University Press).

(2011). Essential Immunology for Surgeons (Oxford University Press).

Appendix

Publications arising from this work

IN REVISION:
Mechanism of succinate efflux upon reperfusion of the ischemic heart,
Hiran A. Prag[1]*, Anja V. Gruszczyk*, Margaret M. Huang, Timothy E. Beach, Efterpi Nikitopoulou, Raimondo Ascione, Anna Hadjihambi, Michael J. Shattock, Luc Pellerin, Kourosh Saeb-Parsy, Christian Frezza, Andrew M. James, Thomas Krieg, Michael P. Murphy, and Dunja Aksentijević
* shared first author

1. Martin JL, Costa ASH, Gruszczyk AV, Beach TE, Allen FM, Prag HA, et al. Succinate accumulation drives ischaemia-reperfusion injury during organ transplantation. Nat Metab. 2019 Oct;1(10):966–74.

2. Martin JL, Gruszczyk AV, Beach TE, Murphy MP, Saeb-Parsy K. Mitochondrial mechanisms and therapeutics in ischaemia reperfusion injury. Pediatr Nephrol. 2019 Jul;34(7):1167–74.

3. Hinchy EC, Gruszczyk AV, Willows R, Navaratnam N, Hall AR, Bates G, et al. Mitochondria-derived ROS activate AMP-activated protein kinase (AMPK) indirectly. J Biol Chem. 2018 Nov 2;293(44):17208–17.

4. Prag HA, Kula-Alwar D, Beach TE, Gruszczyk AV, Burger N, Murphy MP. Mitochondrial ROS production during ischemia-reperfusion injury. In: Oxidative Stress [Internet]. Elsevier; 2020 [cited 2020 Apr 8]. p. 513–38. Available from: https://linkinghub.elsevier.com/retrieve/pii/B9780128186060000262

5. Pell VR, Spiroski A-M, Mulvey J, Burger N, Costa ASH, Gruszczyk AV, et al. Ischemic preconditioning protects against cardiac ischemia reperfusion injury without affecting succinate accumulation or oxidation. J Mol Cell Cardiol. 2018 Oct; 123:88–91.

6. Antonucci S, Mulvey JF, Burger N, Di Sante M, Hall AR, Gruszczyk A, et al. Selective mitochondrial superoxide generation in vivo is cardioprotective through hormesis. Free Radic Biol Med. 2019 Apr; 134:678–87.

7. Bundgaard A, James AM, Gruszczyk AV, Martin J, Murphy MP, Fago A. Metabolic adaptations during extreme anoxia in the turtle heart and their implications for ischemia-reperfusion injury. Sci Rep. 2019 Dec;9(1):2850.

8. Kohlhauer M, Pell VR, Burger N, Spiroski AM, Gruszczyk A, Mulvey JF, et al. Protection against cardiac ischemia-reperfusion injury by hypothermia and by inhibition of succinate accumulation and oxidation is additive. Basic Res Cardiol. 2019 May;114(3):18.

10.1 Supplementary data to Chapter 3

10.1.1 Different ETC inhibitors before induction of ischaemia in mouse heart

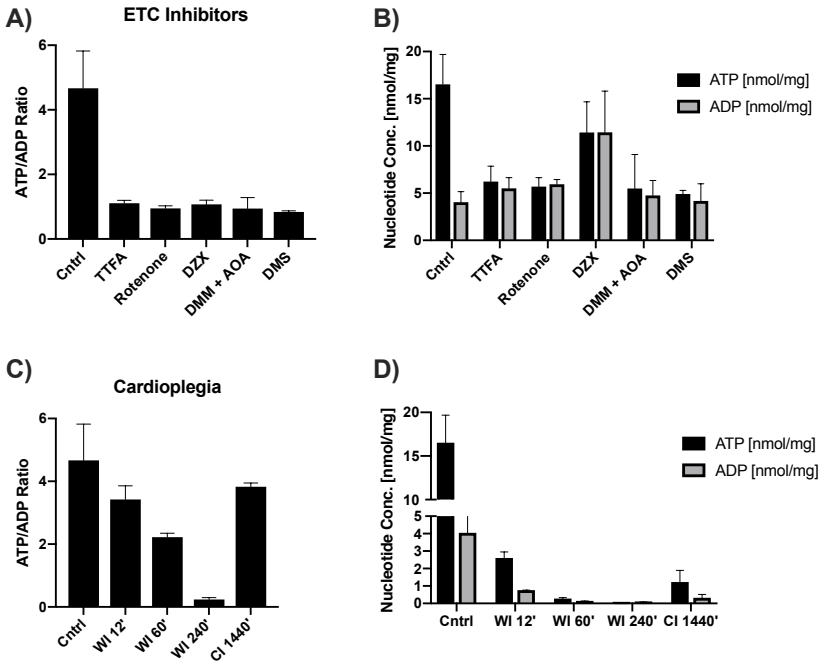

Figure 10.1: Effects of different inhibitors on ATP/ADP ratios in murine heart samples. Adenosine nucleotides were measured in heart tissues using a Luciferase luminescence assay and the change in nucleotides presented as ratio of ATP to ADP (A, C). Nucleotide concentrations are measured in nmol/mg (B, D). Samples were rapidly frozen using Wollenberger clamps and analyse within 1 months. Different ETC inhibitors were injected via IV injection 10 min before retrieval of the heart samples. The hearts were retrieved and subjected to additional warm ischaemia before freezing. The inhibitors were dissolved in saline solution at following concentrations: TTFA, Rotenone, DZX, DMM+ AOA, DMS (A, B). Cardioplegia was induced via potassium injection into the heart immediately before samples were retrieved and subjected to ischaemia at 37°C (WI) or 4°C (CI) for different timepoints (C, D). ETC inhibitors: n= 3, cardioplegia: n= 2 biological replicates, data are mean ± S.E.M.

10.1.2 Rabbit ischaemia and reperfusion

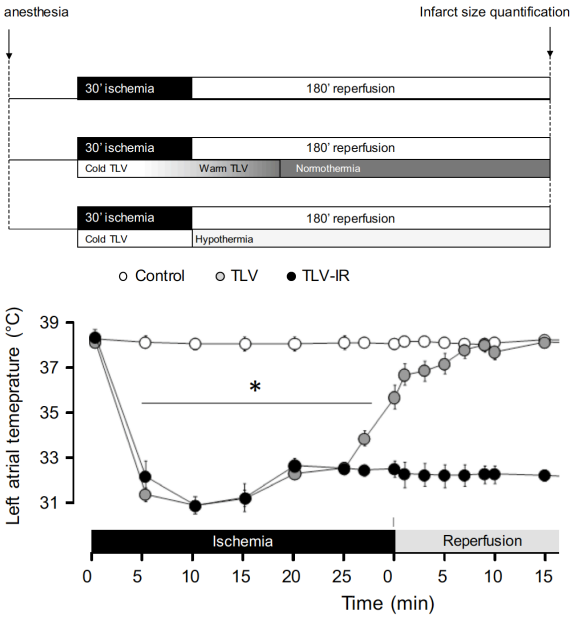

Figure 10.2.: A model for cold ischaemia reperfusion injury in rabbit hearts. Schematic overview of the time course of ischaemia and reperfusion subjected to rabbits modified from REF. (A) After a normoxic equilibration period after induction of anesthesia, ischaemia was induced via LAD occlusion for 30 min followed by 3 h of reperfusion, before samples were snap frozen. (B) Ischaemia was either performed at normothermia (38°C) or hypothermia at 31°C. These samples were retrieved by Dr. Matthias Kohlbauer in Paris, before they were shipped to the MRC MBU in Cambridge and analysed by me. Kohlbauer et al. 2018.

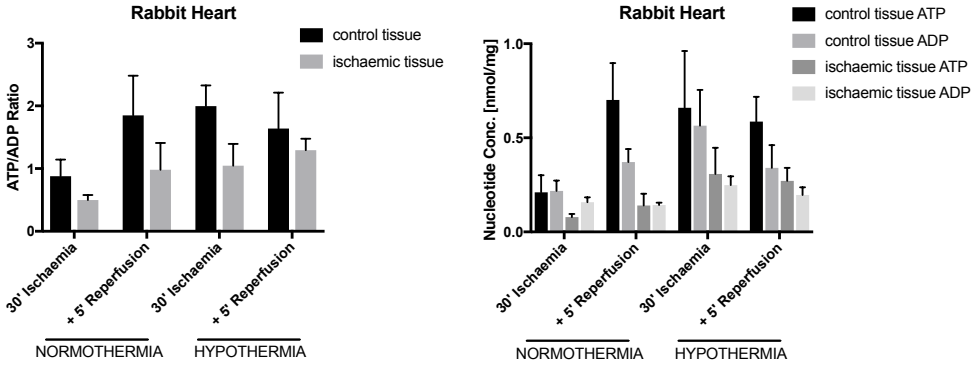

Figure 10.3: Effect of cold ischaemia on adenosine nucleotide changes in rabbit hearts. ATP/ADP ratios in rabbit hearts that have undergone 30 min of ischaemia at normothermia at 38°C or hypothermia at 31°C via LAD occlusion. Tissue samples were retrieved from the ischaemic part of the heart, as well as from a control part of the right ventricle. Samples were snap- frozen at the end of ischaemia or 5 min upon reperfusion and stored at -80°C before being processed within 1 month. Adenosine nucleotides were measured using a Luciferase luminescence assay and the change in nucleotides presented as ratio of ATP to ADP (A). Nucleotide concentrations are measured in nmol/mg (B). The dotted line indicates the control value. n= 4 biological replicates, data are mean ±SEM. statistical test 2- way ANOVA did not show statistical significance.

10.2 Supplementary data to Chapter 4

10.2.1 Development of a HEK cell model for IRI

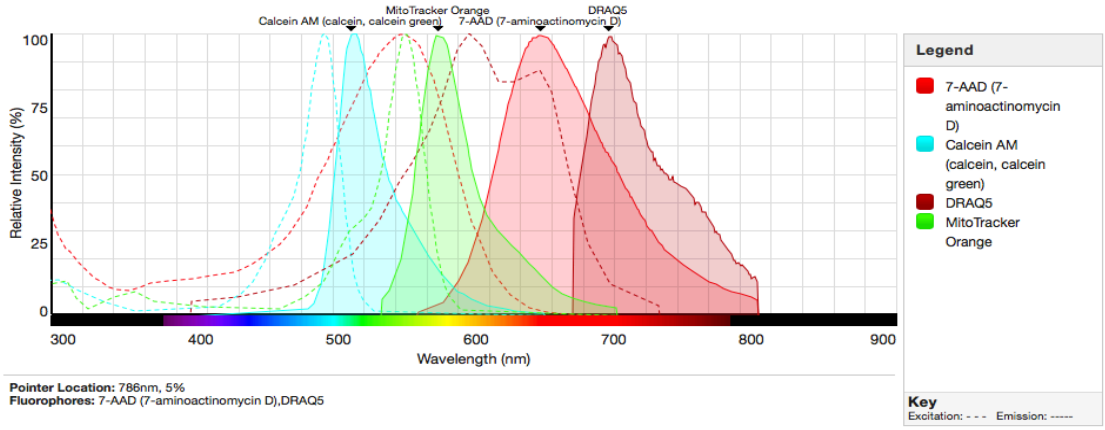

Figure 10.4: Plan to develop a flow cytometry technique to evaluate cell death, MPTP opening and others in isolated cardiomyocytes. The depicted live, death and mitochondrial dyes were supposed to be used. A membrane potential-dependend mitotracker might give insight into mitochondrial membrane potential during anoxia as well. Unfortunately, primary cardiomyocytes were too fragile to be analysed at one of the (to me available) flow cytometers. I therefore looked into establishing another, more robust cell model to try techniques/ drug concentrations first, before utilising the valuable cardiomyocytes (1 mouse heart = 5,000,000 cells)

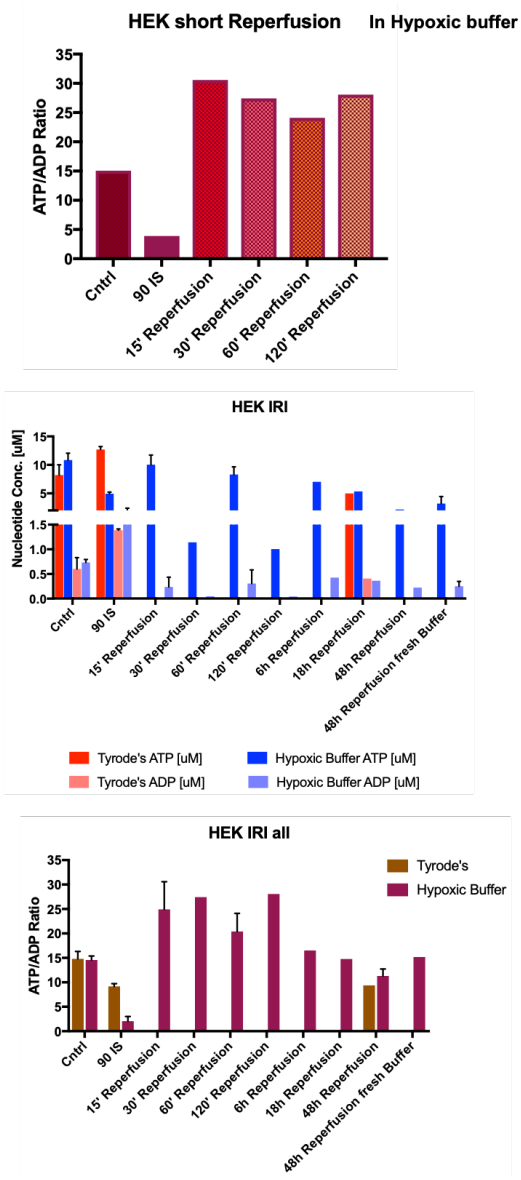

Figure 10.5: Characterisation of HEKcells in response to anoxia and reoxygenation in different buffers. First, their sensitivity to anoxia was measured by inducing different timepoints of anoxia and reperfusion as described before in either hypoxic or Tyrode's buffer. HEK cells respond to ischaemia similar to cardiomyocytes.

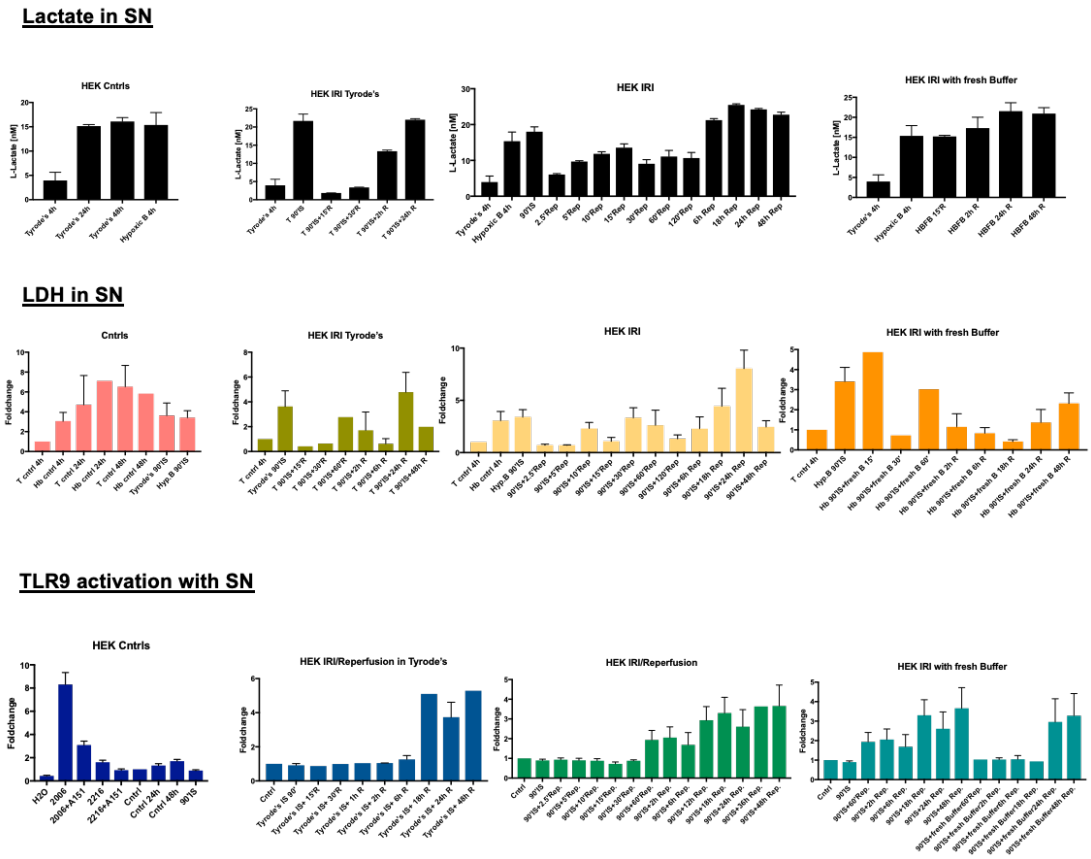

Figure 10.6: Characterisation of HEKcells in response to anoxia and reoxygenation in different buffers. Next, lactate release, cell death and TLR9 activation were assessed upon anoxia and reperfusion and similar although delayed responses were detectable in comparison to cardiomyocytes.

10.3 Supplementary data to Chapter 7

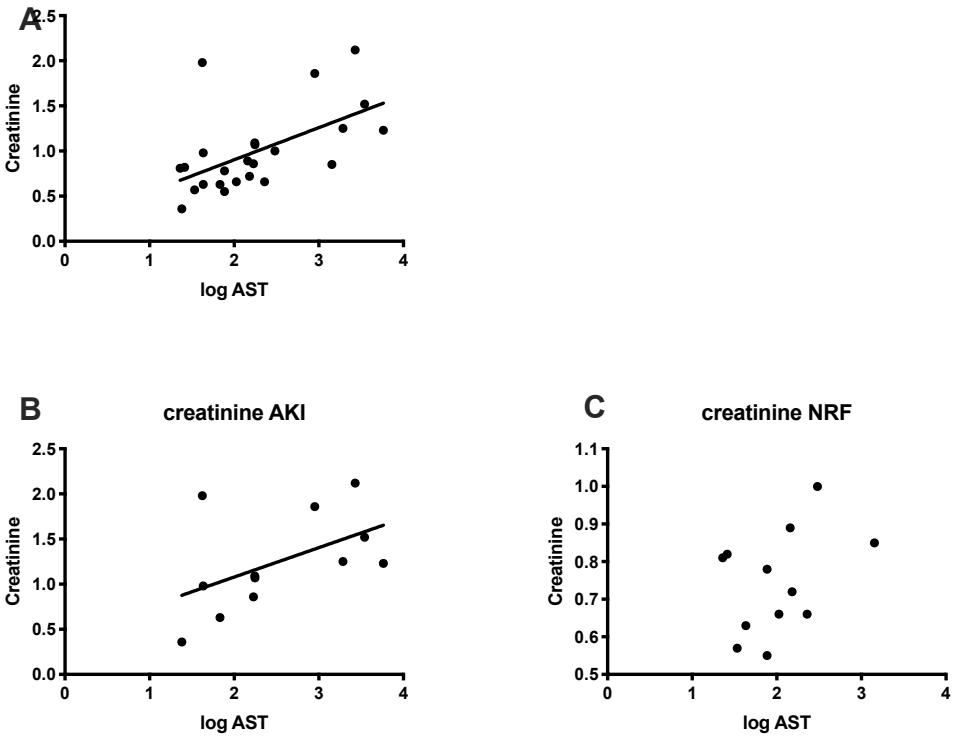

Figure 10.7: Additional correlation data comparing patients that developed AKI upon liver transplantation or had normal renal function. While creatinine and logAST correlate in the whole cohort (A), separated into AKI and NRF groups, the AKI cohort shows a clearer response to kidney damage as measured by the release of damage markers.

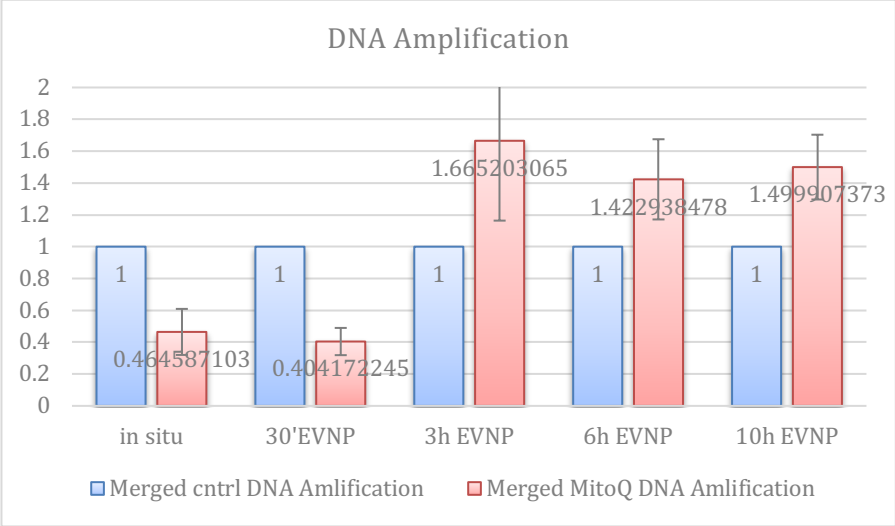

Figure 10.8: Tissue DNA from discarded human kidneys perfused on an EVNP show less DNA damage when perfused with MitoQ. Wedge biopsies were retrieved from human kidneys, that were perfused at an EVNP machine as described in Chapter 7. DNA was extracted as described before and oxidative damage to DNA measured via the previously described qPCR. Kidneys were either perfused with 50 uM MitoQ in leucocyte depleted blood or just blood without any addition.The MitoQ treated bars in red show more DNA amplification after 3 h and longer of perfusion..This might be an indication for the antioxidant function of MitoQ ameliorating damage, or indicate that treatment with the compound upregulates cellular pathways imporving DNA repair.

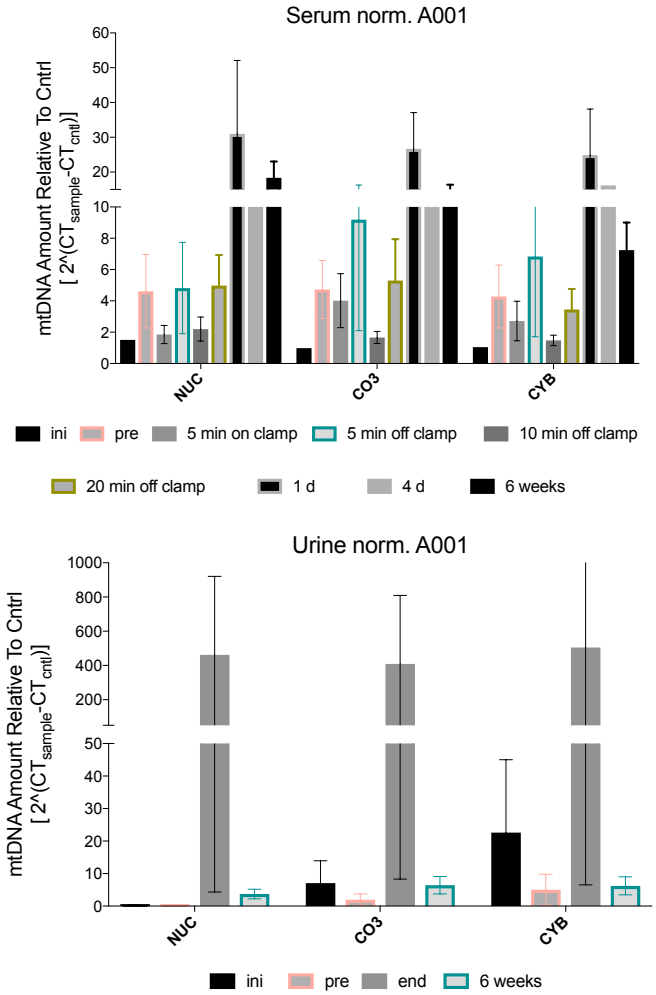

Figure 10.9: Serum and urine samples from patients that underwent partial nephrectomy. Their blood and urine was analysed for circulating DNA utilising RT-PCR (before ddPCR was available). Abundance of the nuclear gene β-actin and the mitochondrial genes CO3 and CYB were investigated and quantified against a standadcurve. The data are displaied relative to control blood samples. Different to data obtained via ddPCR, here, no difference is detectable between nuclear and mitochondrial circulationg DNA. Probably due to the less sensitive RT-PCR detection method as well as due to the fact that RT-PCR overamplifies samples (~40 cycles) resulting in amplification even of genes that are barely abundand. Fazit: ddPCR is more sensitive and gives less false positives. At low amounts of DNA.

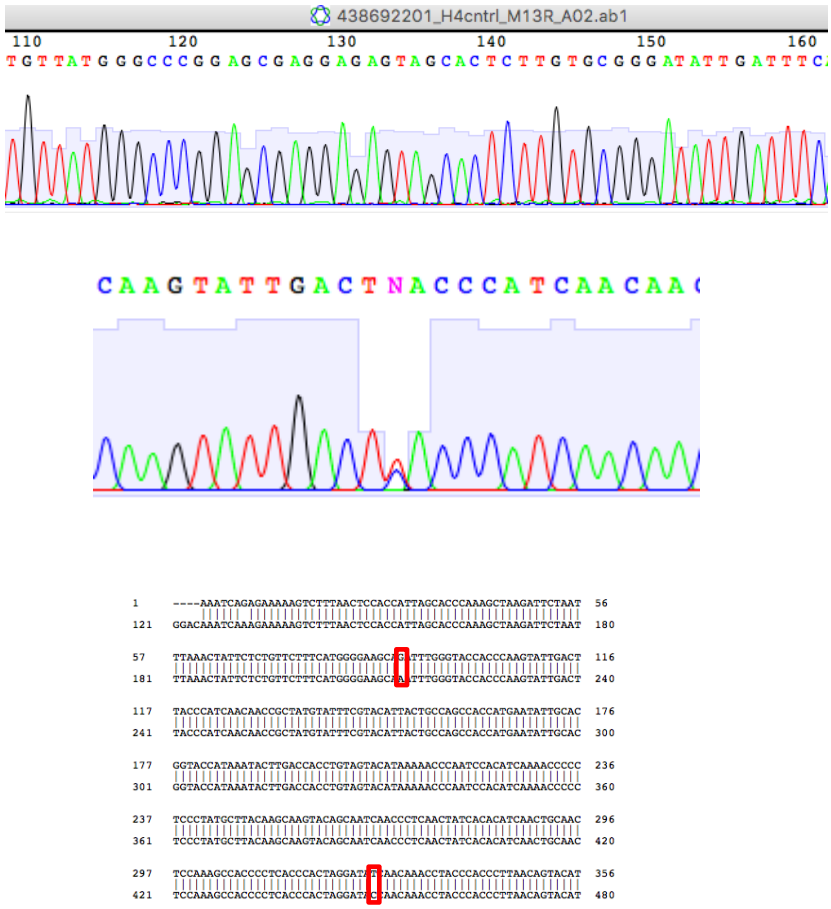

Figure 10.10: Development of a Dloop- Sequencing approach to investigate haplotype differences between organ donors and distinguish between circulating DNA from donor and recipient (same principle as with the conplastic mice). I designed a PCR spanning the highly variable D-loop region on mtDNA. I amplified this Dloop DNA templates in blood samples from the patients that underwent liver transplantation. I sequenced a sample from blood taken before transplantation and one days after transplantation and wanted to investigate if the circulating Dloop changed due to the graft in the recipient. Of all ten patients, just one showed a different sequencing pattern after transplantation than before. In this sample, I could clearly see, that now two SNPs were detectable whch was not the case before surgery. I concluded that most european patients have mtDNA haplotype similar enough to not be picked up with this method.